Microscopic and Beyond-Mean-Field Constraints for a New Generation of Nuclear Energy Density Functionals

Thomas Lesinski

N° d'ordre 141-2008 Année 2008

THÈSE

présentée devant

l'UNIVERSITÉ CLAUDE BERNARD – LYON 1

préparée à l'Institut de Physique Nucléaire de Lyon

(UMR 5822 CNRS/IN2P3 – Université Lyon 1)

pour l'obtention du

DIPLÔME DE DOCTORAT

(arrêté du 7 août 2006)

Spécialité : Physique Théorique

Présentée et soutenue publiquement le 24 septembre 2008

par

M. Thomas LESINSKI

TITRE :

Microscopic and Beyond-Mean-Field Constraints for a New Generation of Nuclear Energy Density Functionals

Directeur de thèse : M. Jacques MEYER

JURY :	M.	Guy CHANFRAY	Président
	M.	Jacek DOBACZEWSKI	} Rapporteurs
	M.	Hubert FLOCARD	
	Mme	Héloïse GOUTTE	
	M.	Jacques MEYER	Directeur
	M.	Karim BENNACEUR	Co-Directeur
	M.	Michael BENDER	} Invités
	M.	Thomas DUGUET	

Ackowledgements / Remerciements

I would first like to thank my advisors, Karim Bennaceur and Jacques Meyer, for their support and the freedom that I enjoyed during the three years I spent as a graduate student in Lyon. I should add Michael Bender and especially Thomas Duguet to complete the list of people who provided me with an open, stimulating and high-level work environment, however geographically scattered. A very special mention should be made at this point of the quality and huge quantity of work performed by Vincent Rotival, whom research will definitely miss, and which eased my way through the work presented in Chapter 5 of the present (highly collective) manuscript. I should also acknowledge Scott Bogner for his valuable help regarding the work presented in the aforementioned chapter.

I also wish to thank every member of the Jury, especially its President Guy Chanfray, Referees Hubert Flocard and Jacek Dobaczewski, and of course Héloise Goutte, for taking the time of an in-depth reading and returning suggestions for improvement. Let me here thank MM. Duguet and Bender a second time and apologize for their "guest" status, due to an optimization performed under administrative constraints.

This thesis was prepared among the Theory group of the *Institut de physique Nucléaire de Lyon*, whom I am grateful for their hospitality. The same applies to the *Espace de Structure Nucléaire Théorique* at the *Service de Physique Nucléaire* of CEA-Saclay, as well as the Theory group of the National Superconducting Cyclotron Laboratory at Michigan State University, which both welcomed me on the occasion of several extended stays. Thanks for their time and hospitality go to the nuclear theory group at INFN Milan, especially Alessandro Pastore.

Bien évidemment, je me dois de remercier toutes les personnes qui font tourner l'IPNL, notamment Lucille Chosson (en lui souhaitant une bonne retraite) et Sylvie Florès, souligner en particulier l'efficacité et la disponibilité du groupe Informatique, notamment Clément, Thierry Olivier, et les "frères Grid" Yoan et Guillaume. Mon expérience a l'IPNL n'aurait pas été la même sans la bonne humeur de ses Thésards, toutes generations confondues. Un grand merci, donc, a Charbel, Clément (x2), David, Elizabeth, Émilie, Fabien, Federica, Hubert, Olivier, Thibaut, Thomas, et ceux et celles que j'ai oublié !

Cette thése fut financée par une allocation de recherche du Ministére de l'Éducation Nationale, de la Recherche et de la Technologie, augmenté d'une allocation de monitorat de l'Université Claude Bernard Lyon 1, ainsi qu'un AP théorie de l'Institut National de Physique Nucléaire et de Physique des Particules (IN2P3).

Contents

1 Introduction **11**

2 Overview of Nuclear Structure Theory **15**
2.1 Microscopic theory of nuclear structure 15
2.1.1 The Nuclear Hamiltonian 15
2.1.2 Single-particle Green's function 17
2.1.3 Perturbation theory (or lack thereof) 20
2.2 Energy Density Functional formalism 21
2.2.1 Mean-field theory and pairing 21
2.2.2 Density functional theory 27
2.2.3 Single- and multi-reference EDF methods 29
2.3 Skyrme energy density functional 34
2.3.1 Quasi-local energy density functional 34
2.3.2 Skyrme energy functional in spherical symmetry 40
2.4 Local pairing functional 40

3 New Constraints for the Nuclear EDF **45**
3.1 Constraining the isovector effective mass 46
3.1.1 Fitting protocol 48
3.1.2 Elementary properties of studied functionals 48
3.1.3 Properties of the nuclear matter EOS 50
3.1.4 Effects on properties of nuclei 51
3.2 Further study of infinite matter 56
3.2.1 Separation of the EOS into (S,T) channels 56
3.2.2 RPA linear response functions and the diagnosis of instabilities 59
3.3 Summary 66

4 Tensor Part of the Skyrme Functional **69**
4.1 Introduction 69
4.2 The fits 73
4.2.1 Properties of tensor terms in spherical symmetry 73
4.2.2 A brief history of tensor terms in the central Skyrme EDF . . 75
4.2.3 General remarks 77
4.2.4 The fit protocol and procedure 77
4.2.5 General properties of the fits 80
4.3 Results and discussion 82
4.3.1 Spin-orbit currents and potentials 82
4.3.2 Single-particle energies 87
4.3.3 Binding energies 102

4.3.4 Radii . . . 109
4.4 Summary and conclusions . . . 113

5 Ab-Initio Description of Nuclear Pairing 117
5.1 Pairing and superfluidity in many-fermion systems . . . 117
5.1.1 BCS theory . . . 118
5.1.2 Experimental evidence and observables . . . 120
5.1.3 Trends in pairing gaps . . . 124
5.1.4 Microscopic theory . . . 124
5.2 Ab-initio input for the pairing EDF . . . 129
5.2.1 The $V_{\mathrm{low}\,k}$ low-momentum NN interaction . . . 130
5.2.2 Separable representation and finite nuclei . . . 131
5.3 A Separable Representation of the NN force . . . 134
5.3.1 Parametrization and fit procedure . . . 134
5.3.2 Fits . . . 137
5.3.3 Separable approximation of the Coulomb interaction . . . 140

6 NN Pairing: Bare Force at First Order 143
6.1 First results . . . 144
6.2 Charge symmetry and Coulomb interaction . . . 146
6.3 Effect of $V_{\mathrm{low}\,k}$ renormalization scale . . . 148
6.4 Summary and outlook . . . 152

7 Conclusion 155

Appendix 159

A Coupling constants of the Skyrme EDF 161

B Separation of the energy into (S,T) channels 165

C P-H Potentials and Residual Interaction 167
C.1 Principle . . . 167
C.2 Definitions . . . 168
C.3 Potential and Residual Interaction . . . 170
C.3.1 Local, density-dependent terms . . . 171
C.3.2 Non-local (effective-mass and current) terms . . . 171
C.4 Infinite matter . . . 172
C.4.1 Parameterization of the residual interaction . . . 172

D Formal aspects of separable interactions 175
D.1 Potentials . . . 175
D.1.1 Partial-wave expansion . . . 176
D.1.2 Two-particle scattering and the Lippmann-Schwinger equation 177
D.2 Phase shifts . . . 177
D.3 Gap equation in infinite matter . . . 178

E Parameters of separable interactions 181

F Separable Force in Spherical Symmetry **185**
F.1 General expression of interaction matrix elements 185
F.2 Computation of the pairing field 187
F.2.1 General technical aspects 187
F.2.2 Center-of-mass/relative coordinate separation 187
F.2.3 Pair densities 188
F.2.4 Pairing fields 190
F.3 Evaluation of Bessel-form factor integrals 191
F.3.1 Simple Gaussian form factor 191
F.3.2 Gaussian × polynomial form factor 191
F.3.3 Coulomb expansion form factor 192
F.4 Some useful expressions 192

G Spherical Bessel Function Basis **195**

List of Abbreviations

ANM	Asymmetric nuclear matter
BCS	Bardeen-Cooper-Schrieffer
BHF	Brueckner-Hartree-Fock
COM	Center-of-mass
CSB	Charge-symmetry breaking
DBHF	Dirac-Brueckner-Hartree-Fock
DFT	Density functional theory
DME	Density matrix expansion
EBHF	Extended Brueckner-Hartree-Fock
EDF	Energy Density Functional
EOS	Equation of state
GCM	Generator coordinate method
GDR	Giant dipole resonance
GMR	Giant monopole resonance
HF	Hartree-Fock
HFB	Hartree-Fock-Bogolyubov
INM	Infinite nuclear matter
ISGMR	Isoscalar giant monopole resonance
IVGMR	Isovector giant monopole resonance
IVGDR	Isovector giant dipole resonance
LCS	Lowest canonical state
LDA	Local density approximation
MR-EDF	Multi-reference energy density functional
NN	Nucleon-nucleon (interaction/scattering)
NNN	Three-nucleon (interaction/scattering)
OES	Odd-even staggering (of binding energies)
PNM	Pure neutron matter
QRPA	Quasiparticle random-phase approximation
RG	Renormalization group
RH	Relativistic Hartree
RMF	Relativistic mean field
RPA	Random-phase approximation
SR-EDF	Single-reference energy density functional
SNM	Symmetric nuclear matter
TRK	Thomas-Reiche-Kuhn
VCS	Variational chain summation

Chapter 1

Introduction

Although the very idea that the positive charge of an atom could be concentrated in a small volume at its center was first proposed by Nagaoka [Nag04], it was Rutherford [Rut11] who gave evidence for this by interpreting the experimental results which Geiger and Marsden obtained by impinging alpha particles on a gold foil [Gei09]. From this point on, the physics of atomic nuclei progressively emerged as a distinct domain from atom physics. However, knowledge of the true composition of nuclei could not be achieved before the discovery of the neutron by Chadwick [Cha32].

A subsequent step was made with the discovery of nuclear fission [Mei39], which showed that quantum tunneling could happen for heavy systems, and gave rise to the description of nuclei and their motion through the liquid drop model [Boh39]. The nucleus was thus understood as a system dominated by collective behavior. This view was supported by the saturation of binding energies per particle, indicating that the interaction between nucleons was short-ranged and extremely strong. As a consequence, quantum correlations were expected to be important. Indeed, after Yukawa's seminal work [Yuk35], the nuclear interaction appeared, in addition to being particularly difficult to understand from first principles, as a non-trivial potential exhibiting a repulsive core even stronger than the attractive part and important spin dependence [Mac89b].

However, it also became known that some nuclei were more bound than their neighbors, causing irregularities on the mass table at well-defined neutron and proton numbers. These "magic numbers", as Wigner called them [Mos96], were explained by Goeppert Mayer via an independent-particle shell model relying on strong spin-orbit coupling for the reproduction of their experimental sequence [GM48, GM49], achieving as well to explain the majority of nuclear spins known at the time [GM50a, GM50b].

The mechanism by which a hard-core interaction can bind many-body systems was due to Brueckner [Bru54b, Bru54a, Bru55b], Bethe and Goldstone [Bet56, Bet57, Gol57]. The reconciliation of collective and single-particle approaches to nuclear structure ensued through the definition of an effective interaction arising in the medium from short-range quantum correlations and useable in a mean-field picture [Foc30], where each particle moves independently in the potential created by the average effect of the others acting through the effective interaction [Bru55c]. The linked-cluster expansion [Bru55a, Bra67] could then extend the mean-field picture to include correlations not re-summed in the effective interaction, and be incorporated in the general framework of many-body perturbation theory

[Hug57, Abr63, Noz63, Fet71] to provide, in principle, an ab-initio description of both single-particle motion and many-body, collective effects in nuclear structure.

From then on, distinct approaches to independent-particle models for nuclear structure emerged. First, models for the nucleon-nucleon interaction in the vacuum were gradually improved [Ham62, Rei68, Lac80, Wir84, Mac87] and used in Brueckner calculations of nuclei [Bec68, Bec74] as well as Brueckner and variational calculations of nuclear matter [Day78]. Nuclei proved stubborn in their habit of coming underbound and too small out of these calculations, while the saturation point of nuclear matter was similarly underbound and occurred at too high a density compared to its empirical position. Coester et al. [Coe70] proved that two-body potentials adjusted on the same nucleon-nucleon scattering data could not reproduce the empirical saturation point. The missing piece was later identified as the three-nucleon force [Pan79, Lag81, Fri81], the existence of which had been previously expected from field-theoretical considerations [Loi67].

Second, shortly after Brueckner's papers, appeared the idea that one could devise simpler effective interactions based on more phenomenological grounds. Skyrme proposed such an effective Hamiltonian consisting of a two-body, velocity-dependent contact interaction and a matching three-body contact interaction [Sky56, Bel56, Sky58a, Sky58b]. The latter was supposed to mimic the medium dependence of Brueckner's effective force more than to reproduce the physics of a bare three-body force. However, Skyrme's idea came to use only later [Vau72], being quantitatively motivated as an approximation to a more realistic effective interaction by the density-matrix expansion method [Neg72, Neg75].

Attempts were also made at finding a potential which could bind nuclei and provide saturation of nuclear matter without needing a hard core for that task [Tab64, Bri67, Gog70]. Such a potential could be employed directly in an independent-particle framework, or in a low-order perturbative expansion where correlations would bring a mere correction to the nuclear wave function, binding energy and other observables. This idea, in the form then envisioned, reached its limits. However, a soft force, augmented by a term depending on the density, was proposed as an approximation to an in-medium effective interaction by Gogny et al. [Gog75a, Dec80, Ber91]. It became the other highly successful non-relativistic nuclear mean-field model, if less widely used than Skyrme's one, due mainly to its higher numerical cost.

An account of nuclear mean-field models would not be complete without a mention of approaches involving effective relativistic Lagrangians, initiated by Walecka [Wal74]. In this model, nucleons interact by exchanging pions and the semi-phenomenological sigma meson. Other degrees of freedom have since been added, aiming at providing better nuclear phenomenology.

Let us now come back to Skyrme's interaction. The latter included quadratic velocity-dependent terms to simulate the range and non-locality of the in-medium effective interaction, and its spin-isospin content was controlled by spin-exchange operators, spin-orbit and tensor terms. A number of parameters thus had to be determined. Given the rather schematic link between a microscopic effective interaction and Skyrme's one, achieving predictive power required fitting the parameters on a set of relevant data. Early choices included the binding energies of stable or exotic nuclei [Bei75b, Ton83, Dob84] and the energies of excited states such as collective vibrations [Kri80, VG81] or fission barriers [Bar82a]. Indeed, Skyrme's

interaction could be successfully used not only to calculate static observables but also collective excitations and nuclear reactions [Eng75, Neg82, Kim97].

The concept of radioactive ion beams, first pioneered by Kofoed-Hansen and Nielsen [KH51], was later implemented in increasingly capable and numerous facilities, starting from ISOLDE at CERN, activated in 1967, and culminating with the many dedicated research centers active today, which employ either isotope separation on line (ISOL) or in-flight fragment separation techniques to produce beams of short-lived isotopes. Work performed at these facilities allowed to measure properties of increasingly unstable nuclei. Naturally, these new data spurred theoreticians to improve the predictive power of available models by adjusting new parameter sets [Rei95, Rei99, Bro98]. With the growing attention paid to the neutron-rich side of the chart of nuclides, it was also realized that experimental data alone could not bring enough constraints on models and that ab-initio calculations could supplement them, when available, for experimentally unreachable systems such as neutron matter [Wir88, Akm98], which, together with data measured for stable nuclei, exerts a strong lever arm on properties of the most neutron-rich ones. Parametrization of Skyrme's interaction built according to these principles by the Saclay-Lyon collaboration [Cha97, Cha98] are still widely used today.

Nowadays, the steady progress of available computational power allows to perform calculations extending the mean-field framework and considering collective correlations in ground and excited states [Bon90, Taj93b, Val00] on a more systematic basis [Ben06a, Ber07, Ter08]. One might thus expect an increase of accuracy, which, however, is taking a long time to come. Contemporary use of Skyrme-mean-field theory is itself put into question concerning its very interpretation as relying on a Brueckner-like effective interaction. Strong resemblances have been found, indeed, with density functional theory, a powerful tool commonly used in condensed-matter physics, which allows in principle to re-sum *all* quantum correlations present in a range of many-particle systems within a universal functional, giving rise to an effective theoretical description by means of independent particles. Using such a formalism for nuclei, though, involves extending it to self-bound, symmetry-breaking systems where single-particle and collective motion are tightly intertwined and both have to be treated explicitly. As a result, in parallel to studies aiming at improving the agreement of the model with experimental data and/or ab-initio calculations, a more formal work is underway to find a rigorous and consistent formal motivation of the method.

The present work is an attempt at improving the predictive power of the "Skyrme interaction" model of nuclear structure. More specifically, our aim is to use the ever-growing amount of data, coming either from experiments, first-principle calculations or microscopic theory of the nuclear interaction itself, to devise new inputs and constraints to be used in the construction of the next generation of models. Most of the following will stay at the mean field level, the precise meaning of which is specified in chapter 2, but we shall, as much as possible, try to keep in mind the necessity to extend our calculations by the addition of collective correlations.

In a first part, we focus on the physical meaning and effect of particular parameters of the Skyrme force, dealing first, in chapter 3, with the momentum-dependence of the mean field and its evolution in neutron-rich nuclei. The spin-isospin content of the force is also studied at this point, both statically, by examining the contribution of different channels of the interaction to the binding energy, and dynamically, by

studying the response of infinite matter, used as a model system, to various perturbations. In will be shown that pathologies of the model can thus be pointed out, and solutions will be proposed. Then, in chapter 4, we add a tensor interaction to the model and study the impact of its parameters on nuclear observables. Single-particle energies, total binding energies and density distributions are considered.

In a second part, we focus on the description of pairing in our model, by making a direct connection with the bare nuclear interaction. In chapter 5, after a brief review of the matter, we detail the formalism and interaction model we use. Then in chapter 6, we perform and study systematic calculations of spherical nuclei across the nuclide chart, discussing the comparison of our results with experimental pairing gaps, giving clues as to the physical origin of nuclear pairing in terms of many-body theory, assessing the importance of the Coulomb interaction in this specific case as well as the care needed when using various bare nuclear-interaction models as an input to our calculations.

Chapter 2

Overview of Nuclear Structure Theory

2.1 Microscopic theory of nuclear structure

Although effective and empirical models have known some success in the theory of atomic nuclei, the quest for a description of the latter from first principles is both a long-standing and current topic of research. As the focus of nuclear theory is, more than ever, on the description of nuclei lying at the fringe of experimental capabilities, the motivation for achieving this is strong.

Let us first specify what we call first principles. The most microscopic theory conceptually applicable to nuclei is the relativistic, non-perturbative Lagrangian of quantum chromodynamics (QCD) ruling all hadronic systems. The latter is most useful, however, at energies above the GeV scale, where asymptotic freedom makes perturbation theory useful again, and for systems made of a few valence quarks which can be simulated thanks to lattice techniques. At lower energies, an effective theory can be built which involves only the physical, observable (i.e. colorless) degrees of freedom: baryons (nucleons and their excitations) and mesons.

This brief foray into the realm of particle and hadron physics allows us to discuss the very first difficulty faced by the study of nuclear structure as an application of quantum many-body theory: the basic Hamiltonian. Practical applications require to treat neutrons and protons as pointlike particles (further reducing them to different states of a single object, the nucleon) interacting via some potential, the theory of which, owing to the compositeness of hadrons and the complexity of their structure and dynamics, is the subject of vast literature. Let us simply mention several relevant facts and assumptions.

2.1.1 The Nuclear Hamiltonian

The notion of a Hamiltonian acting on the sole nucleonic degrees of freedom relies on the hypothesis that the structure of the nucleons, as well as the details of the processes generating the interaction between them, are irrelevant for the study of low-energy processes. Also, the assumption is made that a non-relativistic description of the system, neglecting anti-nucleon degrees of freedom and assuming the usual quadratic expression for the kinetic energy, is valid. The latter is reasonable for 940 MeV-mass particles evolving at about 50 MeV kinetic energy in the nucleus.

Apart from a kinetic term, a realistic Hamiltonian also comprises, at least, two- and three-body interaction terms. The basic experimental input used to determine the two-nucleon interaction is nucleon-nucleon scattering differential cross sections. A large amount of data are available for neutron-proton and proton-proton scattering [SAI, Nij], while some essential features of the neutron-neutron interaction can be obtained in more model-dependent ways. The assumption is made that isospin symmetry is weakly broken, i.e. the potential can be described by a first part which is the same for all combinations of nucleons ($V_{\rm nn} = V_{\rm pp} = V_{\rm np}$) to which one adds a correction breaking charge independence ($V_{\rm nn} = V_{\rm pp} \neq V_{\rm np}$) and an even weaker correction breaking charge symmetry ($V_{\rm nn} \neq V_{\rm pp}$). The probability amplitude of a transition from initial relative momentum $\mathbf{k}'$ to final relative momentum $\mathbf{k}$ for a pair of nucleons at energy E is expressed by the T-matrix obeying the Lippmann-Schwinger (LS) equation ([Bro76], see also appendix D.1.2).

The current leading potential models rely on an effective meson-nucleon Lagrangian. The potential is defined, in this case, as the sum of diagrams entering the scattering amplitude which are irreducible by cutting a pair of nucleon propagation lines [Mac89b]. The repulsive core is either produced by heavy-meson exchange [Mac01] or modeled by phenomenological terms [Wir95]. Scattering data suggest that the interaction is attractive at low energy, while repulsion dominates the scattering of particles having a kinetic energy in the laboratory frame $E_{\rm lab} = \hbar^2 k'^2/m > 250$ MeV, where m is the nucleon mass. At $E_{\rm lab} > 350$ MeV, pion production becomes significant, which indicates that the nonrelativistic NN Hamiltonian picture is inappropriate. Hard-core potentials, however, have non-vanishing matrix elements well into this domain, which is a consequence of the requirement to keep a (mostly) local, i.e. velocity-independent potential. Is is thus obvious that this part of the interaction models is purely effective. In fact, the choice of high-momentum matrix elements of a potential is quite arbitrary and weakly constrained: models of the NN interaction having different matrix elements due to varying choices for the repulsive part yield the same low-energy scattering observables, having been fitted to them.

The above considerations have led to devise a method to produce a universal potential that would not involve any uncontrolled high-energy physics. This was achieved using renormalization group equations [Bog01], and will be further studied in chapter 5. Moreover, a new approach to building NN potentials has been put forward, relying on chiral effective field theory (EFT) [Ent03, Epe05], i.e. an effective Lagrangian including nucleon-pion, pion-pion and nucleon-nucleon contact terms, constrained by chiral symmetry, an essential feature of QCD. This approach allows a systematic, stepwise construction of the potential through a perturbative expansion, which allows to control its accuracy. Moreover, this method has the advantage of naturally producing consistent two-, three- and four-body potentials.

Indeed, a complete description of the nuclear Hamiltonian must include a short-range three-body (NNN) interaction, which is necessary, as a complement to the NN interaction obtained from scattering analysis, to obtain correct saturation properties of nuclear matter [Lag81] and accurate spectroscopy of light nuclei [Pud95, Pie01b]. Several models thus exist also for the three-nucleon interaction [Gra89, Lej00, Pie01a], while current work on the subject focuses on obtaining NNN potentials consistent with the field-theoretical content of NN ones [Epe07, Li08].

Starting from the Hamiltonian detailed above, an ab-initio resolution of the many problem can be undertaken for light and, nowadays, some medium-mass nuclei. For

systems of three and four nucleons, the Faddeev and Faddeev-Yakubovsky equations can be employed, while $A \leq 12$ systems can be treated using quantum Monte-Carlo theory [Pud95, Pie01b], while the no-core shell model, i.e. diagonalization in a full A-body model space [Bog08a], reaches $A = 16$, (or $A = 40$ [Rot07a] with a disputed approximation). Finally, the coupled-cluster method has been employed in doubly-magic nuclei up to $A = 48$ [Hag07, Hag08].

Interacting shell model calculations, which describe correlations explicitly albeit in a reduced model space, implying to "freeze" deeply-bound nucleons [Cau05], are based on microscopically-derived effective Hamiltonians. However, they require slight readjustments of the latter to become accurate [Hon02, Bro06b], and are limited to nuclei up to the fp-shell or lying in the vicinity of closed shells [Cor02].

Beyond lies the realm of effective models. Energy density functional models based on empirical effective interactions allow to treat the majority of nuclides and calculate a variety of observables with a single, reduced parameter set. However, their effective nature means that the meaning of some of the results obtained with them leaves room for interpretation. It is thus useful to put forward some elements of comparison with microscopic many-body theory.

2.1.2 Single-particle Green's function

A recurrent subject of discussion in the following of this work will be single-particle energies. As this section deals with microscopic many-body theory, let us give a short overview of single-particle motion in correlated systems, as understood from Green's functions, and the assumptions underlying EDF theory.

Let us define Fock-space operators $\hat{c}_k^\dagger$ corresponding to a an arbitrary set of single-particle basis states $|k\rangle$ (which can correspond to coordinate-, momentum or configuration-space, but contain all degrees of freedom including spin and isospin – the latter shall not be made explicit or discussed in this part), and their Heisenberg-representation counterpart $\hat{c}_k^\dagger(t)$, with

$$\hat{c}_k^\dagger(t) \equiv e^{i\hat{H}t}\, \hat{c}_k^\dagger\, e^{-i\hat{H}t}, \tag{2.1}$$

These operators allow to define a single-particle Green's function (or propagator) written as a matrix in the above representation

$$G(kt; lt') \equiv i \left\langle \Phi_0(A) \left| \mathcal{T}\left[\hat{c}_k(t)\, \hat{c}_l^\dagger(t')\right] \right| \Phi_0(A) \right\rangle, \tag{2.2}$$

$\mathcal{T}$ being the time-ordering operator, and $|\Phi_0(A)\rangle$ the ground state of the considered A-body system (we shall not go into the details of working with two particle species in this section). An important property is the relation between $G(kt; lt')$ and the density matrix,

$$G(k0; l0^+) = G(k0^-; l0) = -i\rho_{kl}, \tag{2.3}$$
$$G(k0; l0^-) = G(k0^+; l0) = i(\delta_{kl} - \rho_{kl}), \tag{2.4}$$

The time variable introduced above is of little use for stationary problems. In this case, G depends on $t - t'$ only and one can perform the Fourier transform to the energy representation. As of now, we shall measure energies from the Fermi level λ defined as a chemical potential

$$\lambda = \frac{\delta \mathcal{E}_0(A)}{\delta A}. \tag{2.5}$$

The transform reads

$$G(k,l;\omega) = \int dt\, G(kt;lt')\, e^{i(\lambda+\omega)(t-t')}, \tag{2.6}$$

$$G(kt;lt') = \int \frac{d\omega}{2\pi}\, G(k,l;\omega)\, e^{-i(\lambda+\omega)(t-t')}. \tag{2.7}$$

The single-particle Green function describes the propagation, in the considered system, of an additional particle or of the *hole* produced by the removal of a particle. It thus contains information on the excitation spectrum of $A+1$ and $A-1$-particle systems. This can be made explicit thanks to the spectral, or Lehmann representation of G. Defining the particle and hole spectral functions, respectively,

$$\begin{aligned} S^+(k,l;\omega) &= \sum_\nu \langle\Phi_0(A)|\hat{c}_k|\Phi_\nu(A+1)\rangle\, \langle\Phi_\nu(A+1)|\hat{c}_l^\dagger|\Phi_0(A)\rangle \\ &\qquad \times \delta\left(\mathcal{E}_\nu(A+1) - \mathcal{E}_0(A) - \omega - \lambda\right), \end{aligned} \tag{2.8}$$

$$\begin{aligned} S^-(k,l;\omega) &= \sum_\nu \langle\Phi_0(A)|\hat{c}_l^\dagger|\Phi_\nu(A-1)\rangle\, \langle\Phi_\nu(A-1)|\hat{c}_k|\Phi_0(A)\rangle \\ &\qquad \times \delta\left(\mathcal{E}_\nu(A-1) - \mathcal{E}_0(A) - \omega - \lambda\right), \end{aligned} \tag{2.9}$$

where we introduce $\Phi_\nu(A\pm1)$ as the ν^{th} excited state of the system with $A\pm1$ particles, $\mathcal{E}_\nu(A\pm1)$ being the corresponding energy, allows to write the Green function as

$$G(k,l;\omega) = i\int d\omega' \left[-\frac{S^+(k,l:\omega')}{\omega-\omega'-i0^-} - \frac{S^-(k,l:\omega')}{\omega+\omega'-i0^+}\right], \tag{2.10}$$

The ground-state wave function of an A-body system ruled by a single-particle Hamiltonian (let us write it $\hat{H}_0$) is a Slater determinant, i.e. an antisymmetrized product of occupied (hole) states. These hole states belong to the eigenstates of $\hat{H}_0$, which also comprise empty (particle) states. Let us choose, as the representation $|k\rangle$ used above, the eigenstates of $\hat{H}_0$. Adding or removing a particle on such a state yields another eigenstate of $\hat{H}_0$. It is easy to see that the spectral functions then are Dirac functions, and that the Green function reads

$$G(k,l;\omega) = \delta_{kl}\left[-\frac{\delta_{k(p)}}{\omega-\overline{\varepsilon}_k^0-i0^-} - \frac{\delta_{k(h)}}{\omega-\overline{\varepsilon}_k^0-i0^+}\right], \tag{2.11}$$

where $\delta_{k(p)}=1$ if $|k\rangle$ is a particle state, 0 otherwise, the converse being true of $\delta_{k(h)}$, and the single-particle energy ε_k^0 used in the denominator is given by the condition $\hat{H}_0|k\rangle = \varepsilon_k^0|k\rangle$, while $\overline{\varepsilon}_k^0 = \varepsilon_k^0 - \lambda$.

If the Hamiltonian $\hat{H}$ contains an interaction term, its ground state can be expected to contain correlations corresponding to the coherent motion of the interacting particles. In this case, the analytical structure of the Green function is non-trivial, yet it can be expressed in a compact form by introducing the mass operator [Noz63], or proper self-energy [Fet71] $\Sigma(k,\omega)$ (hereafter called simply "self-energy"), for which approximations will be discussed below. For the sake of simplicity, we assume that there exists a representation where the Green function is diagonal for all energies. It is the case in infinite nuclear matter (momentum representation), but the case of finite nuclear systems may be more complicated. This is, anyhow,

beyond the scope of the present discussion. Therefore, let us give the expression of G in this case:

$$G(k,l;\omega) \;=\; \delta_{kl}\left[-\frac{\delta_{k(p)}}{\omega-\overline{\varepsilon}^0_k-\Sigma(k,\omega)-i0^-}-\frac{\delta_{k(h)}}{\omega-\overline{\varepsilon}^0_k-\Sigma(k,\omega)-i0^+}\right]. \quad (2.12)$$

The mass operator is, in general, a complex function. The pole of $G(k,k;\omega)$ thus occurs for $\omega=\omega_k=\overline{\varepsilon}_k-i\Gamma_k$, which is a solution of $\omega_k=\varepsilon^0_k+\Sigma(k,\omega_k)$. In infinite matter, the Green function can be decomposed into a pole part and a background part

$$G(k,l;\omega) \;=\; -\delta_{kl}\frac{z(k)}{\omega-\omega_k}+G_{\rm BG}(k,l;\omega) \quad (2.13)$$

where $z(k)$ is the residue of G at ω_k,

$$z(k) \;=\; \left[1-\left.\frac{\partial\,\Sigma(k,\omega)}{\partial\omega}\right|_{\omega=\omega_k}\right]^{-1}. \quad (2.14)$$

The imaginary part Γ_k is a measure of the correlations present in the system insofar as its non-vanishing value means that no single-particle state $\hat{c}^\dagger_k|\Phi_0\rangle$ is an eigenstate of $\hat{H}$. As for the elementary excitation spectrum, it is given by the real part $\overline{\varepsilon}_k$. Neglecting the imaginary part of $\Sigma(k,\omega)$ (along with setting $z(k)=1$) thus allows to recover the quasiparticle picture.

Single-particle spectrum and effective mass

The single-particle spectrum of a nucleus usually has a non-trivial structure. A essential feature, though, is its density, i.e. the number of levels per unit energy. This is related to the dispersion relation of particles in the medium, which depends on the momentum- and energy-dependence of the self-energy. This is measured by the Landau mass m^*, usually expressed in infinite matter (k then being the momentum of the particle and ε^0_k its kinetic energy), which describes the derivative of the single-particle energy (s.p.e.) with respect to the single-particle (s.p.) momentum.

$$\frac{m^*}{m} \;\equiv\; \left[\,1+\frac{m}{k}\frac{d\,\Re\Sigma(k,\omega_k)}{dk}\,\right]^{-1}, \quad (2.15)$$

where $\Re$ denotes the real part. This quantity integrates the effects of the explicit momentum-dependence of the self-energy, described by the k-mass $\widetilde{m}$,

$$\frac{\widetilde{m}}{m} \;\equiv\; \left[\,1+\frac{m}{k}\left.\frac{\partial\,\Re\Sigma(k,\omega)}{\partial k}\right|_{\omega=\omega_k}\right]^{-1} \quad (2.16)$$

and its energy-dependence, characterized by the e-mass $\overline{m}$,

$$\frac{\overline{m}}{m} \;\equiv\; 1-\left.\frac{\partial\,\Re\Sigma(k,\omega)}{\partial\omega}\right|_{\omega=\omega_k} \;=\; z(k)^{-1} \quad (2.17)$$

where z_k has been introduced above. Both contribute to m^* through

$$\frac{m^*}{m} \;=\; \frac{\overline{m}}{m}\cdot\frac{\widetilde{m}}{m}. \quad (2.18)$$

The s.p. spectrum density is thus a consequence of both the momentum-dependence of the "mean field", or self-energy, and its energy dependence. The latter arises from quantum correlations present in the system, which will not be explicitly included (by definition) in the independent-particle picture necessary to describe heavy nuclei.

2.1.3 Perturbation theory (or lack thereof)

According to the Gell-Mann-Low theorem [GM51], an eigenstate $|\Phi\rangle$ of a Hamiltonian

$$\hat{H} = \hat{H}_0 + \hat{V} \tag{2.19}$$

can be obtained from an eigenstate $|\Phi^0\rangle$ of $\hat{H}_0$ by applying the perturbing operator $\hat{V}$ adiabatically, i.e.

$$|\Phi\rangle = \left. \frac{U^I_\epsilon(0,-\infty)|\Phi^0\rangle}{\langle\Phi^0|U^I_\epsilon(0,-\infty)|\Phi^0\rangle} \right|_{\epsilon\to 0}, \tag{2.20}$$

where $U^I_\epsilon(t,t')$ is the time-evolution operator in the interaction picture for the Hamiltonian $\hat{H}_\epsilon(t) = \hat{H} + \exp(-\epsilon|t|)\,\hat{V}$.

The evolution operator $U^I_\epsilon(t,t')$ can in principle be expanded in powers of the interaction $\hat{V}$, which is the basis of diagrammatic analysis techniques [Noz63, Fet71]. However, this expansion diverges for local NN potentials due to their repulsive core, iterated tensor component and bound state.

The Brueckner-Bethe-Goldstone (BBG) approach can be formulated as a recast of the perturbative expansion in terms of an effective NN vertex [Jeu76, Bal07a]. Indeed, the problematic short-range properties of the interaction can be taken into account by performing the re-summation of diagrams which describe the scattering of a pair of particles in the medium. Compared to the vacuum case, the latter is modified by the Pauli exclusion principle, which blocks the lowest-energy intermediate states, the individual interaction of particles with the medium in the intermediate states, and the three-body force, which is usually treated by averaging over the third particle, yielding a medium-dependent two-body interaction.

An alternative scheme employed in self-consistent Green function approaches to nuclear matter is the Feynman-Galitskii T-matrix approximation [Mut05], which differs from the BBG scheme by the re-summation of hole-hole scattering processes, as shown on Fig. 2.1.

Both schemes, because of the intermediate particle/hole propagation lines, yield results depending on the starting energy. This means, in particular, that an energy-dependence is present, e.g. in the self-energy $\Sigma(k,\omega)$ whenever such an effective vertex is used.

Once the re-summation underlying the scheme chosen has been performed, diagrammatic analysis can be performed with the effective interaction used as an elementary NN vertex, attention being paid to double-counting of diagrams generated by the BBG or Feynman-Galitskii expansion. Fig. 2.2 displays several possible diagrams entering the self-energy. The first line contains the first diagrams of the hole-line expansion practiced in BBG theory. The first term of each series is akin to the Hartree-Fock self-energy (hence the name Brueckner-Hartree-Fock approximation, or BHF), but it must be kept in mind that the G-matrix is energy-dependent.

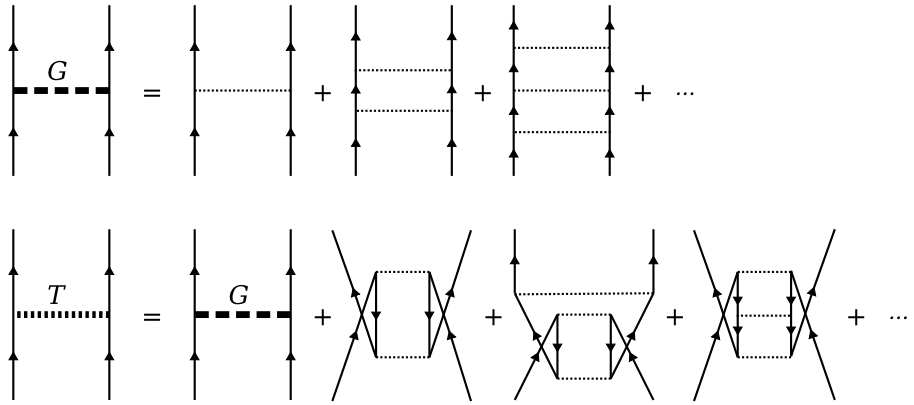

Figure 2.1: Schematic presentation of diagrams re-summed in a Brueckner G-matrix and Feynman-Galitskii T-matrix effective interactions. Whereas the G-matrix only sums particle-particle "ladders", the T-matrix treats particle-particle and hole-hole scattering on an equal footing, yielding additional diagrams.

The two-hole-line diagram for the particle self-energy is commonly referred to as a rearrangement term, since it can be obtained by cutting an intermediate propagation line in the BHF total energy diagram.

The second line of Fig. 2.2 gives diagrams describing the coupling of particles with collective vibrations described by the polarization propagator (or response function) Π, here defined in the ring, or random-phase approximation (RPA), which shall be discussed in chapter 3. This whole contribution is usually not taken into account in infinite matter studies, where the three-hole-line approximation yields well-converged results [Son98] but has been shown to modify the single-particle spectrum significantly in finite nuclei, where surface vibrations play a particular role [Ber80, Lit06].

2.2 Energy Density Functional formalism

The Energy Density Functional (EDF) method is frequently cited as the most general theoretical tool in low-energy nuclear physics. Indeed, it is a microscopic tool, in the sense that it fully takes into account the quantal shell structure of the nucleus, as well as collective effects when extended to its multi-reference variant. At the same time, it is tractable for nuclei going from medium masses to the heaviest ones, as well as nuclei in the crust of neutron stars, the same values of the reduced parameter set associated with the functional being useable for all these systems.

Let us first describe the mean-field approximation which serves as a formal basis, then the EDF method itself.

2.2.1 Mean-field theory and pairing

It has been known, since the work of Bohr, Mottelson and Pines [Boh58], that nuclei have common features with superconductors, and that the clear signatures for pairing between nucleons of the same species abound, from the odd-even staggering

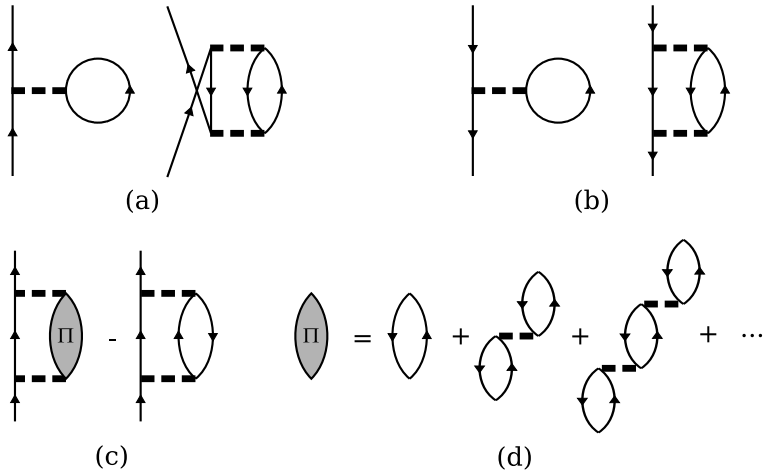

Figure 2.2: Schematic presentation of diagrams entering the self-energy $\Sigma(k,\omega)$. (a) One-hole-line (BHF) and two-hole-line contributions for particle states, (b) same for hole states. (c) Particle-vibration coupling contribution. The polarization propagator Π is defined in (d); for particle states, the second-order term has to be substracted, being already included in the BHF self-energy.

of binding energies to rotational properties.

In this section we shall describe the Hartree-Fock-Bogolyubov formalism, which allows to describe pairing in a mean-field approach and is the starting point of the EDF method. We direct the reader to classic textbooks [Rin00, Fet71] for a discussion of the Hartree-Fock (HF) method it extends and the various derivations and interpretations of the latter. A more thorough discussion of pairing, superfluidity, associated nuclear observables as well as the relevant microscopic theory is contained in chapter 5.

Bogolyubov transformation

Our basic tool to describe the pair condensation phenomenon, while remaining in a framework as easily tractable as the independent-particle (HF) approximation, is the generalized quasiparticle (q.p.) concept. Following the introduction of the Bardeen-Cooper-Schrieffer (BCS) formalism [Bar57a, Bar57b], Bogolyubov and Valatin proposed a canonical transformation which allows to treat elementary excitations of a superfluid state as individual degrees of freedom [Bog58, Val58]. The fully paired ground state of the system is thus a *vacuum* with respect to the operators

$$\hat{\beta}_k^\dagger = \sum_l U_l^k \, \hat{c}_l^\dagger + V_l^k \, \hat{c}_l \tag{2.21}$$

$$\hat{\beta}_k = \sum_l U_l^{k*} \, \hat{c}_l + V_l^{k*} \, \hat{c}_l^\dagger \tag{2.22}$$

where $\hat{c}_l$ and $\hat{c}_l^\dagger$ are the annihilation and creation operators corresponding to an arbitrary representation, as already mentioned in the last section.

The vectors U_l^k and V_l^k fully parametrize the quasiparticle states as well as the vacuum $|\Phi_0\rangle$ defined by the requirement that $\forall k \; \hat{\beta}_k|\Phi_0\rangle = 0$. In the case of vanishing

pairing correlations, we have $U^k = 0$ for hole states and $V^k = 0$ for particle states. Otherwise, pairing correlations are introduced by mixing particles and holes. In the case of a continuous spectrum, this results in the vanishing of the discontinuity of occupation probabilities at the Fermi level.

It is useful to examine the structure of the Bogolyubov transformation. Let us write it under matrix form, arranging the operators $\hat{\beta}_k$ and $\hat{c}_k$ into vectors, then "super-vectors" containing both creation and annihilation operators:

$$\begin{pmatrix} \hat{\beta} \\ \hat{\beta}^\dagger \end{pmatrix} = \mathcal{W}^\dagger \begin{pmatrix} \hat{c} \\ \hat{c}^\dagger \end{pmatrix}. \tag{2.23}$$

The transformation matrix $\mathcal{W}$ can be decomposed, according to the Bloch-Messiah-Zumino theorem [Blo62], as

$$\mathcal{W} = \begin{pmatrix} D & 0 \\ 0 & D^* \end{pmatrix} \begin{pmatrix} \overline{U} & \overline{V} \\ \overline{V} & \overline{U} \end{pmatrix} \begin{pmatrix} C & 0 \\ 0 & C^* \end{pmatrix}. \tag{2.24}$$

This expression involves two transformations of creation and annihilation operators among themselves. The first one, D, transforms the initial basis into the set of *canonical* states among which the Bogolyubov transformation takes a simple form. The matrices $\overline{U}$ and $\overline{V}$, have, themselves, the structure

$$\overline{U} = \begin{pmatrix} u & 0 \\ 0 & u \end{pmatrix}, \qquad \overline{V} = \begin{pmatrix} 0 & v \\ -v & 0 \end{pmatrix} \tag{2.25}$$

where we split the canonical basis in two halves. Hereafter the states belonging to the two halves will be distinguished by the notation $\check{k}$ for the first and $\hat{k}$ for the second one, when necessary. The notation $\overline{k}$ will refer to the state associated with $|k\rangle$ in the Cooper pair. The second block of the $\mathcal{W}$-transform performs the mixing of particles and holes to generate a set of quasiparticles defining the vacuum $|\Phi_0\rangle$. The sub-matrices u and v are diagonal, we call $u_{\check{k}}$ and $v_{\check{k}}$ their eigenvalues, with $\overline{U}_{\check{k}\check{k}} = u_{\check{k}} = \overline{U}_{\overline{k}\overline{k}} = u_{\overline{k}}$ and $\overline{V}_{\check{k}\overline{k}} = v_{\check{k}} = -\overline{V}_{\overline{k}\check{k}} = -v_{\overline{k}}$.

Finally, the C transformation produces a different set of quasiparticles. This last transformation can be used to diagonalize a single-quasiparticle Hamiltonian, as will be discussed in the following.

In the representation $\hat{c}_k$, the density matrix of the system, as well as the particle number, read

$$\begin{aligned} \rho_{kl} &= \langle\Phi_0|\hat{c}_l^\dagger \hat{c}_k|\Phi_0\rangle = \sum_m V_k^{m*} V_l^m, \\ N &= \mathrm{Tr}(\hat{\rho}) = \sum_{km} V_k^{m*} V_k^m. \end{aligned} \tag{2.26}$$

We see that each quasiparticle gives a (generally fractional) contribution to the particle number given by the norm of the corresponding V^k vector. This allows to distinguish between hole-like ($|V^k|^2 > 1/2$) and particle-like ($|V^k|^2 < 1/2$) quasiparticles.

The addition of pairing in the quasiparticle picture involves the definition of the pair tensor, or anomalous density matrix

$$\kappa_{kl} = \langle\Phi_0|\hat{c}_l \hat{c}_k|\Phi_0\rangle = \sum_m V_k^{m*} U_l^m, \tag{2.27}$$

which is nonzero only for states mixing different particle numbers, which is caused by mixing particles and holes in the Bogolyubov transformation.

One can easily infer from the definition of $\hat{\rho}$ and $\hat{\kappa}$ that $\hat{\rho}^\dagger = \hat{\rho}$, and $\hat{\kappa}^\dagger = -\hat{\kappa}^*$ hence $\hat{\kappa}^T = -\hat{\kappa}$, where $\hat{\kappa}^T$ denotes matrix transposition. Additionally, the conservation of fermionic anticommutation rules for the quasiparticles $\hat{\beta}_k, \hat{\beta}_k^\dagger$ imply relations between U and V vectors

$$\begin{aligned} \sum_k (U_k^{m*} U_k^n + V_k^{m*} V_k^n) &= \delta_{mn}, & \sum_m (U_k^m U_l^{m*} + V_k^{m*} V_l^m) &= \delta_{kl}, \\ \sum_k (U_k^m V_k^n + V_k^m U_k^n) &= 0, & \sum_m (U_k^m V_l^{m*} + V_k^{m*} U_l^m) &= 0, \end{aligned} \tag{2.28}$$

which translate into the following relationship between $\hat{\rho}$ and $\hat{\kappa}$

$$\hat{\rho}\,\hat{\rho} - \hat{\kappa}\,\hat{\kappa}^* = \hat{\rho}. \tag{2.29}$$

This expression generalizes the condition that the density matrix of a Slater determinant (vanishing pairing limit of the above) is idempotent, i.e. $\hat{\rho}\hat{\rho} = \hat{\rho}$.

Let us now consider the properties of the canonical basis. From the structure of $\overline{U}$ and $\overline{V}$ matrices, we can see that

$$\rho_{kl} = v_k^2 \delta_{lk}, \qquad \kappa_{kl} = u_k v_k \delta_{l\overline{k}}. \tag{2.30}$$

These expressions allow for an efficient construction of local and quasi-local densities, as well as a simple expression for the particle number (expressed here for a single species, sums and the trace being understood accordingly),

$$N = \langle \Phi_0 | \sum_k \hat{c}_k^\dagger \hat{c}_k | \Phi_0 \rangle = \mathrm{Tr}(\hat{\rho}) = \sum_k v_k^2. \tag{2.31}$$

They imply, moreover, that in the canonical basis the Bogolyubov q.p. vacuum takes the BCS form. Additional properties of this case are discussed in chapter 5.

Time-reversal symmetry

The Bogolyubov transformation involves a pairwise coupling of single-particle states. For each quasi-particle $\hat{\beta}_k$, the states $|l\rangle$ and $|\bar{l}\rangle$ are taken in two different halves of the basis. The distinction is made according to symmetries of the interaction which produces pair condensation and quantum numbers of the Cooper pair. Pairing between particles of the same species, being the most important and readily observable form occurring in nuclei, involves pairs having total spin and angular momentum zero. Accordingly, paired states are related by time-reversal symmetry [And59]. The corresponding operator is antiunitary [Mes58]. Its action on a single-particle wave function expressed in coordinate ($\mathbf{r}$), spin ($\sigma = \pm 1/2$) and isospin ($q = \pm 1/2$) space yields

$$(\hat{\mathcal{T}}\varphi)(\mathbf{r}\sigma q) = (-1)^{1/2-\sigma} \varphi^*(\mathbf{r}\overline{\sigma} q), \tag{2.32}$$

with $\overline{\sigma} \equiv -\sigma$. Moreover the property $\hat{\mathcal{T}}^2 = -1$ holds in the space of states with odd particle number, while $\hat{\mathcal{T}}^2 = 1$ when applied on states with even particle-number parity. For a time-reversal-invariant state, i.e. if $\hat{\mathcal{T}}|\Phi_0\rangle = |\Phi_0\rangle$, the time-reversed

state of each canonical (basis) state can be found in the same basis, which gives a formal definition to the correspondence $k \rightarrow \overline{k}$. It is easy to show that

$$\hat{\mathcal{T}}|k\rangle \;=\; \eta_k|\overline{k}\rangle, \quad \hat{\mathcal{T}}|\overline{k}\rangle \;=\; -\eta_k^*|k\rangle, \tag{2.33}$$

with $|\eta_k| = 1$. We can then choose the states $|k\rangle$ and $|\overline{k}\rangle$ so that $\eta_k = 1$ and, by convention, store the state $|k\rangle$ in the first half of the basis, i.e. $|k\rangle = |\check{k}\rangle$. This fully specifies the two halves through $\eta_{\check{k}} = 1$ and $\eta_{\hat{k}} = -1$.

It may then be interesting to define an *anomalous density matrix* $\tilde{\rho}$ [Dob84],

$$\tilde{\rho}_{kl} \;=\; \eta_l \kappa_{k\bar{l}}, \tag{2.34}$$

which is Hermitian for time-reversal-invariant systems. In particular, this anomalous density can be expressed in coordinate space, where it has a nonvanishing local (diagonal) component. The corresponding local anomalous density occurs naturally in local pairing density functionals for spin-singlet pairing.

Time-reversal symmetry requires the pairwise symmetry between quasiparticles, i.e. $U^k = U^{\overline{k}}$, $V^k = -V^{\overline{k}}$. The resulting vacuum is a sum of Slater determinants having different, but all even, particle numbers. It also implies that time-reversal partner states have the same occupancy. Such a many-body state can thus only describe nuclei with even particle numbers. Odd-mass and odd-odd nuclei require to break this symmetry by creating one or two (unrelated) quasiparticles on top of the *fully paired* vacuum. Such an operation amounts to replacing the corresponding $\hat{\beta}_k$ operator in the set defining $|\Phi_0\rangle$ (through $\hat{\beta}_k|\Phi_0\rangle = 0$) by $\hat{\beta}_k^\dagger$, defining a new vacuum. The latter is said *blocked* since the contributions of the $(\hat{\beta}_k, \hat{\beta}_{\overline{k}})$ q.p. pair to the pair tensor then vanish.

From the definition of $\hat{\beta}_k$ and $\hat{\beta}_k^\dagger$, Eq. (2.22), we see that this operation amounts to exchanging

$$U^k \leftrightarrow V^{k*}, \qquad V^k \leftrightarrow U^{k*}. \tag{2.35}$$

The variations of $\hat{\rho}$ and $\hat{\kappa}$ corresponding to a one-q.p. addition can be deduced from their definitions. In particular, the variation of the particle number is given by

$$\delta N \;=\; \sum_l \left(U_l^k \, U_l^{k*} - V_l^{k*} \, V_l^k \right), \tag{2.36}$$

which is not, in general, an integer number: in order to obtain this way a reasonable wavefunction or density matrix for the intended odd nucleus, a readjustment has to be made to the particle number of the underlying fully-paired vacuum.

Hartree-Fock-Bogolyubov equations

The Hartree-Fock-Bogolyubov method [Rin00] uses the Bogolyubov quasiparticle vacuum as a variational ansatz for the wavefunction of a superfluid system. Considering a system ruled by a Hamiltonian containing a kinetic term and two-body interaction,

$$\hat{H} \;=\; \hat{T} + \hat{V} \;=\; \sum_{kl} t_{kl} \hat{c}_k^\dagger \hat{c}_l + \frac{1}{4} \sum_{klmn} \overline{v}_{klmn} \hat{c}_k^\dagger \hat{c}_l^\dagger \hat{c}_n \hat{c}_m, \tag{2.37}$$

where $\overline{v}_{klmn}$ is the antisymmetrized interaction matrix element

$$\overline{v}_{klmn} = \langle kl|\hat{V}|mn\rangle - \langle kl|\hat{V}|nm\rangle. \tag{2.38}$$

The energy of a configuration $|\Phi\rangle$ reads

$$\mathcal{E}[\Phi] = \langle\Phi|\hat{H}|\Phi\rangle = \sum_{kl} t_{kl}\rho_{lk} + \frac{1}{2}\sum_{klmn}\overline{v}_{klmn}\left(\rho_{mk}\rho_{nl} + \frac{1}{2}\kappa^*_{kl}\kappa_{mn}\right), \tag{2.39}$$

where we take advantage of the antisymmetry of $\overline{v}$. The fact that the q.p. vacuum includes two-body correlations is exhibited by the additional $\kappa^*\kappa$ term extending the factorization of the two-body density matrix $\langle\hat{c}^\dagger_k\hat{c}^\dagger_l\hat{c}_n\hat{c}_m\rangle$ pertaining to a normal Slater determinant.

The HFB approximation for the ground state wave function can be obtained by applying the Ritz variational principle. As already mentioned, however, the Bogolyubov transformation yields a state which mixes wave functions having different particle numbers. It is possible, however, to conserve the average particle number by applying a constraint by introducing Lagrange parameters relative to neutron and proton numbers. The variational procedure can then be applied to the expectation value of the modified Hamiltonian,

$$\hat{\overline{H}} = \hat{H} - \hat{\Lambda} = \hat{H} - \lambda_{\rm n}\hat{N} - \lambda_{\rm p}\hat{Z}, \tag{2.40}$$

$$\tag{2.41}$$

where $\hat{N}$ and $\hat{Z}$ are the neutron and proton number operators, respectively. The expectation value of $\hat{\overline{H}}$ corresponds to the shifted energy

$$\overline{\mathcal{E}}[\Phi] = \langle\Phi|\hat{\overline{H}}|\Phi\rangle = \mathcal{E} - \lambda_{\rm n}N - \lambda_{\rm p}Z, \tag{2.42}$$

This formulation applies, naturally, when no mixing of the two species is considered. The quantities $\lambda_{\rm n}$ and $\lambda_{\rm p}$ can be formally defined as

$$\lambda_{\rm n} = \frac{\delta\mathcal{E}}{\delta N}, \qquad \lambda_{\rm p} = \frac{\delta\mathcal{E}}{\delta Z}, \tag{2.43}$$

which exhibit their role as chemical potentials, and the fact that the HFB/BCS formalism is initially intended to describe systems large enough to be amenable to a statistical treatment or coupled to an external reservoir of particles.

Minimizing the shifted energy Eq. (2.42) with respect to quasiparticle degrees of freedom yields the equations

$$\begin{pmatrix} h-\lambda & \Delta \\ -\Delta^* & -h^*+\lambda \end{pmatrix}\begin{pmatrix} U^k \\ V^k \end{pmatrix} = E_k \begin{pmatrix} U^k \\ V^k \end{pmatrix} \tag{2.44}$$

which involves the particle-hole mean field h and the particle-particle or pairing field Δ, expressed as matrices between single-particle basis states,

$$h_{km} = t_{km} + \sum_{ln}\overline{v}_{klmn}\rho_{nl}, \qquad \Delta_{kl} = -\frac{1}{2}\sum_{mn}\overline{v}_{klmn}\kappa_{mn}. \tag{2.45}$$

In the above expression, λ is a diagonal matrix in isospin space, having diagonal matrix elements $\lambda_{\rm n}$ between neutron states and $\lambda_{\rm p}$ between proton states. The

solution of the above equations can be obtained by iterating until self-consistency is reached.

The ket $|\Phi_0\rangle$ being the state which yields minimal energy $\overline{\mathcal{E}} = \overline{\mathcal{E}}_0$, the modified Hamiltonian can be rewritten, by expressing particle operators through quasiparticle ones and normal-ordering, as [Rin00]

$$\hat{\overline{H}} \;=\; \overline{\mathcal{E}}_0 + \sum_k E_k \; \hat{\beta}_k^\dagger \hat{\beta}_k + \hat{H}_{\rm int}, \tag{2.46}$$

where $\hat{H}_{\rm int}$ is the residual interaction between quasiparticles, which is neglected at the present mean-field level. It is a sum of products of four $\hat{\beta}$ or $\hat{\beta}^\dagger$ operators, each of these products being normal-ordered with respect to the Bogolyubov q.p. vacuum $|\Phi_0\rangle$. As a result, it is easy to check that its expectation values in $|\Phi_0\rangle$ and the elementary excited states $\hat{\beta}_k^\dagger|\Phi_0\rangle$ vanishes. The shifted energy of a one-q.p. state is thus

$$\overline{\mathcal{E}}_k \;=\; \langle\Phi_0|\hat{\beta}_k \hat{\overline{H}} \hat{\beta}_k^\dagger|\Phi_0\rangle \;=\; \overline{\mathcal{E}}_0 + E_k. \tag{2.47}$$

The non-shifted energy can be recovered by adding back the contribution of the constraining term, which yields

$$\mathcal{E}_k \;=\; \langle\Phi_0|\hat{\beta}_k \hat{H} \hat{\beta}_k^\dagger|\Phi_0\rangle \;=\; \mathcal{E}_0 + E_k + \lambda_q \sum_l \left(U_l^k \; U_l^{k*} - V_l^{k*} \; V_l^k\right), \tag{2.48}$$

λ_q being the chemical potential of the species relevant to quasiparticle k, with $q =$ n or p.

As mentioned in section 2.2.1, the one-q.p. state does not have an integer, odd particle number as is practically required. To obtain the latter, the chemical potential has to be adjusted accordingly. As a first-order approximation, though, one can consider that the resulting energy is $\mathcal{E}_k \simeq \mathcal{E}_0 + E_k \pm \lambda_q$, depending whether the q.p. k is hole-like $(-)$ or particle-like $(+)$.

2.2.2 Density functional theory

The electron gas present in solids and molecules is another example of a correlated fermion system. It was demonstrated by Hohenberg and Kohn that the wave function of this system, hence all its properties, could be expressed as a functional of the local electron density [Hoh64]. In particular, the energy of the correlated electron gas can be expressed as a functional of the density, this functional being universal, i.e. valid for all electron numbers and external (ionic) potentials the electrons could be placed in. The density and energy of the ground state can thus be obtained by minimizing the energy functional with respect to the density (taken in the manifold of densities generated from a sensible many-body state).

This result, known as the Hohenberg-Kohn variational principle, was first intended at semiclassical implementations. However, the most successful embodiment of this principle was proposed by Kohn and Sham [Koh65], who suggested generating the density from an auxiliary Slater determinant. The method was later extended to involve the non-local density matrix [Gil75] as well as spin and current densities. It was also shown that superconductivity could be taken into account by including a dependence on the anomalous density in the functional [Oli88, Kur99]. The most

general formulation of density functional theory (DFT) was proposed by Valiev and Fernando [Val97], who showed that one could build a functional of any family of observables corresponding to Hermitian operators.

We restrict this short discussion to one-body operators, making the distinction between particle-hole and particle-particle ones. Following the extended Hohenberg-Kohn procedure, the energy functional of a superfluid system can thus be formally defined as

$$\mathcal{E}[\hat{\rho},\hat{\kappa},\hat{\kappa}^*] \;=\; \mathcal{F}[Q,P,P^*] \;=\; \min_{\Phi\to Q,P}\langle\Phi|\hat{H}_{\rm int}+\hat{V}_{\rm ext}|\Phi\rangle \tag{2.49}$$

where we make the distinction between the intrinsic Hamiltonian $\hat{H}_{\rm int}$ and an external potential $\hat{V}_{\rm ext}$, and $\Phi\to Q,P$ means that the search is performed over trial wave functions Φ which yield the specified input normal and anomalous densities, defined through the operators

$$\hat{Q}(x) \;=\; \sum_{kl} q(x)_{kl}\;\hat{c}_k^\dagger\hat{c}_l, \tag{2.50}$$

$$\hat{P}(x) \;=\; \frac{1}{2}\sum_{kl}\left(p(x)_{kl}\;\hat{c}_k^\dagger\hat{c}_l^\dagger + p(x)^*_{kl}\;\hat{c}_l\hat{c}_k\right), \tag{2.51}$$

$q(x)$ and $p(x)$ being Hermitian and skew-symmetric matrices, respectively, while x is a set of coordinates and indices necessary to specify each density. We then have

$$Q(x) \;=\; {\rm Tr}\left(\hat{Q}(x)\hat{\rho}\right) \;=\; \sum_{kl} q(x)_{kl}\rho_{lk}, \tag{2.52}$$

$$P(x) \;=\; {\rm Tr}\left(\hat{P}(x)\hat{\kappa}\right) \;=\; \sum_{kl} p(x)_{kl}\kappa_{lk}. \tag{2.53}$$

The functional of Eq. (2.49) is *universal* in the sense that it is valid for all particle numbers and external potentials of the form $\hat{V}_{\rm ext} = v\cdot\hat{Q} + w\cdot\hat{P}$, v and w being functions of x and $\cdot$ the scalar product defined by $v\cdot\hat{Q} = \int dx\; v(x)\hat{Q}(x)$.

In the original formulation of DFT, $Q(x)$ is the local particle density. It is tempting to generalize this in order to extract more information from the auxiliary state and potentially improve the predictive power of the functional more efficiently that with a re-summation of all missing effects in the local functional. In addition, a broader range of observables can be contrained this way. However, it should be stressed that in principle, no Kohn-Sham approach can depend on the full density matrix, as it is guaranteed that the latter, being a projector, can *not* be matched with the exact density matrix of a correlated state (the case being less clear for the generalized density matrix which appears with pairing).

Given the exact functional of Eq. (2.49), the ground state energy and densities can be obtained as

$$\mathcal{E}_0 \;=\; \min_{\rho,\kappa,\kappa^*}\mathcal{E}[\rho,\kappa,\kappa^*] \tag{2.54}$$

$$\;=\; \min_{Q,P,P^*}\mathcal{F}[Q,P,P^*]. \tag{2.55}$$

Several remarks are in order concerning the transposition of such a formalism to nuclear structure as is currently envisioned. The first concern to be raised is

related to symmetries of the underlying Hamiltonian. Indeed, any relevant $\hat{H}$ must commute with operator such as total A-body linear and angular momentum, and particle numbers. A nucleus being a self-bound system, contrary to the electron gas in a solid, it has to be considered isolated, without any external potential acting on it. Its wave function then factorizes into a center-of-mass part and an intrinsic part, and the density corresponding to the ground state in the laboratory frame is, trivially, a constant [Kre01].

The intrinsic density, on the other hand, is an A-body operator. However, as shown by Engel for a model system, [Eng07] a useful approximate Kohn-Sham functional of the intrinsic density can be built. Formally adding an external potential term acting only on the center of mass, in order to obtain a localized state amenable to a DFT description has also been proposed [Gir07, Gir08a]. The case of rotation is more complicated, due to the coupling between collective and intrinsic motion as well as the difficulty to properly define angular coordinates, to the point that it was suggested to work only with spherically-symmetric states and densities [Gir08b]. Also, the pair tensor is non-zero only for states mixing different particle numbers. The "exact" pair density should thus be defined from transition matrix elements between A and $A \pm 2$ states, or before projecting onto good particle numbers in an accurate perturbative scheme.

Moreover, since DFT makes no direct reference to the system's wave function whatsoever (the Kohn-Sham Slater determinant should *not* be taken as such), explicit restoration of broken symmetries fails to find a place in its framework. More generally, practical applications of Eq. (2.49) require to build a functional of the relevant densities Q and P able to include all correlations. This implies missing the explicit description of collective effects such as shape coexistence, which is known to be essential for understanding the structure and spectroscopy of many nuclei, such as ^{72,74}Kr [Kor04, Ben06b], ^{100}Zr [Woh86, Mac89a, Ska93] or neutron-deficient lead isotopes [Dug03, Ben04].

No extension of DFT, in the form of a Hohenberg-Kohn existence theorem, able to provide a firm formal ground to calculations "beyond the mean field" has been proposed yet. The definition of the EDF method proceeds by analogy with the self-consistent mean field method, performed with a density-dependent interaction, and its extensions such as the generator coordinate method (GCM) and the random-phase approximation (RPA).

2.2.3 Single- and multi-reference EDF methods

The single-reference (SR) EDF method uses a Bogolyubov quasiparticle vacuum as a reference state to generate the density matrix ρ and pair tensor κ entering the expression for the energy functional, the densities Q and P being in principle matched with their values in the nucleus's rest frame. The approach consisting in writing down the functional and fixing its parameters directly has been attempted on several occasions [Neg72, Fay98, Fay00, Per04, Bal07b, Kor08]. Herafter we shall adopt the more conventional scheme where the functional is expressed as the result of normal and anomalous contractions of distinct effective, density-dependent vertices for the particle-hole (p-h) and particle-particle (p-p) channels, which correspond, respectively, to couplings of Q-densities only, and couplings involving P-densities.

The following general expression for the energy functional results,

$$\mathcal{E}[\hat{\rho},\hat{\kappa},\hat{\kappa}^*] = \sum_{kl} t_{kl}\rho_{lk} + \frac{1}{2}\sum_{klmn}\overline{v}^{\rho\rho}_{klmn}[\hat{\rho}]\rho_{mk}\rho_{nl} + \frac{1}{4}\sum_{klmn}\overline{v}^{\kappa\kappa}_{klmn}[\hat{\rho}]\kappa^*_{kl}\kappa_{mn} \quad (2.56)$$

where t_{kl} is the kinetic Hamiltonian (with an effective correction for spurious center-of-mass motion, see Ref. [Ben03b]), and $\overline{v}^{\rho\rho}[\hat{\rho}]$ and $\overline{v}^{\kappa\kappa}[\hat{\rho}]$ are effective, medium-dependent particle-hole and particle-particle interactions, respectively (regularization subtleties may actually arise in the definition of the particle-particle functional, section 2.4).

Initially, both are devised to match as close as possible the physical content of an effective interaction based on the re-summation of (classes of) diagrams in perturbation theory. The trial state could then be understood as an unperturbed state used as a starting point for the perturbative expansion. This is less clear in the case of a DFT-oriented interpretation, however, and the rather simple effective interactions used up to now lack prominent characteristics of microscopic ones such as energy dependence, or finite range *and* non-locality, which makes a direct link between one and the other rather difficult. As a side note, notice that perturbation theory provides the energy of a system as a functional of the Green function (restricted to the single-particle G for two-body interactions) [Noz63] of which DFT could be formally seen as a special case.

If $\overline{v}^{\rho\rho} = \overline{v}^{\kappa\kappa}$ and the corresponding interaction matrix elements are antisymmetric with respect to interchanging the two particles or holes, the above energy reduces to the standard HFB expression. Nonetheless, perturbative approaches to superfluidity indicate that the effective vertices in the two channels should be different (see chapter 5). Moreover, the antisymmetry of the particle-hole interaction is often broken, either for practical or physical reasons, as this may enable to adjust useful degrees of freedom in the parametrization of the functional. Typical examples are the independent adjustment of isoscalar and isovector spin-orbit terms [Rei95, Rei99], or the use of Landau parameters to fix independently the spin-isospin terms of the functional [Ben02, Zdu05].

Minimizing Eq. (2.56) yields HFB-like equations, Eq. (2.44), with the potentials h and Δ redefined as

$$h_{kl} = \frac{\delta\mathcal{E}}{\delta\rho_{lk}}, \qquad \Delta_{kl} = \frac{\delta\mathcal{E}}{\delta\kappa^*_{lk}}. \quad (2.57)$$

Again, these expressions reduce to the HFB potentials, Eq. (2.45), when the energy of Eq. (2.56) corresponds to the HFB energy. In general, additional rearrangement terms arise in Eq. (2.57) from the functional derivation of the interactions themselves with respect to the density. This will be of some importance in the discussion of single-particle energies below.

Multi-reference (MR) EDF calculations extend SR ones by allowing to mix different reference states (usually obtained from separate SR-EDF calculations). Again, this requires to attribute a certain meaning to the wave functions obtained from the SR-EDF calculations. Just as the wave function used in SR-EDF is the same as in the HFB method, The MR-EDF ansatz is inspired by the generator coordinate method (GCM) [Rin00],

$$|\Phi_0\rangle = \int da f(a)|\Phi^a_0\rangle \quad (2.58)$$

where $|\Phi_0^a\rangle$ is a Bogolyubov quasiparticle vacuum obtained by a constrained calculation (for configuration mixing) or by a group transformation (for symmetry restoration), a being a (set of) collective coordinate(s) and/or order parameters pertaining to the breaking of given symmetries. The mixing is implemented by the weight function $f(a)$, which is given by a group transformation in the case of symmetry restoration, otherwise it is a solution of the Hill-Wheeler equation [Hil53, Rin00]

$$\int db \ \left[\mathcal{H}(a,b) - \mathcal{E}_\nu^{\rm MR}\, \mathcal{I}(a,b)\right] f_\nu(b) \ = \ 0, \tag{2.59}$$

where $\mathcal{E}_\nu^{\rm MR}$ is the energy of the mixed state described by f_ν, $\mathcal{I}$ is the overlap kernel

$$\mathcal{I}(a,b) \ \equiv \ \langle\Phi_0^a|\Phi_0^b\rangle, \tag{2.60}$$

and $\mathcal{H}$ the "Hamiltonian" kernel, which, once more, reduces in the Hamiltonian (HFB/GCM) case to the non-diagonal matrix element

$$\mathcal{H}(a,b) \ \equiv \ \langle\Phi_0^a|\hat{H}|\Phi_0^b\rangle. \tag{2.61}$$

When working with a generalized energy functional, $\mathcal{H}$ is redefined as

$$\mathcal{H}(a,b) \ = \ \mathcal{E}[\hat{\rho}^{ab}, \hat{\kappa}^{ab}, \hat{\overline{\kappa}}^{ab}], \tag{2.62}$$

where the densities obtained in the q.p. vacuum have been replaced by the following transition densities,

$$\rho_{kl}^{ab} \ \equiv \ \frac{\langle\Phi_0^a|\hat{c}_l^\dagger\hat{c}_k|\Phi_0^b\rangle}{\langle\Phi_0^a|\Phi_0^b\rangle}, \qquad \kappa_{kl}^{ab} \ \equiv \ \frac{\langle\Phi_0^a|\hat{c}_l\hat{c}_k|\Phi_0^b\rangle}{\langle\Phi_0^a|\Phi_0^b\rangle}, \qquad \overline{\kappa}_{kl}^{ab} \ \equiv \ \frac{\langle\Phi_0^a|\hat{c}_k^\dagger\hat{c}_l^\dagger|\Phi_0^b\rangle}{\langle\Phi_0^a|\Phi_0^b\rangle}. \tag{2.63}$$

One last time, this choice is consistent with the special HFB/GCM case. In the most complete and involved applications to nuclear structure, a is a set of coordinates corresponding to the gauge angles relative to particle-number symmetry, Euler angles and deformation coordinates, the weight function f_a being partly determined by symmetries and partly by the Hill-Wheeler equation. Symmetry restoration and configuration mixing are thus performed simultaneously [Mey95], yielding a multi-dimensional problem [Ben08]. The full variational problem would require simultaneous optimization of f_a and of the states $|\Phi_0^a\rangle$. In practice, $|\Phi_0^a\rangle$ is optimized with respect to the MR energy functional only when f_a is known a priori, which leads to the variation-after-projection (VAP) approach used in the case of particle-number restoration [She00, Sto07].

A major difficulty arises, though, in the above definitions: the transition densities diverge for orthogonal states. While this is not a concern in the Hamiltonian case [Ang01b], since the corresponding contributions to the energy cancel out, the general EDF kernel $\mathcal{H}$ will indeed diverge. A well-understood case where this can happen is particle-number projection of a wave function where a single-particle level crosses the chemical potential [Dob07]. The terms responsible for this divergence have been recently identified as those contributing to self-interaction and self-pairing, and a correction scheme derived [Lac08]. This correction remains limited, however, to low-order polynomial density dependences in the effective interactions.

The straight generalization of the Hamiltonian "mean field and beyond" picture to a density-functional-inspired one is thus rather tricky. In this work, we shall not perform MR-EDF calculations, yet our results will be analyzed, whenever possible, with the underlying physics in mind.

EDF and single-particle energies

In Kohn-Sham DFT, single-particle (or quasiparticle) energies obtained from the auxiliary potentials $(\hat{h}, \hat{\Delta})$ have *a priori* no particular meaning. However, the prospect of obtaining single-particle spectra from such calculations is of great interest. This has been studied in semiconductors, where, for example, it would allow to extract band gaps [Sha85]. A proper determination of s.p. energies as defined from Green functions, however, involves solving a modified Dyson equation [Sha85, Bha05], i.e. going back to perturbation theory.

On the other hand, provided one can build a functional which is valid not only for the ground state, but also for a sufficient number of excited ones, elementary excitations become a starting point for the general discussion of the excitation spectrum [Gor96]. A first step in this direction is the control of the effective mass, hence the density of s.p. states, through non-local terms [Bha05]. Excited state energies can then be calculated by applying a constraint or adding quasiparticle excitations, which is a rigorous approach when the calculations are performed self-consistently. Physical single-particle energies are thus mass differences between the ground state of the A-nucleon system, and ground or excited states in $A \pm 1$-nucleon ones.

In the very end, nothing prevents us from trying to adjust parameters of the functional to match s.p. energies in addition to other observables. If eigenenergies of the EDF potentials are used, care must be taken to make an explicit link with self-consistent mass differences. For quasi-particles added on top of spherical nuclei, a small rearrangement contribution can be expected in the SR framework [Rut98, Zal08].

Further comments are in order, though, concerning the microscopic definition of s.p. energies and their calculation in a MR-EDF scheme. Nuclear single-particle energies can be measured by stripping and pickup reactions. Such experiments usually yield a non-trivial spectrum where s.p. levels are fragmented due to correlations, i.e. measured states are not pure, single quasiparticles but result from the coupling of the q.p. to other degrees of freedom.

This is commonly discussed in the framework of the interacting shell model as a coupling of several elementary excitations. In such a picture [Cau05], which amounts to decomposing the Hamiltonian into an effective single-particle (monopole) part and a residual interaction acting in a reduced model space, the single-particle energy can be recovered from the spectrum using spectroscopic factors. A similar effect is obtained when performing particle-vibration coupling [Ber80, Lit06] using the (quasiparticle) random phase approximation [Bla77, Sev02] for the collective vibrations. In these cases, the coupling to collective modes fragments the single-particle strength (measured in terms of spectroscopic factors, or spectral functions, Eqs. (2.8) and (2.9)) and yields a lowest fragment with an energy lowered compared to the initial s.p.e. (thus closer to the Fermi level), which translates into a denser spectrum and higher effective mass.

Such a particle-vibration coupling scheme can be understood as an approximation of the full MR-EDF calculation of the odd nucleus, which we take as an idealized standard. Indeed, RPA, or in its EDF-based embodiment, linearized time-dependent EDF [Ben03b], can be considered as a low-amplitude-motion limit of a MR-EDF formalism [Jan64, Sev06].

The EDF method thus has the potential to give a faithful account of single-particle motion, subject to the condition that all relevant collective degrees of free-

dom are taken into account by symmetry restoration and configuration mixing. This clearly remains to be implemented in full-fledged form and on a systematic footing.

Single-particle energies and mass differences

In order to calculate a mass difference between two adjacent nuclei (of masses A and $A \pm 1$), we have to create a quasiparticle on top of the A-body ground state (possibly with a particle number adjusted to obtain the right number of particles in the one-q.p. state, see Eq. (2.48) and chapter 5), then resume self-consistent minimization. Further, it should be ultimately possible to perform a full MR-EDF calculation of the odd system.

In order to understand the workings of the SR-EDF method in this respect, let us express the energy of a the system following the addition of a single quasiparticle (without any self-consistent rearrangement of the nucleus) with an expansion up to second order in the corresponding variation of the density matrix and pair tensor:

$$\begin{aligned}\mathcal{E}[\hat{\rho}+\delta\hat{\rho},\hat{\kappa}+\delta\hat{\kappa},\hat{\kappa}^*+\delta\hat{\kappa}^*] &= \mathcal{E}[\hat{\rho},\hat{\kappa},\hat{\kappa}^*] \\ &+ h_{kl}\delta\rho_{kl} + \frac{1}{2}\left(\Delta_{kl}\delta\kappa^*_{lk} + \Delta^*_{kl}\delta\kappa_{lk}\right) \\ &+ \frac{1}{2}v^{\mathrm{ph}}_{klmn}\delta\rho_{mk}\delta\rho_{nl} + \frac{1}{2}v^{\mathrm{pp}}_{klmn}\delta\kappa^*_{kl}\delta\kappa_{mn} \\ &+ \frac{1}{4}\delta\rho_{lk}\left[\frac{\delta\mathcal{E}}{\delta\rho_{lk}\delta\kappa^*_{nm}}\delta\kappa^*_{nm} + \frac{\delta\mathcal{E}}{\delta\rho_{lk}\delta\kappa_{nm}}\delta\kappa_{nm}\right] \\ &+ \ldots \end{aligned} \tag{2.64}$$

The first line in Eq. (2.64) is the fully paired ground state energy, while the second line corresponds to the quasiparticle energy, as in the HFB case, Eq. (2.48). The third line involves the particle-hole and particle-particle residual interactions,

$$v^{\mathrm{ph}}_{klmn} = \frac{\delta\mathcal{E}}{\delta\rho_{mk}\delta\rho_{nl}}, \qquad v^{\mathrm{pp}}_{klmn} = \frac{\delta\mathcal{E}}{\delta\kappa^*_{kl}\delta\kappa_{mn}}. \tag{2.65}$$

In the strict HFB case, these are (up to a factor) the antisymmetrized interaction Hamiltonian, i.e. $v^{\mathrm{ph}} = \overline{v}$, $v^{\mathrm{pp}} = \overline{v}/2$. In this case the third line vanishes, since

$$\begin{aligned}&\overline{v}_{klmn}\delta\rho_{mk}\delta\rho_{nl} + \frac{1}{2}\overline{v}_{klmn}\delta\kappa^*_{kl}\delta\kappa_{mn} \\ &\quad = \frac{1}{2}\overline{v}_{klmn}\left[\delta\rho_{mk}\delta\rho_{nl} - \delta\rho_{ml}\delta\rho_{nk} + \delta\kappa^*_{kl}\delta\kappa_{mn}\right] = 0,\end{aligned} \tag{2.66}$$

as can be verified by writing down the density variations in terms of quasiparticle U and V vectors. In the general EDF case, the vertices are different, density-dependent (which introduces non-antisymmetric rearrangement terms, which allow the $(A+1)^{\mathrm{th}}$ particle to modify the interaction energy of the A core particles by altering the density on which the interactions depend) and may be non-antisymmetrized. The cancellation of second-order terms does not occur anymore. The energy of a one-q.p. state thus contains a self-interaction contribution (direct terms not cancelled by exchange ones) and a self-pairing one [Lac08]. The latter corresponds to terms of the form $\overline{v}^{\kappa\kappa}_{k\bar{k}k\bar{k}}$, which can be interpreted as the scattering of a pair of particles onto the same state, which gives a spurious pairing energy contribution since it is not cancelled by the opposite particle-hole term arising in strict HFB. As

there is some freedom in the distribution of non-cancelled terms between the two contributions, we may refer to their sum as quasiparticle self-interaction (QSI). The same argument can be put forward for the fourth line, i.e. rearrangement terms of the particle-particle interaction, which vanish in the Hamiltonian case and for density-independent pairing interactions. These can, in any case, be expected to be small.

Also, not included in the above expressions and discussion is the variation of the center-of-mass correction with mass number A [Zal08], which results in a slight and systematic variation of single-particle level spacings.

Self-consistent minimization of the energy will thus yield an energy lower than Eq. (2.64), but the position of the resulting minimal energy with respect to the starting one can not be inferred *a priori*. The fact that QSI occurs in part due to different particle-particle and particle-hole interactions is puzzling, as the latter is required by diagrammatic analysis. One may wonder whether such a self-pairing effect may be found in the latter method, and if it is the case, what kind of physics may be contained therein. This question unfortunately belongs to the list of concerns too involved to be addressed in this manuscript.

Although self-interaction contributions to one-quasiparticle state energies are non-vanishing, they are, qualitatively, effects of order $1/A$ compared to bare q.p. energies generated by the interaction with all nucleons. Depending on the situation, this will have to be compared with the magnitude of the effects under investigation.

2.3 Skyrme energy density functional

The usual *ansatz* for the Skyrme effective interaction [Cha97, Cha98] leads to an energy density functional which can be written as the sum of a kinetic term, the Skyrme potential energy functional that models the effective strong interaction in the particle-hole channel, a pairing energy functional corresponding to a density-dependent contact pairing interaction, the Coulomb energy functional (calculated using the Slater approximation [Sla51]) and correction terms to approximately remove the excitation energy from spurious motion caused by broken symmetries [Ben03b],

$$\mathcal{E} = \mathcal{E}_{\text{kin}} + \mathcal{E}_{\text{Skyrme}} + \mathcal{E}_{\text{Coulomb}} + \mathcal{E}_{\text{pairing}} + \mathcal{E}_{\text{corr}} \,. \tag{2.67}$$

In this section we focus on the particle-hole part of the functional consisting of all the terms mentioned above except the pairing part, which will be the subject of the next section.

2.3.1 Quasi-local energy density functional

Throughout this work, we will use an effective Skyrme energy functional that corresponds to an antisymmetrized density-dependent two-body vertex in the particle-hole channel of the strong interaction, that can be decomposed into a central, spin-orbit and tensor contribution

$$v^{\text{Skyrme}} = v^{\text{c}} + v^{\text{t}} + v^{\text{LS}} \,. \tag{2.68}$$

Other choices for the writing of the Skyrme energy functional are possible and have been made in the literature, which might affect the form of the effective interaction,

its interpretation and the results obtained from it. We will come back to that in section 4.2.2 below.

The Skyrme energy density functional is a functional of local densities and currents

$$\mathcal{E}_{\rm Skyrme} = \int d^3r\ \mathcal{H}^{\rm Skyrme}(\mathbf{r})\,, \tag{2.69}$$

which has many technical advantages compared to finite-range forces such as the Gogny force. All exchange terms have the same structure as the direct terms, which greatly reduces the number of necessary integrations during a calculation.

Local densities and currents

The general density matrix, expressed in coordinate, spin and isospin variables, reads

$$\rho(\mathbf{r}\sigma q, \mathbf{r}'\sigma' q') \;=\; \langle \hat{c}^\dagger_{\mathbf{r}'\sigma' q'} \hat{c}_{\mathbf{r}\sigma q}\rangle. \tag{2.70}$$

Throughout this manuscript we will assume that we have pure proton and neutron states, except for the calculation of the residual interaction, in appendix C.3, where the general framework leads to more compact formulae. The formal EDF framework for the general case including proton-neutron mixing is discussed in Ref. [Per04]. As of now, let us consider that the matrix can be written independently for neutrons and protons,

$$\rho(\mathbf{r}\sigma q, \mathbf{r}'\sigma' q') \;=\; \rho_q(\mathbf{r}\sigma, \mathbf{r}'\sigma')\ \delta_{qq'}, \tag{2.71}$$

and separate the spin part [Dob00]

$$\rho_q(\mathbf{r}\sigma, \mathbf{r}'\sigma') \;=\; \langle \hat{c}^\dagger_{\mathbf{r}'\sigma' q} \hat{c}_{\mathbf{r}\sigma q}\rangle \;=\; \tfrac{1}{2}\,\rho_q(\mathbf{r},\mathbf{r}')\delta_{\sigma\sigma'} + \tfrac{1}{2}\,\mathbf{s}_q(\mathbf{r},\mathbf{r}')\cdot\langle\sigma'|\hat{\boldsymbol{\sigma}}|\sigma\rangle \tag{2.72}$$

where

$$\rho_q(\mathbf{r},\mathbf{r}') \;=\; \sum_\sigma \rho_q(\mathbf{r}\sigma,\mathbf{r}'\sigma), \qquad \mathbf{s}_q(\mathbf{r},\mathbf{r}') \;=\; \sum_{\sigma\sigma'} \rho_q(\mathbf{r}\sigma,\mathbf{r}'\sigma')\ \langle\sigma'|\hat{\boldsymbol{\sigma}}|\sigma\rangle\,. \tag{2.73}$$

The Skyrme energy functional up to second order in derivatives that we will introduce below can be expressed in terms of seven local densities and currents [Per04] that are defined as

$$\begin{aligned}
\rho_q(\mathbf{r}) &= \rho_q(\mathbf{r},\mathbf{r}')\big|_{\mathbf{r}=\mathbf{r}'} \\
\mathbf{s}_q(\mathbf{r}) &= \mathbf{s}_q(\mathbf{r},\mathbf{r}')\big|_{\mathbf{r}=\mathbf{r}'} \\
\tau_q(\mathbf{r}) &= \boldsymbol{\nabla}\cdot\boldsymbol{\nabla}'\ \rho_q(\mathbf{r},\mathbf{r}')\big|_{\mathbf{r}=\mathbf{r}'} \\
T_{q,\mu}(\mathbf{r}) &= \boldsymbol{\nabla}\cdot\boldsymbol{\nabla}'\ s_{q,\mu}(\mathbf{r},\mathbf{r}')\big|_{\mathbf{r}=\mathbf{r}'} \\
\mathbf{j}_q(\mathbf{r}) &= -\tfrac{i}{2}(\boldsymbol{\nabla}-\boldsymbol{\nabla}')\ \rho_q(\mathbf{r},\mathbf{r}')\big|_{\mathbf{r}=\mathbf{r}'} \\
J_{q,\mu\nu}(\mathbf{r}) &= -\tfrac{i}{2}(\nabla_\mu-\nabla'_\mu)\ s_{q,\nu}(\mathbf{r},\mathbf{r}')\big|_{\mathbf{r}=\mathbf{r}'} \\
F_{q,\mu}(\mathbf{r}) &= \tfrac{1}{2}\sum_{\nu=x}^{z}\left(\nabla_\mu\nabla'_\nu+\nabla'_\mu\nabla_\nu\right) s_{q,\nu}(\mathbf{r},\mathbf{r}')\big|_{\mathbf{r}=\mathbf{r}'}
\end{aligned} \tag{2.74}$$

which are the density $\rho_q(\mathbf{r})$, the kinetic density $\tau_q(\mathbf{r})$, the current (vector) density $\mathbf{j}_q(\mathbf{r})$, the spin (pseudovector) density $\mathbf{s}_q(\mathbf{r})$, the spin kinetic (pseudovector) density $\mathbf{T}_q(\mathbf{r})$, the spin-current (pseudotensor) density $J_{q,\mu\nu}(\mathbf{r})$, and the tensor-kinetic

(pseudovector) density $\mathbf{F}_q(\mathbf{r})$. The densities $\rho_q(\mathbf{r})$, $\tau_q(\mathbf{r})$ and $J_{q,\mu\nu}(\mathbf{r})$ are time-even, while $\mathbf{s}_q(\mathbf{r})$, $\mathbf{T}_q(\mathbf{r})$, $\mathbf{j}_q(\mathbf{r})$ and $\mathbf{F}_q(\mathbf{r})$ are time-odd. For a detailed discussion of their symmetries see Ref. [Dob00]. There are other local densities up to second order in derivatives that can be constructed, but when constructing an energy functional they either cannot be combined with others to terms with proper symmetries or they lead to terms that are not independent from the others [Dob96a].

The Cartesian spin-current pseudotensor density $J_{\mu\nu}$ can be decomposed into pseudoscalar, (anti-symmetric) vector and (symmetric) traceless pseudotensor parts, all of which have well-defined transformation properties under rotations

$$J_{\mu\nu}(\mathbf{r}) = \tfrac{1}{3}\delta_{\mu\nu}\, J^{(0)}(\mathbf{r}) + \tfrac{1}{2}\sum_{\kappa=x}^{z} \epsilon_{\mu\nu\kappa}\, J^{(1)}_{\kappa}(\mathbf{r}) + J^{(2)}_{\mu\nu}(\mathbf{r})\,, \tag{2.75}$$

where $\delta_{\mu\nu}$ is the Kronecker symbol and $\epsilon_{\mu\nu\kappa}$ the Levi-Civita tensor. The pseudoscalar, vector and pseudotensor parts expressed in terms of the Cartesian tensor are given by

$$\begin{aligned} J^{(0)}(\mathbf{r}) &= \sum_{\mu=x}^{z} J_{\mu\mu}(\mathbf{r})\,, \qquad (2.76)\\ J^{(1)}_{\kappa}(\mathbf{r}) &= \sum_{\mu,\nu=x}^{z} \epsilon_{\kappa\mu\nu}\, J_{\mu\nu}(\mathbf{r})\,,\\ J^{(2)}_{\mu\nu}(\mathbf{r}) &= \tfrac{1}{2}[J_{\mu\nu}(\mathbf{r}) + J_{\nu\mu}(\mathbf{r})] - \tfrac{1}{3}\delta_{\mu\nu}\sum_{\kappa=x}^{z} J_{\kappa\kappa}(\mathbf{r})\,. \end{aligned}$$

The vector spin current density $\mathbf{J}^{(1)}(\mathbf{r}) \equiv \mathbf{J}(\mathbf{r})$ is often called spin-orbit current, as it enters the spin-orbit energy density. Some authors, though, call $\mathbf{J}(\mathbf{r})$ *spin density*, which is ambiguous when discussing the complete energy density functional including terms that contain the time-odd $\mathbf{s}(\mathbf{r})$.

For the formal discussion of the physical content of the Skyrme energy functional it is of advantage to recouple the proton and neutron densities to isoscalar and isovector densities, for example

$$\rho_0(\mathbf{r}) = \rho_{\rm n}(\mathbf{r}) + \rho_{\rm p}(\mathbf{r})\,, \qquad \rho_1(\mathbf{r}) = \rho_{\rm n}(\mathbf{r}) - \rho_{\rm p}(\mathbf{r}) \tag{2.77}$$

and similarly for all other ones. As we assume pure proton and neutron states, only the $T_z = 0$ component of the isovector density is non-zero, which we have exploited to drop the index T_z from the isovector densities $\rho_{1T_z}(\mathbf{r})$, etc.

Skyrme's central force

In each part of this work, we will use different parametrizations of the density-dependent central Skyrme interaction. The number of density-dependent terms will be chosen as one or two depending on specific requirements. The most general (for our purpose) central Skyrme interaction reads

$$\begin{aligned} \hat{v}^{\rm c}(\mathbf{R},\mathbf{r}) &= t_0\,(1 + x_0\hat{P}_\sigma)\,\delta(\mathbf{r})\\ &+ \tfrac{1}{6}\,t_3\,(1 + x_3\hat{P}_\sigma)\,\rho^{\gamma}(\mathbf{R})\,\delta(\mathbf{r})\\ &+ \tfrac{1}{6}\,t_6\,(1 + x_6\hat{P}_\sigma)\,\rho^{\gamma'}(\mathbf{R})\,\delta(\mathbf{r})\\ &+ \tfrac{1}{2}\,t_1\,(1 + x_1\hat{P}_\sigma)\big[\hat{\mathbf{k}}'^2\,\delta(\mathbf{r}) + \delta(\mathbf{r})\,\hat{\mathbf{k}}^2\big]\\ &+ t_2\,(1 + x_2\hat{P}_\sigma)\,\hat{\mathbf{k}}'\cdot\delta(\mathbf{r})\,\hat{\mathbf{k}} \end{aligned} \tag{2.78}$$

where we use the shorthand notation

$$\mathbf{r} \;=\; \mathbf{r}_1 - \mathbf{r}_2\,, \qquad \mathbf{R} \;=\; \tfrac{1}{2}(\mathbf{r}_1 + \mathbf{r}_2)\,, \tag{2.79}$$

while $\hat{\mathbf{k}}$ is the usual operator for relative momenta

$$\hat{\mathbf{k}} = -\tfrac{i}{2}(\hat{\boldsymbol{\nabla}}_1 - \hat{\boldsymbol{\nabla}}_2) \tag{2.80}$$

and $\hat{\mathbf{k}}'$ its complex conjugate acting on the left. Finally, $\hat{P}_\sigma$ is the spin exchange operator that controls the relative strength of the $S = 0$ and $S = 1$ channels for a given term in the two-body interaction

$$\hat{P}_\sigma = \tfrac{1}{2}\,(1 + \hat{\boldsymbol{\sigma}}_1 \cdot \hat{\boldsymbol{\sigma}}_2)\,. \tag{2.81}$$

As said above, we restrict ourselves to a parametrization of the Skyrme energy functional as obtained from the average value of an effective two-body vertex in the reference quasiparticle vacuum. We decompose the isoscalar and isovector parts of the resulting energy density functional $\mathcal{H}^{\mathrm{c}}$ into a part $\mathcal{H}_t^{\mathrm{c,even}}$ that is composed entirely of time-even densities and currents, and a part $\mathcal{H}_t^{\mathrm{c,odd}}$ that contains terms which are bilinear in time-odd densities and currents and vanishes in intrinsically time-reversal invariant systems

$$\mathcal{H}^{\mathrm{c}}(\mathbf{r}) \;=\; \sum_{t=0,1} \left[\mathcal{H}_t^{\mathrm{c,even}}(\mathbf{r}) + \mathcal{H}_t^{\mathrm{c,odd}}(\mathbf{r})\right]. \tag{2.82}$$

Both $\mathcal{H}_t^{\mathrm{c,even}}$ and $\mathcal{H}_t^{\mathrm{c,odd}}$ are of course constructed such that they are time-even; they are given by [Eng75, Per04]

$$\begin{aligned}
\mathcal{H}_t^{\mathrm{c,even}} &= A_t^{\rho}[\rho_0]\,\rho_t^2 + A_t^{\Delta\rho}\,\rho_t\Delta\rho_t + A_t^{\tau}\,\rho_t\tau_t - A_t^{T}\sum_{\mu,\nu=x}^{z} J_{t,\mu\nu}J_{t,\mu\nu}\,,\\
\mathcal{H}_t^{\mathrm{c,odd}} &= A_t^{s}[\rho_0]\,\mathbf{s}_t^2 - A_t^{\tau}\,\mathbf{j}_t^2 + A_t^{\Delta s}\,\mathbf{s}_t\cdot\Delta\mathbf{s}_t + A_t^{T}\,\mathbf{s}_t\cdot\mathbf{T}_t\,,
\end{aligned} \tag{2.83}$$

where $A_t^{\rho}[\rho_0]$ and $A_t^{s}[\rho_0]$ are density dependent coupling constants that depend on the total (isoscalar) density. The detailed relations between the coupling constants of the functional and the central Skyrme force are given in appendix A. The notation reflects that two pairs of terms in $\mathcal{H}_t^{\mathrm{c,even}}$ and $\mathcal{H}_t^{\mathrm{c,odd}}$ are connected by the requirement of local gauge invariance of the Skyrme energy functional [Dob95a].

Zero-range spin-orbit force

The spin-orbit force used with most standard Skyrme interactions

$$\hat{v}^{\mathrm{LS}}(\mathbf{r}) = iW_0\,(\hat{\boldsymbol{\sigma}}_1 + \hat{\boldsymbol{\sigma}}_2)\cdot\hat{\mathbf{k}}'\times\delta(\mathbf{r})\,\hat{\mathbf{k}} \tag{2.84}$$

is a special case of the one proposed by Bell and Skyrme [Bel56, Sky58b]. As above, the corresponding energy functional [Eng75, Per04] can be separated into a time-even and a time-odd term

$$\mathcal{H}^{\mathrm{LS}}(\mathbf{r}) \;=\; \sum_{t=0,1} \left[\mathcal{H}_t^{\mathrm{LS,even}}(\mathbf{r}) + \mathcal{H}_t^{\mathrm{LS,odd}}(\mathbf{r})\right] \tag{2.85}$$

where

$$\mathcal{H}_t^{\mathrm{LS,even}} \;=\; A_t^{\nabla\cdot J}\,\rho_t\nabla\cdot\mathbf{J}_t, \qquad \mathcal{H}_t^{\mathrm{LS,odd}} \;=\; A_t^{\nabla\cdot J}\,\mathbf{s}_t\cdot\nabla\times\mathbf{j}_t \tag{2.86}$$

which share the same coupling constant as, again, both terms are linked by the local gauge invariance of the energy functional. The relation between the $A_t^{\nabla\cdot J}$ and the one coupling constant of the two-body spin-orbit force W_0 is given in appendix A.

Skyrme's tensor force

Although rather uncommon in the Skyrme parametrizations published so far, the tensor force has been the subject of renewed attention, and will be the main topic of chapter 4.

By convention, the tensor operator in the tensor force is constructed using the unit vectors in the direction of the relative coordinate $\mathbf{e}_r = \mathbf{r}/|\mathbf{r}|$ and subtracting $\hat{\boldsymbol{\sigma}}_1 \cdot \hat{\boldsymbol{\sigma}}_2$

$$\hat{S}_{12} = 3(\hat{\boldsymbol{\sigma}}_1 \cdot \mathbf{e}_r)(\hat{\boldsymbol{\sigma}}_2 \cdot \mathbf{e}_r) - \hat{\boldsymbol{\sigma}}_1 \cdot \hat{\boldsymbol{\sigma}}_2 \,, \tag{2.87}$$

such that its mean value vanishes for a relative S state, which decouples the central and tensor channels of the interaction. The operator $\hat{S}_{12}$ commutes with the total spin $[\hat{S}_{12}, \hat{\mathbf{S}}^2] = 0$, therefore it does not mix partial waves with different spin, i.e. spin singlet and spin triplet states. In particular, it does not act in spin singlet states at all, as $\hat{S}_{12}\hat{P}_{S=0} = 0$ (see section 13.6 of Ref. [Nil95]). As a consequence, there is no point in multiplying a tensor force with an exchange operator $(1 + x_t\hat{P}_\sigma)$ as done for the central force, as this will only lead to an overall rescaling of its strength.

The derivation of the general energy functional from a zero-range two-body tensor force is discussed in detail in Refs. [Flo75, Per04]. We repeat here the details relevant for our discussion, starting from the two zero-range tensor forces proposed by Skyrme [Sky56, Sky58a]

$$\begin{aligned}
\hat{v}^{\mathrm{t}}(\mathbf{r}) \;=\; & \tfrac{1}{2}\,t_e \Big\{ \left[3\,(\hat{\boldsymbol{\sigma}}_1 \cdot \mathbf{k}')\,(\hat{\boldsymbol{\sigma}}_2 \cdot \hat{\mathbf{k}}') - (\hat{\boldsymbol{\sigma}}_1 \cdot \hat{\boldsymbol{\sigma}}_2)\,\hat{\mathbf{k}}'^2\right] \delta(\mathbf{r}) \\
& + \delta(\mathbf{r})\,\left[3\,(\hat{\boldsymbol{\sigma}}_1 \cdot \hat{\mathbf{k}})\,(\hat{\boldsymbol{\sigma}}_2 \cdot \hat{\mathbf{k}}) - (\hat{\boldsymbol{\sigma}}_1 \cdot \hat{\boldsymbol{\sigma}}_2)\,\hat{\mathbf{k}}^2\right] \Big\} \\
& + t_o \left[3\,(\hat{\boldsymbol{\sigma}}_1 \cdot \hat{\mathbf{k}}')\,\delta(\mathbf{r})\,(\hat{\boldsymbol{\sigma}}_2 \cdot \hat{\mathbf{k}}) - (\boldsymbol{\sigma}_1 \cdot \boldsymbol{\sigma}_2)\,\hat{\mathbf{k}}' \cdot\, \delta(\mathbf{r})\,\hat{\mathbf{k}}\right]
\end{aligned} \tag{2.88}$$

where $\mathbf{r}$, $\hat{\mathbf{k}}$ and $\hat{\mathbf{k}}'$ are defined as above, Eqs. (2.79) and (2.80). The corresponding energy density functional can again be decomposed in a time-even and a time-odd part

$$\mathcal{H}^{\mathrm{t}}(\mathbf{r}) \;=\; \sum_{t=0,1} \left[\mathcal{H}_t^{\mathrm{t,even}}(\mathbf{r}) + \mathcal{H}_t^{\mathrm{t,odd}}(\mathbf{r})\right] \tag{2.89}$$

with [Per04]

$$\begin{aligned}
\mathcal{H}_t^{\mathrm{t,even}} \;&=\; -B_t^T \sum_{\mu,\nu=x}^{z} J_{t,\mu\nu} J_{t,\mu\nu} - \tfrac{1}{2}\,B_t^F \left(\sum_{\mu=x}^{z} J_{t,\mu\mu}\right)^2 - \tfrac{1}{2}\,B_t^F \sum_{\mu,\nu=x}^{z} J_{t,\mu\nu} J_{t,\nu\mu} \\
\mathcal{H}_t^{\mathrm{t,odd}} \;&=\; B_t^T\,\mathbf{s}_t \cdot \mathbf{T}_t + B_t^F\,\mathbf{s}_t \cdot \mathbf{F}_t + B_t^{\Delta s}\,\mathbf{s}_t \cdot \Delta\mathbf{s}_t + B_t^{\nabla s}\,(\nabla \cdot \mathbf{s}_t)^2 \,,
\end{aligned} \tag{2.90}$$

where we already used the local gauge invariance of the energy functional [Per04] for the expressions of the coupling constants. The actual expressions for the coupling constants expressed in terms of the two coupling constants t_e and t_o of the tensor forces are given in appendix A.

The "even" term proportional to t_e in the two-body tensor force (2.88) mixes relative S and D waves, while the "odd" term proportional to t_o mixes relative P and F waves. Thus, due to the fact that both act in spin-triplet states only, antisymmetrization implies that the former acts in isospin-singlet states (and hence contributes to the neutron-proton interaction only) and the latter in isospin-triplet

states (contributing both to the like-particle and neutron-proton interactions). The central and spin-orbit interactions as we use them, however, do not contain D or F wave interactions. From this point of view, one might suspect a mismatch when combining the various interaction terms. From the point of view of the energy functional (2.90), however, all contributions from the zero-range tensor force are of the same second order in derivatives as the contributions from the non-local part of the central Skyrme force (2.83) and from the spin-orbit force (2.86).

In the time-even part of the energy functional $\mathcal{H}_t^{\mathrm{t,even}}$, there appear three different combinations of the Cartesian components of the spin current tensor. The term proportional to B_t^T contains the symmetric combination $J_{\mu\nu}J_{\mu\nu}$ as it already appeared in the energy functional from the central Skyrme interaction (2.83), while the term proportional to B_t^F contains two different terms, namely the antisymmetric combination $J_{\mu\nu}J_{\nu\mu}$ and the square of the trace of $J_{\nu\mu}$.

Combining central and tensor interactions

The Skyrme energy functional representing central, tensor, and spin-orbit interactions is given by

$$\begin{aligned}
\mathcal{E}_{\mathrm{Skyrme}} &= \mathcal{E}_{\mathrm{c}} + \mathcal{E}_{\mathrm{LS}} + \mathcal{E}_{\mathrm{t}} \\
&= \int d^3\mathbf{r} \sum_{t=0,1} \Big\{ C_t^{\rho}[\rho_0]\, \rho_t^2 + C_t^{\tau}(\rho_t\tau_t - \mathbf{j}_t^2) + C_t^{\Delta\rho}\rho_t\Delta\rho_t \\
&\quad + C_t^{s}[\rho_0]\, \mathbf{s}_t^2 + C_t^{\nabla s}(\nabla\cdot\mathbf{s}_t)^2 + C_t^{\Delta s}\mathbf{s}_t\cdot\Delta\mathbf{s}_t \\
&\quad + C_t^{T}\Big(\mathbf{s}_t\cdot\mathbf{T}_t - \sum_{\mu,\nu=x}^{z} J_{t,\mu\nu}J_{t,\mu\nu}\Big) \\
&\quad + C_t^{F}\Big[\mathbf{s}_t\cdot\mathbf{F}_t - \tfrac{1}{2}\Big(\sum_{\mu=x}^{z} J_{t,\mu\mu}\Big)^2 - \tfrac{1}{2}\sum_{\mu,\nu=x}^{z} J_{t,\mu\nu}J_{t,\nu\mu}\Big] \\
&\quad + C_t^{\nabla\cdot J}(\rho_t\nabla\cdot\mathbf{J}_t + \mathbf{s}_t\cdot\nabla\times\mathbf{j}_t)\Big\}\,. \qquad (2.91)
\end{aligned}$$

This functional contains all possible bilinear terms up to second order in the derivatives that can be constructed from local densities and that are invariant under spatial and time inversion, rotations, and local gauge transformations [Per04].

Some of the coupling constants are completely defined by the standard central Skyrme force, i.e. $C_t^{\rho} = A_t^{\rho}$, $C_t^{s} = A_t^{s}$, $C_t^{\tau} = A_t^{\tau}$, and $C_t^{\Delta\rho} = A_t^{\Delta\rho}$, two by the spin-orbit force, $C_t^{\nabla J} = A_t^{\nabla J}$, others by the tensor force, $C_t^{F} = B_t^{F}$ and $C_t^{\nabla s} = B_t^{\nabla s}$, while some are the sum of coupling constants from both central and tensor forces, $C_t^{T} = A_t^{T} + B_t^{T}$, and $C_t^{\Delta s} = A_t^{\Delta s} + B_t^{\Delta s}$.

The three terms bilinear in $J_{\mu\nu}$ can be recoupled into terms bilinear in its pseudoscalar, vector, and pseudotensor components $J^{(0)}$, $J^{(1)}$, and $J^{(2)}$, Eq. (2.76), which is preferred by some authors [Per04]

$$\sum_{\mu,\nu=x}^{z} J_{t,\mu\nu}J_{t,\mu\nu} = \tfrac{1}{3}\left(J_t^{(0)}\right)^2 + \tfrac{1}{2}\,\mathbf{J}_t^2 + \sum_{\mu,\nu=x}^{z} J_{t,\mu\nu}^{(2)}J_{t,\mu\nu}^{(2)} \qquad (2.92)$$

$$\tfrac{1}{2}\Big[\Big(\sum_{\mu=x}^{z} J_{t,\mu\mu}\Big)^2 + \sum_{\mu,\nu=x}^{z} J_{t,\mu\nu}J_{t,\nu\mu}\Big] = \tfrac{2}{3}\left(J_t^{(0)}\right)^2 - \tfrac{1}{4}\,\mathbf{J}_t^2 + \tfrac{1}{2}\sum_{\mu,\nu=x}^{z} J_{t,\mu\nu}^{(2)}J_{t,\mu\nu}^{(2)}\,. \qquad (2.93)$$

After combining (2.91) with the kinetic, Coulomb, pairing and other contributions from (2.67), the mean-field equations are obtained by standard functional derivative techniques from the total energy functional, see section 2.2, appendix C.3 and Refs. [Ben03b, Per04].

The complete Skyrme energy functional (2.91) has quite complicated a structure, and in the most general case leads to seven distinct mean fields in the single-particle Hamiltonian [Per04]. In the present manuscript, we enforce spherical symmetry which removes all time-odd densities and all but one out of the nine components of the spin-current tensor $J_{\mu\nu}$ as will be outlined in section 4.2.1.

2.3.2 Skyrme energy functional in spherical symmetry

For the rest of this manuscript, we will concentrate on spherical nuclei, enforcing spherical symmetry of the (A)-body wave functions. As a consequence, the canonical single-particle wave functions φ_i can be labeled by j_i, ℓ_i and m_i. The index n_i labels the different states with same j_i and ℓ_i. The functions φ_i separate into a radial part $u_i(r)$ and an angular and spin part, represented by a tensor spherical harmonic $\Omega_{j\ell m}$

$$\begin{aligned} \varphi_{nj\ell m}(\mathbf{r}) &= \frac{u_{nj\ell}(r)}{r}\,\Omega_{j\ell m}(\hat{r}), \\ \Omega_{j\ell m}(\hat{r}) &= \sum_{m_\ell \sigma} \langle \ell m_\ell s\sigma | jm\rangle\, Y^\ell_{m_l}(\theta,\phi)\,|s\sigma\rangle, \end{aligned} \tag{2.94}$$

with $s \equiv 1/2$. Spherical symmetry also enforces that all magnetic substates of $\varphi_{nj\ell m}$ have the same occupation probability $v^2_{nj\ell m} \equiv v^2_{nj\ell}$ for all $-j \leq m \leq j$. For a static spherical state, all time-odd densities are zero $\mathbf{s}_q(\mathbf{r}) = \mathbf{T}_q(\mathbf{r}) = \mathbf{j}_q(\mathbf{r}) = \mathbf{F}_q(\mathbf{r}) = \mathbf{0}$, as are the corresponding mean fields in the single-particle Hamiltonian.

Altogether, the Skyrme part of the energy density functional in spherical nuclei is reduced to

$$\begin{aligned} \mathcal{H}^{\text{Skyrme}} &= \sum_{t=0,1} \Big\{ C^\rho_t[\rho_0]\,\rho_t^2 + C^{\Delta\rho}_t\,\rho_t\Delta\rho_t \\ &\qquad + C^\tau_t\,\rho_t\tau_t + \tfrac{1}{2}\,C^J_t\,\mathbf{J}_t^2 + C^{\nabla\cdot J}_t\,\rho_t\nabla\cdot\mathbf{J}_t \Big\}, \end{aligned} \tag{2.95}$$

where we have introduced an effective coupling constant C^J_t of the $\mathbf{J}^2_t$ tensor terms at sphericity.

2.4 Local pairing functional

For our EDF to be fully defined, we need to specify its essential pairing part. In this section we focus on local pairing functionals formally generated from zero-range effective pairing interactions, and specific issues associated with them. A different kind of pairing functional will be presented in chapter 5.

Let us write down the coordinate-space expression of the pair density matrix,

$$\tilde{\rho}(\mathbf{r}_1,\sigma_1,q;\mathbf{r}_2,\sigma_2,q) = (-)^{1/2+\sigma_2}\langle \hat{c}_{\mathbf{r}_2\overline{\sigma}_2 q}\hat{c}_{\mathbf{r}_1\sigma_1 q}\rangle, \tag{2.96}$$

as well as the local pair density,

$$\tilde{\rho}_q(\mathbf{r}) = \sum_\sigma \tilde{\rho}(\mathbf{r},\sigma,q;\mathbf{r},\sigma,q) = \sum_\sigma (-)^{1/2+\sigma}\kappa(\mathbf{r},\sigma,q;\mathbf{r},\overline{\sigma},q). \tag{2.97}$$

The pairing functional commonly used in conjunction with the Skyrme-interaction-derived particle-hole functional can be formally derived as the particle-particle contraction of a local, zero-range density-dependent delta interaction (DDDI),

$$v_q^{\rm pair}(\mathbf{r}) \;=\; \mathcal{V}_q^{\rm pair}\,\left(1-c\frac{\rho_0}{\rho_{\rm sat}}\right)\,\frac{1-P_\sigma}{2}\,\delta(\mathbf{r}), \tag{2.98}$$

which is here defined by a strength $\mathcal{V}_q^{\rm pair}$ and a parameter c which determines the density dependence and hence the localization of the pairing field, in the volume of the nucleus (for $c=0$) or at the surface ($c=1$) [JD01]. The corresponding pairing functional reads

$$\mathcal{E}_{\rm pair}[\tilde\rho,\tilde\rho^*] \;=\; \int d^3\mathbf{r}\; C_q^{\tilde\rho}\;\tilde\rho_q^*\;\tilde\rho_q \tag{2.99}$$

where the coupling constant is density-dependent and given as

$$C_q^{\tilde\rho} \;=\; \frac{\mathcal{V}_q^{\rm pair}}{4}\,\left(1-c\frac{\rho_0}{\rho_{\rm sat}}\right). \tag{2.100}$$

Unfortunately, such a theory diverges. Indeed, the pairing field derived from such a functional is local,

$$\begin{aligned}\Delta(\mathbf{r}_1\sigma_2 q;\mathbf{r}_2\sigma_2 q) &= \tilde U_q(\mathbf{r}_1)\;\delta(\mathbf{r}_1-\mathbf{r}_2)\;(-)^{1/2+\sigma_2}\delta_{\sigma_1\overline{\sigma}_2},\\ \tilde U_q(\mathbf{r}) \;=\; \frac{\delta\mathcal{E}}{\delta\tilde\rho_q^*(\mathbf{r})} &= 2C_q^{\rm pair}(\mathbf{r})\;\tilde\rho_q(\mathbf{r}_1)\end{aligned} \tag{2.101}$$

which means that matrix elements of Δ, i.e. pairing gaps are essentially independent from the momentum or energy of single-particle states.

It is useful at this point to make use of the BCS gap equation in infinite matter, which is further discussed in chapter 5.

$$\Delta_q(k) \;=\; -\int_0^{k_{\rm c}}\frac{k'^2dk'}{2\pi^3}\;\mathcal{V}_q^{\rm pair}\;\frac{\Delta_q(k')}{2\sqrt{\overline{\varepsilon}_{k'}^2+\Delta_q(k')^2}}. \tag{2.102}$$

It follows immediately that $\Delta_q(k')$ is in fact a constant. With $\overline{\varepsilon}_k=\hbar^2k^2/2m$, this expression diverges linearly when $k_{\rm c}\to\infty$.

Summing over quasiparticles with non-bounded q.p. energy yields a pair density which diverges as $1/|\mathbf{r}_1-\mathbf{r}_2|$ for $\mathbf{r}_1-\mathbf{r}_2\to 0$ [Bru99, Bul02a], making the pairing energy undefined [Dob96b]. It is thus necessary to regularize $\tilde\rho$, as well as all densities. This can be achieved by substracting the contributions to the density and pair tensor of states lying outside of a pairing window defined as an energy interval in the single-particle (HF), canonical or quasiparticle spectrum. A truncation of single-particle bases is necessary for practical applications whatever the functional used, however for a local pairing functional no convergence of observables is obtained with respect of this truncation, which has to be defined as a part of the model.

As an example and to be more specific, let us give the expressions for the case where the cutoff is implemented in the quasiparticle basis,

$$\begin{aligned}\rho_{kl}^{\rm c} &= \langle\Phi_0|\hat c_l^\dagger\hat c_k|\Phi_0\rangle \;=\; \sum_m f_m\;V_k^{m*}\;V_l^m,\\ \kappa_{kl}^{\rm c} &= \langle\Phi_0|\hat c_l\hat c_k|\Phi_0\rangle \;=\; \sum_m f'_m\;V_k^{m*}\;U_l^m,\end{aligned} \tag{2.103}$$

where f_m and f'_m are equal to one at the Fermi level, and put to zero for states outside a given energy window (which has an upper bound only for f_k, and may also have a lower one for f'_m). In practice, a smooth cutoff is implemented, which alleviates convergence issues due to transitions of q.p. states in and out of the window during iterations:

$$f_m = \frac{1}{1+\exp[(\varepsilon_m - \varepsilon_{\rm c}^+)/\varepsilon_{\rm d}]}, \qquad f'_m = f_m \frac{1}{1+\exp[-(\varepsilon_m + \varepsilon_{\rm c}^-)/\varepsilon_{\rm d}]}, \quad (2.104)$$

where ε_k is the single-particle equivalent energy of quasiparticle k [Ben05], ε_c the cutoff energy and $\varepsilon_{\rm d}$ a diffuseness parameter, typically of the order of 1 MeV.

Thus, the functional actually used involves not the strict local pair density, but a regularized one, the other densities (including in the particle-hole channel) being replaced by their regularized counterparts as well. Such a pairing functional is not, strictly speaking, the expectation value of the effective interactions given thus far, which serves only as a formal intermediate. In addition to the parameters of Eq. (2.98), the functional needs a cutoff energy to be fully defined. Moreover, the strength parameter has to be adjusted consistently with the cutoff, which underlines the fact that $\varepsilon_{\rm c}^{\pm}$ is not only a numerical parameter, but an integral part of the model.

As shown by Matsuo [Mat06], the energy cutoff employed in a local pairing functional plays a role similar to the range of a finite-range interaction with respect to the structure of the non-local pair density, and can be adjusted so as to control the latter rather precisely. The value of $\varepsilon_{\rm c}^+$ that was found appropriate in this respect was of the order of 50 MeV. The fact that a (regularized) local functional can describe nuclear pairing with a satisfactory accuracy comes from the fact that the spatial extension of the Cooper pair wave function (defined, up to a normalization factor, as the non-local part of $\tilde{\rho}$) is typically larger than the range of the underlying interaction, implying that the spatial dependence of the latter is not resolved.

The local or non-local pair density, however, is not an observable, and the fact that an additional parameter is introduced may seem unsatisfactory. To address this issue, Bulgac and Yu [Bul02b] introduced a method to regularize the pair density and obtain a cutoff-independent functional (for sufficiently large cutoffs). The divergence in the pair density is of ultraviolet character, caused by the accumulation of contributions from high-momentum continuum states, for which a local density approximation is reasonable. One can indeed obtain an accurate analytical expression for the divergent part of the pair density at each point $\mathbf{r}$ and for each species q by studying a uniform gas subject to a potential $U_q(\mathbf{r})$, a pairing field $\tilde{U}_q(\mathbf{r})$, an effective mass $m_q^*(\mathbf{r})$ and a chemical potential λ_q. The regularized pair density then reads

$$\tilde{\rho}_q^{\rm reg} = \tilde{\rho}_q^{\rm c} + \tilde{U}_q\, Y(k_{{\rm F}q}, k_{\rm c}), \quad (2.105)$$

where the function $Y(k_{{\rm F}q}, k_{\rm c})$ is given by

$$Y(k_{{\rm F}q}, k_{\rm c}) = \frac{m_q^* k_{\rm c}}{2\pi^2\hbar^2}\left[1 - \frac{k_{{\rm F}q}}{2k_{\rm c}}{\rm Ln}\left(\frac{k_{{\rm F}q}+k_{\rm c}}{k_{{\rm F}q}-k_{\rm c}}\right)\right], \quad (2.106)$$

which involves the position-dependent quantities m_q^*, $k_{{\rm F}q}$ and $k_{\rm c}$, defined by

$$\frac{\hbar^2 k_{{\rm F}q}^2}{2m_q^*} + U_q = \lambda_q, \qquad \frac{\hbar^2 k_{\rm c}}{2m_q^*} + U_q = \varepsilon_{\rm c}^+. \quad (2.107)$$

Here, we consider only an upper bound for the pairing window, with $\varepsilon_{\rm c}^- = -\infty$. The local effective Fermi momentum $k_{{\rm F}q}$ may be an imaginary number where $\lambda_q < U_q$, but it is easy to check that Y stays real in that case. The regularized density is independent from $\varepsilon_{\rm c}^+$ when the latter is taken sufficiently large. One requires, moreover, that observables computed with the regularized functional are also cutoff-independent. Being closely linked with odd-even mass differences, the pairing field $\tilde{U}$ is such a quantity. The pairing functional being quadratic in $\tilde{\rho}$, we must then have

$$\tilde{U}_q \;=\; \frac{\delta\mathcal{E}}{\delta\tilde{\rho}_q^*} \;=\; g_q\tilde{\rho}_q^{\rm reg} \tag{2.108}$$

g_q being a position/density-dependent but cutoff-independent quantity. One may rewrite the above as

$$\tilde{U}_q \;=\; g_q^{\rm reg}\tilde{\rho}_q, \qquad \frac{1}{g_q^{\rm reg}} \;=\; \frac{1}{g_q} - Y(k_{{\rm F}q}, k_{\rm c}). \tag{2.109}$$

We finally rewrite the pairing energy functional as

$$\begin{aligned}
\mathcal{E}_{\rm pair}[\tilde{\rho},\tilde{\rho}^*] \;&=\; \int d^3\mathbf{r}\; \tilde{U}_q\; \tilde{\rho}_q^{{\rm c}*} \;=\; \int d^3\mathbf{r}\; g_q^{\rm reg}\; \tilde{\rho}_q^{{\rm c}*}\; \tilde{\rho}_q^{\rm c} \\
&=\; \int d^3\mathbf{r}\; g_q\; \tilde{\rho}_q^{{\rm c}*}\; \tilde{\rho}_q^{\rm reg} \\
&=\; \int d^3\mathbf{r}\; C_q^{\tilde{\rho}}\; \tilde{\rho}_q^{{\rm reg}*}\; \tilde{\rho}_q^{\rm reg}, \qquad C_q^{\tilde{\rho}} \;=\; \frac{g_q^2}{g_q^{\rm reg}} \;=\; g_q[1 - g_q Y(k_{{\rm F}q}, k_{\rm c})].
\end{aligned} \tag{2.110}$$

We see that the pairing energy is not cutoff-independent; in fact, it is a divergent quantity. However, it is not an observable. The total energy, in turn, is cutoff-independent thanks to a cancellation between the divergent contributions of the pairing and kinetic energies (including effective-mass terms), which behave similarly for large $k_{\rm c}$ [Bul02a].

Chapter 3

New Constraints for the Nuclear Energy Density Functional

The accuracy and predictive power of EDF models needed for unknown regions of the nuclear chart still leave a lot of room for improvement. The phenomenological nature of Skyrme functionals makes their ability to faithfully predict observables or phenomena not linked with those used for their construction quite weak. Indeed, the limited number of adjustable parameters (compared to the wealth of nuclear observables to be matched) turns fitting a Skyrme functional into an overconstrained problem (which, of course, does not prevent some parts of it from being underconstrained).

As a direct consequence, many properties of existing parametrizations are biased to the fitting procedure and the limited analytical form of the Skyrme interaction, rather than to physical reasoning. A well-known example is the equation of state (EOS) of Pure Neutron Matter (PNM), which is sometimes subject to a pathological collapse at high density when not explicitly constrained. This is problematic insofar as one of the major challenges of contemporary nuclear theory is to predict properties of very isospin-asymmetric nuclear systems, i.e. neutron rich nuclei and matter in neutron stars. Experimental data being unavailable in this domain of isospin, one has started relying on ab-initio theoretical results to constrain isovector properties of the functional. It has led to the construction of the "Saclay-Lyon" SLy series of parametrizations [Cha97, Cha98] by fitting (among other quantities) a theoretical equation of state of neutron matter.

Isovector features of the nuclear EOS are crucial for a good understanding of neutron stars, exotic nuclear collisions produced at radioactive beam facilities and to describe the structure of exotic nuclei. For instance, the density dependence of the volume symmetry energy determines the proton fraction in β equilibrium in neutron stars, which ultimately drives the cooling rate and neutrino emission [Lat04]. The high-density part of the symmetry energy, which happens to be strongly model dependent, also influences significantly the isospin diffusion in heavy-ion collisions [Che05]. Finally, the low-density part of the symmetry energy is correlated with the size of neutron skins in finite nuclei [Typ01].

Beyond global isospin-dependent properties of the EOS, the isovector part of nucleon-dependent quantities may influence the behavior of the above mentioned systems. Thus, collision observables depend on the momentum dependence of the mean-field, in particular on its isovector component [Li04a, Li04b]. Also, some

properties of neutron stars require a precise knowledge of isoscalar and isovector nucleon effective masses [Bet90, Far01]. The latter, which drives the *splitting of neutron and proton effective masses* with neutron/proton asymmetry, will serve as a starting point for the study presented in this chapter. Indeed, a lot of efforts has recently been devoted to the microscopic characterization of neutron and proton effective masses in infinite Asymmetric Nuclear Matter (ANM) [Bom91, Kub97, Zuo99, Gre01, Hof01, Liu02, Riz04, Ma04, Dal05a, Sat06]. Either in ANM or in nuclei, the two species acquire different effective masses. This property is quantified by the difference $\Delta m^*(I) = m^*_{\rm n}(I) - m^*_{\rm p}(I)$, where $I = (\rho_{\rm n} - \rho_{\rm p})/(\rho_{\rm n} + \rho_{\rm p})$ is the isospin asymmetry while $\rho_{\rm n}$ and $\rho_{\rm p}$ denote neutron and proton densities, respectively. Note that the different effective masses m^* discussed in the following always refer in fact to the ratio m^*/m, where m is the bare nucleon mass. The latter is taken to be the same for neutrons and protons.

This effective-mass splitting, though, is only one of a wealth of quantities which can be subject to comparison between ab-initio predictions and EDF models. In this chapter we present results of a classical yet long unused test: the separation of infinite Symmetric Nuclear Matter (SNM) potential energy per particle into spin-isospin channels.

We shall also pay particular attention to controlling instabilities (i.e. non-physical spontaneous breaking of spin, isospin and/or spatial symmetries), and correlate $\Delta m^*(I)$ with *vector* properties of the functional. We thus investigate the behavior of the latter with respect to the breaking of time-reversal invariance and the onset of spin polarization, looking for an overall consistency check of its spin-isospin content. Indeed, such properties will become more and more important as one attempts to use full-fledged Skyrme functionals to study odd-mass nuclei, calculate rotational properties through self-consistent cranking calculations, or use more general dynamical methods [Ben02].

This chapter is organized as follows: in section 3.1 we present the set of Skyrme parametrizations used and examine basic properties of nuclear matter and finite nuclei. From then on, in section 3.2 we perform a more detailed study of the spin-isospin content of the functionals and of their stability against finite-size spin and isospin perturbations using response functions in the random-phase approximation (RPA).

3.1 Constraining the isovector effective mass

As mentioned in section 2.1, the nucleon effective mass m^* is a key property characterizing the propagation of (quasi)nucleons through the nuclear medium [Jeu76]. It is a reminder of the non-locality and energy dependence of the nucleon self-energy $\Sigma(k,\omega)$, themselves originating from the finite range and non-locality in time and space of the in-medium effective nucleon-nucleon interaction. Mean-field-like theories of finite nuclei or infinite matter rely on a quasiparticle approximation, and thus include only a limited part of the effects associated with the energy dependence of $\Sigma(k,\omega)$, while neglecting fragmentation of the spectroscopic strength. In this context, either microscopic [Bal99] or making use of phenomenological interactions or functionals [Ben03b], EDF methods do not correspond to a naive Hartree-Fock theory and always amount to renormalizing a certain class of correlations into the effective vertex. However, the energy dependence of the self-energy arising from the

correlations only influences the position of the quasi-particle peak energy.

Let us recall that our approach of the nuclear EDF method is to aim, ultimately, at building functionals which reproduce desired observables at the multi-reference level (MR-EDF), i.e. "beyond the mean field". We thus have to "leave room" for corrections arising from correlations added on top of the single-reference (SR) calculations which we use as an exploration tool.

Thus, the effective mass adjusted at the pure mean-field level is not expected to generate single-particle spectra matching exactly experimental data extracted through binding energy differences from neighboring odd-mass nuclei. In particular, the coupling of single-particle motion to surface vibrations in closed-shell nuclei is known to increase the density of states at the Fermi surface and thus the effective mass [Ber80, Lit06, Gor03]. An isoscalar effective mass $m^*_{\rm s}$ lying in the interval 0.7/0.8 in SNM, is able to account for a good reproduction of both isoscalar quadrupole giant resonances data in doubly closed-shell nuclei [Liu76] and of single-particle spectra in neighboring ones provided particle-vibration coupling has been properly included. When the latter coupling is taken into account, the effective mass becomes greater than one for states near the Fermi surface. Certainly, a lot remains to be done to understand these features microscopically in more involved cases [Cha06b]. This is not only true for mid-shell nuclei where the coupling to both rotational and vibrational states can be important, but also for exotic nuclei where the coupling to the continuum becomes crucial and where shape coexistence and/or large amplitude motion appear more systematically.

In very exotic systems, the isovector behavior of $m^*_{\rm p}$ and $m^*_{\rm n}$ should play an important role. However, so far, no experimental data from finite nuclei has allowed a determination of the effective mass splitting as a function of neutron richness. In this context, ab-initio calculations of ANM are of great help. Non-relativistic Brueckner-Hartree-Fock (BHF) calculations, with or without three-body force, and, with or without rearrangement terms in the self-energy, predicted $\Delta m^*(I)$ to be such that $m^*_{\rm n} \geq m^*_{\rm p}$ in neutron-rich matter, that is, for $I \geq 0$. Such a conclusion was also reached by calculating the energy dependence of the symmetry potential (the Lane potential [Lan62]) within a phenomenological formalism [Li04a]. The latter result was confirmed by microscopic Dirac-Brueckner-Hartree-Fock (DBHF) calculations [Sam05]. The situation regarding the prediction of the effective mass splitting was complexified due to an apparent contradiction between results obtained from BHF [Bom91, Zuo99] and DBHF calculations [Hof01]. However, the situation was finally clarified in Refs. [Ma04, Dal05a] where the importance of the energy dependence of the self-energy and the need to compare the non-relativistic effective mass with the vector effective mass in the relativistic framework [Jam89] were pointed out.

Thus, the sign of the splitting is rather solidly predicted. However, its amplitude is subject to a much greater uncertainty. Starting from that observation, the goal of the present section is to study the impact of the effective-mass splitting on properties of exotic nuclei predicted by Skyrme-EDF calculations. As far as the effective-mass splitting is concerned, one expects consequences onto structure properties of neutron-rich nuclei. As a relatively large asymmetry may be necessary to reveal the influence of the splitting, data from nuclei not yet studied experimentally should provide crucial information in that respect. As the effective mass governs the density of states at the Fermi surface (together with the spin-orbit and the tensor forces),

the amplitude of the splitting may influence properties such as masses and single particle properties of exotic nuclei, the evolution of isotopic shifts across neutron-rich closed-shell nuclei or shell corrections in superheavy nuclei around the ($N = 184, Z = 120$) island of stability [Ben99a, Kru00, Ben01, Ber01]. Also, neutron and proton correlations beyond the mean-field should develop rather differently depending on the direction and amplitude of the effective-mass splitting. This could be true for static and dynamical pairing correlations as well as for the coupling to vibrational and rotational states. Finally, the effective mass splitting should leave its fingerprint onto the characteristics of isovector vibrational states of different sorts in neutron-rich nuclei [Paa05].

3.1.1 Fitting protocol

Trying to keep a coherence, throughout this work, in the way we construct Skyrme functionals, we take the fitting protocol used to define the SLy functionals [Cha97, Cha98] as a basis for the present Study. Also, we pay attention to the fact that any improved or complexified functional includes all features validated by the SLy ones.

We presently take the SLy5 parametrization as a starting point. Thus, the two-body part of the center of mass correction is omitted whereas the $\mathbb{J}^2$ terms are fully kept. The spin-orbit term is the standard one, with a single parameter adjusted on the splitting of the $3p$ neutron level in ^{208}Pb.

Within this general scheme, we have built a series of three new Skyrme interaction parametrizations, denoted hereafter f_-, f_0 and f_+. The departures from the SLy protocol considered presently are (i) a better control of spin-isospin instabilities via Landau parameters (ii) the use of two density-dependent zero-range terms [Coc04] (iii) a constraint on the isovector effective mass, such that, in neutron-rich systems, $m^*_\mathrm{n} < m^*_\mathrm{p}$ for f_-, $m^*_\mathrm{n} = m^*_\mathrm{p}$ for f_0 and $m^*_\mathrm{n} > m^*_\mathrm{p}$ for f_+.

With two density dependent terms, the compressibility and the isoscalar effective mass are no longer bound together and can be chosen independently. However, this is not directly used here and an isoscalar effective mass of $m^*_\mathrm{s} = 0.7$, close to the SLy5 value, is chosen for the three parametrizations f_-, f_0, f_+. The additional freedom brought about by the second density-dependent term is only used to adjust more easily the high-density part of the PNM EOS (see below). In the end, the only parameter subject to variation between f_-, f_0 and f_+ is the isovector effective mass m^*_v which, m^*_s being constant, drives the splitting $\Delta m^*(I)$.

In the present work, we use the SLy5 interaction as a reference, and include a comparison with the LNS parametrization [Cao06] which was also built to match the splitting of effective masses and the neutron matter EOS predicted by BHF calculations. The SkP interaction [Dob84], initially built for the study of pairing effects, will be used for a special purpose in the discussion about instabilities.

3.1.2 Elementary properties of studied functionals

As we focus on the behavior of effective masses m^*_q with isospin asymmetry, we recall that these quantities are related to the dependence of the energy density functional,

Table 3.1: Infinite nuclear matter properties of the Skyrme functionals quoted in the text. The quantities $\rho_{\rm sat}$ and $\mathcal{E}/A$ denote the density and energy per particle at saturation in SNM. The symmetry energy and the compressibility (for symmetric matter) are respectively 32 MeV and 230 MeV for SLy5 and all f_x parametrizations. In the case where $m^*_{\rm s} \sim 0.7$, $\kappa_{\rm s} \sim 0.43$, so we have $\Delta m^* > 0$ if $\kappa_{\rm v} \gtrsim 0.43$.

Parametrization	$\rho_{\rm sat}$	$\mathcal{E}/A$	$m^*_{\rm s}$	$\kappa_{\rm v}$	$m^*_{\rm v}$	Δm^*
SLy5	0.161	-15.987	0.697	0.25	0.800	-0.182
f_-	0.162	-16.029	0.700	0.15	0.870	-0.284
f_0	0.162	-16.035	0.700	0.43	0.700	0.001
f_+	0.162	-16.036	0.700	0.60	0.625	0.170
LNS	0.175	-15.320	0.825	0.38	0.727	0.227
SkP	0.170	-16.590	1.030	0.32	0.760	0.418

Eqs. C.29–C.32, on kinetic densities τ_q, as

$$\begin{aligned} \frac{\hbar^2}{2m^*_q(I)} &= \frac{\partial \mathcal{H}}{\partial \tau_q} = \frac{\hbar^2}{2m} + C^\tau_0\ \rho_0 + qI\ C^\tau_1\ \rho_0 \\ \frac{m}{m^*_q(I)} &\equiv \frac{m}{m^*_{\rm s}} + qI\ \left(\frac{m}{m^*_{\rm s}} - \frac{m}{m^*_{\rm v}}\right) \end{aligned} \tag{3.1}$$

where ρ_0 is the scalar-isoscalar density and $q = +1, -1$ respectively for neutrons and protons. The splitting of effective masses, quantified by

$$\frac{\Delta m^*(I)}{m} = \frac{m^*_{\rm n}(I)}{m} - \frac{m^*_{\rm p}(I)}{m}, \tag{3.2}$$

is governed by the isoscalar and isovector effective masses

$$\frac{m}{m^*_{\rm s}} = 1 + \tfrac{2m}{\hbar^2}\ C^\tau_0\ \rho_0 \equiv 1 + \kappa_{\rm s}, \tag{3.3}$$

$$\frac{m}{m^*_{\rm v}} = 1 + \tfrac{2m}{\hbar^2}\ (C^\tau_0 - C^\tau_1)\ \rho_0 \equiv 1 + \kappa_{\rm v}. \tag{3.4}$$

We use the usual convention for the isovector effective mass, which stems from its definition through the enhancement factor $\kappa_{\rm v}$ of the Thomas-Reiche-Kuhn sum rule [Boh79]. However, $m^*_{\rm v}$ and $\kappa_{\rm v}$ are *not* isovector quantities in the sense of isovector couplings of the functional.

In the following, we shall discuss the value of $\Delta m^*(I)$ at $I = 1$, which we note Δm^* in the following, for the sake of brevity. We have

$$\frac{\Delta m^*}{m} = \frac{2(\kappa_{\rm v} - \kappa_{\rm s})}{(1+\kappa_{\rm s})^2 - (\kappa_{\rm v} - \kappa_{\rm s})^2}, \tag{3.5}$$

such that $\Delta m^* > 0$ for $\kappa_{\rm v} > \kappa_{\rm s}$, or equivalently $m^*_{\rm v} < m^*_{\rm s}$, or $C^\tau_1 < 0$.

Bulk properties of f_x parametrizations are displayed in Table 3.1. We note that, while the position of the saturation point varies little between our parametrizations

(SLy5 and f_x), this consistency is lost in the case of LNS and SkP. These properties depend on the observables used in the fitting procedure. In the case of LNS, the saturation point relates to an Extended Brueckner-Hartree-Fock (EBHF) calculation [Zuo99], predicting values of $(\mathcal{E}/A)_{\rm sat}$ and $\rho_{\rm sat}$ which are larger than empirical ones. A similar but lesser trend is observed for SkP. In this case it seems to be correlated with the choice of effective masses and their interplay with other parameters of the interaction. Indeed, binding energies computed with SkP compare satisfactorily with experimental ones, while LNS suffers in this respect from the lack of readjustment of the saturation point on nuclear data. As it has been shown in Ref. [Ber05], nuclear binding energies are highly sensitive to the choice of the energy at saturation, which is therefore constrained to a very tight interval if one wants to reproduce such quantities. This constraint is especially tight compared to the uncertainty of ab-initio predictions. Despite the fit of surface properties ($C_0^{\Delta\rho}$ parameter) on a set of nuclear data, the accuracy of binding energies predicted by LNS is of the order of 5%, to be compared with less than 1% for SLy5.

3.1.3 Properties of the nuclear matter EOS

It is interesting to note that SLy parametrizations were fitted to PNM EOS with the idea of improving isospin properties of the functionals. One consequence was to generate functionals with $\Delta m^* < 0$, in opposition to ab-initio predictions. On the other hand, older functionals such as SIII [Bei75a] and SkM* [Bar82b], which were not fitted to PNM, had $\Delta m^* > 0$. The same exact situation happens for the Gogny interaction [Cha06a]. Thus, improving global isovector properties (EOS) seems to deteriorate those related to single-particle states ($m^*_{\rm v}$) with currently used functionals. This can be better understood by examining the expressions for SNM and PNM EOS:

$$\frac{\mathcal{E}}{A}(\rho_0, I=0) = \frac{3}{5}\frac{\hbar^2}{2m}\left(\frac{3\pi^2}{2}\right)^{2/3}\rho_0^{2/3} + C_0^\rho(\rho_0)\,\rho_0 + C_0^\tau\frac{3}{5}\left(\frac{3\pi^2}{2}\right)^{2/3}\rho_0^{5/3}, \quad (3.6)$$

$$\frac{\mathcal{E}}{A}(\rho_0, I=1) = \frac{3}{5}\frac{\hbar^2}{2m}\left(3\pi^2\right)^{2/3}\rho_0^{2/3} + [C_0^\rho(\rho_0) + C_1^\rho(\rho_0)]\rho_0 + [C_0^\tau + C_1^\tau]\,\frac{3}{5}\left(3\pi^2\right)^{2/3}\rho_0^{5/3}. \quad (3.7)$$

If $C_t^\rho(\rho_0)$ coefficients only contain one low power of the density ($\propto \rho_0^{1/6}$), the latter influences low-density parts of the EOS more than high-density ones. The effective mass term then determines the high-density part of the EOS. In SNM, this translates into the well-known relation between $m^*_{\rm s}$ and the incompressibility K_∞ [Cha97, Cha98]. In the case of PNM, the EOS above $\rho_{\rm sat}$ is then mostly fixed by the term proportional to $C_0^\tau + C_1^\tau$ in Eq. (3.7), and any attempt to use the density dependence to counteract its effects, results in a very strong constraint on the latter. This in turn degrades the behavior of the functional at and below saturation density and the fit to properties of finite nuclei. We recall at this point that the condition $\Delta m^* > 0$ corresponds to $C_1^\tau < 0$, which drives the high-density PNM EOS down and explains why usual Skyrme functionals predict either a collapse of the PNM EOS if $\Delta m^* > 0$, or, like the SLy functionals fitted to PNM EOS, the wrong sign of the effective mass splitting in neutron rich matter.

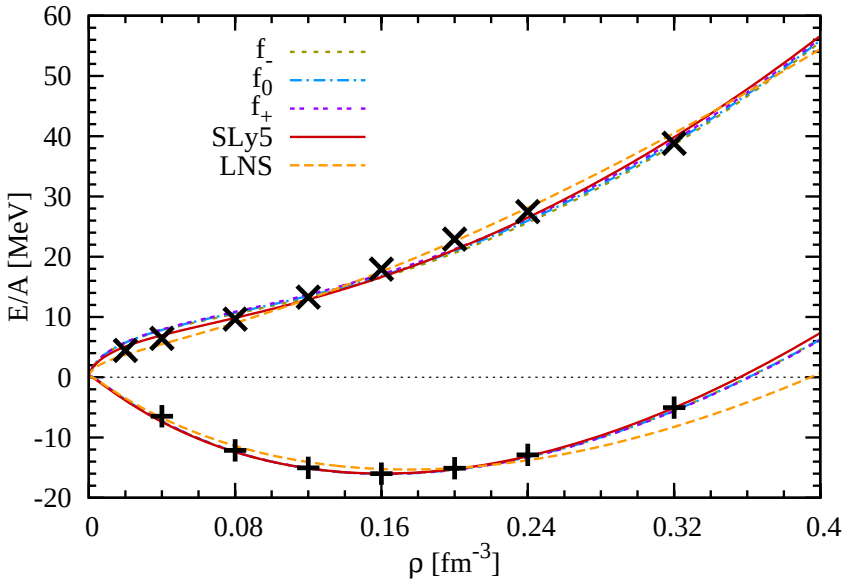

Figure 3.1: SNM and PNM EOS as given by Skyrme functionals presently discussed (see text), compared with VCS results by Akmal *et al.* [Akm98] ($\times$: PNM, $+$: SNM).

If $C_t^\rho(\rho_0)$ coefficients contain an additional density dependence with a higher power, the previous discussion does not apply: using two density-dependent terms in the functional ($\propto \rho_0^{1/3}; \rho_0^{2/3}$) [Coc04] allowed us to construct (f_-, f_0, f_+) with a good fit to PNM EOS, a free choice of effective masses and satisfactory nuclear properties.

The previous discussion already shows the type of problems and information arising from our attempt to improve on the fitting protocol of SLy functionals by using more inputs from ab-initio calculations. Now, Fig. 3.1 shows SNM and PNM EOS as obtained from (f_-, f_0, f_+, SLy5) and as predicted by Variational Chain Summation (VCS) methods [Akm98]. At this point, one can see that the four parametrizations (f_-, f_0, f_+, SLy5) reproduce both microscopic EOS with the same accuracy. However, it remains to be seen whether or not this translates into identical global spin-isospin properties and into similar nuclear structure properties.

3.1.4 Effects on properties of nuclei

We now study the effects of the variation of the isovector effective mass on selected properties of spherical nuclei. We start with HF single-particle energies, then binding energies, ending with a short sum-rule based analysis of isovector giant resonances.

For computations of open-shell nuclei, we use, in the particle-particle channel, a local functional with a density dependent form factor (mixed surface and volume, i.e. $c = 1/2$ in Eq. (2.98)). The local HFB equations are renormalized following the procedure developed by Bulgac and Yu.

The strength V_0 is adjusted to the mean pairing gaps of six semi-magic nuclei (neutron gaps in ^{120}Sn, ^{198}Pb, ^{212}Pb and proton gaps in ^{92}Mo, ^{144}Sm and ^{212}Rn). In

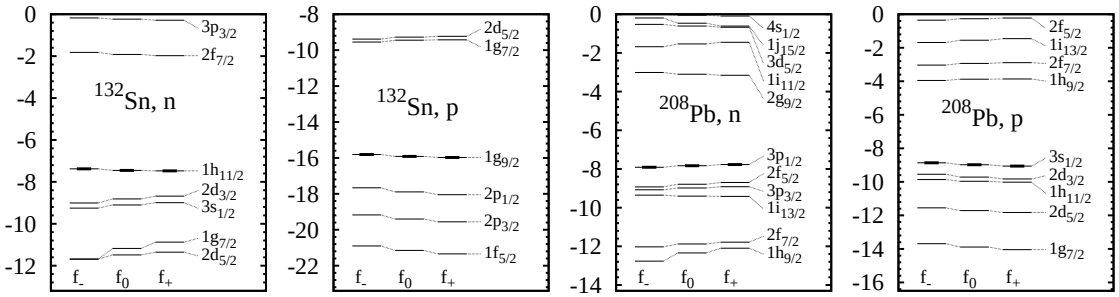

Figure 3.2: Single-particle energies [MeV] in ^{132}Sn and ^{208}Pb computed with indicated interactions. Thick lines indicate the Fermi level ε_F.

this procedure we compute theoretical spectral gaps defined as

$$\langle\Delta\rangle_{\rm th} \;=\; \left[\sum_k \Delta_{k\overline{k}} u_k v_k\right] \Big/ \left[\sum_k u_k v_k\right], \tag{3.8}$$

$\Delta_{k\overline{k}}$ being a pairing field matrix element between canonical states and u_k, v_k the corresponding quasiparticle amplitudes, and adjust each of them upon an experimental gap extracted through a five point difference formula from masses of neighboring nuclei, as suggested in Ref. [Dug01b].

Single-particle energies

Effective masses are known to control the average density of single-particle states. It is thus interesting to check to what extent such statement applies to neutron-rich nuclei when varying $m^*_{\rm v}$. In this part of the study, we are mainly interested in evaluating the change in the single-particle energies generated by the functional for different splittings and not directly by a comparison with experimental results.

Single-particle energies in ^{132}Sn and ^{208}Pb are plotted on Fig. 3.2. The general trend followed by neutron states with increasing Δm^* (from f_- to f_+) corresponds to an increase of the density of neutron states: they tend to come closer to the Fermi energy $\varepsilon_{\rm F}$; notable exceptions being both neutron $1i$ levels in ^{208}Pb. The opposite behavior is observed in proton levels, which spread away from $\varepsilon_{\rm F}$ with increasing Δm^* (except for the proton $1h_{11/2}$ level). However, these trends are rather marginal, which can be linked with the moderate bulk asymmetry of these nuclei ($I = (N-Z)/A = 0.24$ for ^{132}Sn and 0.21 for ^{208}Pb). This moderate asymmetry means that the isovector term in the definition of the effective mass (Eq. (3.1)) is weakly probed.

Let us therefore examine similar spectra for more neutron-rich nuclei, i.e. ^{78}Ni ($I = 0.28$, experimentally observed [Hos05]) and ^{156}Sn ($I = 0.36$). The nucleus ^{156}Sn is used as an example of an extremely asymmetric system, even beyond the reach of planned radioactive beam facilities [sp206]. We observe on the rightmost panel of Fig. 3.3 that the effect of Δm^* on proton single-particle energies at $Z = 50$ is more pronounced in ^{156}Sn than it was in ^{132}Sn. The modification of level densities appears quite clearly in ^{78}Ni also, while neutron levels around $\varepsilon_{\rm F}$ in ^{156}Sn are shifted in a slightly more disordered way.

High-ℓ/low-n orbitals (n, ℓ being respectively the principal and orbital quantum numbers) are in fact more sensitive to variations of the spin-orbit field than to Δm^*

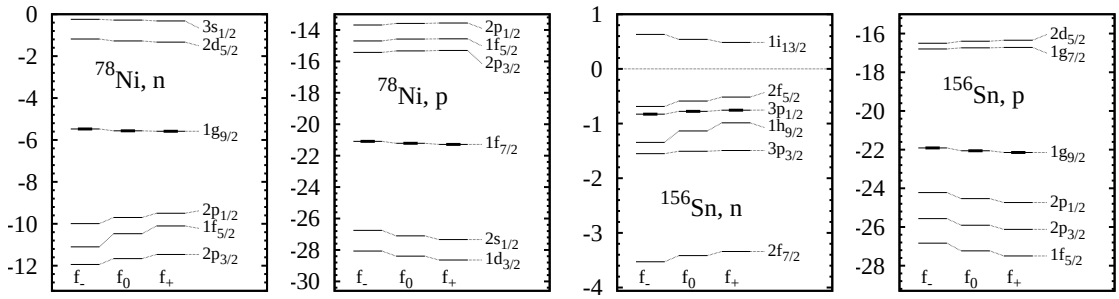

Figure 3.3: Same as Fig. 3.2 in ^{78}Ni and ^{156}Sn.

because of their spatial localization near the surface of the nucleus. The spin-orbit field is modified between functionals by the interplay between $\mathbb{J}^2$-term coefficients and effective mass parameters, since these both depend on the same non-local terms of the Skyrme interaction [Dob06]. The spin-orbit interaction ($\rho\boldsymbol{\nabla}\cdot\mathbf{J}$ terms in the EDF), which is subject to a slight readjustment, does affect the spectra as well. We observed, overall, a marginal increase of the spin-orbit field strength when going from f_- to f_+. This implies that while the global effect of modifying the level density is quite clearly observed when we alter the effective mass parameters, details of the spectroscopy are at least as sensitive to the terms connected to the spin-orbit field.

Pairing gaps

As an example, neutron spectral gaps are plotted on Fig. 3.4 for Sn and Pb series, up to the drip line, against experimental gaps extracted through five-point mass formulas [Dug01a, Dug01b]. The slight change in the level density translates into a modification of the pairing gaps: a higher neutron effective mass (f_+) corresponds to a denser spectrum and higher gaps. The effect, which increases with asymmetry, remains however very small, because of the limited alteration of single-particle levels seen on Figs. 3.2 and 3.3.

In the end, the effect is negligible and would be overwhelmed by any other modification of the particle-hole part of the functional. For example, variations in the detailed level scheme, could alter the shape of gaps. The pairing functional itself is a subject of current debate regarding its density dependence, regularization scheme and finite-range corrections, while the choice of observables to be compared (definition of theoretical an experimental gaps) can be improved. Most of these issues will be addressed in the following of this manuscript.

Binding energies

Let us now study the effect of the aforementioned variation of level densities and pairing gaps on binding energies. On Fig. 3.5 we show the binding energy residuals $E_{\rm th} - E_{\rm exp}$ for Sn and Pb isotopes and $N = 50$ and $N = 82$ isotones. The evolution of $E_{\rm th} - E_{\rm exp}$ along such chains is usually plagued by an underbinding of open-shell nuclei with respect to closed-shell ones which translates into an arch shape of E-residual curves. Although the variation of $m^*_{\rm v}$ seems to impact the arches, again, the effect is negligible compared to the absolute value of deviations from experiment, except in the $N = 82$ series where open-shell nuclei tend to be more underbound in

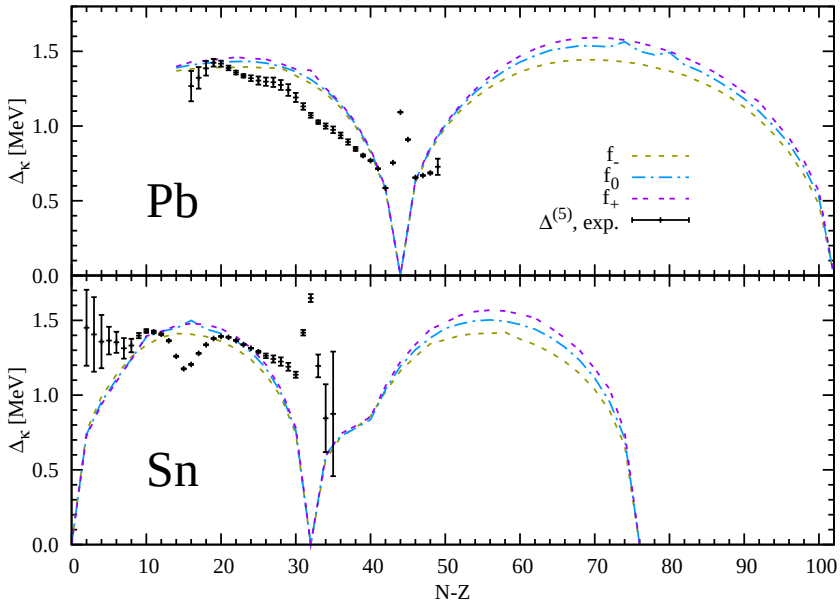

Figure 3.4: Neutron spectral gaps computed in Sn (bottom) and Pb (top) chains with parametrizations f_-, f_0, f_+, as a function of asymmetry. Experimental $\Delta^{(5)}$ gaps extracted from masses [Aud03] are plotted with error bars.

the case of f_+.

Isovector giant resonances

The isovector effective mass is usually defined from the energy-weighted sum rule $\mathfrak{m}_1$ (the Thomas-Reiche-Kuhn sum rule [Boh79]) of the isovector giant dipole resonance (IVGDR):

$$\mathfrak{m}_1(E1\ ;\ T=1) = \frac{\hbar^2}{2m}\frac{NZ}{A}\left(1+\kappa_{\rm v}\right) = \frac{\hbar^2}{2m}\frac{NZ}{A}\frac{m}{m^*_{\rm v}}, \tag{3.9}$$

which exhibits its link with the strength distribution of isovector collective modes. We perform here a schematic overview of dynamical properties of f_-, f_0, f_+ by means of results derived in Ref. [Col95]. Thanks to RPA sum rules similar to Eq. (3.9), it is possible to fit an accurate parametrization of the energy $E_1 = \mathfrak{m}_1/\mathfrak{m}_{-1}$ of isovector giant resonances in a given nucleus as a function of Skyrme parameters. Results for GDR ($L=1$) and isovector giant monopole (IVGMR, $L=0$) modes in ^{208}Pb are shown in Table 3.2, compared to experimental energies (respectively from Refs. [Rit93] and [Ere86] and corrected, as suggested in [Col95], for the shift due to the spreading of the strength by damping effects: 2 MeV for GMR, 1 MeV for GDR).

While f_- predicts both energies lower than experimental ones, values for f_0 and f_+ are compatible with experiment for the $L=0$ mode, and only f_+ approaches the experimental value for the $L=1$ mode. This suggests that values of $\kappa_{\rm v}$ corresponding to a positive value of Δm^* (equal to, or higher than 0.43 in our case) better describe isovector dynamics than lower values.

As a summary, the effect of the splitting of neutron and proton effective masses with isospin asymmetry on single-particle energies, pairing gaps and binding en-

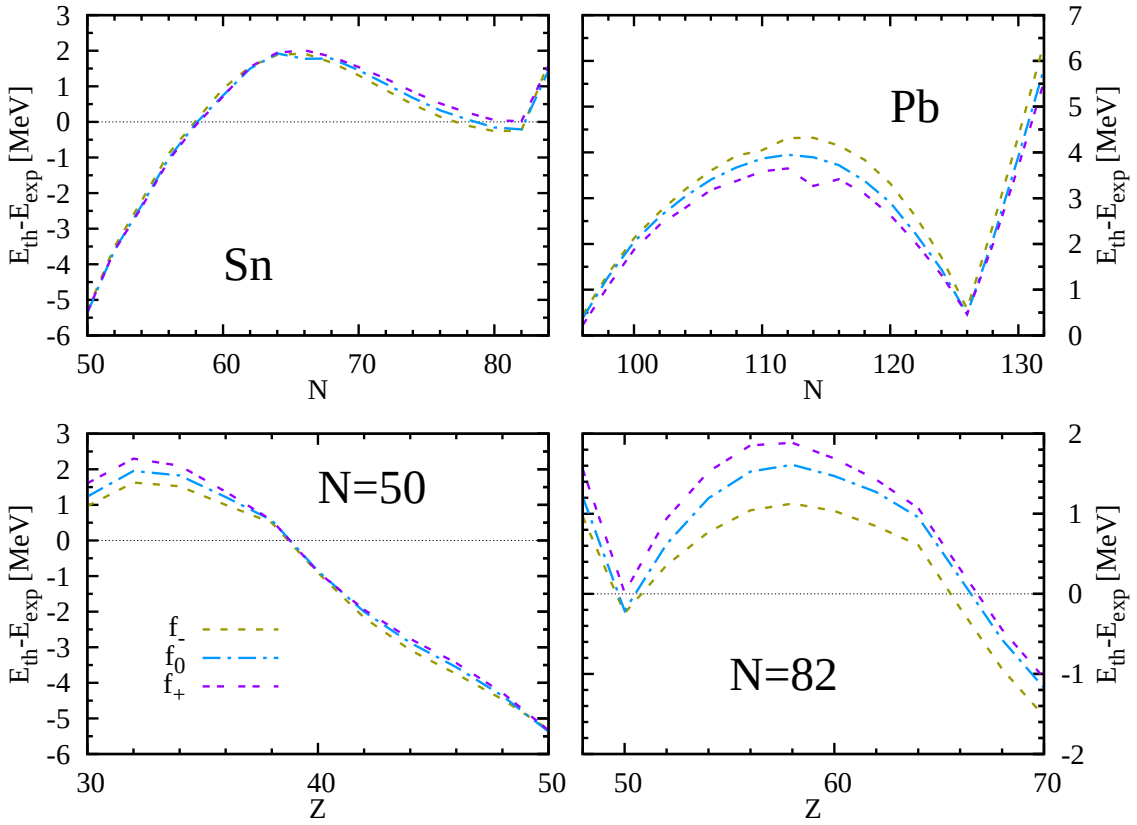

Figure 3.5: Binding energy residuals computed with interactions f_-, f_0 and f_+ for semi-magic series of nuclei, as indicated.

Table 3.2: E_1 energies of ^{208}Pb isovector giant resonances computed thanks to a sum-rule parametrization (see text), compared to experimental energy centroids. Experimental uncertainties are as indicated. We infer from figures in Ref. [Col95] the accuracy of theoretical energies computed with the fits in that reference, with respect to full RPA calculations, to be of the order of 1 MeV.

	$\kappa_{\rm v}$	$E_1(L=0,T=1)$	$E_1(L=1,T=1)$
f_-	0.15	24.55	12.68
f_0	0.43	26.43	13.60
f_+	0.60	27.25	14.01
exp. centroid		26.3 ± 1.1	14.3 ± 0.1

ergies, is noticeable and consistent, yet limited and thus hardly meaningful when compared to the overall (in)accuracy of the predictions made by the current nuclear EDF. In fact, the main reason for not seeing a dramatic modification of EDF predictions when altering Δm^* is the limited amount of strongly asymmetric nuclear matter at high enough density in the ground state of nuclei with realistic isospin as already suggested in [Gor03]. This makes the effect of the isovector effective mass rather marginal. Giant isovector resonances are certainly more fruitful to seek for an effect of a modification of Δm^*. Indeed, a sum-rule-based analysis of isovector collective modes allows a slightly more clear-cut conclusion, with a tendency to favor $\Delta m^* \gtrsim 0$. The conclusion of the phenomenological study done in this section is that, while no observable listed here strongly ask for $\Delta m^* > 0$, there is no reason to omit this constraint in future functionals, since, as already stated, ab-initio predictions for the sign of Δm^* are solid. There remains to check the intrinsic consistency of the functional in terms of other ab-initio inputs and stability criteria, which, as will be discussed below, we have found to be a concern.

3.2 Further study of infinite matter

3.2.1 Separation of the EOS into (S,T) channels

In this section, we discuss the contributions to the potential energy of SNM from the four two-body spin-isospin (S,T) channels. We compare our results with those predicted by BHF calculations [Bal06] using the Argonne v_{18} [Wir95] two-body interaction and a three-body force constructed from meson exchange theory [Gra89, Lej00].

Using projectors on spin singlet and triplet states, respectively

$$\hat{P}_{S=0} = \frac{1}{2}(1-\hat{P}_\sigma), \qquad \hat{P}_{S=1} = \frac{1}{2}(1+\hat{P}_\sigma), \tag{3.10}$$

where $\hat{P}_\sigma$ is the spin-exchange operator, and similar expressions for isospin projectors $\hat{P}_T$ using the isospin exchange operator $\hat{P}_\tau$, yields the potential energy in each (S,T) channel

$$\mathcal{E}^{ST}_{\rm pot} = \frac{1}{2}\sum_{kl}\left\langle kl\left|V\hat{P}_S\hat{P}_T\right|\overline{kl}\right\rangle\rho_{kk}\rho_{ll}, \tag{3.11}$$

where the sum on k,l runs over all HF single-particle eigenstates whereas ρ_{kk} designates the diagonal one-body density matrix. The notation $|\overline{kl}\rangle$ denotes a non-normalized but antisymmetrized two-body state. In order to compare different many-body approaches (ab-initio or EDF), we use the "potential energy" which refers to the total binding energy from which is subtracted the kinetic energy of the non-interacting particle system.

Note that due to the zero-range character of the Skyrme interaction, together with at most second-order derivative terms, only $L = 0, 1$ partial waves occur explicitly whereas higher partial waves contribute to the ab-initio EOS. We find, for

SNM,

$$\frac{\mathcal{E}^{00}_{\rm pot}}{A} = \frac{3}{160}t_2(1-x_2)\left(\frac{3\pi^2}{2}\right)^{2/3}\rho_0^{5/3}, \tag{3.12}$$

$$\frac{\mathcal{E}^{10}_{\rm pot}}{A} = \frac{3}{16}t_0(1+x_0)\rho_0 + \frac{3}{96}t_3(1+x_3)\rho_0^{1+\gamma} + \frac{3}{96}t_6(1+x_6)\rho_0^{1+\gamma'} + \frac{9}{160}t_1(1+x_1)\left(\frac{3\pi^2}{2}\right)^{2/3}\rho_0^{5/3}, \tag{3.13}$$

$$\frac{\mathcal{E}^{01}_{\rm pot}}{A} = \frac{3}{16}t_0(1-x_0)\rho_0 + \frac{3}{96}t_3(1-x_3)\rho_0^{1+\gamma} + \frac{3}{96}t_6(1-x_6)\rho_0^{1+\gamma'} + \frac{9}{160}t_1(1-x_1)\left(\frac{3\pi^2}{2}\right)^{2/3}\rho_0^{5/3}, \tag{3.14}$$

$$\frac{\mathcal{E}^{11}_{\rm pot}}{A} = \frac{27}{160}t_2(1+x_2)\left(\frac{3\pi^2}{2}\right)^{2/3}\rho_0^{5/3}, \tag{3.15}$$

where (t_i, x_i) are coefficients of the Skyrme interaction as defined in Eq. (2.78).

The coefficients occurring in Eqs. (3.12)–(3.15) stem from the antisymmetrization condition $(-)^{L+S+T} = -1$, the relative angular momentum L being even for t_{0i} and t_1 ($\mathbf{k}^2$) terms and odd for t_2 ($\mathbf{k}'\cdot\mathbf{k}$) terms. The expression of the potential energy in channels $(S,T) = (0,0)$ and $(1,1)$ is very simple since only the t_2 term contributes.

Force vs. functional

Previous statements, however, apply only to the case where the EDF is computed as the expectation value of an (antisymmetrized) effective interaction. In the more general case, it is still possible to define (S,T) channels starting from any Hartree-like functional. Indeed, the functional can always be expressed in terms of an effective non-antisymmetrized vertex and one can still plug a projector in the calculation of its matrix elements. In the pure functional case, there is however no more clear definition of partial waves, and spin-isospin channels emerge from the balance between coefficients of (iso)scalar/(iso)vector couplings (see appendix B for the formal definition).

As long as there are not enough inputs to constrain *all* degrees of freedom of a general functional, the effective-interaction approach remains as an acceptable path, and hence shall be used in the following.

Results

Results are plotted against BHF predictions on Fig. 3.6. First, one can observe that results are rather scattered. Second, the main source of binding, from $(S,T) = (0,1)$ and $(1,0)$ channels, is not well described and the detailed saturation mechanism is not captured. It is clear that, even though all four functionals reproduce perfectly PNM and SNM EOS, they do not have the same spin-isospin content, and that the latter is in general rather poor. Thus, fitting the global EOS is an important element but it does not mean that spin-isospin properties of the functional are fixed once and for all. One needs to do more and fitting ab-initio predictions of $E^{(S,T)}_{\rm pot}$ seems to be a good idea in the near future. However, one needs to make sure that the theoretical uncertainty of the data used is smaller than the expected accuracy of the

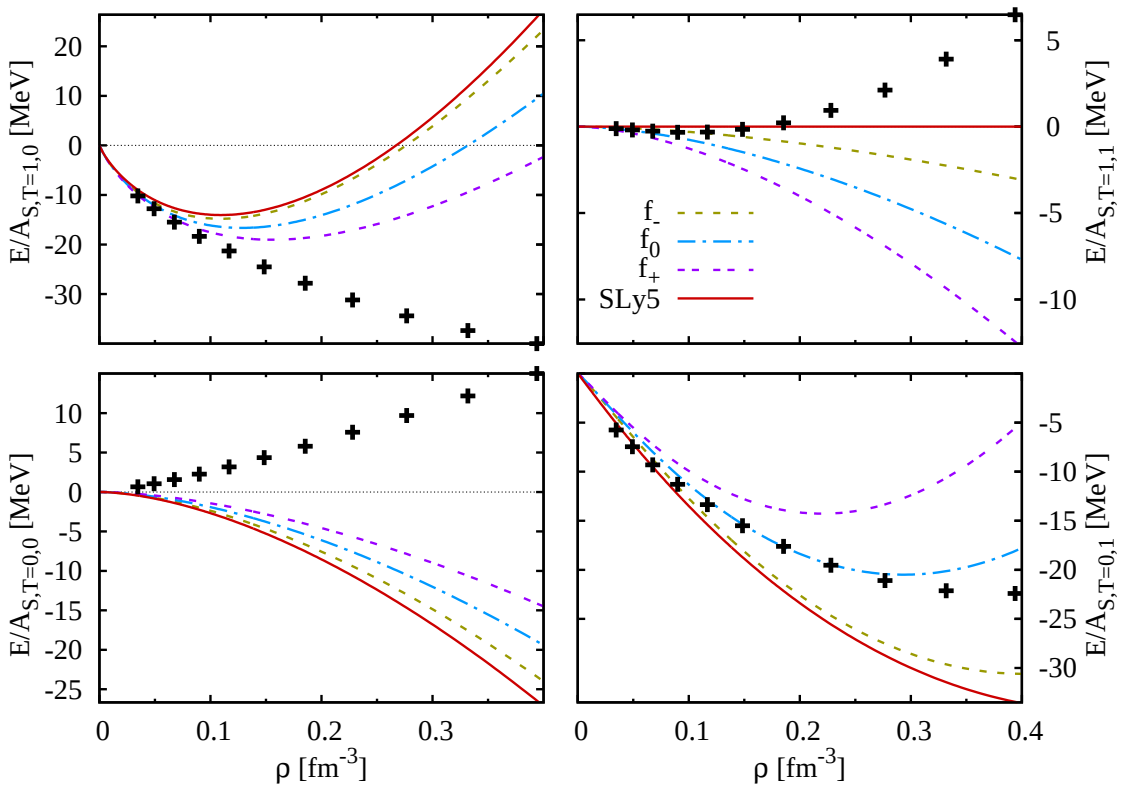

Figure 3.6: Energy per particle in each (S,T) channel for SNM, as a function of density. Crosses refer to the BHF calculations [Bal06].

fit to them. This calls for predictions from other ab-initio methods using the same two-body plus three-body Hamiltonian. Then, those ab-initio calculations should be repeated using different sets of two-body plus three-body Hamiltonians in order to provide a theoretical error bar on those predictions.

The most obvious discrepancy appears in channels $(0,0)$ and $(1,1)$ where Skyrme and BHF data have opposite signs above saturation density. The SLy5 parameter set shows a particular behavior in channel $(1,1)$ due to the choice of $x_2 = -1$ to prevent ferromagnetic instabilities in PNM. Note that in the Skyrme functional, these two channels contain contributions, of the density-independent P-wave term only. The upper-right panel of Fig. 3.6 points out the tendency of Skyrme parametrizations to be attractive in polarized PNM, and hence to cause a collapse of its EOS at high density. At lower densities, BHF data show a distinctive behavior, being slightly attractive below $\rho_{\rm sat}$ and repulsive above. This feature cannot be matched by the standard Skyrme functional which exhibits a monotonous behavior as a function of density in this channel, regardless of the value of (t_2, x_2).

It is also worth noticing that the failure in channel $(1,1)$ becomes more and more prominent as one makes Δm^* closer to the ab-initio predictions (parametrization f_+). The effective masses being governed by the momentum-dependent terms of the interaction, it is not a surprise that the modification of the former impacts channels $(0,0)$ and $(1,1)$. What changes in the coefficients entering Eqs. (3.12-3.15) stems only from the variation of $m^*_{\rm v}$ and the associated rearrangement of parameters in the functional, most notably the $C^{\Delta\rho}_{0,1}$ coefficients closely related to surface and surface-symmetry energies. The relatively tight requirements on the

latter imply that the four parameters of the non-local terms in the standard Skyrme energy functional would be dramatically overconstrained if we were to add the (S,T)-channel decomposition in the fitting data.

In the end, the rather poor properties of the functional in channels $(0,0)$ and $(1,1)$, the degradation of the latter as the effective mass splitting is improved, the idea of using ab-initio (S,T) contributions in the fit, call, at least, for a refinement of the odd-L term in the sense either of a density dependence or of a higher-order derivative term. The latter being prone to numerical instabilities and interpretation problems, a density-dependent $\mathbf{k}' \cdot \mathbf{k}$ term remains as one of the next potential enhancements to be brought to the Skyrme EDF (density-dependent derivative terms have been considered already, but with a focus on even-L terms of the form $t_4(\mathbf{k}^2 + \mathbf{k}'^2)\rho_0^\beta$ [Far97]).

Phenomenological constraints on gradient terms are mainly related to the surface of nuclei, i.e. low-density regions. One can expect that, to first order, BHF data in channel $(S,T) = (1,1)$ can be matched with an extended functional while retaining a good agreement with other (experimental) data. It is less clear in channel $(0,0)$ but further exploration of the extended parameter space may bring Skyrme and BHF data in better agreement.

3.2.2 RPA linear response functions and the diagnosis of instabilities[1]

We attempt here to study general stability conditions of SNM with respect to finite-size density, spin, isospin and spin-isospin perturbations. Our basic ingredient is the RPA response function [Fet71] derived analytically by Garcia-Recio et al. in Ref. [GR92] for the central part of the Skyrme interaction. Recent work was done to incorporate the effect of the spin-orbit part, which was found to be quite negligible [Mar06], and will be omitted in the present work. One starts by defining a one-body perturbing operator

$$\mathcal{Q}^{(\alpha)} \;=\; e^{-i\omega t} \sum_a e^{i\mathbf{q}\cdot\mathbf{r}_a}\, \Theta_a^{(\alpha)}, \tag{3.16}$$

where a indexes particles in the system. The one-body spin-isospin operators $\Theta_a^{(\alpha)}$ are defined as

$$\Theta_a^{\mathrm{ss}} = 1_a, \quad \Theta_a^{\mathrm{vs}} = \hat{\boldsymbol{\sigma}}_a, \quad \Theta_a^{\mathrm{sv}} = \hat{\tau}_a, \quad \Theta_a^{\mathrm{vv}} = \hat{\boldsymbol{\sigma}}_a\hat{\tau}_a, \tag{3.17}$$

where we use the denomination of (iso-)scalar (s) and (iso-)vector (v) channels in order to distinguish the particle-hole spin-isospin channels from the two-body-coupled (particle-particle) (S,T) channels discussed in the previous section. In Eq. (3.17) and the following, the first (second) subscripts denotes the spin (isospin). We then

[1] This chapter is an adapted and corrected version of Ref. [Les06]. Indeed, an an error was made in the derivation of the RPA residual interaction, which, when corrected, yields an additional contribution to the terms discussed. The magnitude of this contribution (and its variation) is smaller than the one discussed but not completely negligible. The quantitative results are modified in a way which does not affect the validity of the method proposed for diagnosing finite-size instabilities. Details of the discussion have been updated accordingly.

study the response to each type of perturbation separately through the *response functions*

$$\Pi^{(\alpha)}(\omega,\mathbf{q}) = \frac{1}{\Omega}\sum_{\nu}|\langle\nu|\mathcal{Q}^{(\alpha)}|0\rangle|^2\left(\frac{1}{\omega-E_{\nu 0}+i\eta}-\frac{1}{\omega+E_{\nu 0}-i\eta}\right), \quad (3.18)$$

at the RPA level, where Ω stands for a normalization volume and $|\nu\rangle$ is an excited state of the system, $E_{\nu 0}$ being the corresponding excitation energy. Since the central residual interaction does not couple the channels defined through Eq. (3.17) in SNM, we can indeed consider each channel separately.

The response function $\Pi^{(\alpha)}$ can be seen as the propagator of the collective perturbation, or polarization propagator, i.e. the positions of its poles in the (q,ω) plane yield the dispersion relation of the mode. In this formalism, the onset of an unstable mode is marked by the occurrence of a pole in $\Pi^{(\alpha)}$ at $\omega = 0$, corresponding to zero excitation energy. Such a pole marks the transition between stable (with our convention, $\Pi^{(\alpha)} < 0$) and unstable ($\Pi^{(\alpha)} > 0$) domains. Unstable modes of infinite wavelength ($q = 0$) are those traditionally discussed in terms of Landau parameters. A pole at finite q characterizes a system which is unstable with respect to the appearance of a spatial oscillation of a given type (density, spin, isospin or spin-isospin) with a given wavelength $\lambda = 2\pi/q$. In unstable domains, an imaginary-energy mode appears.

The evaluation of response functions calls for the residual interaction $\hat{V}^{\rm ph}$, defined as the second-order functional derivative of the energy with respect to the density matrix. Its momentum-space matrix elements can be written, using total momentum conservation, as [GR92]:

$$\begin{aligned}\hat{V}^{\rm ph}(\mathbf{q}_1,\mathbf{q}_2,\mathbf{q}) &= \langle \mathbf{q}_1\ \mathbf{q}_2+\mathbf{q}|\ \hat{V}^{\rm ph}\ |\mathbf{q}_1+\mathbf{q}\ \mathbf{q}_2\rangle,\\ &= \hat{W}_1(q)+\hat{W}_2(q)\ (\mathbf{q}_1-\mathbf{q}_2)^2, \end{aligned}\quad (3.19)$$

with

$$\begin{aligned}\hat{W}_1(q) &= \frac{1}{4}\ [\ W_1^{\rm ss}(q)+W_1^{\rm vs}(q)\ \hat{\boldsymbol{\sigma}}_1\cdot\hat{\boldsymbol{\sigma}}_2+W_1^{\rm sv}(q)\ \hat{\tau}_1\circ\hat{\tau}_2\\ &\quad + W_1^{\rm vv}(q)\ \hat{\boldsymbol{\sigma}}_1\cdot\hat{\boldsymbol{\sigma}}_2\ \hat{\tau}_1\circ\hat{\tau}_2\ ], \end{aligned}\quad (3.20)$$

and a similar expression for $\hat{W}_2$. We find, as an expression for W_1 functions (see also appendix C.3),

$$\begin{aligned}\frac{W_1^{\rm ss}(q)}{4} &= 2C_0^{\rho,0}+C_0^{\rho,\gamma}(\gamma+2)(\gamma+1)\rho_0^{\gamma}+C_0^{\rho,\gamma'}(\gamma'+2)(\gamma'+1)\rho_0^{\gamma'}\\ &\quad -\left[2C_0^{\Delta\rho}+\frac{1}{2}C_0^{\tau}\right]\mathbf{q}^2, \end{aligned}\quad (3.21)$$

$$\frac{W_1^{\rm vs}(q)}{4} = 2C_0^{s,0}+2C_0^{s,\gamma}\rho_0^{\gamma}+2C_0^{s,\gamma'}\rho_0^{\gamma'}-\left[2C_0^{\Delta s}+\frac{1}{2}C_0^{sT}\right]\mathbf{q}^2, \quad (3.22)$$

$$\frac{W_1^{\rm sv}(q)}{4} = 2C_1^{\rho,0}+2C_1^{\rho,\gamma}\rho_0^{\gamma}+2C_1^{\rho,\gamma'}\rho_0^{\gamma'}-\left[2C_1^{\Delta\rho}+\frac{1}{2}C_1^{\tau}\right]\mathbf{q}^2, \quad (3.23)$$

$$\frac{W_1^{\rm vv}(q)}{4} = 2C_1^{s,0}+2C_1^{s,\gamma}\rho_0^{\gamma}+2C_1^{s,\gamma'}\rho_0^{\gamma'}-\left[2C_1^{\Delta s}+\frac{1}{2}C_1^{sT}\right]\mathbf{q}^2, \quad (3.24)$$

where we split the density-dependent coupling constants $C_t^\rho(\rho_0)$ and $C_t^s(\rho_0)$ following the model $C_t^\rho(\rho_0) = C_t^{\rho,0} + C_t^{\rho,\gamma}\rho_0^\gamma + C_t^{\rho,\gamma'}\rho_0^{\gamma'}$, and for W_2 functions,

$$\begin{aligned} \frac{W_2^{\rm ss}(q)}{4} &= C_0^\tau, \qquad \frac{W_2^{\rm vs}(q)}{4} = C_0^{sT}, \\ \frac{W_2^{\rm sv}(q)}{4} &= C_1^\tau, \qquad \frac{W_2^{\rm vv}(q)}{4} = C_1^{sT}. \end{aligned} \tag{3.25}$$

Given the above expression for the residual interaction, one can calculate the response function, which reads

$$\begin{aligned} \Pi^{(\alpha)}(\omega,\mathbf{q}) = 4\Pi_0 \Bigg[& 1 - W_1^{(\alpha)}\Pi_0 - 2W_2^{(\alpha)}k_{\rm F}^2\left(\overline{q}^2 - \frac{\nu^2}{1-\frac{m^*k_{\rm F}^3}{3\pi^2}\,W_2^{(\alpha)}}\right)\Pi_0 \\ & + 2W_2^{(\alpha)}k_{\rm F}^2(2\overline{q}^2\,\Pi_0 - \Pi_2) \\ & + (W_2^{(\alpha)}k_{\rm F}^2)^2\left(\Pi_2^2 - \Pi_0\Pi_4 + 4\overline{q}^2\nu^2\Pi_0^2 - \frac{2m^*k_{\rm F}}{3\pi^2}\overline{q}^2\Pi_0\right) \Bigg]^{-1}, \end{aligned} \tag{3.26}$$

where $\overline{q} = q/2k_{\rm F}$, $\nu = \omega m_{\rm s}^*/qk_{\rm F}$ and $\Pi_{0,2,4}$ are generalized Lindhard functions, see Ref. [GR92].

As already said, the limit $\mathbf{q} \to 0$ corresponds to perturbations of infinite wavelength, keeping the system homogeneous. In this limit, the residual interaction is uniquely determined by Landau parameters F_l, F_l', G_l, G_l', with $l = 0, 1$, and well known stability conditions are obtained under the form [Mig67]:

$$1 + \frac{X_l}{2l+1} > 0, \tag{3.27}$$

where X_l represents any of the Landau parameters. We have used this criterion in the fit of our parametrizations f_x, ensuring that no spin or spin-isospin instability would occur below $2\rho_{\rm sat}$. We observe that, from the point of view of Landau parameters, the most critical channel is the vector-isovector one, with associated instabilities at densities as low as $2\rho_{sat}$ (see the upper-right panel of Fig. 3.9). This behavior is linked to the attractive character of the functional in channel $(S,T) = (1,1)$ which gives rise to a collapse of spin-polarized PNM, and accordingly, a vanishing spin-isospin symmetry energy. Therefore, better reproducing the decomposition into (S,T) channels of EOS obtained from ab-initio methods is not only a matter of microscopic motivation, but also a necessity to avoid unwanted instabilities.

Beyond infinite-wavelength instabilities, we also aim at demonstrating that a more general treatment is needed to fully describe and control unstable modes which arise in the Skyrme EDF framework. Thus, contributions to the residual interaction coming from functional terms of the form $\rho\Delta\rho$ are zero for $\mathbf{q} = 0$, whereas such terms drive finite-size instabilities.

Indeed, we have observed that existing (SkP) or new parametrizations built with a high value of κ_v in order to reproduce the microscopic splitting of effective masses, tend to spatially separate protons from neutrons in spherical mean-field calculations, where enough iterations lead to states with strongly oscillating densities and a diverging energy. Following a preliminary phenomenological reasoning, we could relate this effect to the $C_1^{\Delta\rho}\rho_1\ \Delta\rho_1$ term in the functional, as this term can

Table 3.3: Values of the effective mass splitting (in nucleon mass units), and C_1^τ and $C_1^{\Delta\rho}$ coefficient, in MeV fm^5.

	f_-	SLy5	f_0	f_+	LNS	SkP
Δm^*	-0.284	-0.182	0.001	0.170	0.227	0.418
C_1^τ	22.9	23.8	-0.2	-22.0	-19.5	-41.9
$C_1^{\Delta\rho}$	5.4	16.7	21.4	29.4	33.75	35.0

energetically favor strong oscillations of the isovector density ρ_1 which arise in the case of such a spatial n-p separation.

Moreover, Eqs. (3.21-3.25) show that such a term can yield an attractive contribution to the residual interaction in the case of a short-wavelength (high q) perturbation. We found empirically that parameter sets for which this instability arises are characterized by a high value of $C_1^{\Delta\rho}$, that is $C_1^{\Delta\rho} \gtrsim 30$. However, the term proportional to $\mathbf{q}^2$ in the expression for the residual interaction contains contributions from both the isovector gradient and effective mass (C_1^τ) terms, indicating that Δm^* may also have a direct effect on the phenomenon, which is less intuitive. As seen from Table 3.3, these parameters are strongly correlated together and with the effective mass splitting Δm^* in such a way that for more positive splitting corresponds to more negative C_1^τ (which follows from the definition of effective masses, Eq. (3.1)) and more positive $C_1^{\Delta\rho}$. Given the weighting of both contributions to the residual interaction, we see that it is the attractive (and destabilizing) one from the gradient term which dominates. The effect of the isovector effective mass alone, when going towards microscopic values, is a stabilizing one, and the sole rearrangement of the isovector gradient term is the cause of the fact that a positive splitting, as required by ab-initio predictions, tends to favor instabilities.

Whereas with our fitting protocol we were unable to provide both a fully converged (and hence physically meaningful) and clearly unstable functional to illustrate the previous statements, we found that certain functionals available in the literature present the aforementioned behavior. For example, convergence problems have arisen (and have already been pointed out in another study [Ter07]) for the SkP parameter set [Dob84]. The nature of the instabilities discussed here is illustrated on the left panels of Fig. 3.7, where neutron and proton densities are plotted at various stages of execution of a self-consistent iterative procedure with SkP in ^{56}Ni. We see that strong, opposing oscillations of neutron and proton densities are formed, and steadily increase with iterations. Such a behavior happens after a seemingly converged situation for which the relative energy variation is small but almost constant over a large number of iterations and the evolution of the energy is monotonous.

The study of the linear response function in the scalar-isovector channel allows us to provide a more quantitative ground to the previous observation. By plotting critical densities (lowest density ρ_c of occurrence of a pole in $\Pi^{(\alpha)}(\omega = 0, q)$) for a given q on Fig. 3.8, we see that these critical densities can be lower for $q \approx 2.5$ to 3 fm^{-1} than for $q = 0$, reaching down to about 0.22 fm^{-3}, which is quite near to the saturation density. This is the case for SkP and LNS, with SkP having also lower critical densities at lower values of q. Accordingly, SkP is the most prone to a lack of convergence in HF calculations.

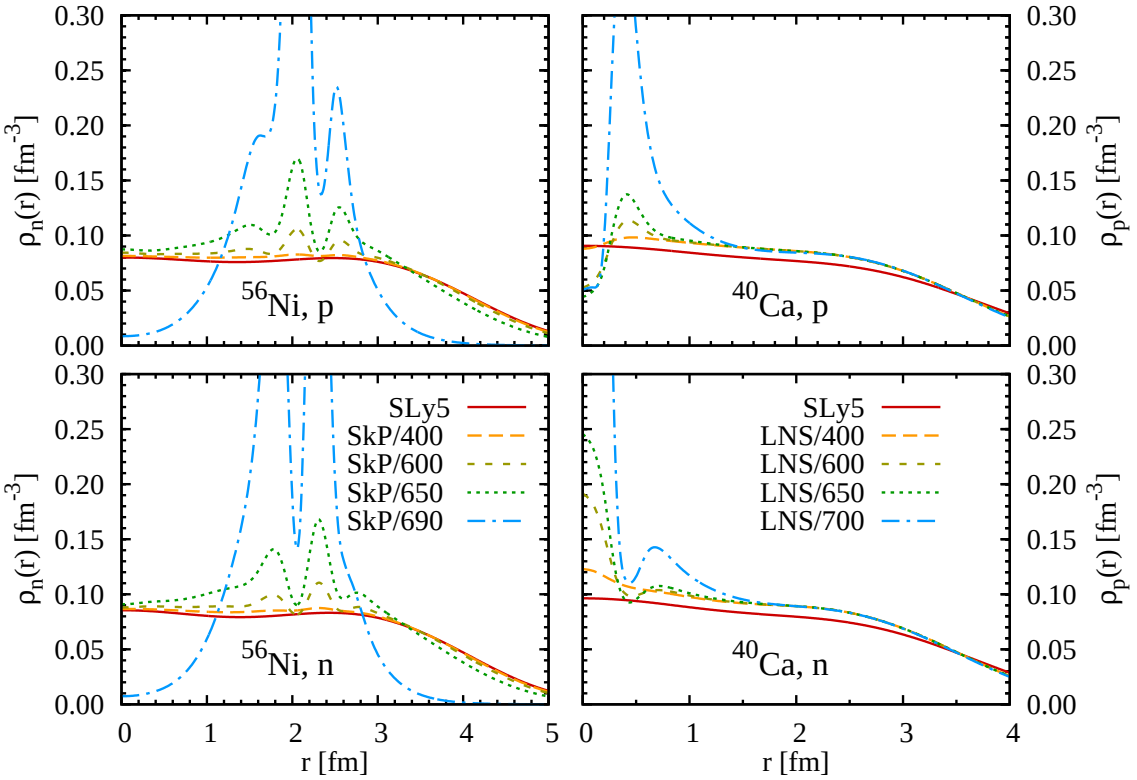

Figure 3.7: Neutron and proton densities in central regions of ^{56}Ni (left panels) and ^{40}Ca (right panels) plotted for a fully converged computation using the SLy5 interaction (solid line; relative variation of energy between iterations less than 10^{-14}) and along a series of iterations done with SkP (for ^{56}Ni) and LNS (for ^{40}Ca). The number of iterations corresponding to each curve is indicated in key. In both cases the collapse happens after a seemingly converged situation ($\sim 10^{-9}$ relative energy variation, steady over a large number of iterations indicating a nearly linear evolution of the energy), which can be mistaken for an energy minimum if too loose a convergence criterion is used.

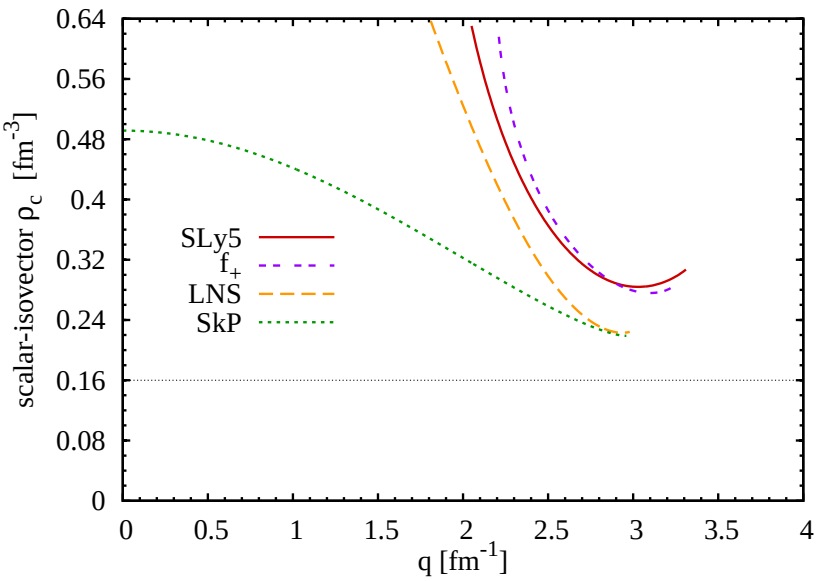

Figure 3.8: The lowest density of occurrence of a pole in $\Pi^{\mathrm{sv}}(\omega = 0, \mathbf{q})$ is plotted against the wave-number q of the scalar-isovector perturbation. The curves end at $q = 2k_F$ since the ground state can not couple to excitations with $\omega = 0, q > 2k_F$.

The link between response functions and convergence problems can indeed be understood by classifying them by their magnitude: in case of a stable but very soft mode, lack of convergence arises from the existence of a continuum of quasi-degenerate mean-field states, among which no minimization or self-consistency algorithm shall be able to decisively find an energy minimum without a considerable amount of iterations. If the soft mode becomes unstable, it causes a divergence of the energy and of other observable such as the densities. We see in the agreement between the RPA study of SNM and the observation of unstable HF calculations of nuclei a qualitative validation of our local-density approximation (LDA)-based treatment of instabilities: soft or unstable modes occurring in INM at densities in the vicinity of the saturation density, happen for the same parameter sets in finite nuclei.

On the other hand, self-consistent calculations of nuclei diverge although no unstable mode appears *strictly* at saturation density, which shows the limits of the transposition of results from INM to nuclei in a LDA scheme: it seems that nuclei probe properties of the functional up to higher densities and momenta than occur in INM at saturation.

The large number of iterations needed for the divergence to occur on Fig. 3.7 is a consequence of the limiting case embodied by SkP, such that the existence of a definite instability is highly dependent on finite-size effects (choice of the nucleus) and discretization details in the numerical procedure. If SkP is a limiting case, LNS also displays a low critical density in the scalar-isovector channel (Fig. 3.8). In this case, we observed proton-neutron separation in ^{40}Ca and for small mesh steps (0.1 fm) only (see Fig. 3.7), while it is more frequent with SkP. Our functional f_+, with a critical density of 0.30 fm^{-3}, which is barely lower than SLy5, while being slightly higher that SkP and LNS, successfully passed the test of computing a set of 134 spherical nuclei. This again demonstrates that testing finite-size instabilities

through response functions constitutes an accurate tool. The critical density (and its proximity to $\rho_{\rm sat}$, keeping in mind that values which yield instabilities in calculations of finite nuclei have been here seen to reach 0.22 fm^{-3}) appears as a good measure of the gravity of the problems one might encounter in finite nuclei. Although the actual occurrence of instabilities is subject to details of the numerical treatment, it is now clear that their origin can be traced back to the choice of parameters in the functional itself.

Nevertheless, even if a functional does not display clear instabilities but only spurious soft collective modes, convergence difficulties shall arise in SR-EDF calculations while such a mode will translate into a non-physical low-lying spectrum in a multi-reference framework. This can then yield excessive correlation energies if one systematically includes correlations in the ground state e.g. in (Q)RPA or GCM-based methods. One should thus make sure that no spurious (even remotely) soft mode occurs at saturation density in order to prevent such problems.

Having demonstrated the importance of finite-size instabilities, let us go back to discussing our original set of functionals and perform a generalization to other spin-isospin channels.

Critical densities are plotted on Fig. 3.9 for the four channels defined in Eq. (3.17). The upper-left panel shows that, while no unstable mode occurs at $q = 0$ thanks to fitting PNM EOS to relatively high density, scalar-isovector instabilities may happen little above $\rho_{\rm sat}$ for $q \approx 2.5$ to 3 fm^{-1}. In addition, there is a clear trend for lowering the critical density when Δm^* is increased, in agreement with the preliminary phenomenological reasoning on $C_1^{\Delta\rho}$. The fact that critical densities for SLy5 lie in the lower range of values obtained with our new parametrizations, despite the negative value of Δm^* it exhibits, must then be attributed to the slightly different fitting protocol involving a single density-dependent term.

Spin channels have been taken care of during the fit thanks to Landau parameters, which describe the residual interaction at $q = 0$. The result can be seen on the right panels of Fig. 3.9, where the critical densities of instability are plotted for spin-flip modes (isoscalar and isovector). As previously stated, the most dangerous $q = 0$ instability is found in the vector-isovector channel. By looking at the upper-right panel of Fig. 3.9 one can see that the critical density is however increased at higher q for our parameter sets.

An even more prominent finite-size effect can be observed in the isoscalar spin-flip channel (lower-right panel of Fig. 3.9) where, while no instability occurs at $q = 0$ as in the case of most Skyrme functionals, finite-size instabilities occur at densities lower than observed in the scalar-isovector channel for pathological parametrizations. These instabilities are linked to the $C_0^{\Delta s}\ \mathbf{s}_0 \cdot \Delta\mathbf{s}_0$ term which makes the vector-isoscalar $V_{\rm p-h}$ attractive at large q whereas it is repulsive at $q = 0$. Values of $C_0^{\Delta s}$, indeed, are as high as 45.85 and 47.32 for SLy5 and f_-, respectively. As a consequence, one can expect divergences in calculations of odd or rotating nuclei with the latter functionals if the aforementioned terms are included. In this case, though, increasing Δm^* pushes the critical density farther from $\rho_{\rm sat}$: f_0 and f_+ functionals are thus the only ones to be free from instabilities near $\rho_{\rm sat}$, f_0 being on the edge of the dangerous region and f^+ well above.

The previous discussion is valid if the full time-odd functional is taken into account. This must be stressed since $\mathbf{s}_0 \cdot \Delta\mathbf{s}_0$ terms, which drive the most critical, finite-size instabilities, have never been included in self-consistent mean field calcu-

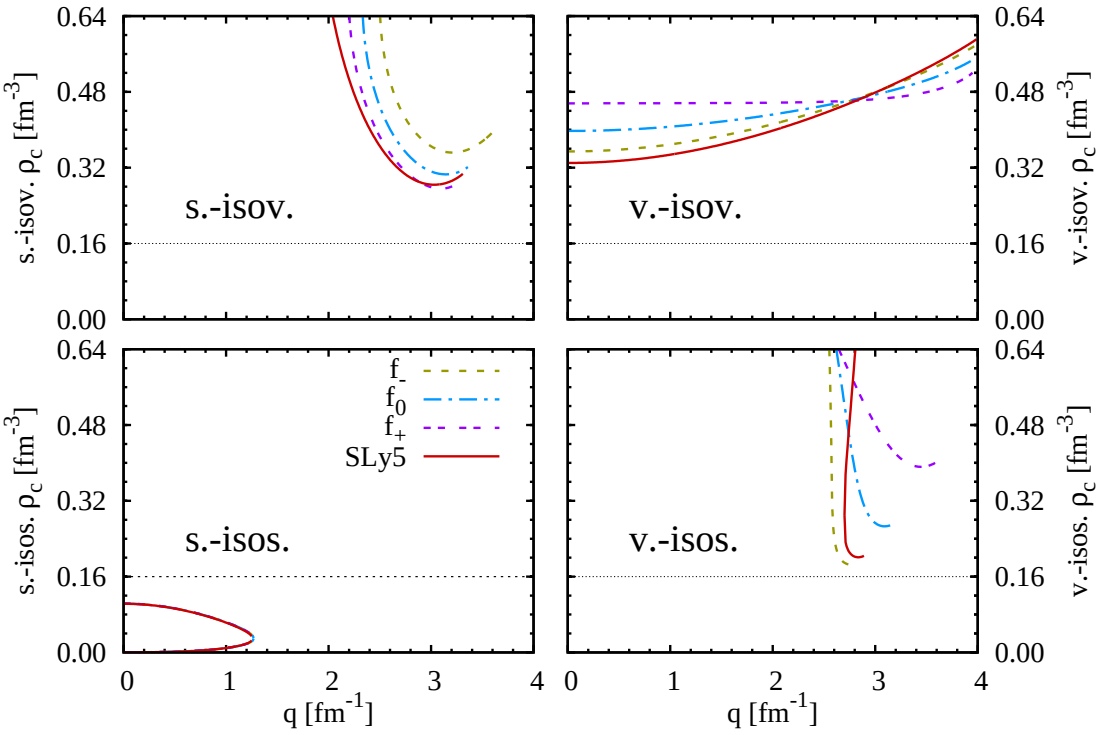

Figure 3.9: Same as Fig. 3.8, for all spin-isospin channels. The lower-left panel shows the region of spinodal instabilities below $\rho_{\rm sat}$. The domain of q covered in this case determines the size of structures formed, while the region between 0.1 and 0.16 fm^{-1} appears as metastable.

lations employing the SLy series of parametrizations. However, RPA calculations are commonly performed by computing the residual interaction matrices directly from the antisymmetrized interaction (plus rearrangement terms), which amounts to implicitly including the contribution to $V_{\rm p-h}$ from all terms in the functional [Ter05a].

The latter findings finalize the picture of a competition between spin and isospin instabilities. All in all, the strong interplay between the various quantities linked to the four parameters of the non-local terms in the Skyrme interaction does not seem to allow for a fully satisfactory compromise between stability criteria and ab-initio constraints on Δm^*. Again, we see that the non-local part of the Skyrme interaction is too simplistic to control all relevant properties. An extension with density- and momentum-dependent terms, allowing the fine-tuning of the functional at various densities, combined with the formal checks advocated in this paper, could prove to significantly improve the predictive power of Skyrme EDF.

3.3 Summary

We have built a series of Skyrme energy density functionals to study the effect of a variation of the splitting of neutron and proton effective masses with isospin asymmetry on properties of this EDF model. Thanks to the use of a second density-dependent term in the underlying effective interaction, we could cover a wide range of effective mass splittings (Δm^*) with a satisfactory fit to nuclear properties. Indeed, nuclear observable predicted by our functionals f_-, f_0 and f_+ show a remark-

able similarity, pointing out that spectra, pairing gaps and masses of bound nuclei are weakly sensitive to Δm^*, mostly due to their relatively low isospin asymmetry. Although observable were affected in a noticeable and consistent way, no clear improvement was seen when altering Δm^* either way.

Beyond this phenomenological study, we have compared the splitting of the equation of state of symmetric infinite matter into spin-isospin channels provided by our functionals and by ab-initio Brueckner-Hartree-Fock calculations. Such a comparison showed an obvious discrepancy in $(S,T) = (0,0)$ and $(1,1)$ channels, where energies predicted by Skyrme functionals and by BHF calculations have opposite signs. The inconsistency in channel $(S,T) = (1,1)$, where the Skyrme functional is attractive, translates into a collapse of polarized neutron matter EOS, related to the onset of spin-isospin instabilities at quite low density ($2\rho_{\rm sat}$). In this channel, ab-initio predictions cannot be matched (in the Skyrme effective-interaction approach) without an extension of the P-wave term. We also identified finite-size isospin instabilities caused by strong isovector gradient terms, which prevent the convergence of SR-EDF calculations. We were able to provide a firm and quantitative basis to these observations through an analysis of finite-size instabilities by use of RPA linear response functions in SNM. The latter showed that finite-size effects in the analysis of instabilities tend to always dominate.

The present study leads us to propose the systematic inclusion of consistency checks with ab-initio predictions of spin-isospin properties in the construction of our future functionals, as well as a systematic diagnosis of finite-size instabilities.

Whereas effective masses are key parameters in the discussion of nuclear single-particle spectra, the latter are determined by the particle-hole potential derived from the whole p-h functional. Most notably, spin-orbit splittings, an essential feature of nuclear structure, are another example of quantity to investigate and control in the quest for better predictive power. This is the subject of the next chapter.

Chapter 4

Tensor Part of the Skyrme Energy Density Functional

4.1 Introduction

The strong nuclear spin-orbit interaction in nuclei is responsible for the observed magic numbers in heavy nuclei [GM48, Hax49, Fee49, GM49]. While a simple spin-orbit interaction allows for the qualitative description of the global features of shell structure, the available data suggest that single-particle energies evolve with neutron and proton number in a manner that cannot be related to the geometrical growth of the single-particle potential with N and Z. Many anomalies of shell structure have been identified that do not fit into simple experimental systematics, and that challenge any global model of nuclear structure.

The evolution of shell structure with N and Z as a feature of self-consistent mean-field models has been known for long. To quote the pioneering study of shell structure in a self-consistent model performed by Beiner et al. [Bei75b], the "most striking effect is the appearance of $N = 16$, 34 and 56 as neutron magic numbers for unstable nuclei, together with a weakening of the shell closure at $N = 20$ and 28". Various mechanisms that modify the appearance of gaps in the single-particle spectra have been discussed in detail in the literature. The two most prominent ones that were worked out by Dobaczewski et al. in Ref. [Dob94], however, play mainly a role for weakly-bound exotic nuclei far from stability, as they are directly or indirectly related to the physics of loosely bound single-particle states, namely that the enhancement of the diffuseness of neutron density distribution reduces the spin-orbit coupling in neutron-rich nuclei on the one hand, and the interaction between bound orbitals and the continuum results in a quenching of shell effects in light and medium systems on the other hand. The former effect was also extensively discussed in the framework of relativistic models by Lalazissis et al. [Lal98a, Lal98b], while the latter triggered a number of studies that discussed the potential relevance of this so-called "Bogolyubov enhanced shell quenching" to explain the abundance pattern from the astrophysical r-process of nucleosynthesis [Che95, Dob95b, Pea96, Pfe97].

These two effects take place in neutron-rich nuclei. In proton-rich nuclei, the Coulomb barrier suppresses both the diffuseness of the proton density and the coupling of bound proton states to the continuum. But the Coulomb interaction itself can also modify the shell structure: for super-heavy nuclei, it begins to destabilize the nucleus as a whole. Mean-field models predict that it amplifies the shell

oscillations of the densities for incomplete filled oscillator shells, which leads to strong variations of the density profile that feed back onto the single-particle spectra [Dec99, Ben99b].

Interestingly, most theoretical papers about the evolution of shell structure from the last decade have speculated about new effects that mainly affect neutron shells in nuclei far from stability in the anticipation of the rare-isotope physics that might become accessible with the next generation of experimental facilities. The known anomalies, some of which have been known for a long time, and many more have been identified recently, concern also proton shells and already appear sufficiently close to stability that "exotic phenomena can be ruled out for their explanation" in most cases, to paraphrase the authors of Ref. [Lan03]. By contrast, this suggests that there exists a mechanism that induces a strong evolution of single-particle spectra already in stable nuclei that has been overlooked for long.

There is a prominent ingredient of the nucleon-nucleon interaction that has been ignored for decades in virtually all global nuclear structure models for medium and heavy nuclei, be it macroscopic-microscopic approaches or self-consistent mean-field methods. It is only very recently, that the systematic discrepancies between model predictions and experiment have triggered a renaissance of the tensor force in the description of finite medium- and heavy-mass nuclei.

The tensor force is a crucial and necessary ingredient of the bare nucleon-nucleon interaction [Wir95, Mac01], and consequently is contained in all *ab-initio* approaches that are available for light, mainly p-shell nuclei [Pie01b, Nav03]. One of the first experimental signatures of the tensor force was the small, but finite quadrupole moment of the deuteron. In a boson-exchange picture of the bare nucleon-nucleon interaction, the tensor force originates from the exchange of pseudoscalar pions, which have both central and tensor couplings, see for example section 2.3 in Ref. [Eis72] or appendix 13A of Ref. [Nil95]. In a nuclear many-body system, the bare tensor force induces a strong correlation between the spatial and spin orientations in the two-body density matrix. For two nucleons with parallel spins, the tensor force energetically favors the configuration where the distance vector is aligned with the spins, while for anti-parallel spins the tensor force prefers when the distance vector is perpendicular to the spins, see the discussion of Fig. 13 in Ref. [Nef03] and of Fig. 3 in Ref. [Rot04]. The authors of these papers also demonstrate very nicely the well-known fact [Bet68, Neg70] that in an approach that starts from the bare nucleon-nucleon interaction, nuclei are not bound without taking into account the two-body correlations induced by the tensor force.

In a perturbation-theory interpretation of the EDF scheme, most of the effect of the bare tensor force on the binding energy is integrated out through the renormalization of the coupling constants associated with a central effective vertex, in a similar fashion as the tensor part of the bare interaction is renormalized into the central one when going from the bare nucleon-nucleon force to a Brueckner G matrix. The tensor terms of the EDF relate to a *residual* tensor vertex, in terms of many-body perturbation theory, that gives nothing but a correction to the spin-orbit splittings, which for light p-shell nuclei might be of the same order as the contribution from the genuine spin-orbit force. The interplay of spin-orbit and tensor forces in the mean field of medium and heavy nuclei was explored in Refs. [Sch76, Goo78, Zhe91], where the particular role of spin-unsaturated shells was pointed out.

Despite the quite recent character of the emphasis seen in the literature on the

tensor part of nuclear EDF models, the effective zero-range non-local interaction proposed by Skyrme in 1956 [Sky56, Sky58a, Bel56, Sky58b] already contained a zero-range tensor force. The first applications of Skyrme's interaction in self-consistent mean-field models that became available around 1970, however, neglected the tensor force, and the simplified effective Skyrme interaction used in the seminal paper by Vautherin and Brink [Vau72] soon became the standard Skyrme interaction that was used in most applications ever since. Until very recently, there was only very little exploratory work on Skyrme's tensor force. In their early study, Stancu, Brink and Flocard [Sta77], who added the tensor force perturbatively to the SIII parametrization, pointed out that some spin-orbit splittings in magic nuclei can be improved with a tensor force. A complete fit including the terms from the tensor force that contribute in spherical nuclei was attempted by Tondeur [Ton83], with the relevant coupling constants of the spin-orbit and tensor terms adjusted to selected spin-orbit splittings in ^{16}O, ^{48}Ca and ^{208}Pb. Another complete fit of a generalized Skyrme interaction including a tensor force was performed by Liu et al. [Liu91], but the authors did not investigate the effect of the tensor force in detail, nor was the resulting parametrization ever used in the literature thereafter.

Similarly, the seminal paper by Gogny [Gog75b] on the evaluation of matrix elements of a finite-range force of Gaussian shape in an harmonic oscillator basis contains the expressions for a finite-range tensor force, which, however, was omitted in the parametrizations of Gogny's force adjusted by the Bruyères-le-Châtel group [Dec80]. It were Onishi and Negele [Oni78] who first published an effective interaction that combined a Gaussian two-body central force, a finite-range tensor force with a zero-range spin-orbit force and a zero-range non-local three-body force, which, however, also fell into oblivion.

The role of the tensor force is slightly different in Skyrme and Gogny interactions. In the Gogny force, the contributions from the central and tensor parts remain explicitly distinct, although, of course, this does not prevent a certain entanglement of their physical effects. In the context of Skyrme's functional, however, the contribution of a zero-range tensor force to the spherical mean-field state of an even-even nucleus has exactly the same form as a particular exchange term from the non-local part of the central Skyrme force.

Thus, one must always keep in mind that both the central and tensor part of the effective vertex contribute to the $\mathbf{J}_t^2$ "tensor" terms of the functional, as they will be referred to in this chapter.

In the context of relativistic mean-field models, the equivalent of the non-relativistic tensor force appears as the exchange term of effective fields with the quantum numbers of the pion, which by construction do not appear in the standard relativistic Hartree models. Only relativistic Hartree-Fock models contain this tensor force, with the first predictive parametrizations becoming available recently [Lon06].

We also mention that there is a large body of work on the tensor force in the interacting shell model, see Ref. [Fay97] for a review, that concentrates on a completely different aspect of the tensor force, namely its unique contribution to excitations with unnatural parity.

The recent interest in the effect of the tensor force in the context of self-consistent mean field models was triggered by the observed evolution of single-particle levels of one nucleon species in dependence of the number of the other nucleon species. Otsuka et al. [Ots05] proposed that at least part of the effect is caused by the proton-

neutron tensor force from pion exchange. Many groups attempt now to explain known, but so far unresolved, anomalies of shell structure in terms of a tensor force. A particularly popular playground is the relative shift of the proton $1g_{7/2}$ and $1h_{11/2}$ levels in tin isotopes, which is interpreted as the reduction of the spin-orbit splittings of both levels with their respective partners with increasing neutron number [Sch04].

Otsuka et al. [Ots06] added a Gaussian tensor force, adjusted on the long-range part of a one-pion+ρ exchange potential, to a standard Gogny force. After a consistent readjustment of the parameters of its central and spin-orbit parts, they were able to explain coherently the anomalous relative evolution of some single-particle levels without, however, being able to describe their absolute distance in energy. Dobaczewski [Dob06] pointed out that a perturbatively added tensor interaction with suitably chosen coupling constants in the Skyrme energy density functional does not only modify the evolution of shell structure, but does also improve the description of nuclear masses around magic nuclei. Then, concentrating of single-particle energies, Zalewski et al. [Zal08] adjusted the tensor and spin-orbit parameters of the Skyrme EDF on spin-orbit splittings in the Ca-Ni region, neglecting somewhat the reproduction of binding energies, which will be discussed in this study. Kortelainen et al. [Kor08] performed a singular-value decomposition analysis of the fit to single-particle energies of a general quasi-local functional, implicitly including the degrees of freedom associated with the tensor in an interaction-derived EDF. Brown et al. [Bro06a] fitted a Skyrme interaction with added zero-range tensor force with emphasis on the reproduction of single-particle spectra. While the authors appreciated the qualitatively correctly described evolution of relative level distances, they pointed out that the combination of zero-range spin-orbit and tensor forces does not and can not correctly describe the ℓ-dependence of spin-orbit splittings. Colò et al. [Col07], and Brink et al. [Bri07] added Skyrme's tensor force perturbatively to the existing standard parametrization SLy5 [Cha97, Cha98], and to the SIII [Bei75b] one, respectively. They investigated some single-particle energy differences: the $1h_{11/2}$ and $1g_{7/2}$ proton states in tin isotopes as well as $1i_{13/2}$ and $1h_{9/2}$ neutron states in $N = 82$ isotones and proposed similar parameters as in Ref. [Bro06a]. The effect of the tensor force on the centroid of the GT giant resonance was also estimated by Colò et al. using a sum-rule approach and found to be substantial. Long et al. [Lon08], demonstrated that the tensor force that emerges naturally in relativistic Hartree-Fock also improves the relative shifts of the proton $1g_{7/2}$ and $1h_{11/2}$ levels in tin isotopes.

Many studies on the tensor force published so far aim at an optimal single parametrization, that establishes a best fit to either the underlying bare tensor force [Ots06, Bro06a] or empirical data [Ton83, Dob06, Col07]. The published results, as well as our first exploratory studies, however, suggest that adding a tensor force to the existing mean-field models gives only a local improvement of the relative change of certain single-particle energies, but not necessarily a global improvement of single-particle spectra or other observables. In the framework of the Skyrme EDF, there is also the already mentioned ambiguity that the contribution from the tensor force to spherical nuclei has the same structure as a term from the central force. In view of this situation, we will pursue a different strategy and investigate the effect of the tensor terms on a multitude of observables in nuclei though a set of Skyrme interactions with systematically varied coupling constants of the tensor terms.

The present study was motivated by the finding that the performance of the

existing Skyrme-type effective interactions for masses and spectroscopic properties is limited by systematic deficiencies of the single-particle spectra [Ben06a, Ben03a, Ben06b, Cha06c] that seem to be impossible to remove within the standard Skyrme interaction. The details of single-particle spectra were so far somewhat outside the focus of self-consistent mean-field methods, on the one hand as they do *not* correspond directly to empirical single-particle energies (we will come back to that below), and on the other hand because many of the observables that are usually calculated with self-consistent mean-field methods are not very sensitive to the exact placement of single-particle levels. By contrast, there is an enormous body of work that examines the infinite and semi-infinite nuclear matter properties of the effective interactions that are the analog of liquid-drop and droplet parameters in great detail. The reason is, of course, that the global trends over the whole chart of nuclei have to be understood before one can look into details. The last few years have seen an increasing demand on predictive power. Moreover, beyond-mean-field approaches of the projected generator coordinate method (GCM), or Bohr-Hamiltonian type, have become widely used tools to analyze and predict spectroscopic properties in medium and heavy nuclei, employing either Gogny or Skyrme interactions. The underlying single-particle spectra thus now deserve more attention, as many of the spectroscopic properties of interest turn out to be extremely sensitive to even subtle details of the single-particle spectra. As the tensor force is the most obvious missing piece in all standard mean-field interactions, it is the natural starting point for the systematic investigation of possible generalizations with the ultimate goal to improve the predictive power of the interactions for spectroscopy.

In the present chapter, we will describe the fit of the parametrizations, analyze the role of the tensor terms for single-particle spectra, then masses and radii of spherical even-even nuclei.

4.2 The fits

4.2.1 Properties of tensor terms in spherical symmetry

As discussed in section 2.3, in time-reversal-invariant systems, only the $\mathbb{J}^2$ terms of the functional generated by the tensor force remains. Furthermore, enforcing spherical symmetry greatly simplifies the spin-current tensor, Eq. (2.76), as both the pseudoscalar and pseudotensor parts of $J_{\mu\nu}$ vanish. From the vector spin-orbit current, only the radial component is non-zero, which is given by [Vau72]

$$J_q(r) \;=\; \frac{1}{4\pi r^3}\sum_{n,j,\ell}(2j+1)\,v^2_{nj\ell}\Big[j(j+1)-\ell(\ell+1)-\tfrac{3}{4}\Big]\,u^2_{nj\ell}(r) \qquad (4.1)$$

so that there is only one out of the nine components of the spin-current tensor density that contributes in spherical nuclei. Unlike the total density ρ and the kinetic density τ, that are bulk properties of the nucleus and grow with the size of the nucleus, the spin-orbit current is a shell effect that shows strong fluctuations. Assume the two shells with same n and ℓ which are split by the spin-orbit interaction, one coupled with the spin to $j = \ell + \frac{1}{2}$, the other to $j = \ell - \frac{1}{2}$. It is easy to verify that their contributions to $J_q(r)$ are equal but of opposite signs such that they cancel when (i) both shells are completely filled and (ii) their radial wave functions are identical

$\psi_{n,\ell+1/2,\ell} = \psi_{n,\ell-1/2,\ell}$. Although the latter condition is never exactly fulfilled, this demonstrates that the spin-orbit current is not a bulk property, but a shell effect that strongly fluctuates with N and Z. It nearly vanishes in so-called *spin-saturated* nuclei, where all spin-orbit partners are either completely occupied or empty, and it might be quite large when only the $j = \ell + 1/2$ level out of one or even several pairs of spin-orbit partners is filled.

In spherical symmetry, the contribution to the energy functional of the $\mathbf{J}^2$ terms is

$$\mathcal{H}^{\mathrm{t}} = \sum_{t=0,1} \tfrac{1}{2}\, C_t^J\, \mathbf{J}_t^2 = \sum_{t=0,1} \left(-\tfrac{1}{2} C_t^T + \tfrac{1}{4} C_t^F\right) \mathbf{J}_t^2 \,. \tag{4.2}$$

The effective coupling constants can be separated back into contributions from the non-local central and tensor forces

$$C_t^J = A_t^J + B_t^J \tag{4.3}$$

which are given by

$$\begin{aligned} A_0^J &= \tfrac{1}{8}\, t_1 \left(\tfrac{1}{2} - x_1\right) - \tfrac{1}{8}\, t_2 \left(\tfrac{1}{2} + x_2\right) \\ A_1^J &= \tfrac{1}{16}\, t_1 - \tfrac{1}{16}\, t_2 \\ B_0^J &= \tfrac{5}{16}\, (t_e + 3t_o) = \tfrac{5}{48}\, (T + 3U) \\ B_1^J &= \tfrac{5}{16}\, (t_o - t_e) = \tfrac{5}{48}\, (U - T)\,, \end{aligned} \tag{4.4}$$

where we also give the expressions using the notation $T = 3t_e$ and $U = 3t_o$ employed in [Flo75, Sta77, Col07].

For the following discussion it will be also illuminating to recouple this expression to a representation that uses proton and neutron densities, where we use the notation introduced in Ref. [Sta77]

$$\mathcal{H}^{\mathrm{t}} = \tfrac{1}{2}\, \alpha\, (\mathbf{J}_n^2 + \mathbf{J}_p^2) + \beta\, \mathbf{J}_n \cdot \mathbf{J}_p \,, \tag{4.5}$$

with

$$\begin{aligned} \alpha = C_0^J + C_1^J \,, \qquad \beta = C_0^J - C_1^J \,, \\ C_0^J = \tfrac{1}{2}\, (\alpha + \beta) \,, \quad C_1^J = \tfrac{1}{2}\, (\alpha - \beta) \,. \end{aligned} \tag{4.6}$$

The proton-neutron coupling constants $\alpha = \alpha_C + \alpha_T$ and $\beta = \beta_C + \beta_T$ can again be separated into contributions from central and tensor forces

$$\begin{aligned} \alpha_C &= \tfrac{1}{8}\, (t_1 - t_2) - \tfrac{1}{8}\, (t_1 x_1 + t_2 x_2) \,, \\ \beta_C &= -\tfrac{1}{8}\, (t_1 x_1 + t_2 x_2) \,, \\ \alpha_T &= \tfrac{5}{4}\, t_o = \tfrac{5}{12}\, U \,, \\ \beta_T &= \tfrac{5}{8}\, (t_e + t_o) = \tfrac{5}{24}\, (T + U) \,. \end{aligned} \tag{4.7}$$

As could be expected, the isospin-singlet tensor force contributes only to the proton-neutron term, while the isospin-triplet tensor force contributes to both.

The spin-orbit potential of the neutrons is given by

$$W_n(r) = \frac{\delta \mathcal{E}}{\delta \mathbf{J}_n(r)} \cdot \mathbf{e}_r = \frac{W_0}{2} \left(2\nabla\rho_n + \nabla\rho_p\right) + \alpha\, J_n + \beta\, J_p \,. \tag{4.8}$$

The expression for the protons is obtained exchanging the indices for protons and neutrons. In spherical symmetry, the tensor force gives a contribution to the spin-orbit potential, but does not alter the structure of the spin-orbit terms in the single-particle Hamiltonian as such. This will be different in the case of deformed mean fields [Per04, Ben09].

The dependence of the spin-orbit potential $W_q(r)$ on the spin-orbit current $J_q(r)$ through the tensor terms is the source of a potential instability. When the spin-orbit splitting becomes larger than the splitting of the centroids of single-particle states with different orbital angular momentum ℓ, the reordering of levels might increase the number of spin-unsaturated levels, which increases the spin-orbit current J_n and feeds back on the spin-orbit potential by increasing it even further, which ultimately leads to an unphysical shell structure.

4.2.2 A brief history of tensor terms in the central Skyrme energy functional

For the interpretation of the parametrizations we will describe below it is important to point out that within our choice of the effective Skyrme interaction as an antisymmetrized vertex the two coupling constants of the contribution from the central force to $\mathcal{H}^T$, Eq. (4.2), either represented through A_0^J, A_1^J or through α_C, β_C, are not independent from the coupling constants A_0^τ, A_1^τ, $A_0^{\Delta\rho}$, and $A_1^{\Delta\rho}$, that appear in Eq. (2.95). Through the expressions given in appendix A, all six of them are determined by the four coupling constants t_1, x_1, t_2, and x_2 from the central Skyrme force, Eq. (2.78). As a consequence, a tensor force is absolutely necessary to decouple the values of the C_t^J from those of the C_t^τ and $C_t^{\Delta\rho}$, which determine the isoscalar and isovector effective masses and give the dominant contribution to the surface and surface asymmetry coefficients, respectively.

This interpretation of the Skyrme interaction is, however, far from being common practice and a source of confusion and potential inconsistencies in the literature. Many authors have used parametrizations of the central and spin-orbit Skyrme energy functional with coupling constants that in one way or the other do not exactly correspond to the functional obtained from Eqns. (2.78) and (2.84), which, depending on the point of view, can be seen as an approximation to or a generalization of the original Skyrme interaction. As the most popular modification concerns the tensor terms, a few comments on the subject are in order. Again, the practice goes back to the seminal paper by Vautherin and Brink [Vau72], who state that "the contribution of this term to [the spin-orbit potential] is quite small. Since it is difficult to include such a term in the case of deformed nuclei, it has been neglected". This choice was further motivated by the interpretation of the effective Skyrme interaction as a density-matrix expansion (DME) [Neg70, Neg72, Neg75, Cam78]. All early parametrizations as SI and SII [Vau72], SIII-SVI [Bei75b], SkM [Kri80] and SkM* [Bar82a] followed this example and did not contain the $\mathbf{J}^2$ terms. Beiner et al. [Bei75b] weakened the case for $\mathbf{J}^2$ terms further by pointing out that they might lead to unphysical single-particle spectra. During the 1980s and later, however, it became more popular to include them, for example in SkP [Dob84], the parametrizations T1-T9 by Tondeur et al. [Ton84], E_σ and Z_σ by Friedrich and Reinhard [Fri86]. Some of the recent parametrizations come in pairs, where variants without and with $\mathbf{J}^2$ terms are fitted within the same

fit protocol, for example (SLy4, SLy5) and (SLy6, SLy7) in Ref. [Cha98], or (SkO, SkO') in Ref. [Rei99].

Interestingly, all but one parametrization of the central Skyrme interaction found in the literature set the coupling constants of the $\mathbf{J}^2$ terms either to their Skyrme force value (A.1) or strictly to zero. The exception is Ref. [Ton83] by Tondeur, where an independent fit of the coupling constants of the $\mathbf{J}^2$ terms was attempted, making explicit reference to a DME interpretation of the energy functional.

Setting the coupling constants of a term to zero when one does not know how to adjust its parameters is of course an acceptable practise when permitted by the chosen framework. For Skyrme interactions fitted without the $\mathbf{J}^2$ terms, the situation becomes confusing when one looks at deformed nuclei and any situation that breaks time-reversal invariance. First of all, Galilean invariance of the energy functional dictates that the coupling constant of the $\mathbf{s} \cdot \mathbf{T}$ terms is also set to zero, as already indicated by the presentation of the energy functional in Eq. (2.91). Second, using a DME interpretation of the Skyrme energy functional in one place, but the interrelations from the two-body Skyrme force in all others is not entirely satisfactory. Many authors who drop the $\mathbf{J}^2$ terms rarely show scruples to keep most of the time-odd terms in the Skyrme energy functional (2.91) with coupling constants A_t^s and $A_t^{\Delta s}$ from (A.1), although they are not at all constrained in the common fit protocols employing properties of even-even nuclei and spin-saturated nuclear matter. For a list of exceptions see Sect. II.A.2.d of Ref. [Ben03b]. An alternative is to set up a hierarchy of terms, as it was attempted by Bonche, Flocard and Heenen in their mean-field and beyond codes, which set $A_t^{\Delta s} = 0$ in addition to the coupling constant of the $\mathbf{J}^2$ terms, as all three terms have in common that they couple two Pauli matrices with two derivatives in different manners, see the footnote on page 129 of [Bon87].

There are also inconsistent applications of parametrizations without $\mathbf{J}^2 - \mathbf{s} \cdot \mathbf{T}$ terms to be found in the literature. For example, almost all applications of Skyrme interactions to the Landau parameters g_ℓ and g'_ℓ and the properties of polarized nuclear matter, include the contribution from the $\mathbf{s} \cdot \mathbf{T}$ terms, although it should be dropped for parametrizations fitted without $\mathbf{J}^2$ terms. Similarly, most RPA and QRPA codes include them for simplicity, see the discussion in Refs. [Eng99, Ben02, Ter05b].

As it is relevant for the subject of the present paper, we also mention another generalization of the Skyrme interaction that invokes the interpretation of the Skyrme energy functional in a DME framework. The spin-orbit force (2.84) fixes the isospin mix of the corresponding terms in the Skyrme energy functional (2.91) such that $A_0^{\nabla J} = 3A_1^{\nabla J}$ (A.2). There are a few parametrizations as MSkA [Sha95], SkI3 and SkI4 [Rei95], SkO and SkO' [Rei99] and SLy10 [Cha98] that liberate the isospin degree of freedom in the spin-orbit functional. A DME interpretation of the energy functional is mandatory for this generalization. It is motivated by the better performance of standard relativistic mean-field models for the kink of the charge radii in Pb isotopes. Note that the standard RMF models are effective Hartree theories without exchange terms, and that the standard Lagrangians have very limited isovector degrees of freedom [Ben03b], both of which suppress a strong isospin dependence of the spin-orbit interaction. It is interesting to note that the existing fits of Skyrme energy functionals with generalized spin-orbit interaction do not improve spin-orbit splittings [Ben99b].

4.2.3 General remarks

In order to study the effect of the $\mathbf{J}^2$ terms, we have built a set of 36 effective interactions that systematically cover the region of coupling constants C_0^J and C_1^J that, in a preliminary exploration of this parameter space, gave a reasonable description of finite nuclei in connection with the standard central and spin-orbit Skyrme forces. At variance with the perturbative approach used in Refs. [Sta77, Col07], each of these parametrizations has been fitted separately, following a procedure nearly identical to that used for the construction of the SLy parametrizations [Cha97, Cha98], as well as that used in the preceding chapter, so that we can keep the connection between the new fits with parametrizations that have been applied to a large variety of observables and phenomena.

The region of effective coupling constants (C_0^J, C_1^J) of the $\mathbf{J}^2$ terms acting in spherical nuclei, as defined in Eq. (2.95), that we will explore, is shown in Fig. 4.1. The parametrizations are labeled TIJ, where indices I and J refer to the proton-neutron (β) and like-particle (α) coupling constants in Eq. (4.5) such that

$$\begin{aligned} \alpha &= 60\,(J-2)\ \text{MeV fm}^5, \\ \beta &= 60\,(I-2)\ \text{MeV fm}^5. \end{aligned} \tag{4.9}$$

The corresponding values of C_t^J can be obtained through Eq. (4.6) or from Fig. 4.1. On the one hand, we cover the positions of the most popular existing parametrizations of the Skyrme interaction that take the $\mathbf{J}^2$ terms from the central force into account, which are SLy5 [Cha98], SkP [Dob84], Z_σ [Fri86], T6 [Ton84], SkO' [Rei99] and BSk9 [Gor05b]. On the other hand, among recent parametrizations including a tensor term, i.e. Skxta [Bro06a], Skxtb [Bro06a, Bro07] as well as those published by Colò et al. [Col07] and Brink and Stancu [Bri07], most fall in a region of negative C_1^J and vanishing C_0^J, that is to the lower left of Fig. 4.1. Parametrizations of this region, which also includes a part of the triangle advocated in the perturbative study of Stancu et al. [Sta77], gave unsatisfactory results for many observables. Moreover, when attempting to fit parametrizations with large negative coupling constants, we sometimes obtained unrealistic single-particle spectra or even ran into the instabilities already mentioned. Parametrizations further to the lower and upper right also have unrealistic deformations properties. The contribution from the $\mathbf{J}^2$ terms vanishes for T22, which will serve as the reference point. For the parametrizations T2J, only the proton-proton and neutron-neutron terms in $\mathcal{H}^{\mathrm{t}}$ are non-zero ($\beta = 0$), while for the parametrizations TI2, only the proton-neutron term in $\mathcal{H}^{\mathrm{t}}$ contributes ($\alpha = 0$). Note that the earlier parametrizations T6 and Z_σ have a pure like-particle $\mathbf{J}^2$ terms as a consequence of the constraint $x_1 = x_2 = 0$ employed for both (and most other early parametrizations of Skyrme's interaction).

4.2.4 The fit protocol and procedure

The list of observables used to construct the cost function χ^2 minimized during the fit (see Eq. (4.1) in Ref. [Cha97]) reads as follows: binding energies and charge radii of ^{40}Ca, ^{48}Ca, ^{56}Ni, ^{90}Zr, ^{132}Sn and ^{208}Pb; the binding energy of ^{100}Sn; the spin-orbit splitting of the neutron $3p$ state in ^{208}Pb; the empirical energy per particle and density at the saturation point of symmetric nuclear matter; and finally, the equation of state of neutron matter as predicted by Wiringa et al. [Wir88].

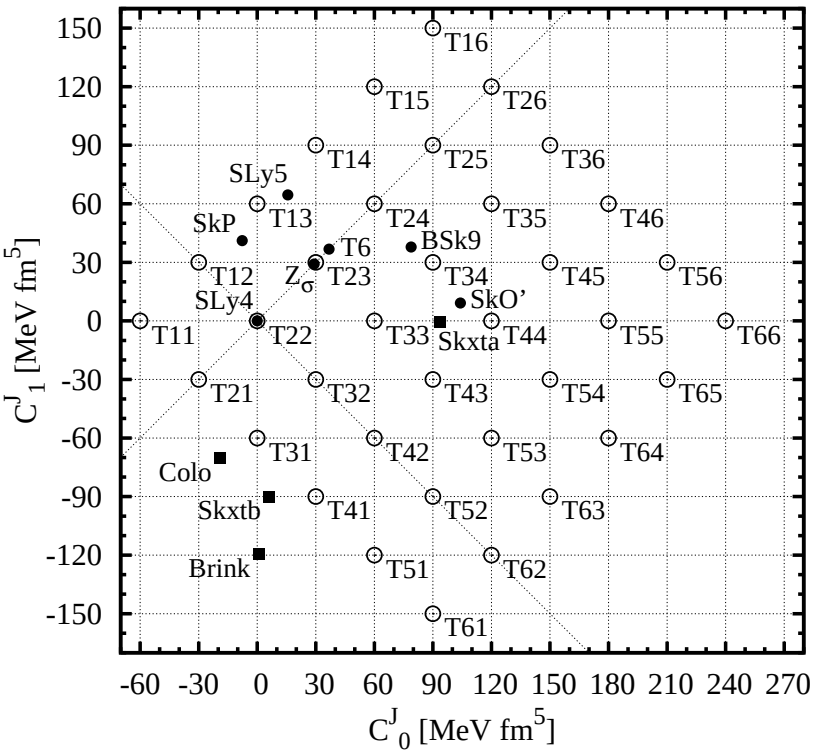

Figure 4.1: Values of C_0^J and C_1^J for our set of parametrizations (circles). Diagonal lines indicate $\alpha = C_0^J + C_1^J = 0$ (pure neutron-proton coupling) and $\beta = C_0^J - C_1^J = 0$ (pure like-particle coupling). Values for classical parameter sets are also indicated (dots), with SLy4 representing all parametrizations for which $\mathbf{J}^2$ terms have been omitted in the fit. Recent parametrizations with tensor terms are indicated by squares.

Furthermore, some properties of infinite nuclear matter are constrained through analytic relations between coupling constants in the same manner as they were in Refs. [Cha97, Cha98]: the incompressibility modulus K_∞ is kept at 230 MeV, while the volume symmetry energy coefficient a_τ is set to 32 MeV. The isovector effective mass, expressed through the Thomas-Reiche-Kuhn sum rule enhancement factor κ_v, is taken such that $\kappa_\mathrm{v} = 0.25$.

When using a single density-dependent term in the central Skyrme force (2.78), the isoscalar effective mass m^*_s cannot be chosen independently from the incompressibility modulus for a given exponent γ of ρ_0. We follow here the prescription used for the SLy parametrizations [Cha97, Cha98] and use $\gamma = 1/6$, which leads to an isoscalar effective mass close to 0.7 in units of the bare nucleon mass for all TIJ parametrizations. Using such a protocol we cannot, contrary to the protocol used in chapter 3, reproduce the isovector effective mass consistent with recent *ab-initio* predictions. Regarding the present exploratory study of the tensor terms this is not a critical limitation, in particular as the influence of this quantity on static properties of finite nuclei, as found previously, turns out to be small.

There are three modifications of the fit protocol compared to [Cha97, Cha98]. The obvious one is that the values for C_0^J and C_1^J are fixed beforehand as the parameters that will later on label and classify the fits. The second is that we have added the binding energies of ^{90}Zr and ^{100}Sn to the set of data. Indeed, we observed that the latter nucleus is usually significantly overbound when not included in the fit, as can be seen on the upper-left panel of Fig. 3.5. The third is that we have dropped the constraint $x_2 = -1$ that was imposed on the SLy parametrizations [Cha97, Cha98] to ensure the stability of infinite homogeneous neutron matter against a transition into a ferromagnetic state. On the one hand, this stability criterion is completely determined by the coupling constants of the time-odd terms in the energy functional [Ben02], that we do not want to constrain here, accepting that the parametrizations might be of limited use beyond the present study. On the other hand, the tensor force brings many new contributions to the energy per particle of polarized nuclear matter that lead to a much more complex stability criterion. The entire discussion concerning the stability with respect to spin polarization in the presence of a tensor force shall not be included in this work, as we expect that addressing finite-size instabilities will be necessary, and the corresponding response-function formalism has not been derived yet, to our best knowledge. It also has to be stressed that the actual stability criterion, as all properties of the time-odd part of the Skyrme energy functional, depends on the choices made for the interpretation of its coupling constants, i.e. antisymmetrized vertex or density functional [Ben02].

The properties of the finite nuclei entering the fit are computed using a Slater determinant without taking pairing into account. The cost function χ^2 was minimized using a simulated annealing algorithm. The annealing schedule was an exponential one, with a characteristic time of 200 iterations (also referred to as "simulated quenching") Thus, assuming a reasonably smooth cost function, we strive to obtain satisfactory convergence to its absolute minimum in a single run, allowing a systematic and straightforward production of a large series of forces. The coupling constants for all 36 parametrizations can be found in Table A.1.

Figure 4.2 displays the value of χ^2 after minimization as a function of the recoupled coupling constants α and β. The first striking feature is the existence of a "valley" at $\beta = 0$, i.e. a pure like-particle tensor term $\sim (\mathbf{J}_\mathrm{n}^2 + \mathbf{J}_\mathrm{p}^2)$. The abrupt rise

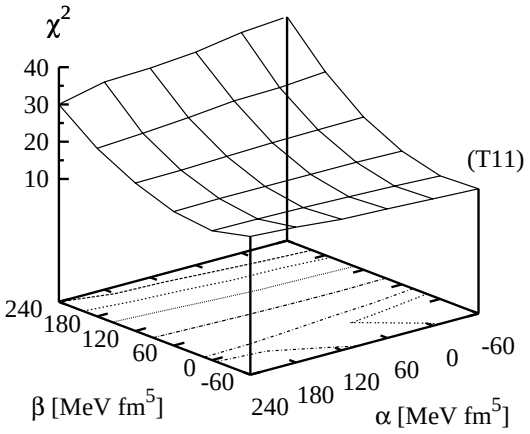

Figure 4.2: Values of the cost function χ^2 as defined in the fit procedure, for the set of parametrizations TIJ. The label "T11" indicates the position of this parametrization in the (α,β)-plane as obtained from Eqs. (4.9). Contour lines are drawn at $\chi^2 = 11$, 12, 15, 20, 25, and 30. The minimum value is found for T21 ($\chi^2 = 10.05$), the maximum for T61 ($\chi^2 = 37.11$).

of χ^2 around this value can be attributed to the term depending on nuclear binding energies, as sharp variations of energy residuals can be seen between neighboring magic nuclei with functionals of the T6J series ($\beta = 240$). For example, ^{48}Ca and ^{90}Zr tend to be significantly overbound in this case. We will come back later to discussing the implications for the quality of the functionals.

4.2.5 General properties of the fits

The coupling constants of the energy functional for spherical nuclei (2.95) obtained for T22 are very similar to those of SLy4, except for a slight readjustment coming from the inclusion of the binding energies of ^{90}Zr and ^{100}Sn in the fit as well as the abandoned constraint on x_2. With its value of -0.945, the x_2 obtained for T22 still stays close to the value -1 enforced for SLy4, which confirms that this is not too severe a constraint for parametrizations *without* effective $\mathbf{J}^2$ terms at sphericity. Increasing the effective tensor term coupling constants C_t^J, however, the values for x_2 start to deviate strongly from the region around -1, which is to a large extent due to the feedback from the contribution of the $\mathbf{J}^2$ terms to the surface and surface symmetry energy coefficients in the presence of constraints on isoscalar and isovector effective masses, all of which also depend on x_2.

From the constrained coupling constants C_0^J and C_1^J, the respective contributions B_0^J and B_1^J from the tensor force can be deduced afterwards using the expressions given in section 2.3.2. Their values, shown in Fig. 4.3, are less regularly distributed, which is a consequence of the non-linear interdependence of all coupling constants. Still, a general trend can be observed, such that all parametrizations are shifted towards the "south-west" compared to Fig. 4.1. In turn, this indicates that the contribution from the central Skyrme force always stays in the small region outlined by SkP, SLy5, Z$_\sigma$, *etc* in Fig. 4.1, with values that range between 28 and 104 MeV fm^5 for A_0^J and between 38 to 62 MeV fm^5 for A_1^J, respectively. This justifies a posteriori to use the tensor force as a motivation to decouple the $\mathbf{J}_t^2$ terms from the central part

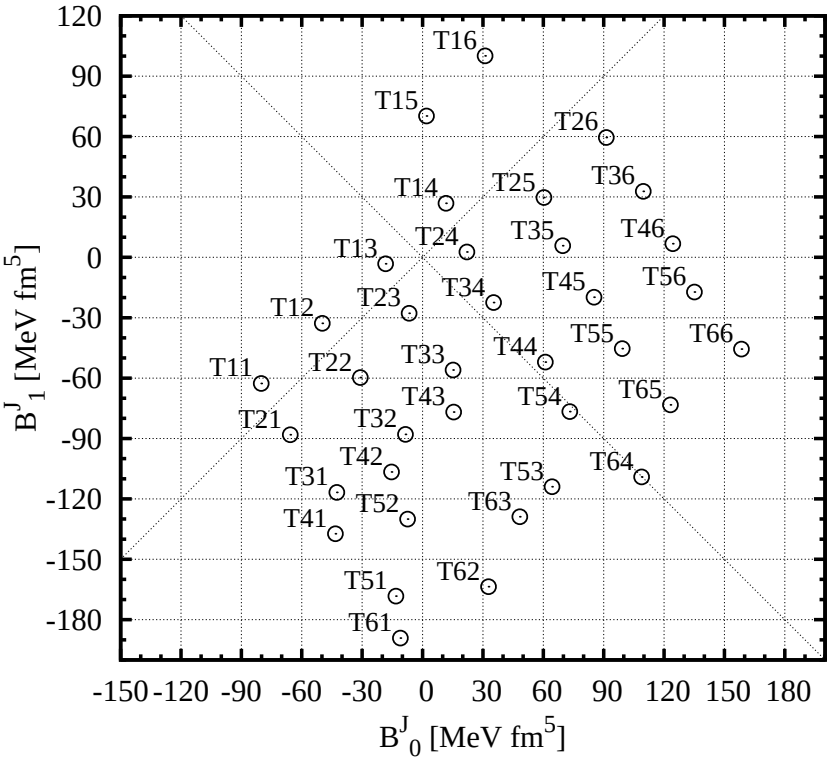

Figure 4.3: The contributions from the tensor force B_0^J and B_1^J to the effective coupling constants of the $\mathbf{J}^2$ term at sphericity. Diagonal lines as in Fig. 4.1. The diagonal where $B_0^J + B_1^J = \alpha_T = 0$ (pure proton-neutron contribution) additionally corresponds to an isospin-singlet force with $t_o \equiv U = 0$.

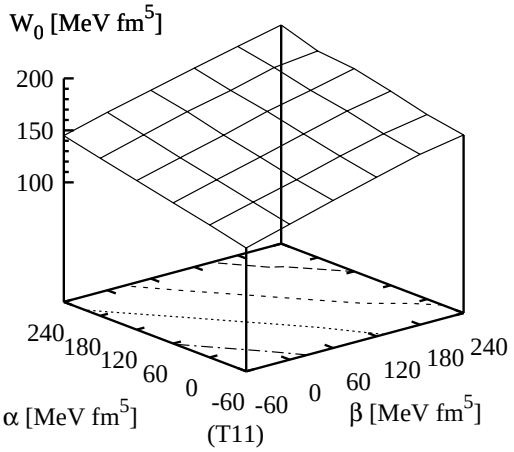

Figure 4.4: Value of spin-orbit coupling constant W_0 for each of the parametrizations TIJ, vs. indices I and J (The "(T11)" label indicates the position of this parametrization in the (α, β)-plane). The contour lines differ by 20 MeV fm^5. The values plotted here range from 103.7 MeV fm^5 (T11) to 195.3 MeV fm^5 (T66).

of the effective Skyrme vertex. We note in passing that all our parametrizations T$I4$ correspond to an almost pure proton-neutron or isospin-singlet tensor force, i.e. the term $\propto t_e$ in Eq. (2.88), as they are all located close to the $\alpha_T = 0$ line.

We also find a particularly strong and systematic variation of the coupling constant W_0 of the spin-orbit force, which varies from $W_0 = 103.7$ MeV fm^5 for T11 to $W_0 = 195.3$ MeV fm^5 for T66, see Fig. 4.4. This variation is of course correlated to the strength of the tensor force. As already shown, the tensor force has the tendency to reduce the spin-orbit splittings in spin-unsaturated nuclei. To maintain a given spin-orbit splitting in such a nucleus, the spin-orbit coupling constant W_0 has to be increased.

4.3 Results and discussion

The calculations presented below include open-shell nuclei treated in the Hartree-Fock-Bogolyubov (HFB) framework. In the particle-particle channel, we use a zero-range interaction with a mixed surface/volume form factor. The HFB equations were regularized with a cutoff at 60 MeV in the quasiparticle equivalent spectrum (see Ref. [Ben05] and section 2.4). The pairing strength was adjusted in ^{120}Sn with the particle-hole mean field calculated using the parameter set T33. The resulting strength was kept at the same value for all parametrizations, which is justified by the fact that the effective mass parameters are the same. Moreover, we thus avoid including, in the adjustment of the pairing strength, local effects linked with changes in details of the single-particle spectrum.

4.3.1 Spin-orbit currents and potentials

As a first step in the analysis of the role of the tensor terms and their interplay with the spin-orbit interaction in spherical nuclei, we analyze the spin-orbit current

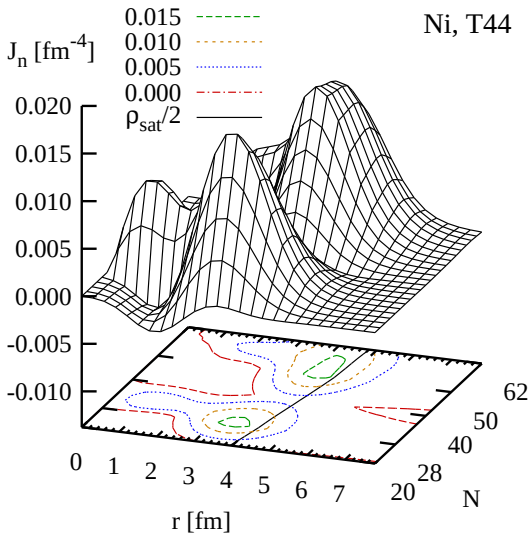

Figure 4.5: Radial component of the neutron spin-orbit current for the chain of Ni isotopes, plotted against radius and neutron number N. The solid line on the base plot indicates the radius where the total density has half its saturation value.

density and its relative contribution to the spin-orbit potential. We choose the chain of nickel isotopes, $Z = 28$, as it covers the largest number of spherical neutron shells and subshells ($N = 20$, 28, 40 and 50) of any isotopic chain, two of which are spin-saturated ($N = 20$ and 40), while the other two are not. Figure 4.5 displays the radial component of the neutron spin-orbit current $\mathbf{J}_\mathrm{n}$ for isotopes from the proton to the neutron drip-lines. The calculations are performed with T44, but the spin-orbit current is fairly independent from the parametrization. Starting from $N = 20$, which corresponds to a completely filled and spin-saturated *sd*-shell, the next magic number at $N = 28$ is reached by filling the $1f_{7/2}$ shell, which leads to the steeply rising bump in the plot of $\mathbf{J}_\mathrm{n}$ in the foreground, peaked around $r \simeq 3.5$ fm. Then, from $N = 28$ to $N = 40$ the rest of the fp shell is filled, which first produces the small bump at small radii that corresponds to the filling of the $2p_{3/2}$ shell, but ultimately leads to a vanishing spin-orbit current when the $1f$ and $2p$ levels are completely filled for the $N = 40$ isotope, visible as the deep valley in Fig. 4.5. Adding more neutrons, the filling of the $1g_{9/2}$ shell leads again to a strong neutron spin-orbit current at $N = 50$. For the remaining isotopes up to the neutron drip line, the evolution of $\mathbf{J}_\mathrm{n}$ is slower with the filling of the $2d$ and $3s$ orbitals.

A few further comments are in order. First, the spin-orbit current clearly reflects the spatial probability distribution of the single-particle wave function in pairs of unsaturated spin-orbit partners. Within a given shell, the high-ℓ states contribute at the surface, represented by the solid line on the base of Fig. 4.5, while low-ℓ states contribute at the interior. The peak from the high-ℓ orbitals, however, is always located on the inside of the nuclear surface, as defined by the radius of half saturation density. Second, within a given shell, the largest contributions to the spin-orbit current density obviously come from the levels with largest ℓ, as they have the largest degeneracy factors in (4.1), and because they do not have nodes, which leads to a single, sharply peaked contribution. Third, the spin-orbit current is not exactly zero for nominally "spin-saturated" nuclei, exemplified by the $N = 20$

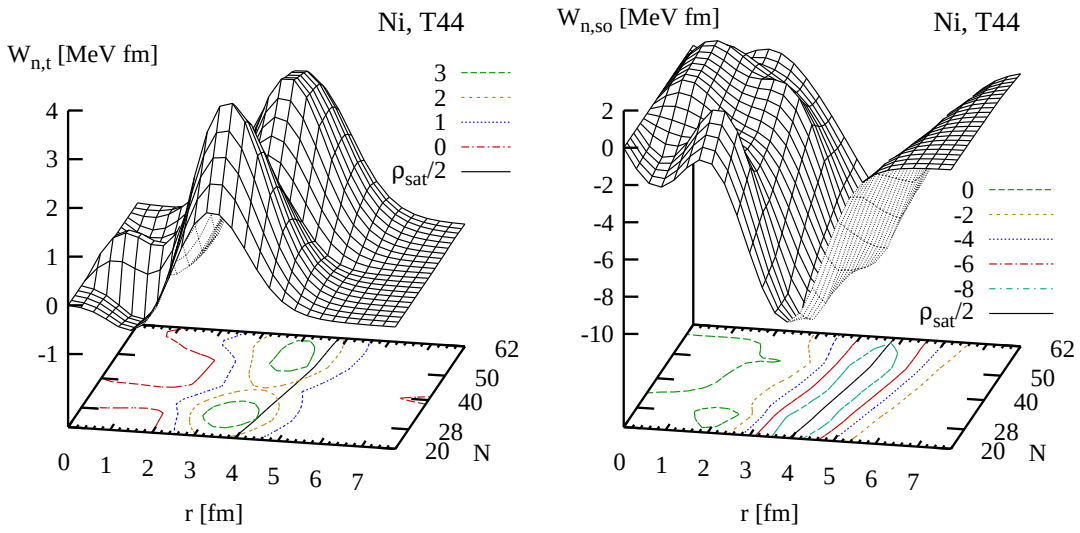

Figure 4.6: Contribution from the tensor terms (left panel) and the spin-orbit term (right panel) to the neutron spin-orbit potential for the chain of Ni isotopes as obtained with the parametrization T44. The solid line on the base plot indicates the radius where the isoscalar density ρ_0 crosses half its saturation value.

and $N = 40$ isotopes in Fig. 4.5, as the radial single-particle wave functions are not exactly identical for all pairs of spin-orbit partners, which is a necessary requirement to obtain $\mathbf{J}_n = 0$ at all radii (cf. the example of the $\nu\, 2d$ states in ^{132}Sn in Fig. 4.12 below). Fourth, pairing and other correlations will always smooth the fluctuations of the spin-orbit current with nucleon numbers, as levels in the vicinity of the Fermi energy will never be completely filled or empty.

Next, we compare the contributions from the tensor terms and from the spin-orbit force to the spin-orbit potentials of protons and neutrons, Eq. (4.8). The contributions from the tensor force to the spin-orbit potential are proportional to the spin-orbit currents of protons and neutrons. For the Ni isotopes, the proton spin-orbit current is very similar to that of the neutrons at $N = 28$ displayed in Fig. 4.5. For the parametrization T44 we use here as an example, we have contributions from both proton and neutron spin-orbit currents, which come with equal weights. Their combined contribution to the spin-orbit potential of the neutron W_n might be as large as 4 MeV, which is more than a third of the maximum contribution from the spin-orbit force to W_n (see Fig. 4.6). The latter is proportional to a combination of the gradients of the proton and neutron densities, $2\nabla\rho_n(r) + \nabla\rho_p(r)$, see Eq. (4.8). As a consequence, it has a smooth behavior as a function of particle number, with slowly and monotonically varying width, depth and position. Only limited local variations can be seen on the interior due to small variations of the density profile originating from the successive filling of different orbits. Furthermore, one can easily verify that the contribution from the spin-orbit force is peaked at the surface of the nucleus (the solid line on the base plot). The strongest variation of the depth of this potential occurs just before the neutron drip line at $N = 62$, where is becomes wider and shallower due to the development of a diffuse neutron skin, which reduces the gradient of the neutron density [Dob94, Lal98a, Lal98b].

Adding the contributions from the proton and neutron tensor terms to that

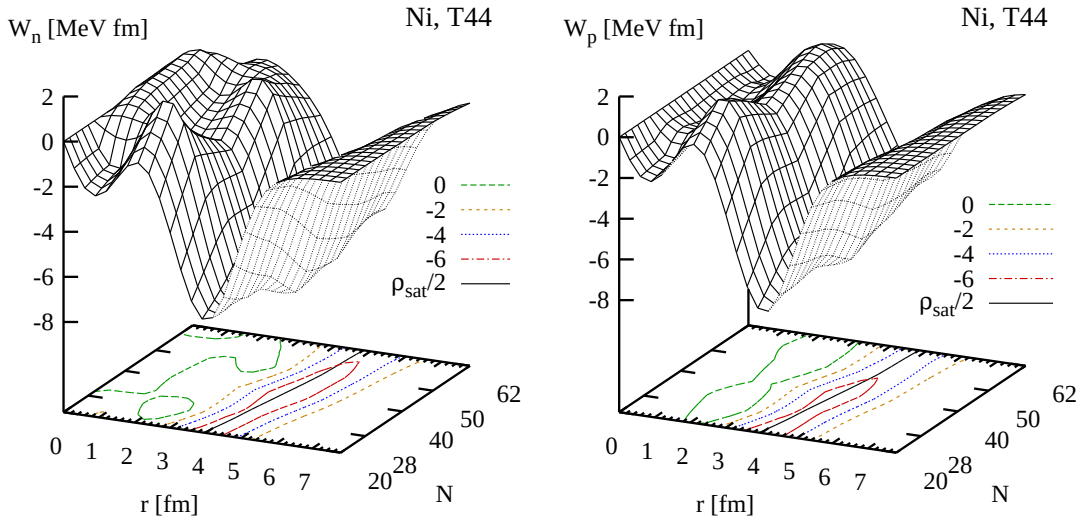

Figure 4.7: Total neutron (left panel) and proton (right panel) spin-orbit potentials for the chain of Ni isotopes as obtained with the parametrization T44. The solid line on the base plot indicates the radius where the isoscalar density ρ_0 crosses half its saturation value.

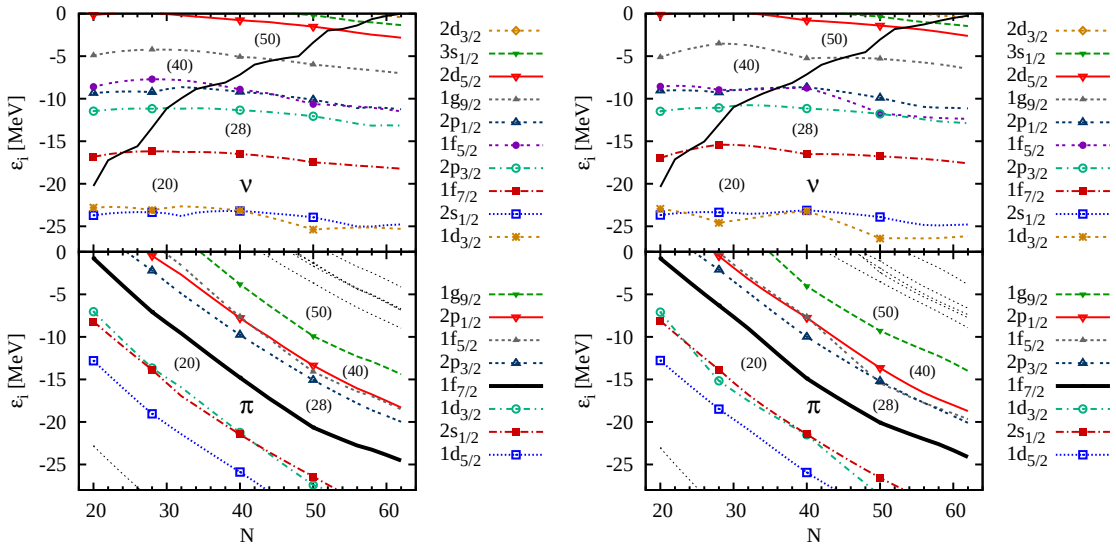

Figure 4.8: Single-particle spectra of neutrons (upper panels) and protons (lower panels) for the chain of Ni isotopes, as obtained with the parametrization T22 with vanishing combined $\mathbf{J}^2$ terms (left) and T44, with proton-neutron and like-particle tensor terms of equal strength (right). The thick solid line in the upper panels denotes the Fermi energy for neutrons.

from the spin-orbit force, the total neutron spin-orbit potential for neutrons in Ni isotopes is shown on the left panel of Fig. 4.7. For the parametrization T44 used here (and most others in the sample of parametrizations used in this study) the dominating contributions from the spin-orbit and tensor forces to the spin-orbit potential are of opposite sign. For Ni isotopes, $\mathbf{J}_p$ is always quite large, while $\mathbf{J}_n$ varies as shown in Fig. 4.5. Notably, both are peaked inside of the surface. When examining the combined contribution from the spin-orbit and tensor forces to the spin-orbit potential (4.8), one must keep in mind that they are peaked at different radii. Moreover, the variation of tensor-term coupling constants among a set of parametrizations implies a rearrangement of the spin-orbit term strength, as will be discussed later. As a consequence, taking into account the tensor force modifies the width and localization of the spin-orbit potential $W_q(r)$ much more than it modifies its depth through the variation of the spin-orbit currents.

Our observations also confirm the finding of Otsuka et al. [Ots06] that the spin-orbit splittings might be more strongly modified by the tensor force than they are by neutron skins in neutron-rich nuclei through the reduction of the gradient of the density.

The right panel of Figure 4.7 shows the spin-orbit potential of the protons for the chain of Ni isotopes. Here, the contribution from the spin-orbit force has a larger contribution coming from the gradient of the proton density that just grows with the mass number, without being subject to varying shell fluctuations. The same holds for the proton contribution from the tensor terms. Only the neutron contribution from the tensor terms varies rapidly, proportional to $\mathbf{J}_n$ displayed in Fig. 4.5, which has a very limited effect on the total spin-orbit potential, though.

With that, we can examine how the tensor terms affect the evolution of single-particle spectra. To that end, Fig. 4.8 shows the single-particle energies of protons and neutrons along the chain of Ni isotopes for the parametrization T22 with vanishing combined tensor terms, which will serve as a reference, and for the parametrization T44 with proton-neutron and like-particle tensor terms of equal strength. For the latter, the variation of the neutron spin-orbit current with N influences both neutron and proton single-particle spectra. The effect of the tensor terms is subtle, but clearly visible: for T22, the major change of the single-particle energies is their compression with increasing mass number, while for T44 the level distances oscillate on top of this background correlated to the neutron shell and sub-shell closures at $N = 20$, 28, 40 and 50. As shown above, the neutron spin-orbit current vanishes for $N = 20$, where it consequently has no effect on the spin-orbit potentials and splittings. By contrast, the neutron spin-orbit current is large for $N = 28$ and 50, where its contribution to the spin-orbit potential reduces the splittings from the spin-orbit force.

The strong variation of the spin-orbit current with nucleon numbers is typical for light nuclei up to about mass 100. For heavier nuclei, its variation becomes much smaller. This is exemplified in Fig. 4.9 for the neutron spin-orbit current in the chain of Pb isotopes. There remain the fast fluctuations at small radii which we already saw for the Ni isotopes and that reflect the subsequent filling of low-ℓ levels with many nodes, but which have a very limited impact on the spin-orbit splittings when fed into the spin-orbit potential. The dominating peak of the spin-orbit current, just beneath the surface shows only small fluctuations, as the overlapping spin-orbit splittings of levels with different ℓ never give rise to a spin-saturated configuration

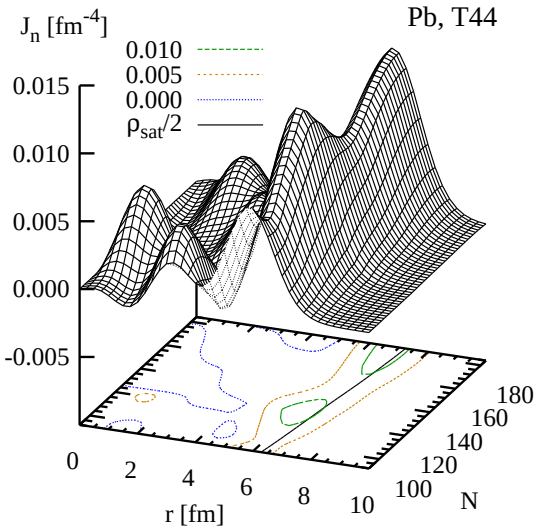

Figure 4.9: Radial component of the Neutron spin-orbit current for the chain of Pb isotopes plotted in the same manner as in Fig. 4.5.

in heavy nuclei.

Note that both the spin-orbit current $\mathbf{J}$ and the spin-orbit potential are exactly zero at $r = 0$ as they are vectors with negative parity.

4.3.2 Single-particle energies

As a next step, we analyze the modifications that the presence of $\mathbf{J}^2$ terms brings to single-particle energies in detail. Before we do so, let us recall that we ultimately expect our functional to be used in a multi-reference EDF framework, which has implications on the comparison between single-particle energies obtained at the single-reference level and experimental mass differences which will be used in this section. In essence, single-particle spectra of nuclei sufficiently magic and robust with respect to collective motion are expected to see their density renormalized by correlations, with an increase of the effective mass. Care should be taken not to include data too strongly affected by deformation of the odd nucleus, or the fragmentation of spectroscopic strength due to particle-vibration coupling.

It should be kept in mind that the obvious, coarse discrepancies between the calculated spectra of ϵ_μ and the empirical single-particle energies are often larger than the uncertainties coming from the missing correlations, as long as one observes some elementary precautions. We took care to ensure that the states used in the analysis below were one-quasiparticle states weakly coupled to core phonons. First, we checked that the even-even nucleus of interest could be described as spherical, indicated by a sufficiently high-lying 2^+ state. Second, we avoided all levels which were obviously correlated with the energies of 2^+ states in the adjacent semi-magic series, as this indicates strong coupling with core excitations. Finally, we carefully examined states, lying above the 2^+ energy and/or twice the pairing gap of adjacent semi-magic nuclei, in order to eliminate those more accurately described as an elementary core excitation coupled to one or more quasiparticles, which generally appear as a multiplet of states. We did not attempt to use energy centroids calculated with use of spectroscopic factors, as these are not systematically available. Indeed,

our requirement is that if some collectivity is present, it should be similar among all nuclei considered, in order to be easily subtracted out. Empirical single-particle levels shown below are determined from the lowest states having given quantum numbers in an odd-mass nucleus.

Spin-orbit splittings

The primary effect one expects from a tensor term is that it affects spin-orbit splittings by altering the strength of the spin-orbit field in spin-unsaturated nuclei, according to Eq. (4.8). One should remember, though, that the spin-orbit coupling itself is readjusted for each pair of coupling constants C_0^J, and C_1^J. The effect of this readjustment is generally opposite to that of the variation of the isoscalar tensor term coupling constant. It should thus be stressed that the effects described result from the balance between the variation of tensor and spin-orbit terms, which for most of our parametrizations pull into opposite directions.

Common wisdom states that the energy spacing between levels that are both above or both below the magic gap are not much affected by correlations, even when their absolute energy changes; hence it is common practice to confront only the spin-orbit splittings between pairs of particle or hole states with calculated single-particle energies from the spherical mean field. The left panel of Fig. 4.10 shows the relative error of single-particle splitting of such levels for doubly-magic nuclei throughout the chart of nuclei. The calculated values are typically 20 to 60 % larger than the experimental ones, with the exception of ^{16}O, where the splittings of the neutron and proton $1p$ states are acceptably reproduced at least for the parametrizations T22, T24 and T42, i.e. those with the weakest tensor terms in the sample.

It is noteworthy that the calculated splittings depend much more sensitively on the tensor terms for light nuclei with spin-saturated shells (protons and neutrons in ^{16}O, protons in ^{90}Zr) than for the heavy doubly-magic ^{132}Sn and ^{208}Pb, which are quite robust against a variation of the tensor terms. The reason will become clear below.

Connection between tensor and spin-orbit terms

The finding that our parametrizations systematically overestimate the spin-orbit splittings deserves an explanation. It was earlier already noted that all standard Skyrme interactions, including the SLy parametrizations that share our fit protocol, have an unresolved trend that overestimates spin-orbit splittings in heavy nuclei [Ben99b, Ben03b, LQ00]. Adding the tensor terms, however, further deteriorates the overall description of spin-orbit splittings, instead of improving it. It is particularly disturbing that the spin-orbit splitting of the $3p$ level in ^{208}Pb that was used to constrain W_0 in the fit is overestimated by 30 to 40%, which is larger than the relative tolerance of 20% included in the fit protocol. In fact, it turns out that the coupling constant W_0 of the spin-orbit force is more tightly constrained by the binding energies of light nuclei than by this or any other spin-orbit splitting. In the HF approach used during the fit, the structure of ^{40}Ca, ^{48}Ca, and ^{56}Ni differs by the occupation of the neutron and proton $1f_{7/2}$ levels. First, we have to note that the terms in the energy functional that contain the spin-orbit current play an important role for the energy difference between ^{40}Ca and ^{56}Ni. The combined contribution from the tensor and spin-orbit terms varies from a near-zero value in the

spin-saturated ^{40}Ca to about -60 MeV in ^{56}Ni for all our parametrizations, which is a large fraction of the -142 MeV difference in total binding energy between both nuclei. The $Z = 40$ subshell and $Z = 50$ shell are another example of abrupt variation of the spin-orbit current with the filling of the $1g_{9/2}$ level, which strongly affects the relative binding energy of $N = 50$ isotones ^{90}Zr and ^{100}Sn. Second, the fit to phenomenological data can take advantage of the large relative variation of these terms to mock up missing physics in the energy functional that should contribute to the energy difference, but that is absent in it. The consequence will be a spurious increase of the spin-orbit and tensor term coupling constants. The resulting energy functional will correctly describe the mass difference, but not the physics of the spin-orbit and tensor terms.

In order to test the above interpretation, we performed a refit of selected TIJ parametrizations without taking into account the masses of ^{40}Ca, ^{48}Ca, ^{56}Ni and ^{90}Zr in the fit procedure. In the resulting parametrizations, the spin-orbit coefficient W_0 is typically 20 % lower than in the original ones. As a consequence, the empirical value for the spin-orbit splitting of the neutron $3p$ level in ^{208}Pb is met well within tolerance, at the price of binding energy residuals in light nuclei being unacceptably large, i.e. ^{56}Ni being underbound by 5 MeV while ^{40}Ca and ^{90}Zr are overbound by up to 10 MeV. While the global trend of the spin-orbit splittings shown in Fig. 4.10 is enormously improved with these fits, in particular for heavy nuclei, the overall agreement of the single-particle spectra with experiment is not, so that we had to discard these parametrizations. This finding hints at a deeply rooted deficiency of the Skyrme energy functional. The spin-orbit and, when present, tensor terms indeed do simulate missing physics of the energy functional at the price of unrealistic spin-orbit splittings. This also hints why perturbative studies, as those performed in [Sta77, Col07] give much more promising results than what we will find below with our complete refits. We will discuss mass residuals in more detail in Sect. 4.3.3 below.

During the fit, the masses of light nuclei do not only compromise the spin-orbit splittings, they also establish a correlation between W_0 and C_0^J in all our parametrizations. The combined spin-orbit and spin-current energy of a given spherical nucleus (N, Z) is given by (keeping only the isoscalar part since we shall focus on the $N = Z$ nuclei ^{40}Ca and ^{56}Ni)

$$E_0^{\text{spin}}(N,Z) = C_0^{\nabla J}\,\mathcal{I}_0^{\nabla J}(N,Z) + C_0^J\,\mathcal{I}_0^J(N,Z) \tag{4.10}$$

with

$$\mathcal{I}_0^{\nabla J}(N,Z) \;=\; \int \mathrm{d}^3r\;\rho_0 \boldsymbol{\nabla}\cdot\mathbf{J}_0, \qquad \mathcal{I}_0^J(N,Z) \;=\; \int \mathrm{d}^3r\;\mathbf{J}_0^2\,. \tag{4.11}$$

The difference of E_0^{spin} between ^{56}Ni and ^{40}Ca

$$E_0^{\text{spin}}\left(^{56}\text{Ni}\right) - E_0^{\text{spin}}\left(^{40}\text{Ca}\right) = \Delta E^{\text{spin}} \tag{4.12}$$

turns out to be fairly independent from the parametrization. Averaged over all 36 parametrizations TIJ used here, ΔE^{spin} has a value of -58.991 MeV with a standard deviation as small as 3.202 MeV, or 5.4%.

The integrals in Eqs. (4.11) are fairly independent from the actual parametrization. For a rough estimate, we can replace them in Eq. (4.10) by their average

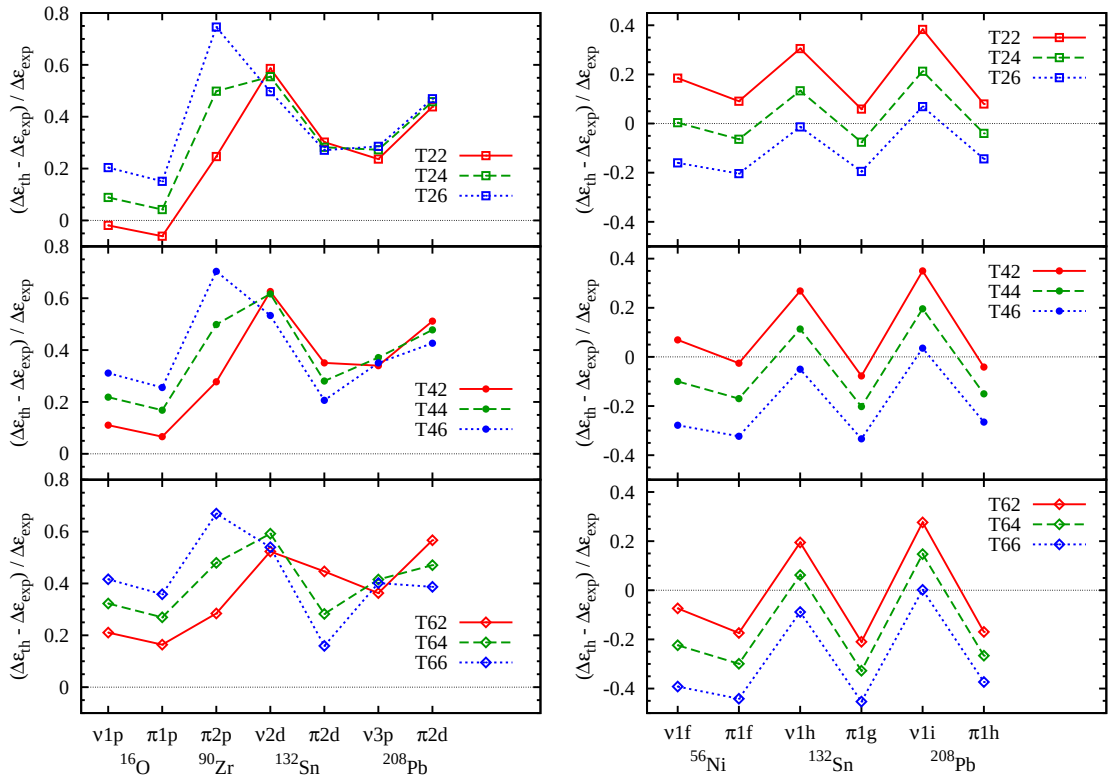

Figure 4.10: Left panel: relative error of the spin-orbit splittings in doubly-magic nuclei for $\ell \leq 2$ levels. Right panel: Spin-orbit splittings of high-ℓ levels in magic nuclei, corresponding to s.p.e. differences across the Fermi energy. The calculated values are less robust against correlation effects than those shown on the left panel and have to be interpreted with caution (see text).

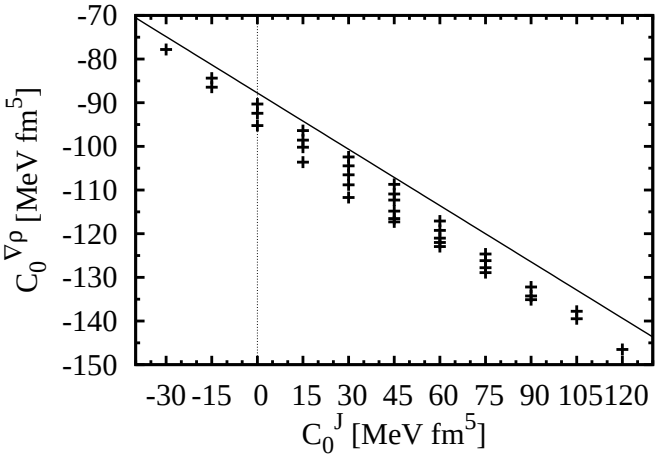

Figure 4.11: Correlation between the values of spin-orbit coupling constant $C_0^{\nabla J}$ and the isoscalar spherical effective spin-current coupling constant C_0^J. Dots: values for the actual parametrizations TIJ, solid line: trend estimated through Eq. (4.13) (see text).

values. Plugged into Eq. (4.12) this yields

$$C_0^{\nabla J} = \frac{\Delta E^{\text{spin}} - C_0^J \langle \mathcal{I}_0^J\,(^{56}\text{Ni}) - \mathcal{I}_0^J\,(^{40}\text{Ca})\rangle}{\langle \mathcal{I}_0^{\nabla J}\,(^{56}\text{Ni}) - \mathcal{I}_0^{\nabla J}\,(^{40}\text{Ca})\rangle}\,. \tag{4.13}$$

Figure 4.11 compares the values of $C_0^{\nabla J}$ as obtained through (4.13) with the values for the actual parametrizations. The estimate works very well, which demonstrates that $C_0^{\nabla J} = -\frac{3}{4}W_0$ and C_0^J are indeed correlated and cannot be varied independently within a high quality fit of the energy functional (2.95). As the combined strength of the spin-orbit and tensor terms in the energy functional is mainly determined by the mass difference of the two $N = Z$ nuclei ^{40}Ca and ^{56}Ni, the spin-orbit coupling constant W_0 depends more or less linearly on the isoscalar tensor coupling constant C_0^J, while for all practical purposes it is independent from the isovector one, see also Fig. 4.4 above.

Splitting of high-ℓ states and the role of the radial form factor

As stated above, it is common practice to confront only the spin-orbit splittings between pairs of particle or hole states with calculated single-particle energies from the spherical mean field. The spin-orbit splitting of intruder states is rarely examined. The right panel of Fig. 4.10 displays the relative deviation of the spin-orbit splittings of the intruder states with $\ell \geq 3$ that span across major shell closures and are thus given by the energy difference of a particle and a hole state. These splittings are not "safe", i.e. they can be expected to be strongly decreased by polarization and correlation effects [Rut98, Ber80, Lit06]. To leave room for this effect, a mean-field calculation should overestimate the empirical spin-orbit splittings. We observe, however, that mean-field calculations done here give values that are quite close to the experimental ones, or even smaller for parametrizations with large positive isoscalar tensor coupling (cf. the evolution from T22 to T66).

This means that the spin-orbit splittings are not too large in general, as might be concluded from Fig. 4.10, but that there is a wrong trend of the splittings with ℓ with the strength of the spin-orbit potential establishing a compromise between the in-shell splittings of small ℓ orbits that are too large and the across-shell splittings of the intruders that are tentatively too small. In fact, the levels in the right panel of Fig. 4.10 obviously have in common that their radial wave functions do not have nodes, while the levels on the left panel have one or two nodes, with the notable exception of the $1p$ levels in ^{16}O, for which we also find smaller deviations of the spin-orbit splittings than for the other $\ell \leq 2$ levels.

Underestimating the spin-orbit splittings of intruder levels has immediate and obvious consequences for the performance of an effective interaction, as this closes the magic gaps in the single-particle spectra and compromises the predictions for doubly-magic nuclei, as we will demonstrate in detail below. By contrast, the spin-orbit splittings of the low-ℓ states within the major shells have no obvious direct impact on bulk properties. Their deviation from empirical data is less dramatic, as the typical bulk observables discussed with mean-field approaches are not very sensitive to them. It is only in applications to spectroscopy that their deficiencies become evident. It is noteworthy that the parametrization T22 *without* effective tensor terms at sphericity provides a reasonable compromise between the tentatively underestimated splittings of the intruder levels and the tentatively overestimated

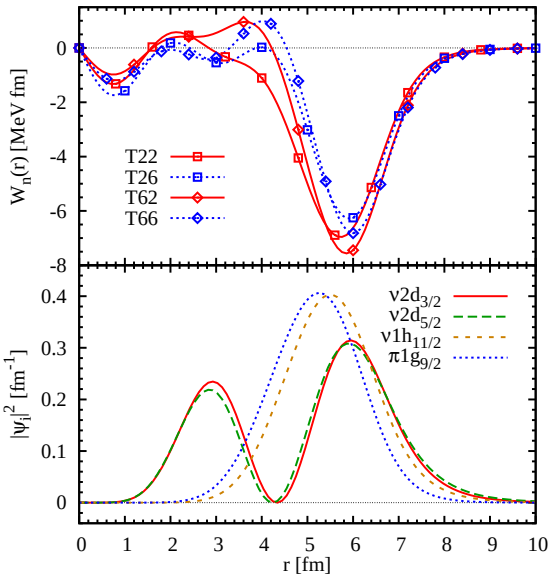

Figure 4.12: Neutron spin-orbit potential (top) and the radial wave function of selected orbitals (bottom) in ^{132}Sn.

splittings of the levels within major shells, both shown in Fig. 4.10 above, while for parametrizations with tensor terms this balance is lost.

There clearly is a proton-neutron staggering in Fig. 4.10, such that calculated proton splittings are relatively smaller than the neutron ones. The effect appears both when comparing proton and neutron levels with different ℓ in the same nucleus, and when comparing proton and neutron levels with the same ℓ in the same or different nuclei (see the $1h$ levels in ^{132}Sn and ^{208}Pb). The staggering for the intruder levels is even amplified for parametrizations with large proton-neutron tensor term, as T62, T64 or T66. The effect is particularly prominent for the heavy ^{132}Sn and ^{208}Pb with a large proton-to-neutron ratio N/Z, which might hint at unresolved isospin dependence of the spin-orbit interaction, although alternative explanations that involve how single-particle states in different shells should interact through tensor and spin-orbit forces are possible as well, see also the next paragraph.

Note that also the spin-orbit splittings of the low-ℓ levels shown in Fig. 4.10 exhibit a staggering, which is of smaller amplitude, though. It has been pointed out by Skalski [Ska01], that an exact treatment of the Coulomb exchange term (compared to the Slater approximation used here and nearly all existing literature) does indeed slightly increase the spin-orbit splittings of protons across major shells. This effect might give a clue to the staggering observed for the $N = Z$ nucleus ^{56}Ni, but the magnitude of the effect reported in Ref. [Ska01] is too small to explain the large staggering we find for the heavier $N \neq Z$ nuclei.

Next, we use the example of ^{132}Sn to demonstrate why the spin-orbit splittings of nodeless high-ℓ states are more sensitive to the tensor terms than low-ℓ states with one or several nodes, see Fig. 4.12. The lower panel shows the neutron spin-orbit potential in ^{132}Sn for four different parametrizations, while the upper panel shows selected radial single-particle wave functions. The ν $1h_{11/2}$ and π $1g_{9/2}$ levels give the main contribution to the neutron and proton spin-orbit currents in this nucleus, and consequently to the tensor contribution to the spin-orbit potential. Indeed, the largest differences between the spin-orbit potentials from the chosen

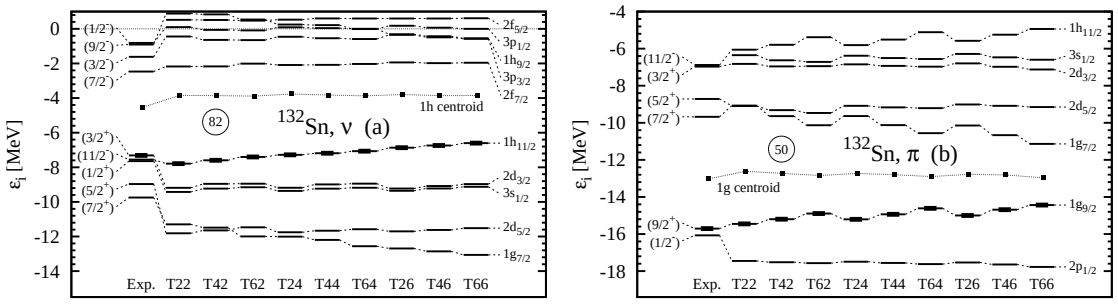

Figure 4.13: Single-particle energies in ^{132}Sn for a subset of our parametrizations. We also show the centroid of the intruder levels, defined through Eq. (4.14) Top panel: neutron levels, bottom panel: proton levels. A thick mark indicates the Fermi level.

parametrizations are caused by the varying contribution from the tensor terms and appear for the region between 3 and 6 fm, where the wave functions of the $1g$ and $1h$ states are peaked. This region corresponds to the inner flank of the spin-orbit potential well, while the outer flank is much less affected. While the $1g$ and $1h$ wave functions are peaked at the inner flank, the $2d$ orbitals have their node in this region. Consequently, the splittings of the $1g$ and $1h$ levels are strongly modified by the tensor terms, while those of the $2d$ orbitals are quite insensitive.

As a rule of thumb, the tensor contribution to the spin-orbit potential in doubly-magic nuclei comes mainly from the nodeless intruder states, which, when present, in turn mainly affect their own spin-orbit splittings, leaving the splittings of the low-ℓ states with one or more nodes nearly unchanged for reasons of geometrical overlap.

We note in passing that the slightly different radial wave functions of the $2d$ orbitals demonstrate nicely that their contribution to the spin-orbit current, Eq. (4.1), cannot completely cancel.

In fact, when regarding more specifically the evolution of the spin-orbit potential between the parametrizations T22 and T66, it is striking that for T66 it is essentially narrowed and its minimum slightly pushed towards larger radii, while its depth remains unaltered. Recalling that T66 shows a pathological behavior of too weak spin-orbit splitting of the intruder states, it appears that a correct ℓ-dependence of spin-orbit splittings might require to modify the radial dependence of the spin-orbit potential such that it becomes wider towards smaller radii. This uncalled-for modification of the shape of the spin-orbit field has previously been put forward by Brown et al. [Bro06a] as an argument for a negative like-particle $\mathbf{J}^2$ coupling constant α. However, as will be discussed in paragraph 4.3.2 below, the evolution of single-particle levels along isotopic chains calls for $\alpha > 0$, see also [Bro06a].

Single-particle spectra of doubly-magic nuclei

After we have examined the predictions for spin-orbit splittings, we will now turn to the overall quality of the single-particle spectra of doubly-magic nuclei. Figure 4.13 shows the single-particle spectrum of ^{132}Sn. It is evident that as a consequence of the underestimated spin-orbit splittings of the intruder levels that we discussed in the last section, the spectrum is deteriorated for large positive isoscalar tensor

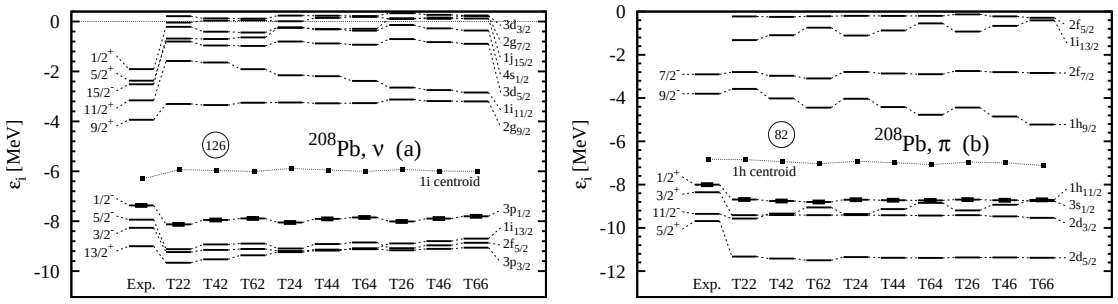

Figure 4.14: Same as Fig. 4.13 for ^{208}Pb.

term coupling constants C_0^J (see T66), as, for example, a decrease of the spin-orbit splitting of the neutron $1h$ shell pushes the $1h_{11/2}$ further up, closing the $N = 82$ gap. As a consequence, the presence of the tensor terms cannot remove the problem shared by all standard mean-field methods that always wrongly put the neutron $1h_{11/2}$ level above the $2d_{3/2}$ and $3s_{1/2}$ levels [Ben03b], which compromises the description of the entire mass region. For the same reason, the proton spectrum of ^{132}Sn also excludes interactions with large positive C_0^J, which reduces the $Z = 50$ gap between the $1g$ levels to unacceptable small values.

Figure 4.13 also shows the energy centroids of the ν $1h$ and π $1g$ levels, defined as

$$\varepsilon^{\text{cent}}_{qn\ell} = \frac{\ell+1}{2\ell+1}\,\varepsilon_{qn\ell,j=\ell+1/2} + \frac{\ell}{2\ell+1}\,\varepsilon_{qn\ell,j=\ell-1/2}\,. \tag{4.14}$$

The position of the centroid is fairly independent from the parametrization. Assuming that the calculated energy of the centroid of an intruder state is more robust against corrections from core polarization and particle-vibration coupling that its spin-orbit splitting, we see that the $\nu\,1h$ centroid is clearly too high in energy by about 1 MeV. In combination with its tentatively too small spin-orbit splitting, see Fig. 4.10, this offers an explanation for the notorious wrong positioning of the ν $1h_{11/2}$, $2d_{3/2}$ and $3s_{1/2}$ levels in ^{132}Sn [Ben03b]. The near-degeneracy of the ν $2d_{3/2}$ and $3s_{1/2}$ levels is always well reproduced, while the $1h_{11/2}$ comes out much too high. As the $1h_{11/2}$ is the last occupied neutron level, self-consistency puts it close to the Fermi energy, which, in turn, pushes the $2d_{3/2}$ and $3s_{1/2}$ levels down in the spectrum.

The overall situation is similar for ^{208}Pb, see Fig. 4.14. Again, the high-ℓ intruder states move too close to the $Z = 82$ and $N = 126$ gaps for large positive C_0^J. The effect is less obvious than for ^{132}Sn as the intruders and their spin-orbit partners are further away from the gaps. Still, the level ordering and the size of the $Z = 82$ gap become unacceptable for parametrizations with large tensor coupling constants. For strong tensor term coupling constants (both like-particle and proton-neutron), a $Z = 92$ gap opens in the single-particle spectrum of the protons that is also frequently predicted by relativistic mean-field models [Rut98, Ben99b] but absent in experiment [Hau01].

The single-particle spectra for the light doubly magic nuclei ^{40}Ca (Fig. 4.15), ^{48}Ca (Fig. 4.16), ^{56}Ni (Fig. 4.17), ^{68}Ni (Fig. 4.18) and ^{90}Zr (Fig. 4.19), all have in common that the relative impact of the $\mathbf{J}^2$ terms on the ordering and relative distance of single-particle levels is even stronger than for the heavy nuclei discussed above. But not all of the strong dependence on the coupling constants of the $\mathbf{J}^2$ terms that we see in the figures is due to the actual contribution of the tensor

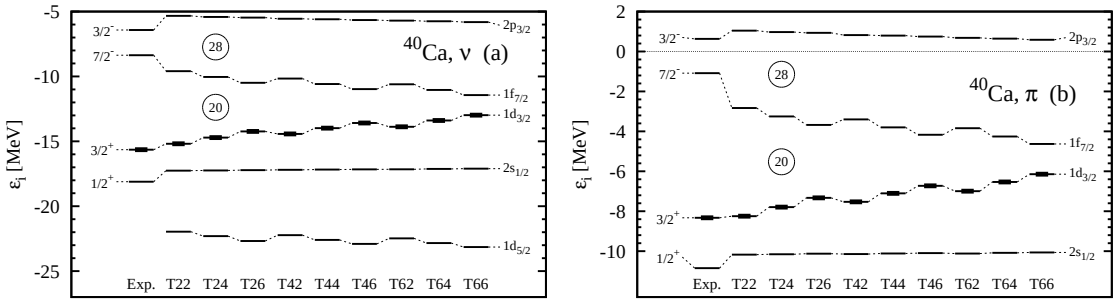

Figure 4.15: Same as Fig. 4.13 for ^{40}Ca.

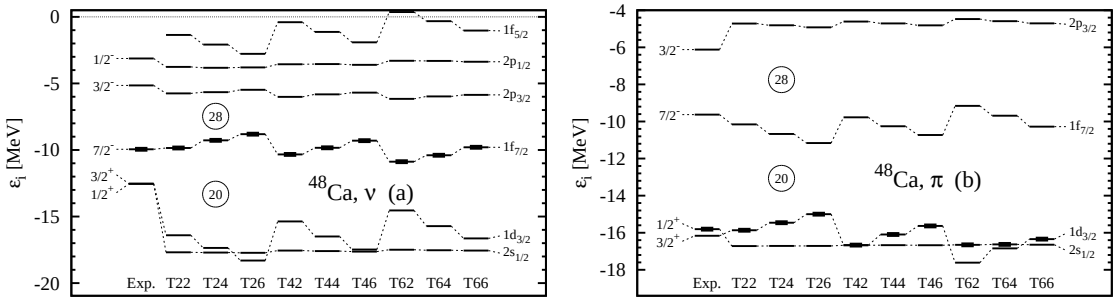

Figure 4.16: Same as Fig. 4.13 for ^{48}Ca.

terms to the spin-orbit potential. This is most obvious for ^{40}Ca, where protons and neutrons are spin-saturated so that the $\mathbf{J}^2$ terms do not contribute to the spin-orbit potentials. Still, increasing their coupling constants increases the spin-orbit splittings, which manifests the readjustment of the spin-orbit force to a given set of C_0^J and C_1^J (see Fig. 4.4). The evolution of the spin-orbit splittings in ^{40}Ca visible in Fig. 4.15 is the background which we have to keep in mind when discussing the impact of the tensor terms on nuclei with non-vanishing spin-orbit currents. Note that the spin-orbit coupling constant W_0 is correlated with isoscalar tensor coupling constant C_0^J, such that the single-particle spectra obtained with T24 and T42 are very similar, as they are for T26, T44 and T62.

For ^{48}Ca, Fig. 4.16, the protons are still spin-saturated with vanishing proton spin-orbit current $\mathbf{J}_\mathrm{p}$, while for neutrons we have a large $\mathbf{J}_\mathrm{n}$. Depending on the nature of the tensor terms in the energy functional – i.e. like-particle or proton-neutron or a mixture of both – the spin-orbit current will either contribute to the spin-orbit potential of the neutrons or that of the protons or both, see Eq. (4.8). For the parametrizations with dominating like-particle $\mathbf{J}^2$ term, for example T24 and T26, the situation for the protons is the same as for ^{40}Ca: there is no contribution from the tensor terms to the proton spin-orbit splittings, but compared to T22 the proton $Z = 20$ gap is reduced through the readjustment of the spin-orbit force, leading to values that are too small. For the same parametrizations, the large contribution from $\mathbf{J}_\mathrm{n}$ to W_n opens up the $N = 20$ gap to values that are tentatively too large, as it reduces the neutron spin-orbit splittings and thereby compensates, even overcompensates, the effect from the readjustment of the spin-orbit force. At the same time the $N = 28$ gap is reduced. The opposite effect is seen for parametrizations with large proton-neutron tensor term, for example T42 or T62. For those, the proton spin-

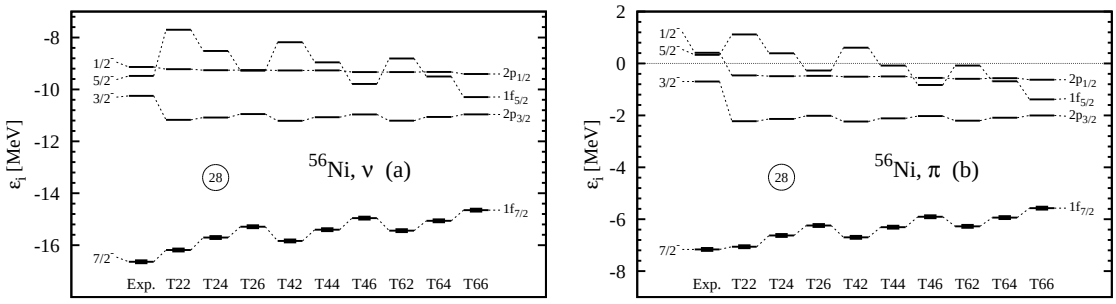

Figure 4.17: Same as Fig. 4.13 for ^{56}Ni.

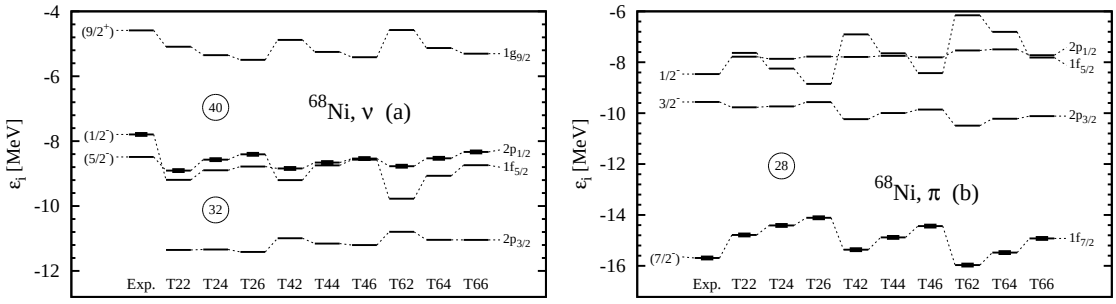

Figure 4.18: Same as Fig. 4.13 for ^{68}Ni.

orbit splitting is reduced, opening up the $Z = 20$ gap compared to T22, while the neutron spin-orbit splittings are increased by the background effect from the readjusted spin-orbit force.

For ^{56}Ni, Fig. 4.17, we have large $\mathbf{J}_\mathrm{n}$ and $\mathbf{J}_\mathrm{p}$. In this $N = Z$ nucleus, the like-particle or proton-neutron parts of the tensor terms cannot be distinguished. The spectra depend only on the overall coupling constant of the isoscalar tensor term C_0^J, on the one hand directly through the contribution of the tensor terms to the spin-orbit potentials, and on the other hand through the background readjustment of W_0 that is correlated to C_0^J as well. As already mentioned, results for T24 and T42 are very similar, as they are for T26, T44 and T62. All parametrizations have in common that the proton and neutron gaps at 28 are too small. The variation of the single-particle spectra among the parametrizations is smaller than for ^{40}Ca, mainly because the tensor terms compensate the background drift from the readjustment of W_0.

The slightly neutron-rich ^{68}Ni combines a spin-saturated sub-shell closure $N = 40$ that gives a vanishing neutron spin-orbit current with the magic $Z = 28$ that gives a strong proton spin-orbit current. The variation of the single-particle spectra in dependence of the coupling constants of the tensor terms is similar to those of ^{48}Ca, with the roles of protons and neutrons exchanged.

The nucleus ^{90}Zr combines the spin-saturated proton sub-shell closure $Z = 40$ with the major neutron shell closure $N = 50$. The high degeneracy of the occupied ν $1g_{9/2}$ level leads to a very strong neutron spin-orbit current, while the proton spin-orbit current is zero. Even in the absence of a tensor term contributing to their spin-orbit potential for parametrizations with pure like-particle tensor terms, the proton single-particle spectra are dramatically changed by the feedback effect from

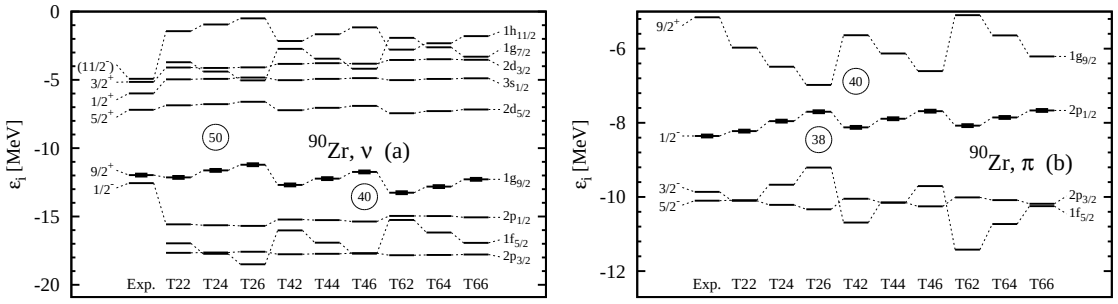

Figure 4.19: Same as Fig. 4.13 for ^{90}Zr.

the readjusted spin-orbit force; see the evolution from T22 to T26. The $\pi\, 1g_{9/2}$ comes down, and closes the $Z = 40$ sub-shell gap. For parametrizations with pure proton-neutron tensor term, one has the opposite effect, this time because the contribution from the tensor terms overcompensates the background effect from the spin-orbit force. The effect of the tensor terms on the neutron spin-orbit splittings is less dramatic, but still might be sizable.

We have to point out that the calculations displayed in Fig. 4.19 were performed without taking pairing into account, as the HFB scheme breaks down in the weak pairing regime of doubly magic nuclei. For some extreme (and unrealistic) parametrizations, however, the gaps disappear which, in turn, would lead to strong pairing correlations if the calculations were performed within the HFB scheme. This happens, for example, for neutrons in ^{90}Zr when using T26 and T46. Interestingly, the pairing correlations for neutrons break the spin saturation, which leads to a substantial neutron spin-orbit current $\mathbf{J}_{\rm n}$. As these parametrizations use values of the like-particle coupling constant significantly larger than the neutron-proton one, $\mathbf{J}_{\rm n}$ feeds back onto the neutron spin-orbit potential only, Eq. (4.8). As the corresponding coupling constant α is positive for T26 and T46, the contribution from the tensor terms reduces the spin-orbit splittings, in particular those of the $1g_{9/2}$ and $1f_{5/2}$. As a result, this counteracts the reduction of the $N = 40$ gap predicted by T26 and T46 in calculations without pairing. Moreover, if pairing sets in, the relevant quantities to be compared to odd-even mass differences are quasiparticle energies, instead of HF single-particle ones. A contribution from the pairing gap thus supplements the shell gap. Such a strong reduction of a gap across the Fermi level is thus unlikely to be observed.

Evolution along isotopic chains: *np* coupling

In the preceding sections, we have analyzed characteristics of the single-particle spectra for isolated doubly-magic nuclei. We found that larger tensor terms do not lead to an overall improvement of the single-particle spectra. However, we also argued that it might be essentially due to deficiencies of the central (and possibly spin-orbit) interactions and that it should not be used to discard the tensor terms as such. In any case, the results gathered so far on single-particle spectra of doubly-magic nuclei do not permit to narrow down a region of meaningful coupling constants of the tensor terms. The analysis must be complemented by looking at other observables. A better suited observable is provided by the evolution of spin-orbit splittings along an isotopic or isotonic chain, which ideally reflects the nucleon-number-dependent

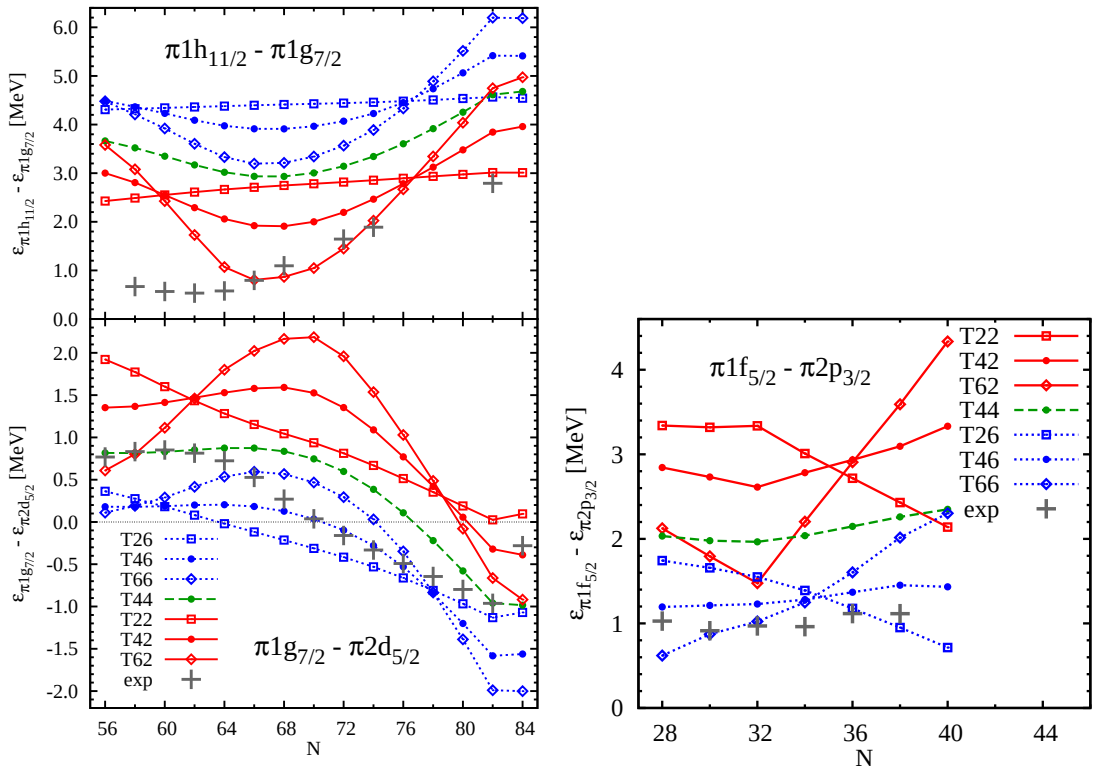

Figure 4.20: Left panel: Distance of the proton $1h_{11/2}$ and $1g_{7/2}$ levels (top) and of the proton $2d_{5/2}$ and $1g_{7/2}$ levels (bottom), for the chain of tin isotopes. Right panel: Distance of the proton $1f_{5/2}$ and $2p_{3/2}$ in the chain of Ni isotopes. The "best" parametrization cannot and should not be determined with a χ^2 criterion, see text.

contribution from the $\mathbf{J}^2$ terms to the spin-orbit potentials. Unfortunately, safe experimental data for the evolution of spin-orbit partners are scarce; hence, one has to content oneself to the evolution of the energy distance of levels with different ℓ, assuming that the effect is primarily caused by the evolution of the spin-orbit splittings of each level with its respective partner. A popular playground for such studies is the chain of Sn isotopes, where two such pairs of levels have gained attention; the $\pi\ 2d_{5/2}$ and $\pi\ 1g_{7/2}$ on the one hand, and the $\pi\ 1g_{7/2}$ and $\pi\ 1h_{11/2}$ on the other hand. The left panel of Figure 4.20 shows these two sets of results for a selection of our parametrizations.

Experimentally, the $2d_{5/2}$ and $1g_{7/2}$ levels cross between $N = 70$ and 72, such that the $2d_{5/2}$ provides the ground state of light odd-A Sb isotopes, and $1g_{7/2}$ that of the heavy ones, see for example Ref. [She05]. The crossing as such is predicted by many mean-field interactions and most of the parametrizations of the Skyrme interaction we use here. It has also been studied in detail with the standard Gogny force (without any tensor term) using elaborate blocking calculations of the odd-A nuclei [Por05]. The crossing, however, is never predicted at the right neutron number, see Fig. 4.20. As we have learned above, we should not assume that the absolute distance of the two levels will be correctly described by any of our parametrizations (as the centroids of the ℓ shells will not have the proper distance and the spin-orbit splittings have a wrong ℓ dependence within a given shell). Hence, the neutron number where the crossing takes place cannot and should not be used as a quality criterion. What does characterize the tensor terms is the bend of the curves in Fig. 4.20, as ideally it reflects how the spin-orbit splittings of both levels change in the presence of the tensor terms. Similar caution has to be exercised in the analysis of the unusual relative evolution of the proton $1g_{7/2}$ and $1h_{11/2}$ levels that was brought to attention by Schieffer et al. [Sch04]. Their spacing has been investigated in terms of the tensor force before [Ots05, Ots06, Bro06a, Col07]. Again, we pay attention to the qualitative nature of the bend without focusing too much on the precise value by which the splitting changes when going from $N \approx 58$ to $N = 82$. Indeed, the matching of the lowest proton fragment with quantum number $1h_{11/2}$ seen experimentally with the corresponding empirical single-particle energy is unsafe because of the fractionization of the strength as discussed in Ref. [Bro06a].

For both pairs of levels, the evolution of their distance can be attributed to the tensor coupling between the proton levels and neutrons filling the $1h_{11/2}$ level below the $N = 82$ gap. Unfortunately, this introduces an additional source of uncertainty: as can be seen in Fig. 4.13, the ordering of the neutron levels in ^{132}Sn is not properly reproduced by any of our parametrizations, with the $1h_{11/2}$ level being predicted above the $2d_{3/2}$ level, while it is the other way round in experiment. This means that in the calculations, the contribution from the $1h_{11/2}$ level to the neutron spin-orbit current builds up at larger N than what can be expected in experiment. As a consequence, the prediction for the relative evolution of the levels might be shifted by up to four mass units to the right compared to experiment for both pairs of levels we examine here.

In the end, the trend of both splittings is best reproduced when using a positive value of the neutron-proton $\mathbf{J}_\mathrm{n} \cdot \mathbf{J}_\mathrm{p}$ coupling constant β such that the filling of the neutron $1h_{11/2}$ shell decreases the spin-orbit splittings of the proton shells. The parametrizations from the T4J and T6J series indeed do reproduce the bend of empirical data, with, however, a clear shift in the neutron number where it occurs,

as expected from the previous discussion. A value of $\beta = 120$ MeV fm^5, which corresponds to the series of T4J parametrizations, matches its magnitude best (see for example T44).

A similar analysis can be performed for the proton $1f_{5/2}$ and $2p_{3/2}$ levels in the chain of Ni isotopes, see the right panel of Fig. 4.20. This case is interesting as no distinctive feature can be observed in the empirical spectra, yet the standard parametrizations without tensor terms like T22 do not reproduce them. In fact, to keep the $1f_{5/2}$ and $2p_{3/2}$ at a constant distance, two competing effects have to cancel. First, the increasing diffuseness of the neutron density with increasing neutron number diminishes the proton spin-orbit splittings through its reduced gradient in the expression for the proton spin-orbit potential when going from $N = 32$ to $N = 40$. Second, the filling of the neutron $1f_{5/2}$ state reduces the neutron spin-orbit current which in turn increases the proton spin-orbit splittings for interactions with sizable proton-neutron tensor contribution to the proton spin-orbit potential when going from $N = 32$ to $N = 40$. The former effect can be clearly seen for parametrizations T2J with vanishing proton-neutron tensor term, $\beta = 0$. Again, parametrizations of the T4J series seem to be the most appropriate to describe the evolution of these levels.

The evolution of single-particle levels is the tool of choice to determine the sign and magnitude of the proton-neutron tensor coupling constant. The value which we favor, as a result of our semi-qualitative analysis is $\beta = 120$ MeV fm^5. This value is only slightly larger than the value of 94 to 96 MeV fm^5 advocated by Brown et al. in Ref. [Bro06a], which was adjusted to *theoretical* level shifts in the chain of tin isotopes obtained from a G-matrix interaction. We can consider this as a reasonable agreement.

Let us defer the discussion of this value to the end of this section and study in the next paragraph the like-particle tensor-term coupling constant α.

Evolution along isotopic chains: nn coupling

In order to narrow down an empirical value for the neutron-neutron tensor coupling constant, the ideal observable would be the evolution of neutron single-particle levels along an isotopic chain. Unfortunately, these are only accessible at the respective shell closures. We shall therefore compare neutron single-particle spectra of pairs of doubly-magic nuclei belonging to the same isotopic chain. Again, the necessity to extract pure single-particle effects calls for precautions. We choose pairs of particle or hole levels which are close enough in energy that their absolute spacing is not much affected by particle-vibration coupling. Of course, one also has to be careful if both states appear at relatively high excitation energy in the neighboring odd isotope because the fractionization of their strength could again interfere with the analysis. In the following, we choose pairs of orbitals which are as safe as possible.

To remove the uncertainties from the deficiencies of the central and spin-orbit parts of the effective interaction that we have identified above, we will look at a double difference, where, first, we construct the energy difference between the neutron $1d_{3/2}$ and $2s_{1/2}$ levels separately for ^{40}Ca and ^{48}Ca, and then compare the value of this difference in both nuclei

$$\delta^{\mathrm{Ca}} = \left(\varepsilon^{^{48}\mathrm{Ca}}_{1d_{3/2}} - \varepsilon^{^{48}\mathrm{Ca}}_{2s_{1/2}}\right) - \left(\varepsilon^{^{40}\mathrm{Ca}}_{1d_{3/2}} - \varepsilon^{^{40}\mathrm{Ca}}_{2s_{1/2}}\right). \tag{4.15}$$

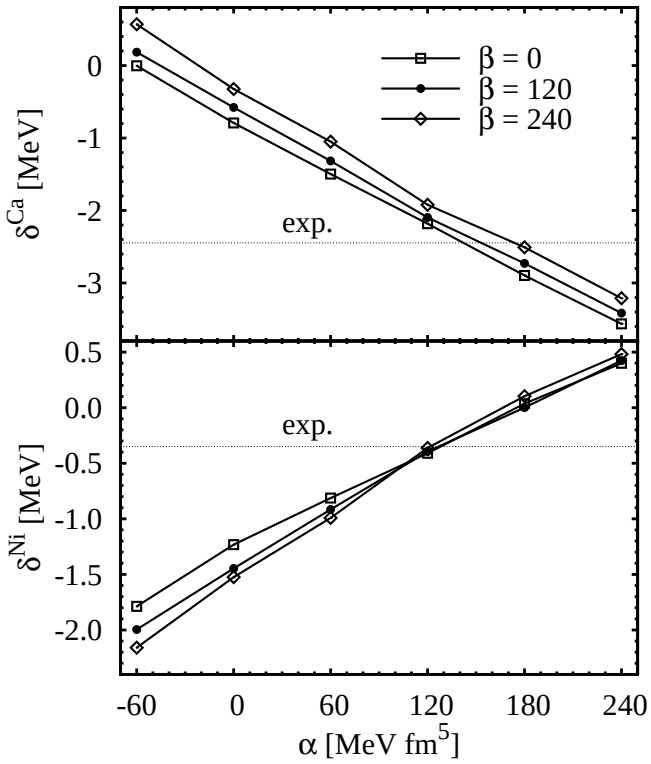

Figure 4.21: Shift of the distance between the neutron $1d_{3/2}$ and $2s_{1/2}$ levels when going from ^{40}Ca to ^{48}Ca, Eq. (4.15) (top) and of the neutron $1f_{5/2}$ and $2p_{1/2}$ levels when going from ^{56}Ni and ^{68}Ni, Eq. (4.16) (bottom).

Assuming that the problems from the central and spin-orbit forces discussed in Sects. 4.3.2 and 4.3.2 have the same effect in both nuclei, they will cancel out in δ^{Ca}.

The interesting feature of this pair of states is that they are separated by more than 2 MeV in ^{40}Ca, while they are nearly degenerate in ^{48}Ca, see Figs. 4.15 and 4.16. Such a shift can only be reproduced with a positive (140-180 MeV fm^5) value of α, which decreases the splitting of the neutron $1d$ shell when the neutron $1f_{7/2}$ level is filled.

A similar analysis can be performed for the $1f_{5/2}$ and $2p_{1/2}$ neutron states in the Ni isotopes ^{56}Ni and ^{68}Ni

$$\delta^{\mathrm{Ni}} = \left(\varepsilon^{^{68}\mathrm{Ni}}_{1f_{5/2}} - \varepsilon^{^{68}\mathrm{Ni}}_{2p_{1/2}}\right) - \left(\varepsilon^{^{56}\mathrm{Ni}}_{1f_{5/2}} - \varepsilon^{^{56}\mathrm{Ni}}_{2p_{1/2}}\right). \tag{4.16}$$

Going from ^{56}Ni to ^{68}Ni, the neutron $1f_{5/2}$ level comes further down in energy than the $2p_{1/2}$ level for parametrizations without tensor terms (T22), see Figs. 4.17 and 4.18. The reason for this trend is the geometrical growth of the nucleus, which on the one hand lowers the centroid of the $1f$ levels in the widening potential well, and on the other hand pushes the spin-orbit field to larger radii, which has opposite effects on the splittings of $2p$ and $1f$ states. The like-particle tensor terms can compensate this trend through a reduction of the spin-orbit splitting of the $1f$ levels. The observed downward shift by 0.3 MeV can be recovered with a value of α around 120 MeV fm^5, see Fig. 4.21.

It is also gratifying to see that the analysis of Ca and Ni isotopes suggests nearly the same value for the like-particle tensor term coupling constant α.

4.3.3 Binding energies

Our ultimate goal, although far beyond the scope of the present paper, is the construction of a universal nuclear energy density functional that simultaneously describes bulk properties like masses and radii, giant resonances, and low-energy spectroscopy, such as quasiparticle configurations and collective rotational and vibrational states. To crosscheck how our findings on single-particle spectra and spin-orbit splittings translate into bulk properties, we will now analyze the evolution of mass residuals and charge radii along isotopic and isotonic chains. It has been repeatedly noted in the literature that the mass residuals from mean-field calculations show characteristic arches [Dob84, Fri86, Cha98, Pat99, Ben03b, Lun03, Dob04, Ben06a], where heavy mid-shell nuclei are usually underbound compared to the doubly magic ones that are located at the bottom of deep ravines. For light nuclei, the patterns are often less obvious. Part of this effect can be explained and removed taking large-amplitude correlations from collective shape degrees of freedom into account through suitable beyond-mean-field methods. In turn, this means that the mass residuals should leave room for the extra binding of mid-shell nuclei from correlations. However, it turns out that for typical effective interactions the amplitude of the arches is larger than what is brought by correlations [Ben06a]. Furthermore, this effect seems not to be of the same size for isotopic and isotonic chains, which altogether hints at deficiencies of the current effective interactions.

Recently, Dobaczewski pointed out [Dob06] that the strongly fluctuating contribution brought by the $\mathbf{J}^2$ terms to the total binding energy could remove at least some of the ravines found in the mass residuals around magic numbers. The hypothesis was motivated by calculations that evaluate the tensor terms either perturbatively, or self-consistently, using in this case an existing standard parametrization without tensor terms for the rest of the energy functional. Our set of refitted parametrizations with varied coupling constants of the tensor terms gives us a tool to check how much of the argument persists to a full fit.

Semi-magic chains

Figure 4.22 displays binding energy residuals along various isotopic and isotonic chains of semi-magic nuclei for a selection of our parametrizations: T22 is the reference with vanishing $\mathbf{J}^2$ terms at sphericity; T24 has a substantial like-particle coupling constant α and vanishing proton-neutron coupling constant β, which is similar to most of the published parametrizations which take the $\mathbf{J}^2$ terms from the central Skyrme force into account; T42 and T62 are parametrizations with substantial proton-neutron coupling constant β and vanishing like-particle coupling constant; T44 has a mixture of like-particle and proton-neutron tensor terms that is close to what we found preferable for the evolution of spin-orbit splittings above; and T46 is a parametrization that gives the best root-mean-square residual of binding energies for spherical nuclei, as we will see below. Finally, T66 is a parametrization with large and equal proton-neutron and like-particle tensor-term coupling constants.

Tensor terms have opposite effects in light and heavy nuclei: The curves obtained with T22, the parametrization without $\mathbf{J}^2$ term contribution at sphericity, are relatively flat for the light isotopic and isotonic chains, but show very pronounced arches with an amplitude of 5 or even more MeV for the heavy Sn and Pb isotopic chains. By contrast, the most striking effect of the $\mathbf{J}^2$ terms is that they induce

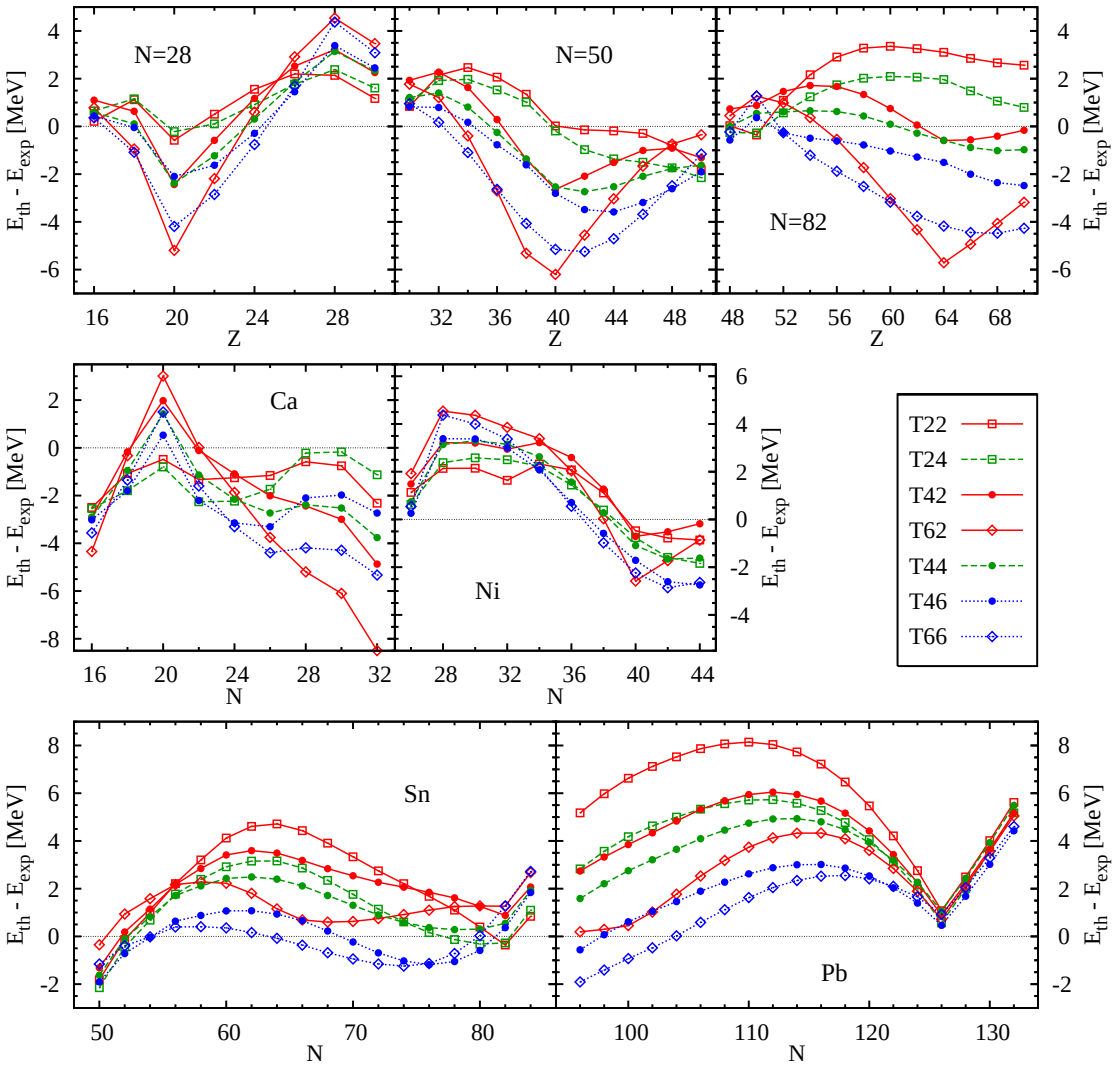

Figure 4.22: Mass residuals $E_{\rm th} - E_{\rm exp}$ along selected isotopic and isotonic chains of semi-magic nuclei for the parametrizations as indicated. Positive values of $E_{\rm th} - E_{\rm exp}$ denote underbound nuclei, negative values overbound nuclei.

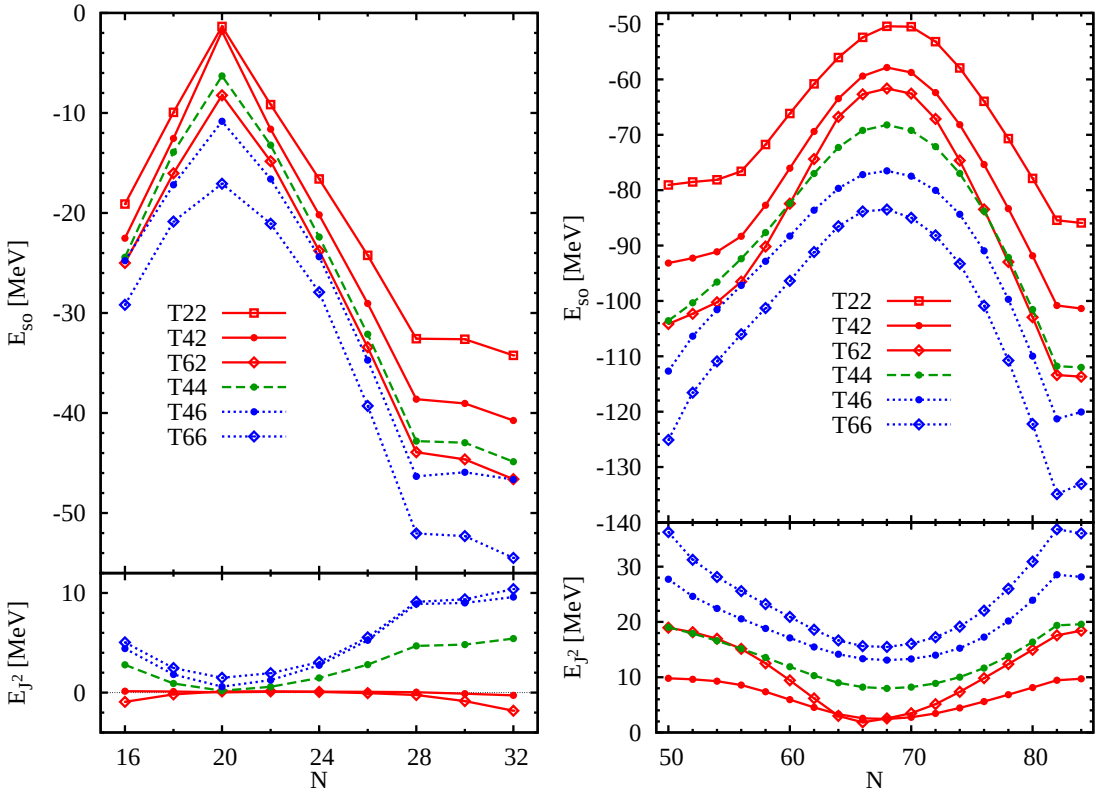

Figure 4.23: Evolution of spin-orbit current (J_t^2) energy (bottom panels, zero by construction for T22) and spin-orbit energy (top panels) with neutron number N in the chain of Ca isotopes ($Z = 20$, left) and Sn isotopes ($Z = 50$, right).

large fluctuations of the mass residuals in light nuclei, while they flatten the curves in the heavy ones.

The strong variation between the parameter sets for light nuclei are of course the direct consequence of the strong variation of the spin-orbit current $\mathbf{J}$ that enters the spin-orbit and tensor terms when going back and forth between nuclei where the configuration of at least one nucleon species is spin-saturated. The variations seen are a result of the modifications of tensor-term coupling constants and the associated readjustment of the spin-orbit strength W_0. For example, ^{48}Ca is overbound with respect to ^{40}Ca and ^{56}Ni for parametrizations with a proton-neutron coupling constant $\beta > 0$, while the like-particle coupling constant α has a more limited effect. Since only the neutron core is spin-unsaturated in this nucleus, this must be attributed to the increase in the readjusted spin-orbit strength W_0 (correlated with $C_0^J = \frac{1}{2}(\alpha + \beta)$) which dominates when β is increased and α kept at zero, and counterbalances the effect of α when the latter varies. See the parameter sets T62 and T66 in Figures 4.22 and 4.23. The large overbinding of nuclei around ^{90}Zr ($Z = 40$, $N = 50$) for parametrizations with large proton-neutron tensor coupling constant has the same origin. For a given parametrization and a given nucleus, the energy gain from the spin-orbit term seems to be almost always larger than the energy loss from the $\mathbf{J}^2$ one, see Fig. 4.23 for Ca and Sn isotopes. Of course, other terms in the energy functional compensate for a part of the gain from the spin-orbit term, but the overall trends of the mass residuals suggest that the spin-orbit energy has a

much larger contribution to the differences between the parametrizations visible in Fig. 4.22 than the $\mathbf{J}^2$ terms.

We have to note that the spin-orbit current does not completely vanish for the nominally proton and neutron spin-saturated ^{40}Ca for parametrizations with large coupling constants of the $\mathbf{J}^2$ terms. For those, the gap at 20 is strongly (and non-physically) reduced, see Fig. 4.15. The small gap at 20 does not suppress pairing correlations anymore in our HFB approach. The resulting scattering of particles from the *sd* shell to the *fp* shell breaks the spin-saturation, such that there is a finite, in some cases quite sizable, contribution from the spin-orbit term to the total binding energy. Owing to the compensation between all contributions, the total energy gain compared to a HF calculation without pairing is usually small and rests on the order of 200 keV for the parametrizations shown in Fig. 4.22.

It is also important to note that some of the light chains in Fig. 4.22 are sufficiently close to or even cross the $N = Z$ line that they are subject to the Wigner energy, which still lacks a satisfying explanation, not to mention a description in the framework of mean-field methods [Sat97]. The Wigner energy is not taken into account in our fits, while it turned out to be a crucial ingredient of any HFB [Ton00, Sam02, Gor03] or other mass formula. In fact, as shown in Fig. 14 of Ref. [Ben06a], the missing Wigner energy clearly sticks out from the mass residuals for SLy4 (which is very similar to T22) when they are plotted for isobaric chains. This local trend around $N = Z$ is, however, overlaced with a global trend with mass number, such that the missing Wigner energy cannot be spotted anymore when looking at the mass residuals for the isotopic chain of Ca isotopes, similar to what is seen for T22 in Fig. 4.22. Within our fit protocol, the correlation between the masses of ^{40}Ca, ^{48}Ca and ^{56}Ni, that is brought by the spin-orbit force (see Sect. 4.3.2) does not tolerate a correction for the Wigner energy for standard central and spin-orbit Skyrme forces, as this will lead to an unacceptable underbinding of ^{48}Ca. This, however, might change when the $\mathbf{J}^2$ terms are added. Indeed, Fig. 4.22 suggests that adding a phenomenological Wigner term around ^{40}Ca and ^{56}Ni to a parameter set like T44, which is consistent with the evolution of single-particle levels, would flatten the curves for the mass residuals in the Ca, Ni and $N = 28$ chains. The mass residuals for the chain of oxygen isotopes that are not shown here would be improved in a similar manner. However, extreme caution should be exercised before jumping to premature conclusions, as the spin-orbit splittings and level distances in light nuclei are far from realistic for all our parametrizations; as a consequence it is difficult to judge if the room we find for the Wigner energy is fortuitous or indeed a feature of well-tuned $\mathbf{J}^2$ terms. Note that the HFB mass formulas that do include a correction for the Wigner energy side-by-side with the $\mathbf{J}^2$ terms from the central Skyrme force give satisfying mass residuals for light nuclei [Ton00, Sam02, Gor03], but have nuclear matter properties that are quite different from ours; *cf.* BSk1 and BSk6 with SLy4 in Table I of Ref. [Rei06]. Our constraints on the empirical nuclear matter properties (same as those on SLy4) that are absent in these HFB mass fits might be the deeper reason for this conflict.

Large tensor-term coupling constants straighten the arches in the mass residuals in the heavy Sn and Pb isotopic chains, but the improvements are not completely satisfactory. Large, combined proton-neutron and like-particle coupling constants tend to transform the arch for the tin isotopic chain into a an s-shaped curve, which is not very realistic from the standpoint of expected corrections through collective

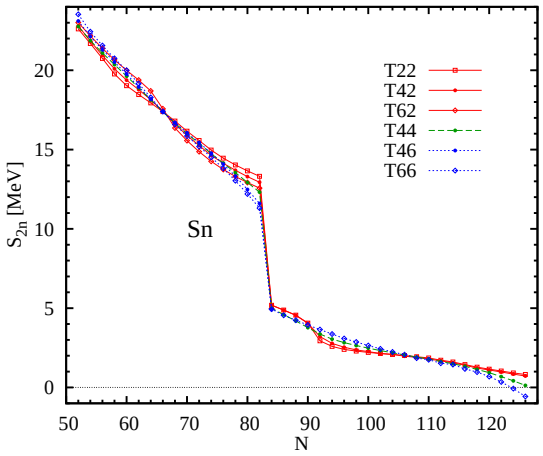

Figure 4.24: Two-neutron separation energy along the chain of isotopes ($Z = 50$).

effects. It can again be assumed that the deficiencies of the single-particle spectra pointed out in Fig. 4.13 are responsible, where the $\nu\ 1h_{11/2}$ and $\pi\ 1g_{9/2}$ are placed too high above the rest of the single-particle spectra in heavy Sn isotopes. For Pb isotopes, large values of the tensor terms tend to overbind the neutron-deficient isotopes. It is noteworthy that the tensor terms seem to not much affect the mass residuals of the heavy Pb isotopes above $N = 126$, which are on the flank of a very deep ravine that becomes visible when going towards heavier elements, *cf.* the SLy4 results in Ref. [Ben06a].

It has been often noted that effective interactions that give a similar satisfying description of masses close to the valley of stability give diverging predictions when extrapolated to exotic nuclei. The standard example is the two-neutron separation energy $S_{2n}(N,Z) = E(N,Z-2) - E(N,Z)$ for the chain of Sn isotopes. Results obtained with a subset of our parametrizations are shown in Fig. 4.24. It is noteworthy that the differences for neutron-rich nuclei beyond $N = 82$ are not larger than those for the isotopes closer to stability. Around the valley of stability, increasing the coupling constants of tensor terms, in particular the like-particle ones, tilts the curve, pushing it up for light isotopes and pulling it down it for heavy ones, which reflects of course the position of the $\nu\ 1h_{11/2}$ level that is pushed into the $N = 82$ gap, see Fig. 4.13. For the neutron-rich isotopes, small differences appear around $N = 90$, which reflects the change of level structure above the $\nu\ 2f_{7/2}$ level and at the drip line, but they are much smaller than the differences seen between parametrizations obtained with different fit protocols, see Fig. 5 of Ref. [Ben03b].

Systematics

In the preceding section we showed how the $\mathbf{J}^2$ terms in the energy functional modify the trends of mass residuals along isotopic and isotonic chains, in particular the amplitude of the arches between doubly-magic nuclei. In this section, we want to examine how this translates into quality criteria for the overall performance of the parametrizations for masses.

Figure 4.25 displays the root-mean-square deviation of the mass residuals for all our 36 parametrizations, evaluated for a set of 134 nuclei predicted to have spherical mean-field ground states when calculated with the parametrizations SLy4 [Ben06a].

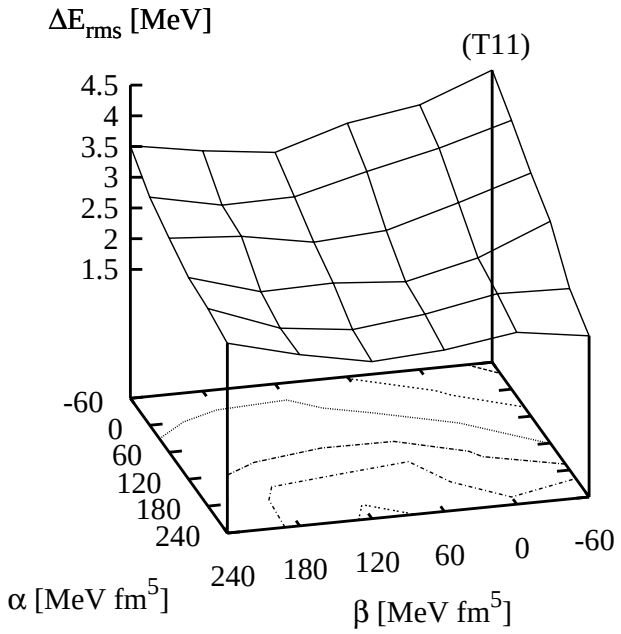

Figure 4.25: Root-mean-square deviation from experiment of the binding energies of a set of 134 spherical nuclei, for each of the forces TIJ, *vs.* α and β (The "(T11)" label indicates the position of this parametrization in the (α, β)-plane). Contour lines at $\Delta E_{\rm rms} = 2.0, 2.25, 2.5, 3.0, 3.5, 4.0$ MeV. The minimal value is found for T46 ($\Delta E_{\rm rms} = 1.96$ MeV).

One observes a clear minimum around T46, i.e. $(\alpha, \beta) = (240, 120)$, with $(E_{\rm th} - E_{\rm exp})_{\rm r.m.s.} = 1.96$ MeV, compared with 3.44 MeV for T22 ($\alpha = \beta = 0$). We found even slightly better values with even more repulsive isoscalar and isovector coupling constants, but the single-particle spectra of these interactions turn out to be quite unrealistic, *cf.* Sect. 4.3.2. This already demonstrates that in the presence of the $\mathbf{J}^2$ terms a good fit of masses does not necessarily lead to satisfactory single-particle spectra.

Figure 4.26 demonstrates how the distribution of the mass residuals $E_{\rm th} - E_{\rm exp}$ affects the evolution of their r.m.s. value for a subset of 9 parametrizations. For T22 ($\alpha = \beta = 0$), the distribution is centered at positive mass residuals, with only very few nuclei being overbound. Increasing β to 120 MeV fm^5 (T42) or even 240 MeV fm^5 (T62) shifts the median of the distribution to smaller values, which yields more and more overbound nuclei. For large values of β, the distribution spreads out more, which diminishes the improvement from centering the distribution closer to zero. For given β, increasing α mainly shifts the median of the distribution without spreading out its overall shape, which is preferable to optimize the r.m.s. value.

These considerations, however, have to be taken with caution. As said above, we aim at a model where certain correlations beyond the mean-field are treated explicitly, which asks for a distribution of *mean-field* mass residuals with an asymmetric distribution towards positive mass residuals, and a width that is similar to the difference between the maximum and minimum correlation energies to be found.

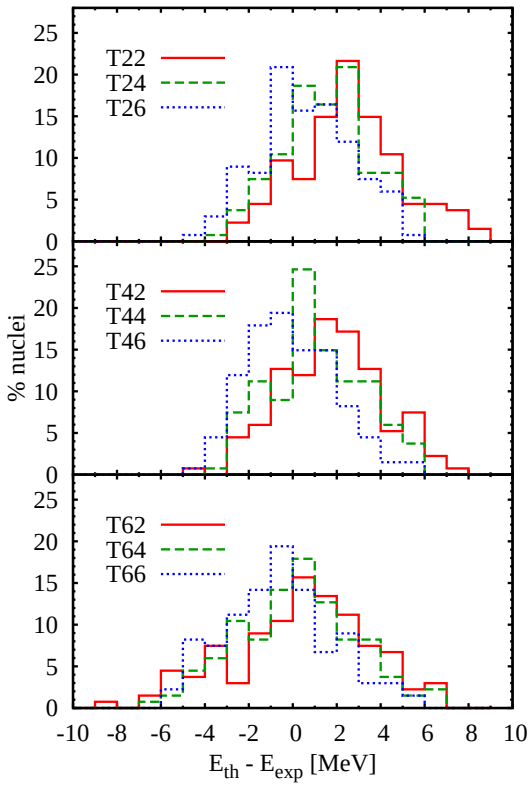

Figure 4.26: Distribution of deviations from experiment of the binding energies of a set of 134 spherical nuclei (1 MeV bins) for a subset of parametrizations. Each panel corresponds to a given value of β (from top to bottom: $\beta = 0$, 120, 240 MeV fm^5).

4.3.4 Radii

The evolution of nuclear charge radii along isotopic chains reflects how the mean field of the protons changes when neutrons are added in the system. In the simplistic liquid-drop model, it just follows the geometrical growth of the nucleus $\sim A^{1/3}$, but data show that there are many local deviations from this global trend. On the one hand, radii are of course subject to correlations beyond the mean field [Rei79, Gir82, Bon91, Hee93, Ben06a] On the other hand, they are also sensitive to the detailed shell structure, which, in turn, might be influenced by tensor terms. We will concentrate here on two anomalies of the evolution of charge radii, both of which are not much influenced by collective correlations beyond the mean-field (at least in calculations with the Skyrme interaction SLy4) [Ben06a]: that the root-mean-square (r.m.s.) charge radius of ^{48}Ca is almost the same as the one of the lighter ^{40}Ca or possibly slightly smaller, and the kink in the isotopic shifts of mean-square (m.s.) charge radii in the Pb isotopes, where Pb isotopes above ^{208}Pb are larger than what could be expected from liquid-drop systematics. In both cases it is plausible that shell effects are the determining factor, although alternative explanations that involve pairing effects have been put forward for the latter case as well [Taj93a, Fay00].

Charge radii have been calculated with the approximation used in Ref. [Cha97][1] and derived from Ref. [Ber72]

$$r_{\rm ch}^2 = \langle r^2 \rangle_{\rm p} + r_{\rm p}^2 + \frac{N}{Z} r_{\rm n}^2 + \frac{1}{Z} \left(\frac{\hbar}{mc} \right)^2 \sum_i v_i^2 \mu_{q_i} \langle \boldsymbol{\sigma} \cdot \boldsymbol{\ell} \rangle_i \,, \tag{4.17}$$

where the mean-square (m.s.) radius of the point-proton distribution $\langle r^2 \rangle_{\rm p}$ is corrected by three terms: the first two estimate the effects of the intrinsic charge distribution of the free proton and neutron (with m.s. radii $r_{\rm p}^2$ and $r_{\rm n}^2$) and the third adds a correction from the magnetic moments of the nucleons. Since we will consider the shift of charge radii for different isotopes of the same series, the actual value of $r_{\rm p}^2$ cancels out. For the second correction term, which is independent from the interaction, we take $r_{\rm n}^2 = -0.117$ fm^2 [Ben03b]. Finally, the magnetic correction can only depend weakly on the details of the interaction through the occupation factors v_i^2 when non-magic nuclei are considered. The same expressions had been used during the fit of our parametrizations.

We begin with the Ca isotopes. Most parametrizations of Skyrme's interaction are not able to reproduce that the charge radius of ^{48}Ca has about the same size as that of ^{40}Ca, see Fig. 11 in Ref. [Ben03b]. The middle panel of Fig. 4.27 shows the difference of the m.s. radii of ^{48}Ca and ^{40}Ca in dependence of the tensor term coupling constants α and β. First, this difference is almost independent of α, the strength of the like-particle tensor terms. Second, it is strongly correlated with β, the strength of the proton-neutron tensor term, with large positive values of β bringing the difference of radii into the domain of experimentally acceptable values [Ott89] or even below, with a best match obtained for $\beta = 80$ MeV fm^5. This effect can be explained by looking at the proton single-particle spectra of ^{40}Ca (Fig. 4.15) and ^{48}Ca (Fig. 4.16). Indeed, one observes that a positive neutron-proton tensor coupling constant decreases the strength of the proton spin-orbit field in ^{48}Ca, which in turn

[1] There is a typographical error in Eq. (4.2) in Ref. [Cha97], that was copied to Eq. (110) in Ref. [Ben03b]: the $\hbar/mc$ factor should be squared, as is trivially found by dimensional analysis and confirmed by Ref. [Ber72].

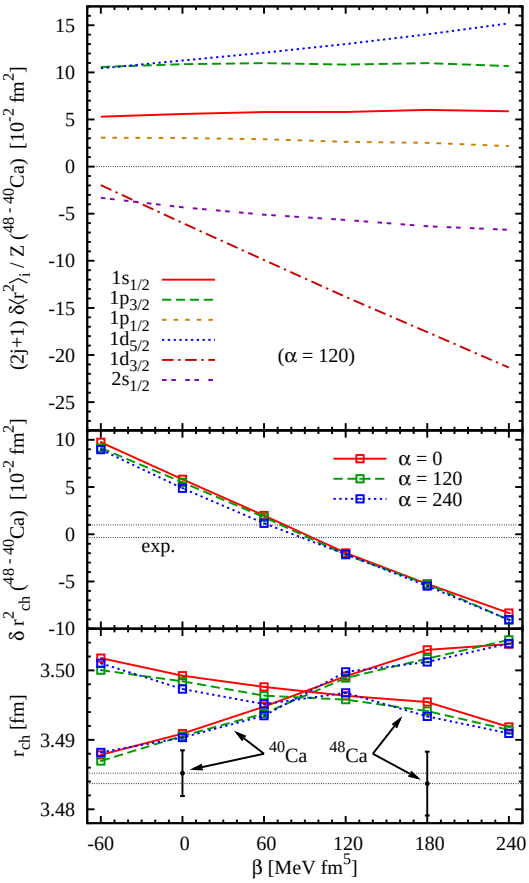

Figure 4.27: Middle panel: Difference of mean-square charge radii between ^{40}Ca and ^{48}Ca as a function of the proton-neutron tensor term coupling constant β for three values of α. The experimental value (with error bar) is represented by the two horizontal black lines. Bottom panel: Root-mean-square charge radii of ^{40}Ca and ^{48}Ca. Top panel: Contribution of the single-particle proton states to the difference of the charge radii (mean square radius of the point proton distribution, see Eq. (4.17)).

lowers the π $1d_{3/2}$ level in ^{48}Ca (compare the parametrizations TIJ in Fig. 4.16 with increasing I for given J). As a consequence, the m.s. radius of this state decreases as it sinks deeper into the potential well of ^{48}Ca. At the same time, this level is pushed up in ^{40}Ca, which slightly increases the contribution of this state to the charge m.s. radius of this nucleus. This effect is demonstrated in the top panel of Fig. 4.27, which displays the degeneracy-weighted and normalized change of the m.s. radii of proton hole states between ^{40}Ca and ^{48}Ca as a function of the proton-neutron tensor term coupling constant β for forces with a like-particle tensor term coupling constant $\alpha = 120$ MeV fm^5. Indeed, the decreasing contribution from the $\pi 1d_{3/2}$ state to the m.s. radius significantly decreases the isotopic shift between both Ca isotopes. It has to be noted that the m.s. value of the charge radii of ^{40}Ca and ^{48}Ca are almost independent of alpha and that their absolute values are not reproduced for any of our parametrizations.

The latter study demonstrates the correlation between the isotopic shift of m.s. charge radius between ^{40}Ca and ^{48}Ca and the absolute single-particle energy of the proton $1d_{3/2}$ state. This level can be moved around within the single-particle spectrum with the $\mathbf{J}^2$ terms. However, the agreement of the calculated single-particle energy of the proton $1d_{3/2}$ state in both nuclei with experiment is not necessarily improved for the parametrizations that reproduce the isotopic shift of the m.s. charge radius. Furthermore, a good reproduction of the isotopic shift does not guarantee that the absolute values of the charge radii are well reproduced, see the bottom panel in Fig. 4.27. In fact, they are predicted too large for all of our parametrizations, which again points to deficiencies of the central field. Altogether, this suggests that in spite of its sensitivity to the coupling constants of the $\mathbf{J}^2$ terms, the isotopic shift of m.s. charge radius between ^{40}Ca and ^{48}Ca should not be used to constrain them before one has gained sufficient control over the central interaction.

A few further words of caution are in place. The charge radii of all light nuclei are significantly increased by dynamical quadrupole correlations, see Fig. 23 of Ref. [Ben06a]. Correlations beyond the static self-consistent mean field are also at the origin of the arch of the ms charge radii between ^{40}Ca and ^{48}Ca that is neither reproduced by any pure mean-field model, see again Fig. 11 in Ref. [Ben03b], nor by the beyond-mean-field calculations with SLy4 of Ref. [Ben06a], while the shell model allows for a satisfactory description [Cau01].

Many explanations have been put forward to explain the kink in the isotopic shifts of Pb radii. As it qualitatively appears in relativistic mean-field models, but not in non-relativistic ones using the standard spin-orbit interaction (2.84), it has been used as a motivation to generalize the isospin mix of the standard spin-orbit energy density functional, Eq. (2.86), to simulate the isospin dependence of the relativistic Hartree models [Sha95, Rei95]. The resulting parametrizations are not completely satisfactory, as the price for the improvement of the radii is a further deterioration of spin-orbit splittings [Ben99b], while the relativistic mean field gives a satisfactory description of both. Some standard Skyrme interactions that take the tensor terms from the central Skyrme force into account also give a kink, but it is by far too small to reproduce the experimental values [Cha98].

Plotting the m.s. radii along the chain of Pb isotopes as a function of N, the slopes are nearly linear when looking separately at the isotopes below and above ^{208}Pb. We will concentrate on the change in the slope at ^{208}Pb that is brought by the tensor terms, which can be quantified through the second finite difference of the

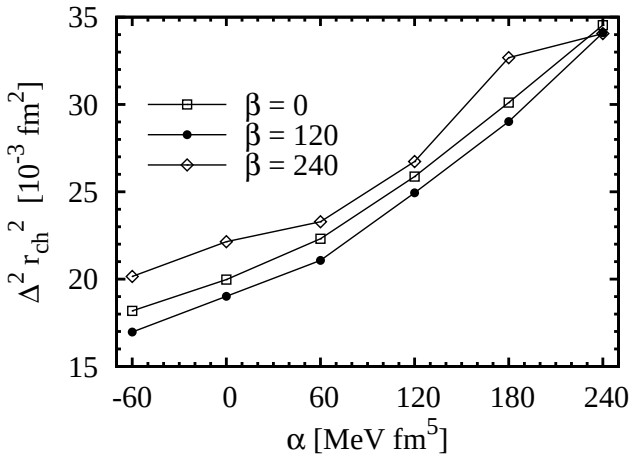

Figure 4.28: Change of slope in the m.s. charge radii $\Delta^2 r^2_{\rm ch}$ around ^{208}Pb, Eq. (4.18), in fm^2 as a function of α for three values of β. The experimental value is about one and a half times as large as the largest theoretical value shown here, see text.

m.s. radii at ^{208}Pb

$$\Delta^2\langle r^2_{\rm ch}\rangle(^{208}{\rm Pb}) \;=\; \tfrac{1}{2}\left[r^2_{\rm ch}(^{206}{\rm Pb}) - 2\,r^2_{\rm ch}(^{208}{\rm Pb}) + r^2_{\rm ch}(^{210}{\rm Pb})\right]. \qquad (4.18)$$

There are two conflicting values to be found in the literature, either 46.4 ± 1.4 fm^2 [Ott89] and the significantly larger 59 ± 3 fm^2 [Ang04]. Figure 4.28 shows the change of slope around ^{208}Pb as defined through Eq. (4.18) as a function of the like-particle tensor coupling constant α and for three different values of β. It is striking to see that this quantity is almost independent of the neutron-proton tensor coupling constant β, so the change is mainly induced by the tensor interaction between particles of the same kind. It has been noted before that the kink in the isotopic shift of the charge radii in Pb isotopes is correlated to the single-particle spectrum of neutrons above $N = 126$, in particular the position of the $1i_{11/2}$ level. (This has to be contrasted with the Ca isotopic chain discussed above, where the difference of charge radii between ^{40}Ca and ^{48}Ca appears to be particularly sensitive to the single-particle spectrum of the protons.) The closer the $1i_{11/2}$ level is to the $2g_{9/2}$ level that is filled above $N = 126$, the more the $1i_{11/2}$ becomes occupied through pairing correlations. Through the shape of its radial wave function, the partial filling of the nodeless $1i_{11/2}$ increases the neutron radius faster than filling only the $2g_{9/2}$, and in particular faster than for the isotopes below $N = 126$. As the protons follow the density distribution of the neutrons, the charge radius grows rapidly beyond $N = 126$. This offers an explanation why the kink increases with the like-particle tensor term coupling constant α: for large values of the weight α of the neutron spin-orbit current in the neutron spin-orbit potential, Eq. (4.8), the spin-orbit splitting of the ν $1i$ levels is reduced such that the $1i_{11/2}$ approaches the $2g_{9/2}$ level in ^{208}Pb, see Fig. 4.14.

While the kink is clearly sensitive to the tensor terms, they cannot be responsible for the entire effect, as even for extreme parametrizations that give unrealistic single-particle spectra the calculated kink hardly reaches about three quarters of its experimental value.

4.4 Summary and conclusions

In this chapter, we have reported a systematic study of the effects of the $\mathbf{J}^2$ (tensor) terms in the Skyrme energy functional for spherical nuclei. The aim of the present study was not to obtain a unique best fit of the Skyrme energy functional with tensor terms, but to analyze the impact of the tensor terms on a large variety of observables in calculations at a pure SR-EDF level and to identify, if possible, observables that are particularly, even uniquely, sensitive to the $\mathbf{J}^2$ terms. To reach our goal, we have built, using a protocol very similar to that of the SLy parametrizations, a set of 36 parametrizations that cover the two-dimensional parameter space of the coupling constants of the $\mathbf{J}_t^2$ terms that does not give obviously unphysical predictions for a wide variety of observables we have looked at. The parametrizations were fitted independently on the same set of data, in order to keep an agreement with the physics associated with the latter.

As a result of our study, we have obtained a long list of potential deficiencies of the Skyrme energy functional, most of which can be expected to be related to the properties of the central and spin-orbit interactions used. In fact, these deficiencies become more obvious the moment one adds a tensor force, as it appears that the presence of a tensor force unbalances a delicate compromise within various terms of the Skyrme interaction that permits to get the global trend of gross features of the shell structure right.

Our conclusions, however, have to be taken with a grain of salt. On the one hand, some might depend on the fit protocol; and on the other hand, we have to stress that (within the framework of our study – and all others available so far using mean-field methods) the comparison between calculated and empirical single-particle energies is not straightforward and without the risk of being misled.

However, without even looking at single-particle spectra, we find that a strong rearrangement of the spin-orbit terms occurs, linked with a strong constraint coming from the fit to the masses of Ca and Ni nuclei. The latter, again, appears to be model-dependent and linked with the specificities of the central and spin-orbit terms. The rearrangement of the spin-orbit strength with the isoscalar tensor coupling means that single-particle spectra of spin-saturated nuclei are strongly affected by the latter, which can lead to unrealistic situations.

Besides, the particular constraints used in our protocol, focused on doubly-magic nuclei, favor parametrizations with a vanishing neutron-proton tensor coupling β. By contrast, the mass residuals of a test set of 134 spherical even-even nuclei are minimized for interactions with large α (like-particle) and β couplings. Finally, tensor terms were shown to have an influence, through single-particle level shifts, on the difference of charge radii between ^{40}Ca and ^{48}Ca. The corresponding spectra, however, are not fully satisfactory, which is another example of incompatible constraints.

Concerning the global properties of the spin-orbit current $\mathbf{J}$ and its contribution, through the tensor terms, to the spin-orbit potential, we have shown that it was dominated, in spin-unsaturated nuclei, by single intruder orbitals, which implies a specific localization in regions just below the nuclear surface, slightly different from the localization of the spin-orbit contribution to the spin-orbit field.

The main motivation to add $\mathbf{J}^2$ terms is of course to improve the single-particle spectra. All observations and conclusions concerning those have to be taken with

care, however, due to the caveat already mentioned and repeated. When looking at the single-particle spectra in doubly-magic nuclei (or semi-magic nuclei combined with a strong subshell closure of the other species) we find that, as a consequence of the localization of the spin current density, state-dependent modifications of spin-orbit splittings occur when varying tensor parameters, due to the coupling of nodeless intruder states to themselves being maximized. The addition of tensor terms thus modifies the dependence with principal and/or orbital quantum number of spin-orbit splittings in disagreement with experimental input, as shown already in Ref. [Bro06a]. The isospin dependence of spin-orbit splittings, moreover, has been found to be affected by the specific localization of the spin-orbit field in a non-physical and model-dependent way. In addition, the discussion of splittings stemming from the comparison of theoretical and experimental spectra of heavy nuclei is impeded by the position of spin-orbit doublet centroids, which lie tentatively too high compared to levels of the nearest shells. This is unambiguously a defect of the central potential and corresponding part of the functional.

The principal effect of the tensor terms, that most of the recent studies concentrate on, is the evolution of spin-orbit splittings with N and Z. Unfortunately, there are no data for the splittings themselves, such that one relies on data for the evolution of the distance of two levels with different ℓ. The comparison is compromised by the global deficiencies of single-particle spectra listed above.

Still, a careful comparison of calculations and experiment suggests that the evolution of the proton $1h_{11/2}$, $1g_{7/2}$ and $2d_{5/2}$ levels in the chain of Sn isotopes and that of the proton $1f_{5/2}$ and $2p_{3/2}$ levels in Ni isotopes call for a positive proton-neutron tensor coupling constant β with a value around 120 MeV fm^5, consistent with the findings of Refs. [Bro06a, Col07, Bri07]. Meanwhile, The evolution of the neutron $1d_{3/2}$ and $2s_{1/2}$ levels between ^{40}Ca and ^{48}Ca calls for a like-particle tensor coupling constant α with a similar value around 120 MeV fm^5. This it at variance to the findings of the aforementioned papers, but in qualitative agreement with the parametrization skxta of Brown et al. [Bro06a] for which the tensor terms were derived from a microscopic interaction but disregarded thereafter because of its poor description of spin-orbit splittings. We expect this mismatch to be alleviated if the position of doublet centroids is kept under control.

This particular study is only a limited contribution to the improvement of the Skyrme energy density functional. Also, it does not exhaust the range of studies to be performed in order to understand the role of tensor terms in this model. The study of deformation properties of selected parametrizations TIJ, for example, should allow to distinguish between the effects of central and tensor contributions to $\mathbb{J}^2$ terms, which are no longer identical when breaking spherical symmetry. This work will be published in the near future [Ben09].

Moreover, the influence of the terms depending on time-odd densities and currents in the complete energy functional (2.91) on nuclear matter and finite nuclei (rotational bands etc) is under investigation as well. The existing stability criteria of polarized matter have to be generalized as the tensor force introduces new unique terms, for example in the Landau parameters [Hae82].

It is evident that improvements of the central and spin-orbit parts of the energy density functional are necessary, which will require a generalization of its analytical form. This confirms and extends the conclusions of chapter 3. Furthermore, a systematic implementation of MR-EDF calculations will be needed, so as to assess

not only the variation of single-particle spectra, but also the effect of correlations on the ensuing odd-nucleus excitation spectrum. Particle-vibration coupling in the random-phase approximation should thus be an invaluable tool.

These comments close the first part of this manuscript. As we have in mind the properties and, unfortunately, limitations of the particle-hole part of the nuclear EDF derived from a Skyrme effective interaction, let us shift the discussion to the particle-particle part.

Chapter 5

Ab-Initio Description of Nuclear Pairing

5.1 Pairing and superfluidity in many-fermion systems

The structure and dynamic properties of a nucleus greatly depends on the parity of its neutron and proton numbers. It was realized soon that an empirical mass formula had to take into account an additional binding energy contribution for nuclei with even N or Z, compared to those with odd N or Z, of the order of $12A^{-1/2}$ MeV [Boh98]. Moreover, excitation spectra of even-even nuclei show a distinct gap between the ground and first excited states, a feature absent in nuclei with an odd N or Z. These observations were explained by Bohr, Mottelson and Pines [Boh58], who made the link between them and the pair condensation mechanism, which had been put forward as a model for electronic superconductivity by Bardeen, Cooper and Schrieffer (BCS) [Bar57a, Bar57b], then for the superfluidity of Helium-3.

In BCS theory, fermion pair condensation is explained by an attractive interaction between particles at the Fermi surface of an otherwise non-interacting gas. In this sense, it remains within the mean-field scheme, and can be formulated within a density functional theory formalism [Oli88]. A more fundamental and general approach to pair condensation has since been derived within the framework of many-body perturbation theory [Noz63, Abr63].

Generally speaking, pair condensation consists in the appearance of a two-body bound state in the medium. Besides, the possibility, for arbitrarily weak attractive interactions, to form a two-electron bound state (so-called "Cooper pair") near the Fermi surface of an electron gas, [Coo56], was fundamental in the derivation of the BCS formalism [Bar57a]. In an infinite system, such a bound state will be clearly distinct from the continuum of scattering states corresponding to elementary excitations, which is the origin of a gap in the elementary excitation spectrum. In other words, building an excitation first requires breaking a pair into independent particles before exciting one of them. This is the main cause of the specific properties of superfluid/superconducting media.

5.1.1 BCS theory

The BCS ansatz for the wave function of a system of fermions condensed into a superfluid phase consists of a coherent superposition of Slater determinants differing by the addition of pairs of particles or holes, created in pairs of single-particle basis states. States in a such a pair belong to two different "halves" of the basis, and are associated according to symmetries of the system and properties of the interaction. The quantum numbers upon which the distinction between single-particle states is made are related to those of the Cooper pair. In the case of spin-singlet, or $S = 0$ pairing, S being here the total spin of the Cooper pair, states associated in the BCS wave function are related by time-reversal symmetry [And59] which, e.g. in infinite systems, associates the state $|\mathbf{k}\sigma\rangle$, $\mathbf{k}$ being the momentum and σ the spin of the particle, to $|\text{-}\mathbf{k}\text{-}\sigma\rangle$. This is the conventional choice in BCS theory, appropriate for most superconductors, low-density neutron matter and the description of same-species nucleon pairing, in the ${}^1S_0$ state, which is the dominant process in nuclei. In the spin-triplet case, a similar role seems to be played by parity [And84], which transforms $|\mathbf{k}\sigma\rangle$ into $|\text{-}\mathbf{k}\sigma\rangle$. This spin-triplet pairing occurs in exotic, high-T_C superconductors [Gor85], neutron-proton pairing in symmetric nuclear matter as well as high-density neutron matter where neutron pairs form in the ${}^3P - F_2$ state.

Hereafter we shall deal with spin-singlet ($S = 0$), isospin-triplet ($T = 1$, like-particle) nuclear pairing, yet the expressions put forward will usually stay as general as possible.

In a first step, we shall work with an arbitrary single-particle basis $|k\rangle$. We note with a $\check{}$ sign ($|\check{k}\rangle$) single-particle states belonging to the first half and with a $\hat{}$ sign ($|\hat{l}\rangle$) s.p. states belonging to the second half. The state associated with $|\check{k}\rangle$ in a pair operator is written $|\overline{k}\rangle$, omitting the $\check{}$ since no ambiguity should occur. The same principle applies for $|\hat{l}\rangle$. States without a $\check{}$ or $\hat{}$ symbol can belong to either half of the basis. We will mostly work with creation/annihilation operators corresponding to the single-particle states, i.e. $|k\rangle = \hat{c}_k^\dagger|-\rangle$, where $|-\rangle$ is the bare vacuum.

The BCS wavefunction can be expressed as

$$|\Phi_0\rangle = \prod_{\check{k}} (u_{\check{k}}^2 + v_{\check{k}}^2 \hat{c}_{\check{k}}^\dagger \hat{c}_{\overline{\check{k}}}^\dagger)|-\rangle. \tag{5.1}$$

Bogolyubov [Bog58] and Valatin [Val58] introduced the canonical transformation (which transforms the initial fermion operators into quasiparticle operators conserving the fermionic anticommutation rules)

$$\hat{\alpha}_k = u_k \hat{c}_k - v_k \hat{c}_{\overline{k}}^\dagger \tag{5.2}$$

$$\hat{c}_k = u_k \hat{\alpha}_k + v_k \hat{\alpha}_{\overline{k}}^\dagger \tag{5.3}$$

with $u_k = u_{\overline{k}}$, $v_k = -v_{\overline{k}}$. The new quasiparticle basis defines the BCS state as a quasiparticle vacuum with $\alpha_k|\Phi_0\rangle = 0$ for all k. One can check that for the state $|\Phi_0\rangle$ to be normalized, one must have

$$u_k^2 + v_k^2 = 1. \tag{5.4}$$

Another important property is the probability that a (pair of) s.p. state(s) is occupied, i.e. the diagonal density matrix element $\left\langle \Phi_0 \left| \hat{c}_k^\dagger \hat{c}_k \right| \Phi_0 \right\rangle = v_k^2$. Summing v_k^2 over all s.p. states thus yields the particle number.

The energy of the system is defined as the functional of u_k and v_k parameters [Bar57a]

$$\mathcal{E}_0 \equiv \mathcal{E}_{\text{s.p.}} + \mathcal{E}_{\text{pair}}, \tag{5.5}$$

$$\mathcal{E}_{\text{s.p.}} \equiv \sum_k \varepsilon_k v_k^2, \tag{5.6}$$

$$\mathcal{E}_{\text{pair}} \equiv \frac{1}{4}\sum_{kl} \overline{v}_{k\overline{k}l\overline{l}}\, u_k v_k\, u_l v_l, \tag{5.7}$$

where $\mathcal{E}_{\text{s.p.}}$ is the sum of single-particle energies ε_k of the particles, and $\mathcal{E}_{\text{pair}}$ is the pairing energy corresponding to the anomalous contractions of the pairing interaction [Rin00].

The energy $\mathcal{E}_{\text{pair}}$ is nonzero only for a state which breaks particle-number conservation. The wave function Eq. (5.1), indeed, does not conserve particle number, which is characteristic of a finite-order perturbative treatment of pair condensation. In order to determine the parameters u_k and v_k , we should minimize $\mathcal{E}$. However, since we no longer work in a manifold of Slater-determinant eigenstates of the particle number operator $\hat{N}$, we have to apply a constraint, at least, on the average particle number. This is done through the use of a Lagrange multiplier, defining the quantities

$$\overline{\mathcal{E}}_0 \equiv \mathcal{E}_0 - \lambda N = \overline{\mathcal{E}}_{\text{s.p.}} + \mathcal{E}_{\text{pair}}, \tag{5.8}$$

$$\overline{\mathcal{E}}_{\text{s.p.}} = \sum_k \varepsilon_k v_k^2 - \lambda \sum_k v_k^2 = \sum_k \overline{\varepsilon}_k v_k^2, \tag{5.9}$$

$$\overline{\varepsilon}_k \equiv \varepsilon_k - \lambda, \tag{5.10}$$

$$\lambda \equiv \left.\frac{\partial \mathcal{E}}{\partial N}\right|_{N=N_0}, \tag{5.11}$$

$\overline{\varepsilon}_k$ is thus the single-particle energy measured from the chemical potential λ, which is set so as to ensure the conservation of the average particle number at its target value N_0.

Minimizing $\overline{\mathcal{E}}$ yields the equation

$$2\,\tilde{\varepsilon}_k u_k v_k + \Delta_k(v_k^2 - u_k^2) = 0, \tag{5.12}$$

with

$$\tilde{\varepsilon}_k \equiv \frac{1}{2}(\overline{\varepsilon}_k + \overline{\varepsilon}_{\overline{k}}), \qquad \Delta_k \equiv -\frac{1}{2}\sum_l \overline{v}_{k\overline{k}l\overline{l}}\, u_l v_l, \tag{5.13}$$

where $\tilde{\varepsilon}_k$ is a s.p. energy averaged over partner states (whose energies can be different in the most general case), whereas Δ_k is the gap parameter. Eqs. (5.12) and (5.4) allow one to determine u_k and v_k as

$$v_k^2 = \frac{1}{2}\left(1 - \frac{\tilde{\varepsilon}_k}{E_k}\right), \qquad u_k^2 = \frac{1}{2}\left(1 + \frac{\tilde{\varepsilon}_k}{E_k}\right), \tag{5.14}$$

where $E_k \equiv \sqrt{\tilde{\varepsilon}_k^2 + \Delta_k^2}$ is the quasiparticle energy. Indeed, in the case where $\overline{\varepsilon}_k = \overline{\varepsilon}_{\overline{k}}$, one can show that $|\Phi_0\rangle$ is the ground state of the single-(quasi)particle Hamiltonian [Noz63]

$$\hat{\overline{H}}_{\text{BCS}} = \sum_{\check{k}} \left\{ \overline{\varepsilon}_{\check{k}} \left(\hat{c}_{\check{k}}^\dagger \hat{c}_{\check{k}} + \hat{c}_{\overline{k}}^\dagger \hat{c}_{\overline{k}} \right) + \Delta_{\check{k}} (\hat{c}_{\check{k}}^\dagger \hat{c}_{\overline{k}}^\dagger + \hat{c}_{\overline{k}} \hat{c}_{\check{k}}) \right\} \tag{5.15}$$

with energy $\overline{\mathcal{E}}_0$. One then has, for one-quasiparticle states, the property

$$\hat{\overline{H}}_{\rm BCS}\,|\Phi_k\rangle \;\equiv\; \hat{\overline{H}}_{\rm BCS}\,\hat{\alpha}_k|\Phi_0\rangle \;=\; \overline{\mathcal{E}}_0 + E_k\,|\Phi_k\rangle. \tag{5.16}$$

By plugging back Eq. (5.14) into the definition of Δ_k, Eq. (5.13) one obtains the BCS *gap equation*

$$\Delta_k \;=\; -\frac{1}{2}\sum_l \overline{v}_{k\overline{k}l\overline{l}}\,\frac{\Delta_l}{E_l}, \tag{5.17}$$

which can be solved by self-consistent iterations to obtain all other quantities presented in this section.

Quasiparticle energies $E_k = \sqrt{\tilde{\varepsilon}_k^2 + \Delta_k^2}$, in the case of nonvanishing pairing gap Δ_k, are themselves nonzero even for states whose energy is in the vicinity of the chemical potential λ. This is at the origin of a staggering of binding energies between nuclei with odd and even particle number in an isotope or isotone chain. Indeed, whereas the BCS wave function, Eq. (5.1) is not an eigenstate of the particle number operator, it only has components with even particle numbers. Thus, a system with an odd number of particles shall be better described as a one-quasiparticle state $\alpha_k^\dagger|\Phi_0\rangle$ which exhibits an excess energy with respect to the even-number parity state it is built upon.

The quasiparticle operator $\alpha_k^\dagger$ annihilates the particle in state $|\overline{k}\rangle$ and creates one in state $|k\rangle$, with corresponding amplitudes, respectively, v_k and u_k. The corresponding variation of particle number equals $u_k^2 - v_k^2$. Adding back the constraining term λN to the Hamiltonian $\hat{\overline{H}}_{\rm BCS}$, one obtains the energy of the one-quasiparticle state

$$\mathcal{E}_k \;=\; \mathcal{E}_0 + E_k + \lambda(u_k^2 - v_k^2), \tag{5.18}$$

i.e. the energy gained is equal to E_k only if the quasiparticle $|k\rangle$ corresponds to a s.p. level whose energy is equal to the chemical potential λ. The quasiparticle energy corresponds to the pairing gap Δ_k in the same conditions.

It should be noted, though, that this perturbative scheme for the description of an odd-particle-number state is inaccurate. Indeed, creating a single quasiparticle breaks the symmetry between the two halves of the basis (time-reversal symmetry in nuclear ${}^1S_0$, $T = 1$ pairing) since $\hat{\alpha}_k$ and $\hat{\alpha}_{\overline{k}}$ are distinct operators. This is negligible for infinite systems, but for finite nuclei this symmetry breaking lifts the degeneracy of pairs of s.p. states. Whereas in the theory of superconductors it is generally believed that exact time-reversal symmetry is necessary for the onset of $S = 0$ pairing (the large number of particles making a single non-paired particle irrelevant), in nuclei the addition of a single quasiparticle is a significant but weak enough perturbation to allow pairing to be maintained. However, the description of such a system has to use the full time-reversal-symmetry-breaking HFB scheme, i.e. the variation of the s.p. states on top of which the BCS state is built. Expressions for the latter and the gap equation then hold in the canonical basis.

5.1.2 Experimental evidence and observables

Fermion pairing causes the appearance of a condensed phase having properties very different from those of a non-interacting gas. In infinite matter, as the bound state

is clearly separated from the continuum of free elementary excitations, excited states breaking the symmetries of the ground state require a finite energy to be reached. This makes the superfluid irrotational (states with non-vanishing angular momentum are pushed to higher energies) and prevents dissipation in hydrodynamic flows.

In atomic nuclei, manifestations of pairing mainly consist of spins of even and odd nuclei, energy gaps in the spectra of even-even nuclei, moments of inertia lower than their rigid-body counterparts, and odd-even staggering of binding energies.

The ground state of even-even nuclei can be described as a fully-paired vacuum, i.e. all particles participate to forming pairs. The necessity for this behavior was pointed as early as 1950 by Goeppert Mayer [GM50a, GM50b] as an explanation, in the context of the shell model, for the spin 0 observed in these nuclei. Moreover, the latter exhibit an excitation spectrum where no excitation of an individual character exists below an energy of several hundred keV to several MeV. Thus, low-lying states in such a nucleus have a highly collective character, i.e. correspond to the recoupling of a large number of quasiparticle excitations. As a result, the lowest excited states of a spherical even-even nucleus is most often a 2^+ quadrupole-vibrational state, while low-energy excitation spectrum of a deformed one is dominated by a rotational band. To the contrary, low-lying quasiparticle structure, associated with excitations of the single non-paired particle, is visible in nuclei with odd N and/or Z at energy scales of 100 keV.

Moments of inertia extracted from low-energy rotational spectra were immediately noticed as being lower than those expected from a supposedly rigid rotating quantum system [Boh55, Ald56]. Only later was the link made with a possible superfluid behavior of the nucleons [Boh58]. Another significant effect associated with pair condensation is the possibility to break pairs, yielding a higher moment of inertia. Whereas at low angular momentum broken-pair states lie higher in energy than the fully-paired quasiparticle vacuum, their higher moment of inertia means that they gain energy more slowly with angular momentum. This implies that energy vs. angular momentum curves for rotational bands corresponding to these different configurations will eventually cross [Joh71]. Another way to interpret the phenomenon is by studying the coupling of nucleon spins to the rotation of the nuclear reference frame via the Coriolis effect [Mot60]. A distinct signature of this phenomenon is the backbending effect [Ste72].

More recently, the advent of radioactive ion beam facilities, together with the development of supernova simulations in computational nuclear astrophysics, has shifted the focus of nuclear-structure research to neutron- and proton-rich nuclei. Such nuclei present particular challenges to many-body theory due to the low neutron (or proton) separation energy, which implies the existence of low-lying excitations of nucleons to continuum, scattering states. Precautions concerning the discretization of the continuum have to be taken when computing such systems, see Refs. [Dob84, Ben99c, Dob96b]. One prominent effect occurring at the drip lines is the presence of halos. Following the discovery of this phenomenon in ^{11}Li [Tan85b], halos have been observed in several other light nuclei [Tan85a, Tan88, Rii94]. In medium-mass and heavy ones, though, no experimental evidence exists of the presence of halos, and theory has to rely on the EDF method. Pairing is especially important in this case, as it hinders the appearance of a halo by modifying the asymptotic behavior of the density [Ben00]. Recent studies performed in single-reference [Rot07c, Rot07b] and multi-reference [Sch08] EDF frameworks indeed confirm that

the appearance of a halo is sensitive to details of the pairing scheme used, as are other properties of nuclei at the neutron drip line.

Finally, the most prominent signature of pairing is the large odd-even staggering (OES) of nuclear masses: odd nuclei are found to have an energy systematically higher than the mean energies of the neighboring even nuclei, i.e. they lie on different smooth $\mathcal{E}$ vs. N (Z) curves [Hei32]. As a measure of this effect, the quantities

$$\Delta^{(3)}_{\rm n}(N,Z) \;=\; \frac{(-1)^N}{2}\left[E(N-1,Z)-2E(N,Z)+E(N+1,Z)\right], \quad (5.19)$$

and $\Delta^{(3)}_{\rm p}$, obtained by exchanging the roles of N and Z, are most often used. They have positive values for both odd and even N (Z). In a BCS-like quasiparticle picture, the excess energy found in an odd nucleus corresponds to the energy of the quasiparticle created in order to obtain a one-q.p. ("blocked") odd-number-parity state.

Eq. (5.19) is the difference between separation energies of consecutive nuclei. In a self-consistent mean-field/EDF scheme without pairing, due to Koopmans' theorem [Koo34], it measures the spacing of single-particle levels, i.e. (in the case of neutrons)

$$\Delta^{(3)}_{\rm n,HF}(N,Z) \;=\; \frac{(-1)^N}{2}\left[\varepsilon_{(N+1)}-\varepsilon_{(N)}\right], \quad (5.20)$$

where $\varepsilon_{(N)}$ is the energy of the single-particle level on which the $N^{\rm th}$ neutron is added. Due to the twofold degeneracy of single-particle states in even-even nuclei whose ground state is invariant under time reversal, one-neutron separation energies calculated at the HF level (i.e., more generally, without pairing) for a N-neutron nucleus (even N) and its $N+1$ neighbor are almost identical, while separation energies for $N+1$ and $N+2$ are usually different, except in the case of a large spherical j-shell degeneracy. Thus, $\Delta^{(3)}_{\rm n}(N,Z)$ with even N may contain a significant contribution from the splitting of single-particle energies, which may explain a significant part of the odd-even staggering of $\Delta^{(3)}(N,Z)$ itself. Satuła, Dobaczewski et al. [Sat98, Dob01] used this result to propose restricting oneself to $\Delta^{(3)}_{\rm n}(N,Z)$ calculated at odd N values (hereafter called $\Delta^{(3)}_{\rm odd}$) in the discussion of pairing.

However, the twofold degeneracy of single-particle levels, and the equality between $\varepsilon_{(N+1)}$ and $\varepsilon_{(N)}$ for even N, is not exact. Indeed, time-reversal symmetry breaking caused by the addition of a single nucleon lifts this degeneracy in the odd nucleus, resulting in a rearrangement (or "polarization") of the nucleus, which is a nuclear embodiment of the Jahn-Teller effect [Jah37]. Although the deformation degree of freedom is mostly blocked due to pairing itself [Sat98], limiting the magnitude of the Jahn-Teller contribution to the OES, core polarization can decrease the energy of the blocked configuration. This polarization brings a negative contribution to the OES that Rutz et al. estimated at up to 30 % of the "bare" gap in relativistic Hartree (RH) models [Rut99].

Duguet et al. revisited the interpretation of the structure of an odd nucleus in terms of a fully paired BCS/HFB vacuum (with an even number parity and an odd average particle number) on top of which a quasiparticle corresponding to a s.p. orbital lying close to the chemical potential was created [Dug01a]. Starting from the calculation of such HFBE (for HFB-Even) states and fully self-consistent HFB blocking calculations, an analysis of different measures of the pairing gap was made

[Dug01b], i.e. a comparison of $\Delta_{\rm n}^{(3)}(N,Z)$ and

$$\Delta_{\rm n}^{(5)}(N,Z) = -\frac{(-1)^N}{8}\big[E(N-2,Z)-4E(N-1,Z) + 6E(N,Z)-4E(N+1,Z)+E(N+2,Z)\big], \quad (5.21)$$

which is an average of $\Delta^{(3)}$ over a nucleus and its neighbors. They decomposed mass-difference formulae as

$$\Delta^{(n)} = \Delta^{(n)}_{\rm HFBE} + \overline{E}_{\rm LQP} + \overline{E}_{\rm pol.} \quad (5.22)$$

where $\Delta^{(n)}_{\rm HFBE}$ contains the $(n-1)^{\rm th}$-order derivative of the "smooth" part of the energy curve corresponding to fully paired, even-number-parity vacua. The latter has been verified as being significant for $n=3$, which corresponds to a curvature due to non-linear terms in the mass formula such as, principally, the symmetry energy, whereas it vanished almost completely for $n=5$. The curvature contribution $\Delta^{(n)}_{\rm HFBE}$ is generally observed to decrease with mass and, contrary to the HF contribution to the OES, it has a sizeable value in spherical nuclei. $E_{\rm LQP}$ is a Lowest QuasiParticle energy averaged over one or more neighboring nuclei. This is the quantity that we are attempting to extract since the main contribution to its value, for well-paired nuclei, is the HFB pairing gap (diagonal pairing field matrix element) Δ_k. Finally, $\overline{E}_{\rm pol.}$ is the (similarly averaged) polarization energy, i.e. the difference between the energy of the odd nucleus calculated in a fully self-consistent blocking scheme, and the perturbative value obtained by adding the quasiparticle energy to the HFBE ground state energy. It was found that, whereas $\Delta^{(5)}$ was the most accurate measure of the sum of pairing and polarization contributions, a cancellation occurred between $\overline{E}_{\rm pol.}$ and $\Delta^{(3)}_{\rm HFBE}$ terms in $\Delta^{(3)}_{\rm odd}$, which confirms it as a good measure of pure pairing effects.

In the Jahn-Teller mechanism, a system is expected to lower its energy consequently to lifting the degeneracy of its ground state. In the HFB method, the underlying variational principle could be expected to make an odd nucleus calculated in self-consistent blocking follow this scheme. Therefore, $\overline{E}_{\rm pol.}$ should be negative, which is the case in the work by Rutz et al. [Rut99] but not in those by Satuła et al. [Sat98] and Duguet et al. [Dug01b]. One possible reason for this is the self-interaction present in an energy density functional when the latter is not strictly built as the HFB expectation value of a Hamiltonian, or explicitly corrected for self-interaction [Per81]. Despite the inclusion of time-odd components of the functional, quasiparticle self-interaction, i.e. self-interaction and self-pairing terms [Lac08] can be present and break the link between quasiparticle energies resulting from the HFBE calculation and the true energy of the one-quasiparticle state as calculated explicitly through the functional (see Eq. (2.64) and accompanying discussion). As of this work's writing there is no more accurate check of the magnitude of this effect, though, which might be required if one expects to fully understand the precise influence of pairing in the nuclear EDF.

Beyond these qualitative considerations, performing yet another analysis of the link between nuclear masses and pairing gaps is beyond the scope of the present work. We shall thus use the rather consensual measure $\Delta^{(3)}_{\rm odd}$ when performing comparisons with experiment. On last remark may be required, i.e. that this quantity should not be used near shell closures $(N, Z\pm 2)$ for the comparison with a SR-EDF calculation, since dynamical pairing effects may play a significant role.

5.1.3 Trends in pairing gaps

Several studies have dealt with the mass- and isospin-dependence of pairing gaps. As already mentioned, the A-dependence of both proton and neutron gaps was identified early [Boh98] as a decreasing function. The question of the relative importance of neutron and proton gaps and their dependence with respect to particle numbers of the two species was first investigated by fitting simple analytic functions of (N, Z) without explicit knowledge of the quantal structure of nuclei. It was observed that neutron and proton gaps were similar for light nuclei, while proton gaps were slightly larger than neutron ones in heavy nuclei, especially in the actinide region [Boh98, Nem62]. As for the neutron-excess dependence, simple analytic fits yielded gaps decreasing with $(N-Z)/A$ for both species [Vog84, Mad88]. Later on, Möller and Nix [Möl92] performed an analysis of gaps across the mass table using a microscopic-macroscopic approach. Pairing was treated in the BCS and BCS-Lipkin-Nogami schemes, with a pairing strength parametrized through an "effective-interaction gap", the connection between the latter being made through a calculation performed on a schematic s.p. spectrum with shell corrections smoothed out. Thus, quantal effects due to (sub-)shell structure and variations of the latter with deformation were substracted. It was found that no explicit neutron-excess dependence was needed in the effective interaction to reproduce trends observed in the data.

Proton and neutron $\Delta^{(3)}_{\rm odd}$ values extracted from Ref. [Aud03] are plotted on Fig. 5.1. We only show mass differences centered on nuclei with an even number of particles for the species *not* under consideration, in order to avoid including in the data odd-odd nuclei where the coupling between the non-paired proton and neutron may impede the discussion.

As was noted in Ref. [Vog84], neutron-excess dependence appears most clearly in the region of $50 < Z < 82$ and $82 < N < 126$. The lowest gaps in this region occur in nuclei situated in the middle of neutron and proton shells, which corresponds to the limit of known nuclei on the neutron-rich side. As was suggested already in Ref. [Nem62], these nuclei are well-deformed and exhibit a low level density at the Fermi level due to the presence of deformed shell closures, resulting in a reduction of pairing. Such an effect is clearly visible in a systematic calculation such as [Hil06, Hil07], and could be hinted by the crescent-shaped distribution of higher gaps around the middle of major neutron and proton shells on Fig. 5.1.

Thus, the variation of pairing gaps with neutron excess observed more recently in the Hafnium ($Z = 72$) and Tungsten ($Z = 74$) chains [Lit05] could be attributable mainly to local shell effects. In this case, work on improving models which fail to reproduce this variation would benefit from concentrating on single-particle spectroscopy and deformation properties. Also, it would explain why attempts at liquid-drop or LDA-based description of gaps across the mass table [Jen86] fail in this region.

5.1.4 Microscopic theory

Nuclei and nuclear matter are highly correlated quantum systems. However useful for the qualitative understanding of nuclear pairing and as the basis for pairing-enabled density functional theory, the BCS gap equation is not a rigorous starting point for the ab-initio description of superfluidity. Such a description has been the aim of many studies performed in the context of nuclear or neutron matter [Dea03].

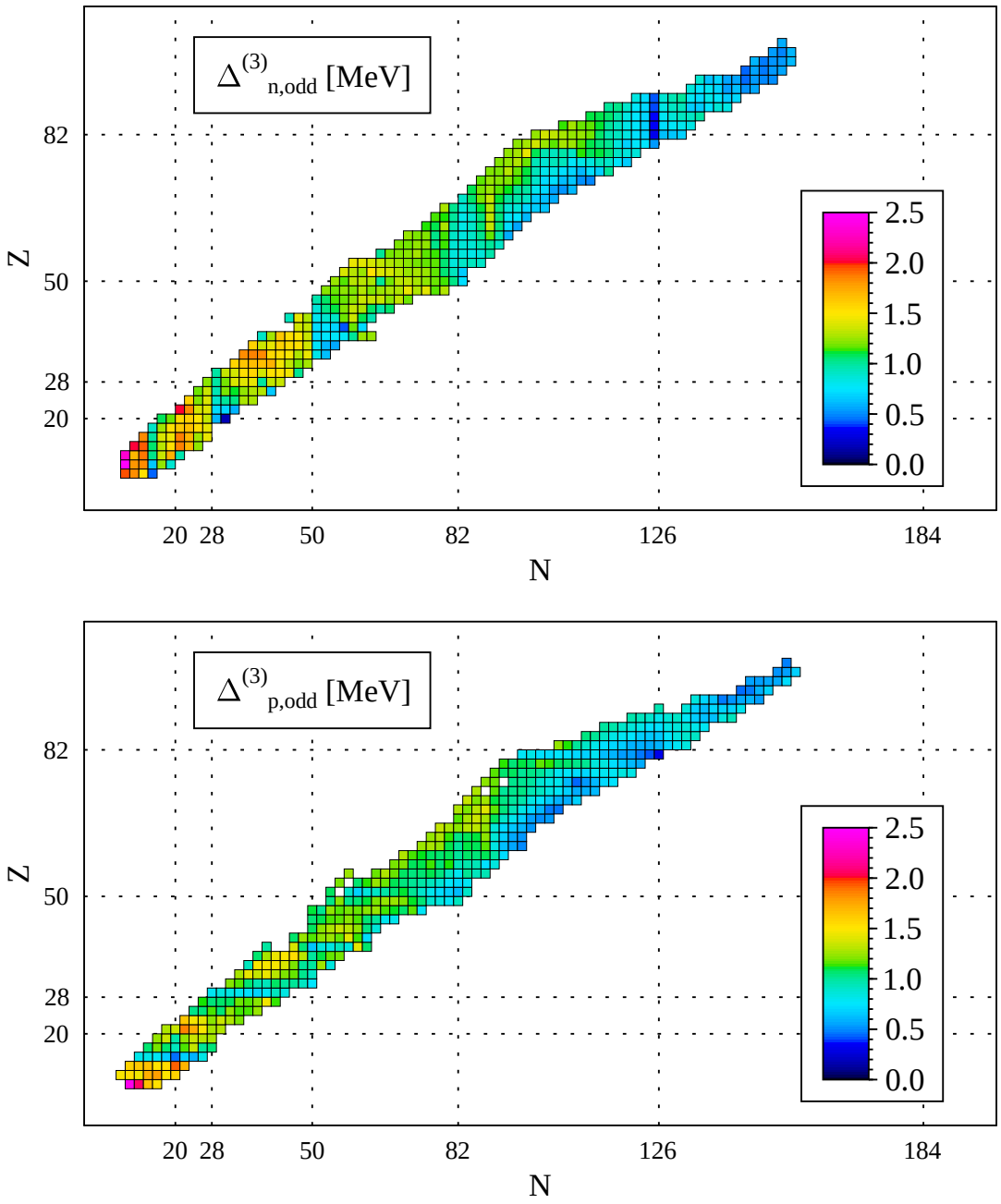

Figure 5.1: Experimental gaps extracted from the mass table [Aud03] by a three-point finite difference formula ($\Delta_q^{(3)}$, Eq. (5.19)) centered on nuclei with an odd number of the considered species and an even number of the other species. Top panel: neutron gaps, bottom panel: proton gaps.

Results obtained are interesting not only as a theoretical input for nuclear models applied to finite nuclei, but also as the sole means of studying the nature of matter in the crust of neutron stars.

Indeed, superfluidity plays a key role in these compact stars, as suggested early by Migdal [Mig60]. Pulsar glitches could be related to the pinning of vortices to nuclei in the superfluid neutron matter of their crust [Avo07]. Pairing also has a significant impact on the specific heat of the crust of neutron stars, which affects its cooling rate [Mon07]. In deeper and denser regions, protons could become superfluid and thus superconducting, which has strong implications for magnetic properties, while neutrons would form pairs in the anisotropic $^3P - F_2$ state [Bal98].

The self-consistent microscopic description of superfluidity in nuclear matter has been attempted using correlated basis function, or Monte-Carlo methods [Cha04, Fab05, Gan08]. However, the most useful method to understand how pairing is built into the correlated ground state is probaby to include correlations step by step through perturbation theory (or a Brueckner-Goldstone recast thereof). Conventional many-body perturbation theory (MBPT) [Hug57, Fet71] breaks down for superfluid nuclear systems, as the onset of pairing is approximately related to divergences occurring at the Fermi level in the G-matrix [Eme59], and exactly corresponds to a similar singularity appearing in the Feynman-Galitskii T-matrix [Eme60], together with the divergence of Weinberg eigenvalues [Ram07], which marks the transition to a nonperturbative regime. The same results were obtained in a finite-temperature formalism [Alm96]. Indeed, phase transitions such as the onset of pairing are not amenable to a perturbative expansion [Noz63]. We thus have to redefine the starting point and work with pair condensation incorporated at every level.

Such a theory can be built as an extension to MBPT, as proposed by Nambu and Gorkov [Gor58, Nam60], through the definition of anomalous propagators [Sch64, Abr63].

We suppose the system is ruled by a Hamiltonian $\hat{\overline{H}} = \hat{T} + \hat{V} - \lambda\hat{N}$, where $\hat{T}$ groups all one-body terms (kinetic term and external potential) and $\hat{V}$ is a two-body interaction, while a chemical potential λ, as in the BCS scheme, is used to conserve the average particle number.

Following [Noz63], we make use of the generalized two-body propagators

$$F_1(k;\omega) = \frac{\overline{\varepsilon}^0_k + \omega + \Sigma(\overline{k};-\omega)}{D(k;\omega)}, \tag{5.23}$$

$$F_2(k;\omega) = \frac{\Delta(k;\omega)}{D(k;\omega)}, \tag{5.24}$$

$$D(k;\omega) = [\overline{\varepsilon}^0_k + \omega + \Sigma(\overline{k};-\omega)][\overline{\varepsilon}^0_k - \omega + \Sigma(k;\omega)] + \Delta(k,\omega)^2, \tag{5.25}$$

with $\overline{\varepsilon}^0_k = \varepsilon^0_k - \lambda$, and ε^0_k is the s.p. energy determined by the one-body $\hat{T}$ (for an infinite system, the appropriate representation is $|k\rangle = |\mathbf{k}\sigma\rangle$, and $\varepsilon^0_k = \hbar^2\mathbf{k}^2/(2m)$, $\mathbf{k}$ being the s.p. momentum).

F_1 corresponds to the normal propagator, while F_2 is defined through an anomalous contraction. $\Sigma(k;\omega)$ is the (proper) self-energy entering the Dyson equation (for the sake of simplicity, we consider Σ to be diagonal in the chosen representation, as is the case in the plane wave basis for infinite systems). It sums all diagrams which are irreducible by cutting a single one-particle propagator line. A standard approxima-

tion used in nuclear matter is to use for $\Sigma(k;\omega)$ the first-order diagram involving the Brueckner G-matrix, yielding the Brueckner-Hartree-Fock (BHF) approximation.

$\Delta(k,\omega)$, on the other hand, is an anomalous self-energy obtained by solving the generalized Bethe-Salpeter equation, which describes the scattering of a pair of particles, involving generalized propagators. The latter yields, as an equation for Δ,

$$\Delta(k;\omega) = \int \frac{d\omega'}{2\pi} \sum_l I(k\overline{k}\omega; l\overline{l}\omega')\, F_2(l;\omega') \tag{5.26}$$

$$= \int \frac{d\omega'}{2\pi} \sum_l \frac{I(k\overline{k}\omega; l\overline{l}\omega')\, \Delta(l,\omega')}{[\overline{\varepsilon}^0_{\overline{l}} + \omega' + \Sigma(\overline{l};-\omega')][\overline{\varepsilon}^0_l - \omega' + \Sigma(l;\omega')] + \Delta(l,\omega')^2}, \tag{5.27}$$

where the interaction kernel $I(k\overline{k}\omega; l\overline{l}\omega')$ is the sum of diagrams which are irreducible by cutting a *pair* of single-particle lines [Bog58, Noz63, Hen64, Mig67, Bal90, Elg96]. Thus, diagrams entering the Brueckner G-matrix or the T-matrix beyond first order in V are forbidden in I, as they are already generated by the Bethe-Salpeter scattering equation itself: this would lead to double counting. Including anyway such effective vertices in the pairing channel [Amu85, Bal90, Wam93] yields markedly increased pairing gaps, compared to using the bare NN potential. The lowest-order contribution to $I(k\overline{k}\omega; l\overline{l}\omega')$ is thus the bare interaction matrix element $V_{l\overline{l}k\overline{k}}$. In this case I, as well as the anomalous self-energy Δ, are energy-independent. At following orders, we start to sum polarization diagrams corresponding to the particle-hole induced interaction, i.e. the many-body process of two particles interacting via the exchange of medium fluctuations [Hei00, She03].

Many-body effects do impact the anomalous self-energy Δ even if the bare interaction is taken as a pairing interaction kernel. Eq. (5.27) involves a non-trivial energy integral, which is the manifestation of the potential presence of effects beyond the quasiparticle picture. The complex values and energy-dependence of $\Sigma(k,\omega)$ indicate that quasiparticle excitations have a finite lifetime, i.e. they are not eigenstates of the Hamiltonian. It also signals the depletion of the Fermi sea on top of which pairing takes place.

Elementary excitation energies are given by the poles of the propagator, which occur at $\omega = \pm E_k$, with

$$E_k = \tfrac{1}{2}\left[\Sigma(k,E_k) - \Sigma(k,-E_k)\right] + \left\{[\overline{\varepsilon}^0_k + \tfrac{1}{2}(\Sigma(k,E_k) + \Sigma(k,-E_k))]^2 + \Delta(k,E_k)^2\right\}^{1/2}, \tag{5.28}$$

where we keep the energy-dependence of Δ for the sake of generality. We see that the energy dependence modifies the BCS expression for the quasiparticle energy, which is, however, recovered for an ω-independent self-energy (confirming the role of $\Delta(k;E_k)$ as the pairing gap). In the case of vanishing pairing (or for states far from the Fermi level where $\Sigma(k,E_k) \gg \Delta(k,E_k)$) we have $E_k = |\overline{\varepsilon}_k|$, where $\overline{\varepsilon}_k$ is the on-shell single-particle energy. For simplicity, we will skip imaginary parts in the following. We thus have

$$\overline{\varepsilon}_k = \overline{\varepsilon}^0_k + \Sigma(k,\overline{\varepsilon}_k). \tag{5.29}$$

Its explicit energy integral makes Eq. (5.27) quite impractical. Due to the non-trivial structure of the self-energies, an analytical reduction can only be achieved

by performing some approximation of the latter. An efficient choice is the pole approximation [Bal00a, Bal01, Bal02, Bal07c]. It consists, first, in neglecting the imaginary part of $\Sigma(k,\omega)$, which is reasonable for states lying next to the Fermi level and dominating the integrand of the gap equation. Then, the generalized propagator entering Eq. (5.27) is replaced by its pole part. One obtains

$$\Delta(k) \;=\; -\sum_{l} \frac{V_{k\bar{k}l\bar{l}}\; z_{\rm s}(l)\; \Delta(l)}{2\sqrt{(\overline{\varepsilon}^{\rm s}_l)^2+\Delta(l)^2}}, \tag{5.30}$$

where $\overline{\varepsilon}^{\rm s}_l$ is the *symmetrized* effective single-particle energy

$$\overline{\varepsilon}^{\rm s}_k \;=\; \overline{\varepsilon}^{0}_k + \tfrac{1}{2}[\Sigma(k,E_k)+\Sigma(k,-E_k)], \tag{5.31}$$

and $z_{\rm s}(k)$ is the residue of $1/D(k;\omega)$ at each of its (symmetric) poles. Near the Fermi level and in the $\Delta = 0$ limit (in nuclear matter we have $\Delta \simeq 3$ MeV for kinetic energies of the order of 50 MeV), $z_{\rm s}(k)$ can be identified with the normal-phase z-factor. A further approximation relies on the assumption of a smooth energy dependence of the self-energy. One then obtains the expression [Bal02, Bal07c, Lom01]

$$\widetilde{\Delta}(k) \;=\; -\sum_{l} \frac{z(k)\; V_{k\bar{k}l\bar{l}}\; z(l)\; \widetilde{\Delta}(l)}{2\sqrt{\overline{\varepsilon}^{2}_l+\widetilde{\Delta}(l)^2}}, \tag{5.32}$$

which involves, this time, the *on-shell* s.p. energy $\overline{\varepsilon}_k$ and a renormalized gap $\widetilde{\Delta}(k) = z(k)\Delta(k)$. Similar expressions have been obtained in the self-consistent Green's function approach involving T-matrix-derived self-energies [Mut05, Boz99, Boz03].

To first order in ω in the expression of $\Sigma(k;\omega)$, the symmetrized single-particle energy can be approximated as

$$\overline{\varepsilon}^{\rm s}_k \;\simeq\; \overline{\varepsilon}^{0}_k + \Sigma(k,\omega=0) + \mathcal{O}(E_k^2). \tag{5.33}$$

Next to the Fermi level the self-energy can be expected to vary sufficiently smoothly between $-E_k$ and E_k for this approximation to hold. We thus see that Eq. (5.30) involves a single-particle spectrum which does not take into account dispersive effects. The corresponding effective (Landau) mass is the pure k-mass $\widetilde{m}$. On the other hand, the on-shell prescription for the s.p. energies in Eq. (5.32) implies that both energy- and momentum-dependence are taken into account, which the additional z-factor compensates for. Indeed, $z(k) < 1$ at the Fermi level, while energy dependence increases the density of the s.p. spectrum, yielding an e-mass higher than the k-mass. It is interesting to mention some results in the ultraweak-coupling regime, where an analytical expression for the Fermi-level gap can be obtained [Bal01, Bal02]:

$$\Delta(k_{\rm F}) \;=\; 8\frac{mE_{\rm F}}{\widetilde{m}(k_{\rm F})}\; \exp\left[-\frac{m}{\pi^2 n_0 I(k_{\rm F})\widetilde{m}(k_{\rm F})z(k_{\rm F})}\right], \tag{5.34}$$

where $E_{\rm F}$ is the Fermi kinetic energy, $\widetilde{m}(k_{\rm F})$ is the k-mass at the Fermi level, n_0 is the Fermi gas level density, and $I(k_{\rm F})$ is the typical interaction kernel matrix element between states lying at the Fermi level. Because of the property $m^*(k) = \widetilde{m}(k)/z(k)$, we see that in this limit, Eqs. (5.30) and (5.32) are indeed equivalent: the pairing gap is determined by the quantity $I(k_{\rm F})\widetilde{m}(k_{\rm F})z(k_{\rm F}) = I(k_{\rm F})m^*(k_{\rm F})z(k_{\rm F})^2$.

5.2 Ab-initio input for the pairing part of the nuclear energy density functional

In this work, we aim at achieving a first step leading towards two distinct goals. First, we expect to improve our understanding, in terms of the relative importance of different diagrams in the pairing interaction kernel $I(k\bar{k}\omega; l\bar{l}\omega')$, of the microscopic origin of pairing between identical nucleons in nuclei. This requires to go beyond extrapolations of results obtained in nuclear matter and implement a method to perform calculations of finite nuclei, building the pairing gaps (i.e. HFB pairing field) explicitly from the bare interaction, either at first order or including higher-order diagrams. Such calculations have been attempted, the bare interaction being included to first order, for a slab of nuclear matter [Bal00b, Bal03, Pan06, Pan07], however self-energy effects were neglected. The few studies performed in a finite nucleus until now tend to show that the bare interaction alone can only account for a fraction of experimental pairing gaps [Bar04, Bar05], and that induced interactions due to coupling of individual motion with collective modes [Bar99, Ter02, Gio02] can explain the remainder [Bar04, Gor05a, Pas08a]. Due to the complexity of the calculations involved in the above mentioned works, only a single nucleus (^{120}Sn) could be studied. We thus hope to bring additional information into the discussion by performing a more systematic study of gaps obtained with the first-order contribution of the bare NN potential to I, thanks to the method explained below. We shall treat the NN contribution as fully as possible, including the Coulomb interaction, however we will not treat the three-nucleon interaction at this point. We will not, either, extend this work to incorporating higher-order contributions, owing to the complexity of first choosing then implementing a sound method to do so. We hope, ultimately, to treat induced interactions e.g. by including the exchange of phonons calculated in the RPA approximation using the residual interaction deduced from the Skyrme EDF. Of course, deriving the residual interaction from the bare NN potential would be the most consistent approach, and might become possible in the future using low-momentum interactions.

Second, we expect to produce a pairing functional yielding trustworthy predictions in regions of the mass table where pairing-related experimental data are unavailable. Indeed, existing local pairing functionals employed in self-consistent nuclear structure calculations are characterized by a number of parameters (strength factor, pairing active window/regularization scheme, density dependence) which are not all well constrained by available data. In fact, models which yield consistent predictions near the valley of stability can exhibit very different behaviors when extrapolated towards the neutron drip-line [Dug05]. These differences occur despite the fact that, except for recent works [Mar07, Mar08], isovector-density dependence of pairing functionals has not been employed.

For this purpose, we shall perform calculations with our microscopic model across the mass table, including regions far from the valley of stability. As will be detailed below, our method is, for now and within reasonable computing time and storage requirements, restricted to calculations in spherical symmetry. The results thus generated will provide a reference for comparison with other models useable in more general cases such as local pairing functionals. Note however that we do not necessarily expect, at this point, to obtain a good agreement with available experimental data.

Our approach to building HFB equations relies on devising a separable representation of the NN interaction. This separable interaction can then be used to build a pairing functional having some of the simplifying properties of a local one, allowing for the efficient construction and diagonalization of the HFB matrix. As a starting point, we use the $V_{\mathrm{low}\ k}$ low-momentum NN interaction, which, as will be discussed below and in section 5.3.2, lends itself well to separable approximations.

5.2.1 The $V_{\mathrm{low}\ k}$ low-momentum NN interaction

Several models exist for the nucleon-nucleon (NN) interaction. The most recent ones, either representing a mix of one-boson exchange parts and semi-phenomenological short-range terms [Wir95, Mac01], or consistently built from chiral effective field theory (EFT) [Ent03, Epe05], achieve an accurate description of available scattering data for energies reaching up to 350 MeV in the laboratory frame. These models are clearly different in terms of their matrix elements. However, it was shown that a universal NN interaction could be obtained by applying to either of several recent NN potentials a renormalization group (RG) transformation eliminating high-energy degrees of freedom [Bog01, Bog03a, Bog03b].

A NN interaction is thus obtained, called $V_{\mathrm{low}\ k}$, which couples only states of relative motion below a certain cutoff momentum, or renormalization scale Λ, while conserving two-body observables in the low-energy domain [Bog07b] thanks to the scale-invariance enforced for the scattering T-matrix. In particular, it does not present the high-energy/short-range repulsion characteristic of the hard core in traditional NN potentials, which makes it suitable for ab-initio nuclear structure calculations in reduced model spaces via variational [Nog04, Bog06a] shell model [Bog02], no-core shell model [Bog08a] or coupled cluster [Hag07] methods. Also, the RG transformation yields a NN interaction which, below a certain value of Λ, is *perturbative*, i.e. a perturbative expansion in terms of interaction vertices of the two-body scattering amplitude [Bog06b] or many-body ground state [Bog05] converges term-after-term, whereas only the formal re-summation of infinite series (such as the Brueckner G-matrix) yields a definite result when using the starting high-momentum potential. This feature is important as it allows to control the accuracy of such perturbative expansions through power counting as is done in chiral EFT.

The $V_{\mathrm{low}\ k}$ approach, therefore, opens new ways of studying nuclear structure. This, however, comes at a price. First, the interaction resulting from the RG transformation cannot be represented as a local potential anymore: it is a set of numerical matrix elements with significant non-locality. Second, while two-body observables are conserved, it is not true of higher-particle-number operators, and conservation of A-body physics requires, strictly speaking, the introduction of up to A-body interactions. In practice, the importance of interactions involving higher body numbers is expected to increase slowly when running Λ down. Although low-momentum three-body forces generated from NN+NNN Hamiltonians through RG equations are currently unavailable, it is expected that they will show marked resemblance with NNN forces from chiral EFT [Nog04, Bog05]. Work towards obtaining a complete $V_{\mathrm{low}\ k}$ NN+NNN Hamiltonian is currently underway [Bog07a, Bog08b].

The RG equation for the $V_{\mathrm{low\ k}}$ matrix elements is obtained by introducing a cutoff Λ in the Lippmann-Schwinger equation and running it down while conserving the half-off-shell T-matrix (making $V_{\mathrm{low}\ k}$ energy-independent) or the fully off-shell

one (yielding an energy-dependent $V_{\text{low } k}$, which can be rendered energy-independent by converting energy- to momentum-dependence and hermitizing). The cutoff can actually be applied in a smooth manner, yielding an interaction with continuous matrix elements in the k, k'-plane. Possible cutoff functions are [Bog07c]

$$f_{\text{sharp}}(k^2) \equiv \Theta(\Lambda^2 - k^2), \tag{5.35}$$

$$f^n_{\text{exp}}(k^2) \equiv \exp\left[-\left(\frac{k^2}{\Lambda^2}\right)^n\right], \tag{5.36}$$

$$f^\epsilon_{\text{FD}}(k^2) \equiv \frac{1}{1+\exp\left(\frac{k^2-\Lambda^2}{\epsilon^2}\right)}, \tag{5.37}$$

respectively called "sharp", "exponential" and "Fermi-Dirac" regulators. We then have

$$T_{\text{low k}}(k, k'; E) = f(k^2) T(k, k'; E) f(k'^2), \tag{5.38}$$

i.e. the T-matrix is conserved exactly for the sharp cutoff, and approximately, up to a factor corresponding to the regulating function used, for smooth ones.

5.2.2 Separable representation and finite nuclei

In atomic nuclei, Cooper pairs are expected to form principally between nucleons of the same species and in the $S = 0$, $L = 0$ state of relative motion. It is an interesting feature of NN scattering physics that the two-nucleon system exhibits in this channel ($^1S_0$) a virtual, quasi-bound state at low energy, which translates into large attractive phase shifts and, correspondingly, a large negative scattering length. Scattering theory [Bro76] tells us that the T-matrix corresponding to such a system is dominated by a single pole at the energy of the virtual state, which means that it is, to a good approximation, separable of rank one close to this energy. A potential describing the two-body scattering problem in this energy range may thus have the same structure, i.e. $V(k, k') = \lambda\ g(k)\ g(k')$ [Hai84]. Such a potential, however, cannot describe NN scattering beyond an energy $E_{\text{lab}} = 250$ MeV due to the inversion of the sign of phase shifts (and hence of diagonal T-matrix elements) at this point. Nevertheless, this property could be used by Duguet [Dug04], who built a low-momentum approximation to the Argonne v_{18} potential having similar properties with respect to pairing in infinite nuclear matter. The form of this interaction was a simple one, and further approximations were proposed in order to make nuclear structure calculations feasible. In this work, we aim at extending the work of Ref. [Dug04], both by building accurate separable representations of the $V_{\text{low } k}$ NN interaction and by using them to compute nuclear properties at the HFB level without further assumptions regarding the form of the pairing interaction/functional.

Even beyond a rank-one approximation, it is a general feature of low-momentum potentials that they can be more easily approximated by separable forms. This can be understood by studying Weinberg eigenvalues, i.e. solutions η_i of the equation

$$\hat{V}\ G_0(E)\ |\psi_i\rangle = \eta_i\ |\psi_i\rangle, \tag{5.39}$$

where $\hat{V}$ is the two-body potential, $G_0(E)$ the free two-particle propagator and $|\psi_i\rangle$ the corresponding eigenstate. When RG evolution is applied to a NN potential,

running down the cutoff Λ drives more and more eigenvalues close to zero, resulting in fewer ones retaining a significant contribution. The potential not only becomes perturbative, but it can also, then, be approximated through a separable expression of lower and lower rank [Bog06b].

An interaction acting solely in the ${}^1S_0$ channel can be decomposed as

$$\hat{V}^{^1S_0} = \hat{V}^S \hat{P}_{S=0}, \tag{5.40}$$

where $\hat{V}^S$ is the spatial part acting in the $L=0$ state of relative motion and $\hat{P}_{S=0}$ is the spin-singlet projector defined as

$$P_S = \frac{1+(-1)^S \hat{P}_\sigma}{2}, \tag{5.41}$$

$\hat{P}_\sigma$ being the spin-exchange operator. Momentum- and coordinate-space matrix elements of the spatial part can be expressed, respectively, as

$$\langle \mathbf{k}_1\mathbf{k}_2|\hat{V}^S|\mathbf{k}_3\mathbf{k}_4\rangle = V_{^1S_0}(k_{12},k_{34})\ (2\pi)^3\delta(\mathbf{K}_{12}-\mathbf{K}_{34}), \tag{5.42}$$

$$\langle \mathbf{r}_1\mathbf{r}_2|\hat{V}^S|\mathbf{r}_3\mathbf{r}_4\rangle = V_{^1S_0}(s_{12},s_{34})\ \delta(\mathbf{R}_{12}-\mathbf{R}_{34}). \tag{5.43}$$

The center-of-mass (CoM)/relative coordinates are defined as: $\mathbf{s}_{ij}=\mathbf{r}_i-\mathbf{r}_j$, $\mathbf{R}_{ij}=(\mathbf{r}_i+\mathbf{r}_j)/2$, $\mathbf{k}_{ij}=(\mathbf{k}_i-\mathbf{k}_j)/2$ and $\mathbf{K}_{ij}=\mathbf{k}_i+\mathbf{k}_j$. This interaction has, in general, a finite-range and a finite non-locality. It is true of any finite-range interaction when one isolates a single partial wave, whether or not one starts with a non-local interaction such as $V_{\text{low }k}$. The separable approximation to the matrix elements enters the definition of $V_{^1S_0}$ functions,

$$V_{^1S_0}(k,k') = \sum_{\alpha\beta} g_\alpha(k)\ \lambda_{\alpha\beta}\ g_\beta(k'), \tag{5.44}$$

$$V_{^1S_0}(s,s') = \sum_{\alpha\beta} G_\alpha(s)\ \lambda_{\alpha\beta}\ G_\beta(s'), \tag{5.45}$$

where $1\le\alpha,\beta\le M$, M is the rank of the interaction, and $g_\alpha(k)$ and $G_\alpha(s)$ are interaction form factors in momentum and coordinate space, respectively; $\lambda_{\alpha\beta}$ is a strength matrix.

The two representations are linked by the following relation between momentum- and coordinate-space form factors:

$$G_\alpha(s) = \int \frac{d^3\mathbf{k}}{(2\pi)^3}\, e^{-i\mathbf{k}\cdot\mathbf{s}}\, g_\alpha(k) = \frac{1}{2\pi^2 s}\int kdk\ \sin(ks)\ g_\alpha(k). \tag{5.46}$$

Given four states $\check{\imath}\hat{\jmath}\check{k}\hat{l}$ belonging to a single-particle basis, with $\check{\imath}$ and $\check{k}$ taken in the first half and $\hat{\jmath}$ and $\hat{l}$ in the second half of the basis, as defined by the Bogolyubov transform of the system's reference state, one can express the corresponding matrix element of the interaction as

$$(\overline{v}^{^1S_0}_{\text{sep}})_{\check{\imath}\hat{\jmath}\check{k}\hat{l}} = \iint d^3\mathbf{R}_{12}d^3\mathbf{R}_{34}\ \sum_{\alpha\beta}\left[\int d^3\mathbf{s}_{12}\ G_\alpha(s_{12})\ \Psi^*_{\check{\imath}\hat{\jmath}}(\mathbf{r}_1,\mathbf{r}_2)\right] \times\ \lambda_{\alpha\beta}\ \delta(\mathbf{R}_{12}-\mathbf{R}_{34})\left[\int d^3\mathbf{s}_{34}\ G_\beta(s_{34})\ \Psi_{\check{k}\hat{l}}(\mathbf{r}_3,\mathbf{r}_4)\right] \tag{5.47}$$

$$(\overline{v}^{^1S_0}_{\text{sep}})_{\check{\imath}\hat{\jmath}\check{k}\hat{l}} = \int d^3\mathbf{R}\ \sum_{\alpha\beta}\breve{\Psi}^{\alpha*}_{\check{\imath}\hat{\jmath}}(\mathbf{R})\ \lambda_{\alpha\beta}\ \breve{\Psi}^{\beta}_{\check{k}\hat{l}}(\mathbf{R}), \tag{5.48}$$

with

$$\breve{\Psi}^{\alpha}_{\check{i}\hat{j}}(\mathbf{R}) \equiv \int d^3\mathbf{s}\; G_\alpha(s)\Psi_{\check{i}\hat{j}}(\mathbf{R}+\mathbf{s}/2,\mathbf{R}-\mathbf{s}/2) \tag{5.49}$$

$$= \int d^3\mathbf{s}\; G_\alpha(s)\sum_\sigma(-)^{s-\sigma}\;\varphi_{\check{i}}(\mathbf{R}+\mathbf{s}/2,\sigma)\;\varphi_{\hat{j}}(\mathbf{R}-\mathbf{s}/2,\overline{\sigma}), \tag{5.50}$$

where $\Psi_{\check{i}\hat{j}}$ is the spin-singlet part of the two-body product wave function (see appendix F.1). At first order in the interaction, the pairing energy can be written

$$\mathcal{E}_{\rm pair} = \frac{1}{4}\sum_{\check{i}\hat{j}\check{k}\hat{l}}(\overline{v}^{\,^1S_0}_{\rm sep})_{\check{i}\hat{j}\check{k}\hat{l}}\;\kappa_{\check{i}\hat{j}}\;\kappa_{\check{k}\hat{l}} = \frac{1}{4}\int d^3\mathbf{R}\;\sum_{\alpha\beta}\lambda_{\alpha\beta}\;\breve{\chi}^*_\alpha(\mathbf{R})\;\breve{\chi}_\beta(\mathbf{R}), \tag{5.51}$$

where $\kappa_{\check{i}\hat{j}}$ is the pair tensor and the effective pair densities $\breve{\chi}_\alpha$ are defined as

$$\breve{\chi}_\alpha(\mathbf{R}) = -\sum_{\check{i}\hat{j}}\breve{\Psi}^{\alpha}_{\check{i}\hat{j}}(\mathbf{R})\;\kappa_{\check{i}\hat{j}}, \tag{5.52}$$

The key point in the above expression is that the pairing energy can be written as a functional of pair densities which are *local* in the sense that they depend on one spatial coordinate only. All the range and non-locality of the interaction, which were contained in the $G_\alpha(s)$ functions, are now hidden in the densities defined by Eq. (5.52). The elements of the strength matrix $\lambda_{\alpha\beta}$ play the role of coupling constants of the functional. Effective pair densities can also be expressed starting from the non-local spin-singlet pair density

$$\breve{\chi}_\alpha(\mathbf{R}) = \int d^3\mathbf{s}\; G_\alpha(s)\tilde{\rho}(\mathbf{R},\mathbf{s}), \tag{5.53}$$

$$\tilde{\rho}(\mathbf{R},\mathbf{s}) \equiv -\sum_{\check{i}\hat{j}}\Psi_{\check{i}\hat{j}}(\mathbf{R}+\mathbf{s}/2,\mathbf{R}-\mathbf{s}/2)\kappa_{\check{i}\hat{j}}, \tag{5.54}$$

which exhibits the non-locality of our functional.

Matrix elements of the pairing field Δ in the chosen basis can be obtained via functional differentiation, yielding

$$\Delta_{\check{i}\hat{j}} = \sum_\alpha\int\; d^3\mathbf{R}\;\breve{\Psi}^{\alpha*}_{\check{i}\hat{j}}(\mathbf{R})\,\breve{\Delta}_\alpha(\mathbf{R}), \tag{5.55}$$

where we use local intermediate quantities (or effective fields) to fully represent the pairing field,

$$\breve{\Delta}_\alpha(\mathbf{R}) \equiv -\tfrac{1}{2}\sum_\beta\lambda_{\alpha\beta}\;\breve{\chi}_\beta(\mathbf{R}). \tag{5.56}$$

This form of a pairing functional allows to build the HFB equations, expressed in the chosen basis representation, with a computational burden similar to the case of a local functional. Although the expression Eq. (5.51) still does not allow to work efficiently in an explicit coordinate-space representation, the calculation of pairing matrix elements is considerably faster using Eq. (5.55) ($\mathcal{O}(n^2)$, n being the typical number of s.p. basis states in a block of the pair tensor $\kappa_{\check{i}\hat{j}}$) than when using the matrix elements of the interaction directly ($\mathcal{O}(n^4)$).

Two difficulties arise, though, in addition to the workings of a basis-representation Skyrme-HFB code. Indeed, in order to achieve the $\mathcal{O}(n^2)$ scaling of computational cost, we have to calculate and store the $\breve{\Psi}^{\alpha}_{ij}(\mathbf{R})$ functions for all pairs of basis states potentially coupled by the pairing field given the symmetries chosen for the representation. Storage requirements are thus larger than in the case of a local pairing functional. The second, formal, difficulty is to design and implement a center-of-mass/relative coordinate separation for use in Eq. (5.50). This is trivial when working in Cartesian coordinates, but storage and time requirements imply, at least in a first step, to work in spherical symmetry.

The details of the method we use, being non-essential for the physical discussion, are exposed in appendix F.

5.3 A Separable Representation of the NN force

Before performing calculations, as described in the previous chapter, employing the $V_{\mathrm{low}\ k}$ interaction in the pairing channel, we have to devise a separable representation of it. Several techniques have been proposed for building separable approximations of local or other potentials [Wei63, Ern73, Hai84, Bal86, Bal87]. Most focus on reproducing the low-energy physics of the interaction, such as the M lowest-energy poles of the T-matrix in the case of the Gamow separable approximation [Bal86], by diagonalizing an operator derived from the interaction, in some cases adding weight on a particular region of the momentum space. Such is the case of the Weinberg procedure, which, by diagonalizing $VG_0(E)$, $G_0(E)$ being here the free two-particle propagator in the vacuum, yields a good approximation mainly around the chosen energy E (although in practice, the range of accuracy of the approximation is more extended, at least for $V_{\mathrm{low}\ k}$ [Bog06b]). In our case, the focus on low-energy degrees of freedom is already taken care of by the $V_{\mathrm{low}\ k}$ procedure. In particular, the matrix elements of $V_{\mathrm{low}\ k}$ are of finite support because of the RG cutoff. Provided they are also smooth enough, this guarantees the existence of an accurate, finite separable expansion in the whole (k, k')-plane. Moreover, any analytic property of a given scheme would probably be lost in the process of devising a parametrization of the numerically-obtained separable representation.

Therefore, the first step of our method for producing a separable approximation of $V_{\mathrm{low}\ k}$ is even simpler: we diagonalized the potential itself, i.e. its ${}^1S_0$ matrix elements. Let us note that a similar approach was followed in Ref. [Bal98] for use in infinite matter. We then fitted analytic formulae to the eigenvectors, yielding a first separable representation which was improved by refitting all its parameters, first on the original $V_{\mathrm{low}\ k}$ matrix elements, then on half-on-shell T-matrix values calculated with the latter.

5.3.1 Parametrization and fit procedure

When choosing the form of the functions $g_\alpha(k)$ entering the separable form, the basic principle was to keep the fit as "linear" as possible in order to have a (cost/merit) function close to a quadratic form with respect to the parameters. We also had to ensure the possibility to perform the Bessel-Fourier transform of the momentum-space form factors to their coordinate-space equivalent analytically. Several families

of form factors were tested, corresponding in each case to a master function determining the range of the corresponding interaction term (through the only range parameter) multiplied by a linear combination of power functions which modulate the shape of the master function. The most convenient master function was found to be a Gaussian. The form factors $g_\alpha(k)$ thus read

$$g_\alpha(k) \;=\; \left[\sum_{i=0}^{m} x_{\alpha i}\left(\frac{a_\alpha^2 k^2}{2}\right)^{n_i}\right]\exp\left(-\frac{a_\alpha^2 k^2}{2}\right). \tag{5.57}$$

Here the exponents n_i take integer values in the range $0\ldots10$. Due to the redundancy between the overall magnitude of $g_\alpha(k)$ and the coupling constants $\lambda_{\alpha\beta}$, it is necessary to normalize one of them. Here the $g_\alpha(k)$'s were normalized by setting in each case one of the x's to 1 (typically the one corresponding to the lowest order n_i, or the largest one if it is significantly larger). The corresponding term is then labelled with $i = 0$.

The parameters of the force (labeled $V_{\rm fit}$ in the following) were adjusted by minimizing a chi-square-like quantity, built with tolerances which reflect the *desired* accuracy of the fit to the various quantities involved rather than true uncertainties. We strive to keep as much of the physics contained in the raw data while obtaining a necessarily imperfect parametrization.

The procedure we used was stepwise. In a first step the matrix $V_{\rm low\ k}(k_i,k_j)$ was diagonalized, yielding a set of normalized numerical form factors $g_\alpha^{\rm diag}(k_i)$ and corresponding coupling constants $\lambda_\alpha^{\rm diag}$. Only the form-factor/coupling pairs with the largest $|\lambda_\alpha^{\rm diag}|$ were kept, and analytical expressions, Eq. (5.57), were fitted on the values of corresponding $g_\alpha^{\rm diag}(k_i)$. This preliminary fit involved a systematic search of the optimal range a_α and coefficients x_n determined by performing a linear least-squares fit for a number of values of the range and all possible combinations of exponents n, taken as a fixed number N_n of values picked between 0 and $n_{\rm max}$ (see below for actual values). The best parametrization of $g_\alpha(k)$ was kept and refitted with respect to all its parameters using a standard minimization algorithm.

In a second step, raw matrix elements were constrained by minimizing, with respect to all continuous parameters of the force, the quantity

$$\chi_V^2 \;=\; \frac{2}{N_k(N_k+1)}\sum_{i\geq j}\frac{\left(V_{\rm fit}(k_i,k_j)-V_{\rm low\ k}(k_i,k_j)\right)^2}{\sigma_V(k_i,k_j)^2}, \tag{5.58}$$

where i,j are indices referring to points on a lattice in the (k,k')-plane, with $k_i = i\,\delta k$ while N_k is the number of points in the k or k' direction (taken the same for both). $V_{\rm fit}(k,k')$ was computed thanks to Eqs. (5.44) and (5.57). The tolerances σ were defined as

$$\sigma_V(k_i,k_j) \;=\; \sigma_{\Delta V}(k_i,k_j)\;\times\;\frac{1+\nu}{\kappa+\nu}\;\left[1+(\kappa-1)\left|\frac{k_i-k_j}{k_i+k_j}\right|^\nu\right] \tag{5.59}$$

where κ and ν are parameters which control the relative weighting of diagonal and off-diagonal matrix elements (κ: ratio between tolerances of the most-off-diagonal and diagonal points, ν: power law according to which σ varies. The formula here keeps the average value along the $k-k'$ direction at $\sigma_{\Delta V}$), while the σ_Δ are given

by

$$\sigma_{\Delta V}(k_i,k_j) = \begin{cases} \sigma_{\rm med} + \dfrac{\sigma_{\rm max}-\sigma_{\rm med}}{\Delta^V_{\rm max}}\,\Delta^V(k_i,k_j), & \Delta^V(k_i,k_j) > 0 \\ \sigma_{\rm med} + \dfrac{\sigma_{\rm min}-\sigma_{\rm med}}{\Delta^V_{\rm min}}\,\Delta^V(k_i,k_j), & \Delta^V(k_i,k_j) < 0 \end{cases} \tag{5.60}$$

where $\sigma_{\rm min}$, $\sigma_{\rm med}$ and $\sigma_{\rm max}$ are tolerances affected to the points (averaged over the $k-k'$ direction) having resp. the lowest($\Delta^V_{\rm min}$), zero and highest ($\Delta^V_{\rm max}$) values of the quantity

$$\begin{aligned} \Delta^V(k_i,k_j) &= 4V_{\text{low k}}(k_i,k_j) \\ &\quad -V_{\text{low k}}(k_{i+1},k_j) - V_{\text{low k}}(k_i,k_{j+1}) - V_{\text{low k}}(k_{i-1},k_j) - V_{\text{low k}}(k_i,k_{j-1}), \end{aligned} \tag{5.61}$$

which is simply a finite-difference expression for a Laplacian of the function $V(k,k')$, and expresses the local "curvature" of the matrix elements. This has been devised to allow for a lower weighting of regions where $V_{\text{low }k}$ matrix elements have a highly angular behavior, which our analytical expressions for the matrix elements $V_{\rm fit}(k,k')$ cannot accurately match. Such an increased tolerance in this region allows to "sacrifice" them and avoid propagation of the error made there to neighboring regions where a much more accurate fit is possible.

As a third step, starting from the previous solution, we minimized the quantity $\chi^2_V + \chi^2_T$, where

$$\chi^2_T = \frac{1}{N'_k(N'_k+1)} \sum_{ij} \frac{\left(T_{\rm fit}(k'_i,k'_j;E_{k'_j}) - T_{\text{low }k}(k'_i,k'_j;E_{k'_j})\right)^2}{\sigma_T(k'_i,k'_j)}, \tag{5.62}$$

$T_{\rm fit}(k'_i,k'_j;E_{k'_j})$ being the half-on-shell T-matrix in the ${}^1S_0$ channel calculated with our model separable interaction, while $T_{\text{low }k}(k'_i,k'_j)$ are the corresponding values obtained from the original $V_{\text{low }k}$ potential [Rot08a], and

$$\sigma_T(k'_i,k'_j) = \frac{\sigma^0_T}{k'_i+k'_j} \times \frac{1+\nu'}{\kappa'+\nu'} \left[1 + (\kappa'-1)\left|\frac{k'_i-k'_j}{k'_i+k'_j}\right|^{\nu'}\right]. \tag{5.63}$$

Again we apply a weighting scheme which constraints diagonal matrix elements, directly related in this case to phase shifts, more than off-diagonal ones. The $1/(k'_i+k'_j)$ factor make the tolerances on the diagonal T-matrix elements correspond to approximately constant tolerances on phase shifts, since the latter satisfy $T(k,k;E_k) = k\cot(\delta(k))$.

We thus have a simple constraint better connected with the physics of the interaction and which ensures that not only the matrix elements of our force match those of $V_{\text{low k}}$ locally, but that an optimum fit of the *function* $V_{\rm fit}(k,k')$ to the *whole set* of data is achieved. Indeed, physical observables, in general, integrate the effect of matrix elements over a significant portion of the (k,k') plane, especially phase shifts, which are known to be closely related to pairing gaps.

In our procedure, the result of step three turned out to be a slight readjustment of the result obtained at step two, thus giving us confidence that we attained a globally optimal solution. Moreover, while after step two we generally had $\chi^2_T \gg \chi^2_V$, step three yielded a significant reduction of χ^2_T, with only a slightly increased χ^2_V, which shows that a purely local constraint on $V(k,k')$ misses important degrees of freedom in the set of matrix elements.

5.3.2 Fits

We performed fits on a range of $V_{\mathrm{low}\ k}$ interactions built from either the Argonne v_{18} [Wir95] or the CD-Bonn [Mac01] potential. The choice of which interactions were parametrized stems from requirements of our study: First, we built representations of $V_{\mathrm{low}\ k}$ /Argonne, for $\Lambda = 1.8$ and $2.5\,\mathrm{fm}^{-1}$, in both the neutron-neutron and proton-proton channels. In the latter case, we switched off the electromagnetic part of the interaction in order to study the effect of charge symmetry breaking in the hadronic part. Second, we built a set of representations of $V_{\mathrm{low}\ k}$ for higher values of Λ, in order to study the Λ-dependence of pairing at the HFB level. In this case, we had to use the CD-Bonn potential as an input due to numerical instabilities observed in the RG evolution of the Argonne potential. All these fits were based on the neutron-neutron channel of the interaction.

The cutoff function $f(k^2)$ was chosen, in each case, as a compromise between the necessity to have a cutoff sharp enough to conserve the T-matrix accurately and the requirement that it be smooth enough to allow for the reproduction of matrix elements near Λ with an analytic function. We thus used a Fermi-Dirac function with $\epsilon = 0.5\,\mathrm{fm}^{-1}$ for the lowest cutoff value ($\Lambda = 1.8\,\mathrm{fm}^{-1}$) and an exponential one in the other cases.

Finally, we performed a separable parametrization of the ${}^1S_0$ nn matrix elements of the Argonne v_{18} potential. Yielding a rank-9 representation, it lies arguably at the edge of the capacities of our method. Nonetheless, this makes it useable in systematic calculations using our HFB code. On the other hand, the CD-Bonn potential could not be accurately reproduced with a separable form.

The parameters used in the fit procedure were chosen so as to focus on diagonal matrix elements and phase shifts. We used the values $\kappa = \nu = 2$, $\kappa' = 3, \nu' = 2$, $\sigma_T^0 = 10^{-2}$, which translates into a tolerance on phase shifts of around $0.3°$.

We investigated the use of both a diagonal and non-diagonal coupling matrix $\lambda_{\alpha\beta}$ in the final refit. The minimization algorithm tends to favor large off-diagonal couplings and similar form factors. In the rank-2 case, by diagonalizing the $\lambda_{\alpha\beta}$ matrix produced by such a fit, one observes that the form factors corresponding to its eigenvectors are the sum and the difference of the similar-looking form factors which differ by just slightly different ranges. Such a difference, in the limit of functions that are identical up to a range parameter, corresponds to ($\eta \ll 1$)

$$f(a(1+\eta)x) - f(x) \quad \simeq \quad \eta a x \frac{df}{dx}, \tag{5.64}$$

or in the case of a simple Gaussian,

$$\exp\left(-\frac{(a(1+\eta)x)^2}{2}\right) - \exp\left(-\frac{(ax)^2}{2}\right) \quad \simeq \quad -\eta(ax)^2 \exp\left(-\frac{(ax)^2}{2}\right), \tag{5.65}$$

i.e. the optimization code tries to build a form factor with a higher order in k. The purpose of this obviously lies in the reproduction of the quite abrupt variations of $V_{\mathrm{low}\ k}$ matrix elements near the cutoff. However, such a scheme seems quite artificial and, moreover, one faces the problem that the large off-diagonal couplings are not well defined – it seems impossible to get a firm convergence as the $\lambda_{\alpha\beta}$'s keep growing albeit for only a slight reduction of χ^2. Thus, we preferred using only diagonal couplings, at the expense of a slightly worse description of the data near the cutoff,

$V_{\rm NN}$	Λ	Cut. function	M	N_n	Par.	$n_{\rm max}$	$\sigma_{\rm min,med,max}$	χ^2_V	χ^2_{V+T}
AV18, nn	1.8	FD $\epsilon = 0.5$	2	6	14	6	3, 3, 80	0.10	2.41
AV18, nn	2.5	exp. $n = 6$	3	6	21	10	3, 3, 3	0.26	3.02
AV18, pp	1.8	FD $\epsilon = 0.5$	2	6	14	6	3, 3, 80	0.10	1.85
AV18, pp	2.5	exp. $n = 6$	3	6	21	10	3, 3, 3	0.27	2.93
CD-B, nn	1.8	FD $\epsilon = 0.5$	2	6	14	6	3, 3, 80	0.10	1.77
CD-B, nn	2.5	exp. $n = 6$	3	5	18	10	3, 3, 3	0.20	2.20
CD-B, nn	3.0	exp. $n = 6$	5	4	25	10	3, 3, 3	0.22	0.66
CD-B, nn	4.0	exp. $n = 6$	5	4	25	10	3, 3, 3	0.22	0.42
CD-B, nn	8.0	exp. $n = 6$	6	5	36	10	3, 3, 3	0.55	1.21
CD-B, nn	15.0	exp. $n = 6$	7	5	42	10	3, 3, 3	0.70	9.55
AV18, nn	—	—	9	5	54	10	3, 3, 3	0.44	1.26

Table 5.1: Fitting parameters and resulting χ^2 values. $V_{\rm NN}$: starting bare potential (AV18: Argonne v_{18}, CD-B: CD-Bonn). Λ: RG cutoff, in fm^{-1} . Cutoff: cutoff function in RG equation (Eqs. (5.37) and (5.37)). M: rank of the separable representation. N_n: number of values of the exponent n of $(a_\alpha^2\ k^2)/2$ in each form factor, Eq. (5.57). Par.: total number of parameters. $n_{\rm max}$: maximum value of exponent n. $\sigma_{\rm min,med,max}$: tolerance parameters for potential matrix elements in Eq. (5.60), χ^2_V: residual error on potential matrix elements, Eq. (5.58), χ^2_{V+T}: total residual error on potential, Eq. (5.58) and T-matrix, Eq. (5.62).

but allowing for a reduced number of parameters (1 less for rank-2, 3 less for rank-3, etc.).

Forces we used as input for fitting, as well as parameters defining the form of separable representations we built are summarized in Table 5.1, together with resulting values of χ^2_V and χ^2_T. The complete set of parameters resulting from the fits and defining these separable representations is given in appendix E.

The rank and number of terms in the form factors of the separable force, which define the number and type of parameters, were adjusted to obtain a final $\chi^2_V + \chi^2_T$ value of order unity with as low a number of parameters as possible. This could be achieved in all cases except for $\Lambda = 15$ fm^{-1} $V_{{\rm low}\ k}$ /CD-Bonn, which will see more limited use than the other representations anyway. As expected, though, the rank necessary for an accurate reproduction of potential matrix elements and of the T-matrix grows steadily with the cutoff. In the case of Argonne v_{18}, the number of parameters in our separable form (54) is larger than in the initial force (48). This has to be attributed to the practical constraints on the analytic form taken by our interaction. Since the latter is not connected to the form of the original potential, our parameter set contains information corresponding to the expression of v_{18} in addition to its parameters.

Fig. 5.2 displays phase shifts calculated with our potential parametrizations. The cutoff is clearly visible in the collapse of $\delta(k)$ at high k. Below Λ, all our forces predict similar values despite originating from different hard-core potentials, which only signals that the latter have been fitted to the same data. It is worth pointing out, here, that the shape of the smooth cutoff implies that the collapse occurs slightly below Λ. Charge-symmetry breaking (left panel) brings only a small correction to the phase shifts by making the interaction marginally less attractive.

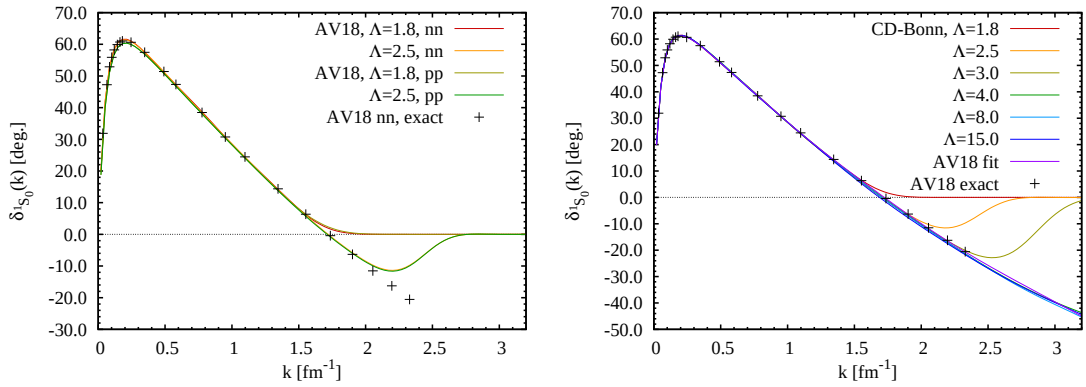

Figure 5.2: Phase shifts calculated from our separable potentials. Left panel: nn and pp $V_{\mathrm{low}\,k}$ potentials generated from Argonne v_{18}. Right panel: nn $V_{\mathrm{low}\,k}$ potentials generated from CD-Bonn and separable representation of Argonne v_{18}.

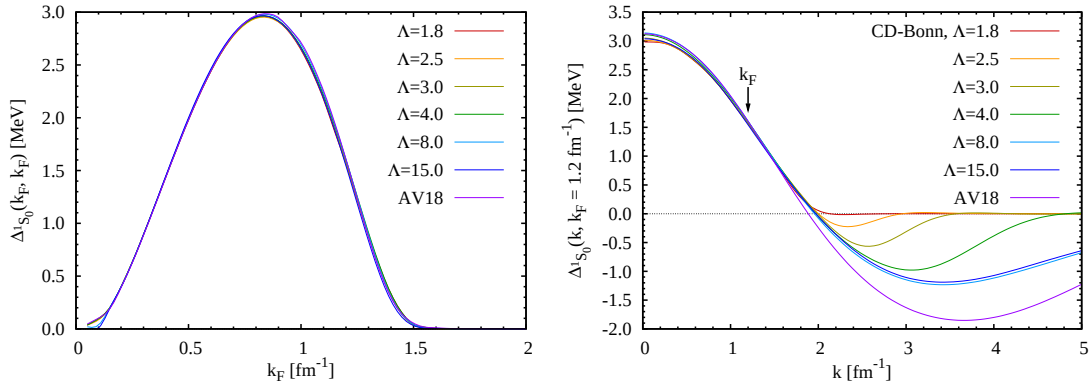

Figure 5.3: BCS infinite-matter pairing gaps calculated with a kinetic spectrum from our separable representations of $V_{\mathrm{low}\,k}$ /CD-Bonn potentials and bare Argonne v_{18}. Left panel: Fermi level gaps. Right panel: momentum-dependent gaps at $k_F = 1.2$ fm^{-1} .

Pairing gaps calculated at the BCS level for a kinetic spectrum are shown on Fig. 5.3. Whereas gaps calculated at the Fermi level (left panel) are identical to each other, up to fitting errors and a slight Λ-dependence (which is known to decrease gaps with lower Λ), momentum-dependent gaps (right panel) exhibit markedly different structures at high momenta. For $V_{\mathrm{low}\,k}$ /CD-Bonn interactions, the repulsive core develops between $\Lambda = 1.8$ and 8.0 fm^{-1} , where gaps are almost identical to the case $\Lambda = 15.0$ fm^{-1} , signalling a saturation of the RG evolution of this potential. Although we were not able to produce a separable representation of CD-Bonn, this potential, once evolved to this range of cutoffs can be treated with our separation method and can be expected to be very close to the original potential. The Argonne potential appears to be even more repulsive at momenta larger than 2 fm^{-1} . We thus have at hand, with the parametrizations used in the right panel of Fig. 5.3, a range of potentials of various "hardness", which will be useful for the study of the effect of their high-momentum matrix elements.

We have thus built a set of separable parametrizations of the $V_{\mathrm{low}\,k}$ interaction as well as the Argonne v_{18} potential. These parametrizations will now allow us to

perform systematic EDF calculations with the bare NN interaction in the pairing channel. To obtain a full NN potential, though, there remains to treat the electromagnetic interaction, which had to be switched off when treating the proton-proton channel, whereas it is, obviously, non-negligible in this case.

5.3.3 Separable approximation of the Coulomb interaction

The electromagnetic potential between protons is dominated by the Coulomb force, i.e. the electric part of the one-photon exchange potential. We take the proton charge distribution as pointlike. Momentum-space matrix elements of the latter in the S-wave read [Bro76]

$$V_{\mathrm{Coul},\ell=0}(k,k') = \frac{4\pi e^2}{2kk'} \ln\left|\frac{k+k'}{k-k'}\right|, \tag{5.66}$$

where e is the electromagnetic unit charge (in MeV fm). They diverge at $k = k'$, which forbids separable expansions. One can devise, though, a separable expansion of an approximate Coulomb potential restricted to a finite range, by setting (in usual notations)

$$V^a_{\mathrm{Coul}}(r) = \begin{cases} e^2/r & \text{for} \quad r \le a \\ 0 & \text{for} \quad r > a \end{cases}, \tag{5.67}$$

a being a range parameter. Provided a is chosen larger than the diameter of the finite nucleus, this range truncation should yield a satisfactory approximation for use in the proton-proton pairing channel, as the non-local part of the pair density quickly vanishes when a particle is outside of the nucleus and, thus, no matrix element of the pairing tensor probes the part of the potential that has been put to zero. In an infinite system, the above approximation should be useful provided a is made much larger than the coherence length, which requires the latter to be finite, and better, not too large.

The S-wave part of the above potential can be calculated through its definition

$$V^a_{\mathrm{Coul},\ell=0}(k,k') \equiv 4\pi \int_0^a r^2 dr\; j_0(kr)\, \frac{e^2}{r}\, j_0(k'r), \tag{5.68}$$

$$= 4\pi \frac{e^2}{2kk'} \big[\mathrm{Ci}(a(k-k')) - \ln(a(k-k')) - \mathrm{Ci}(a(k+k')) + \ln(a(k+k'))\big], \tag{5.69}$$

j_n being a spherical Bessel function and Ci a cosine-integral function. The above expression has a separable expansion[1]:

$$V^a_{\mathrm{Coul},\ell=0}(k,k') = 2\pi e^2 a^2 \sum_{n=0}^{\infty} (2n+1)\, j_n^2\left(\frac{ak}{2}\right)\, j_n^2\left(\frac{ak'}{2}\right). \tag{5.70}$$

This corresponds to our usual separable form with the definitions ($\alpha = n+1$)

$$\lambda_{\alpha\beta} = \delta_{\alpha\beta}\,(2\alpha-1)\, e^2 a^2, \tag{5.71}$$

$$g_\alpha(k) = \sqrt{2\pi}\, j_{\alpha-1}^2\left(\frac{ak}{2}\right). \tag{5.72}$$

[1] Numerically tested, proof pending.

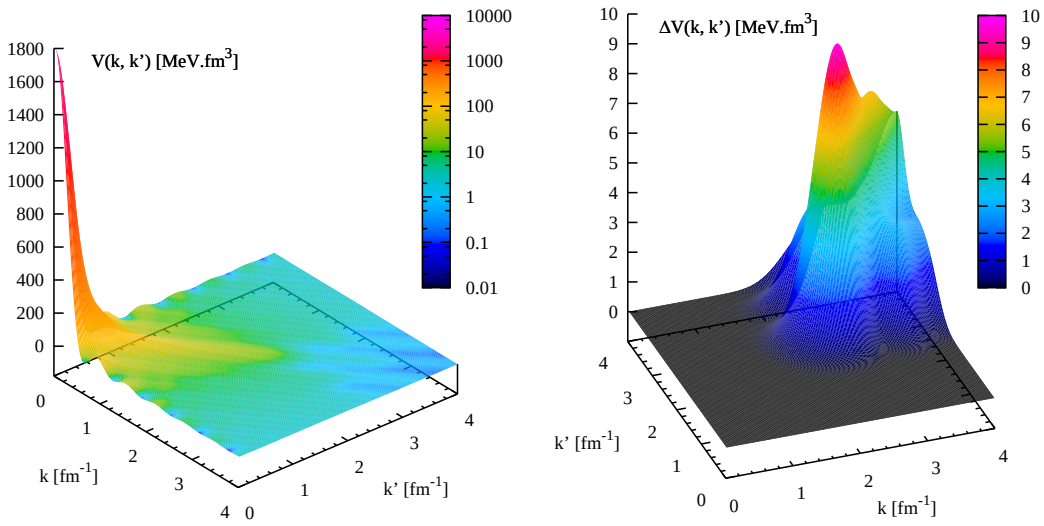

Figure 5.4: Left panel: S-wave matrix elements of the separable Coulomb potential with $a = 10$ fm, $N_{\mathrm{Coul}} = 10$. Right panel: Difference between the exact range-truncated Coulomb potential and the latter finite separable expression.

Truncating the sum in Eq. (5.70) to the first N_{Coul} terms yields a separable potential reproducing the physics of the Coulomb interaction, which can be added to the hadronic terms and poses no challenge for its implementation in the method outlined in section 5.2.2.

S-wave matrix elements of such a potential with $a = 10$ fm and $N_{\mathrm{Coul}} = 10$ are plotted on Fig. 5.4, along with matrix elements substracted through truncation of the sum in Eq. (5.70). It is striking that, once the singularity at $k = k'$ has been regularized by discarding the long-range part, the largest matrix elements occur near $k = k' = 0$. The sum-truncation error only involves matrix elements acting between high-momentum states, which are small anyway (notice the different scales between panels of Fig. 5.4, and recall that hadronic matrix elements are typically of the order of hundreds of MeV.fm^3.) Bessel functions $j_n(x)$ having, for sufficiently large n, significant values only for $x \gtrsim n$, one can guarantee that neglected terms only contribute to matrix elements at $k, k' \gtrsim 2n/a$, which evaluates to 2 fm^{-1} for $n = a/\mathrm{fm}$ (this is different from the decimation of high-momentum matrix elements performed by the $V_{\mathrm{low}\ k}$ RG evolution, which affects regions with k *or* k' greater than Λ). The assumptions leading to this approximate form of the Coulomb potential in the S-wave are thus well motivated. They are, moreover, easily controllable by varying truncation parameters.

Chapter 6

NN Pairing: Bare Force at First Order

In this chapter we present the results of the calculations performed with the functional presented in section 5.2, the representation of the bare NN vertex at the origin of the pairing part of the functional being described in section 5.3.

The method of solving the HFB-like equations that we use is efficient enough to perform systematic calculations of large sets of spherical nuclei across the mass table on single-CPU systems. We take advantage of this feature to investigate trends with mass, isospin and major single-particle shells, beyond the "local" comparisons which can be made with a single calculation. Indeed, it is clear that in most nuclei, the single-particle spectrum determined by the effective s.p. potentials, themselves derived from the particle-hole part of the functional, only matches gross features of experimental s.p. energies (see chapter 4). Since pairing-related observables depend on the level density next to the Fermi energy, notably on the magnitude of a subshell gap if present, a direct comparison with experimental data in a single nucleus can be prone to a model-dependent bias. However, we expect such issues to be less critical when computing a sufficiently large and dispersed set of nuclei, since then, besides local fluctuations of pairing gaps, global trends shall depend on the *average* density of single-particle energies only.

Results presented in this section have been obtained by performing HFB calculations in spherical symmetry with the functional SLy4 [Cha98] in the particle-hole channel. For our purpose, the essential feature of the latter is its isoscalar effective mass, $m^*/m = 0.7$ at saturation density, which is entirely generated by the nonlocality of the particle-hole potential and thus corresponds to a k-mass. This value is consistent with k-mass values obtained from BHF calculations [Jeu76, Dal05b] at the Fermi level in symmetric nuclear matter at saturation density. The Skyrme effective mass, contrary to the microscopic case, is momentum-independent, i.e. the non-locality of the potential acts on the whole spectrum, whereas it is physically meaningful only around the Fermi level. This implies that only the spectrum close to the Fermi level should be probed in a scheme building correlations on top of the independent-particle picture, which is one of the characteristics of the Skyrme functional which confine it to low-energy physics. As a result, the $V_{\mathrm{low}\ k}$ NN interaction is well suited for the application we envision.

The HFB equations were discretized on a set of spherical Bessel functions (see appendix G), which allows for an efficient treatment of separable finite-range and

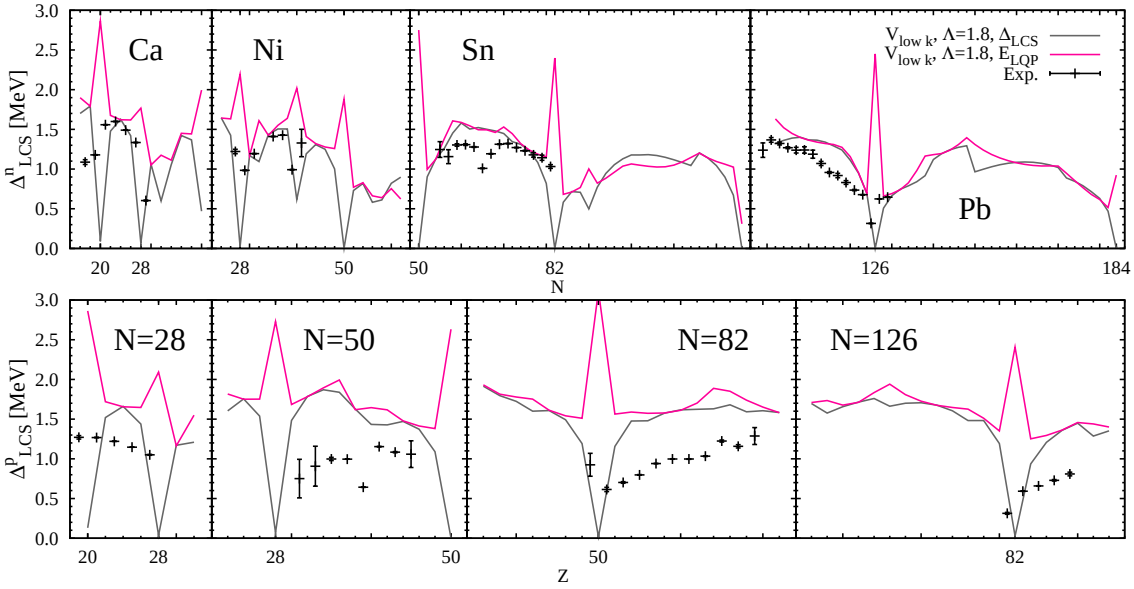

Figure 6.1: Lowest Canonical State (LCS) gaps and Lowest QuasiParticle energies. Top panel: neutron gaps, bottom panel: proton gaps.

non-local potentials in the pairing channel (see appendix F).

6.1 First results

One of the questions we would like to address is the proportion of the total pairing gap which is due to the first-order contribution ("direct term") of the nucleon-nucleon interaction.

We use, as a measure of experimental pairing gaps, the quantity $\Delta_q^{(3)}(N,Z)$, Eq. (5.19), with odd values of the particle number of the species in consideration. As is reviewed in some detail in chapter 5, this gives a good estimate of the pure pairing contribution to odd-even staggering, i.e. the lowest quasiparticle energy. This energy is itself approximately equal, in the case of strong pairing and tightly-spaced single-particle levels (which reduces the s.p.e. contribution ε_k to the quasiparticle energy) to the pairing gap Δ_k, where k corresponds to the index of the lowest quasiparticle. For each nucleus and each nucleon species, we call $E_{\rm LQP}$ the lowest quasiparticle energy and $\Delta_{\rm LCS}$ the pairing potential matrix element of the *canonical* state with the lowest quasiparticle energy. We use the canonical basis in this case, since we found the usual way to compute the quasiparticle pairing gap [Ben05] to yield, on some occasions, dubious values. Although this reminds somewhat of a BCS approximation, we should stress that the values presented below come from full HFB calculations.

Fig. 6.1 displays values of $E_{\rm LQP}$ and $\Delta_{\rm LCS}$ computed with the neutron-neutron part (used in both neutron and proton pairing channels) of the separable $V_{\text{low } k}$ with $\Lambda = 1.8$ fm^{-1}, built starting from the Argonne v_{18} potential. This is the softest charge-symmetric pairing interaction of our set. The computations were performed for all major magic isotopic and isotonic chains, between proton and neutron drip lines. In this case, the HFB equations were solved in a box of 24 fm radius, with a mesh step of 0.3 fm and a momentum cut-off in the Bessel s.p. basis $k_{\rm cut} = 4.0$ fm^{-1},

which describes single-particle states up to about 300 MeV.

The evolution of lowest-quasiparticle energies and LCS gaps show characteristic patterns around magic nuclei, where $\Delta_{\rm LCS}$ collapses due to the depletion of the spectrum around the Fermi level while $E_{\rm LQP}$ rises to a value corresponding to half the single-particle shell gap. Equality (approximately) of the two quantities indicates that the chemical potential lies in a densely-packed set of s.p. levels, which minimizes the $\overline{\varepsilon}_k$ contribution to $E_{\rm LQP}$. This is the case where a static SR-EDF description is the safest.

As expected from the expression of a BCS quasiparticle energy, we have $\Delta_{\rm LCS} < E_{\rm LQP}$ for most nuclei. Notable exceptions are the neutron-rich sides of tin and lead chains, where an inversion occurs. This is a signature of the mixing of different s.p. orbitals by the HFB pairing field, which allows to lower the first quasiparticle energy below the corresponding canonical quasiparticle-equivalent energy, which is allowed because of the larger variational space explored by HFB equations compared to the BCS gap equation. The fact that this signature mainly occurs in regions approaching the neutron drip line confirms the importance of solving the full HFB problem for nuclei where the chemical potential lies just beneath the scattering continuum [Dob84].

Fig. 6.1 also shows experimental values of the gaps, where available. The method we have chosen to extract the latter yields data with a general behavior similar to that of $\Delta_{\rm LCS}$, which allows for a meaningful comparison . Around shell closures, though, theoretical gaps increase more slowly away from magic particle numbers than data, resulting in lower theoretical gaps in these regions. It is known that particle-number projection, or an approximate variant thereof such as the Lipkin-Nogami method, increase gaps near shell closures. We can thus blame the pairing scheme on this inaccuracy. Although the exact shape of the gap curves does not match the data perfectly, the magnitude of theoretical and experimental pairing gaps is clearly similar in the case of neutrons. Calcium and nickel chains are especially well reproduced, probably owing to the simplicity of the underlying single-particle spectrum. Tin and lead chains, on the other hand, exhibit features in the data which are absent from the calculation. A depletion of gaps around $N = 65$ in tin, for example, suggests the existence of a sub-shell closure not predicted as large by SLy4. In lead isotopes, the decrease before $N = 126$ is steeper in the calculated gaps, which suggests a level density which is too high in the corresponding sub-shell. The latter is consistent with the $\nu 1i_{13/2}$ level lying too high in the s.p. spectrum (see chapter 4). Again, except these local defects, which can be rather directly related to the s.p. structure produced by the functional SLy4, the global magnitude of the theoretical neutron pairing gaps matches that of the experimental ones very well.

The case of protons is different. We see a general over-estimation of proton gaps by the calculation performed with a charge-symmetric pairing functional. In fact, calculated proton gaps are, in the heaviest isotonic chains, higher than neutron gaps calculated in neighboring magic isotopic chains, with values standing above 1.5 MeV for protons and between 1 and 1.5 MeV for neutrons. It is known that proton gaps are similar in magnitude, or marginally larger, than neutron ones in heavy nuclei [Nem62], yet the difference observed here clearly overestimates the one present in experimental data.

Given that our pairing functional is charge-symmetric, the charge asymmetry observed in the results may be traced back to the intrinsic properties of the un-

derlying NN vertex. Heavy nuclei globally exhibit a neutron excess. Save for a thin neutron skin, the spatial extension of neutron and proton distributions in these nuclei are similar, which implies that proton densities are lower than neutron ones. Consequently, the effective Fermi momentum is also lower for protons than neutrons, or, more accurately, momentum-space density distributions corresponding to states close to the chemical potential are peaked at lower momenta. As a result, the proton pairing tensor probes more attractive matrix elements of the NN interaction than the neutron one, which potentially explains the observed difference. The same effect can be invoked for the neutron-excess-dependence of gaps: neutron $\Delta_{\rm LCS}$ values decrease noticeably with N for all four chains present on Fig. 6.1, due to the increase of the neutron density and effective Fermi momentum with N. Proton gaps exhibit a less marked decrease with Z, the difference being probably attributable to the centrifugal effect due to the curvature of the particle-hole Coulomb field.

Agreement with experiment of calculated neutron and proton gaps is very uneven. We can thus question the validity of using an charge-symmetric pairing functional in our approach. Improving the latter aspect is the matter of the following section.

6.2 Charge symmetry and Coulomb interaction

Charge-symmetry breaking (CSB) in the nucleon-nucleon interaction has two distinct origins: the most obvious one is the electromagnetic interaction, which produces the principal contribution to CSB as the Coulomb interaction between protons. However, the term CSB is usually used to refer to the hadronic part of the NN interaction, which breaks this symmetry in a more subtle way, being just slightly less attractive between protons than between neutrons.

We have performed four sets of calculations of the same nuclei as in the previous section. Keeping the functional SLy4 in the particle-hole channel, we used different potentials in the particle-particle channel: (i) a charge-symmetric separable $V_{{\rm low}\ k}$, generated starting from the neutron-neutron part of the Argonne v_{18} potential, with $\Lambda = 2.5\ {\rm fm}^{-1}$, (ii) a CSB separable potential with neutron-neutron and hadronic proton-proton terms generated separately from the corresponding matrix elements of $V_{{\rm low}\ k}$ built with the same parameters, (iii) A separable $V_{{\rm low}\ k}$ potential which is charge-symmetric except for the addition of a separable truncated Coulomb term (with 16 terms and a truncation range $a = 16$ fm; see section 5.3.3), (iv) A separable $V_{{\rm low}\ k}$ potential incorporating both nuclear CSB and Coulomb. Discretization parameters were otherwise kept from the previous calculation.

Our method for dealing with the electromagnetic part of the proton-proton interaction consists in replacing it with a separable expansion of the ${}^1S_0$ part of a range-truncated Coulomb potential. Several approximations are thus involved.

First, we neglect the finite size of the proton, which modifies the short-range part of the electromagnetic potential. Although, due to the relatively small extension of the nucleon Cooper pair wave function, the effect could be expected to be larger than in the case of the Hartree term in the particle-hole channel, this only affects the innermost 1 fm and can thus be considered a higher-order correction. The same comments apply to the neglected higher-order quantum field theory and nucleon structure effects (such as magnetic moments) beyond simple one-photon exchange.

Second, neglecting higher partial waves is potentially worse for a long-range

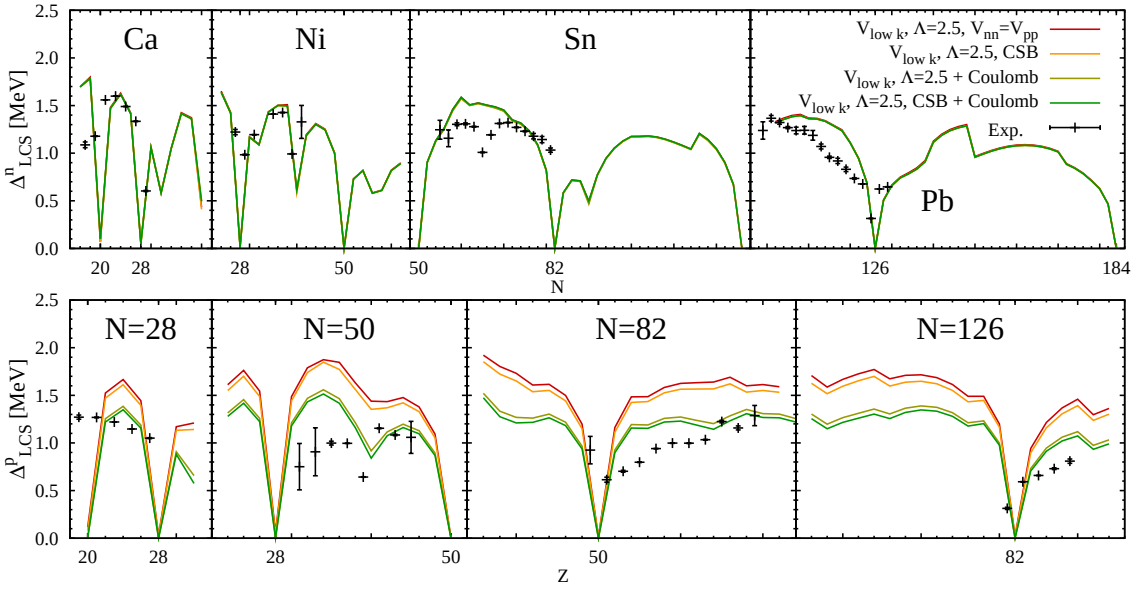

Figure 6.2: LCS gaps with charge-symmetric $V_{\text{low } k}$, charge-symmetry breaking (CSB) included in the nuclear part of the interaction and the Coulomb interaction included (see key). The neutron-neutron pairing vertex is the same in all cases, the corresponding curve is given for reference.

interaction than a short-range one. Indeed, the coordinate-space pair tensor does contain such components, due to the finite size of the nucleus and despite the use of a pure $^1S_0$ pairing interaction, and these components are peaked at larger relative separations than the S-wave one. We do not expect this concern to be essential for the following discussion, but it would have to be checked more accurately if one aimed at high precision results.

Third, we take the electromagnetic part into account by adding an approximate Coulomb potential directly to the $V_{\text{low } k}$ interaction without taking into account the modification of the former through the RG evolution. As explained in section 5.3.3, the Coulomb interaction is most important for its long-range part, which yields large matrix elements for very low momenta. Its contribution to matrix elements beyond $k = 2$ fm^{-1} is minimal and can be expected not to alter the RG evolution and the resulting $V_{\text{low } k}$ potential. Moreover, the matrix elements remaining beyond the RG cutoff are negligible for all practical purposes.

Fourth, we use the separable approximation described in section 5.3.3. The accuracy of this approximation is the easiest to assess by performing a benchmark calculation with higher values of the corresponding parameters (truncation range a and number of terms N_{Coul}). With respect to the latter, we have checked that diagonal pairing matrix elements were converged to better than 100 eV.

Pairing gaps resulting from calculations with functionals (i)-(iv) are displayed on Fig. 6.2. The global effect of CSB and the Coulomb interaction of proton gaps can be assessed quickly, since, as we could have expected, they are clearly of very different magnitudes. Whereas hadronic CSB only produces a slight shift of gap curves, Coulomb decreases Δ_{LCS} values by 20 to 30% of their original value. In this case, the magnitude of proton gaps is either well reproduced ($N = 28$ chain, $N = 50$ chain above Zirconium, proton-rich end of $N = 82$) or slightly overestimated ($N = 50$ below Zirconium, $N = 82$ next to the $_{50}$Sn shell closure and $N = 126$).

The global agreement is comparable to the one oberved for neutron gaps. In N=50 isotones, the relative magnitude of gaps below and above $Z = 40$ is not captured. This hints that level spacings predicted by SLy4 in this region are inappropriate, the position of the $1g_{9/2}$ state being too high.

We are aware of only one other systematic HFB calculation including the Coulomb interaction in the proton pairing channel. It was performed by the Madrid group [Ang01a] with the Gogny D1 and D1S effective interactions, in a triaxial harmonic-oscillator basis. Although no explicit study has been made of pairing gaps in this work, it was found that pairing energies were reduced by 30 to as much as 60% (for semi-magic ^{90}Zr) when including the Coulomb pairing term self-consistently in the variational procedure. Lowest two-quasiproton energies, which are the most relevant quantities of this work to be directly compared to pairing gaps, were reduced, in the same conditions, by 20 to 30% (see Fig. 1 and Tables 1 and 2 in Ref. [Ang01a]). The magnitude of the reduction of proton pairing observed in our results thus confirms observations of this previous work.

The apparent value of proton gaps would thus be explained by our study as the result of the cancellation of the effects of the hadronic component of the NN interaction, which is more attractive at the Fermi level, in heavier nuclei, in the case of protons than it is for neutrons, and the electromagnetic part, which, being strictly repulsive, yields lower pairing gaps when taken into account.

This reduction of pairing gaps due to the Coulomb interaction is large enough for its CSB effect to be systematically taken into consideration in HFB calculations. In particular, it fully validates using distinct values of neutron and proton pairing parameters (i.e. isospin dependence) in empirical models based on local pairing functionals [Gor06].

6.3 Effect of $V_{\mathrm{low}\ k}$ renormalization scale

The results we have presented to this point indicate that the magnitude of proton and neutron pairing gaps in the set of spherical nuclei in consideration can be explained by the interaction of nucleons at lowest order in the bare NN potential. This is at variance with results obtained previously through HFB calculations in ^{120}Sn using the SLy4 functional together with the Argonne v_{14} potential in the neutron particle-particle channel. In a first work, Barranco et al. [Bar04] obtained a pairing gap of ca. 700 keV. It was concluded that the bare NN interaction could not explain the magnitude of the experimental pairing gap, which is close to 1.3 MeV in this nucleus.

However, it should first be noted that this HFB calculation was performed using a set of single-particle orbitals and energies produced by a modified SLy4 parametrization of the Skyrme EDF (see reference/note 17 in Ref. [Bar04]). The reduction of the spin-orbit strength parameter by 15% reduces spin-orbit splittings by, roughly, the same ratio. More specifically, it significantly reduces the s.o. splitting of the $\nu 1h$ shell in ^{120}Sn, which results in the (experimentally spurious) gap between the $\nu 3s_{1/2}$ and $\nu 2d_{3/2}$ levels on the one hand, and the $\nu 1h_{11/2}$ level on the other hand, to be increased by 1 MeV. This creates, in fact, an important sub-shell closure in the neutron spectrum of the nucleus, which results in a partial suppression of pairing. Restoring the original SLy4 EDF yields a Δ_{LCS} gap slightly larger than 1 MeV [Pas08a, Pas08b]. In our calculation, with the Argonne v_{14} potential replaced with

a $V_{\mathrm{low}\,k}$ one evolved to a low renormalization scale $\Lambda = 1.8$ or $2.5\,\mathrm{fm}^{-1}$ we consistently find $\Delta_{\mathrm{LCS}} \simeq 1.45$ MeV. There remains, thus, to explain the difference of roughly 30 % seen between our calculation performed with $V_{\mathrm{low}\,k}$ and those using a hard-core potential.

In order to investigate this issue on a more systematic footing, we have repeated the previous calculations with $V_{\mathrm{low}\,k}$ interactions evolved to higher Λ values. Hadronic charge-symmetry breaking was neglected, being largely irrelevant for the present discussion, while the Coulomb interaction was included in all cases in the proton pairing channel. These interactions, since they couple low-energy degrees of freedom to higher-energy ones, require a larger basis to achieve convergence of the HFB equations in terms of the truncation of the latter. Barranco et al. [Bar04] used a HF basis cut off at a s.p. energy of 800 MeV, which corresponds, approximately, to $k_{\mathrm{cut}} = 6\,\mathrm{fm}^{-1}$ in the representation we use. We performed calculations with $V_{\mathrm{low}\,k}$ potentials generated from CD-Bonn [Mac01] with RG scales up to $8.0\,\mathrm{fm}^{-1}$, using bases truncated at k_{cut} values equal to $4\,\mathrm{fm}^{-1}$ for $\Lambda < 3\,\mathrm{fm}^{-1}$ or $\Lambda + 1.0\,\mathrm{fm}^{-1}$ for $\Lambda > 3\,\mathrm{fm}^{-1}$.

For another calculation, performed with our separable approximation to the Argonne v_{18} potential, k_{cut} was set to $12\,\mathrm{fm}^{-1}$, which yields s.p. state energies reaching 3.9 GeV. Indeed, in benchmark calculations of ^{120}Sn, we observed a rather slow convergence of gaps with k_{cut}, with a value of Δ_{LCS} varying by 76 keV between $k_{\mathrm{cut}} = 6$ and $8\,\mathrm{fm}^{-1}$. We finally obtained a LCS neutron gap of 925 keV in ^{120}Sn, which is about 100 keV smaller than results from Refs. [Pas08a, Pas08b].

To save computing time, we reduced the basis size for high-Λ forces by using smaller boxes, checking that no sizeable effect on the calculated gaps occurred near the valley of stability. The box radius R_{box} was thus reduced from 24 fm (CD-Bonn, $\Lambda = 1.8\,\mathrm{fm}^{-1}$) to 18 fm (CD-Bonn, $\Lambda = 8.0\,\mathrm{fm}^{-1}$) and down to 15 fm for Argonne v_{18}. Total CPU time for the calculation of the set of 176 nuclei presented in the figures of this chapter amounts to around 10 hours for the softest forces, up to 100 hours for Argonne v_{18} on a desktop computer.

Values of Δ_{LCS} obtained with the set of pairing functionals described above are plotted on Fig. 6.3. While the curves for $\Lambda = 1.8$, 2.5 and $3.0\,\mathrm{fm}^{-1}$ sit essentially on top of each other, gaps calculated for $\Lambda = 4.0\,\mathrm{fm}^{-1}$ are slightly lower, while the $V_{\mathrm{low}\,k}$ /CD-Bonn at $\Lambda = 8.0\,\mathrm{fm}^{-1}$ and v_{18} interactions yield gaps reduced, respectively, by ca. 10-20% and 30% with respect to the latter, indeed below experimental $\Delta^{(3)}_{\mathrm{odd}}$ data. The latter values apply to mid-shell nuclei with strong pairing, while gaps are depleted even more at sub-shell closures.

Fig. 6.4 displays local and non-local values of the neutron spin-singlet pair density in ^{120}Sn. The long-range behavior of this quantity has been analyzed in [Pil07], we shall thus focus on the short-range part. First, the local, or zero-range part (top-left panel) is strongly depleted when increasing Λ, i.e. going from softer to harder-core interactions. In the Argonne v_{18} case, the local pair density is almost completely suppressed. This suppression is, relatively to calculations employing low-Λ interactions, much stronger than the one observed for pairing matrix elements. In fact, an accurate understanding of the situation requires to look at non-local components, also plotted on Fig. 6.4. The quantity $\tilde{\rho}(\mathbf{R}, \mathbf{s})$ is, up to a normalization factor, the spin-singlet part of the Cooper pair wave function. Its $\mathbf{s} = 0$ components, i.e. the local part usually included in local pairing functionals, are thus linked with the probability amplitude of observing the paired nucleons in contact. It is therefore

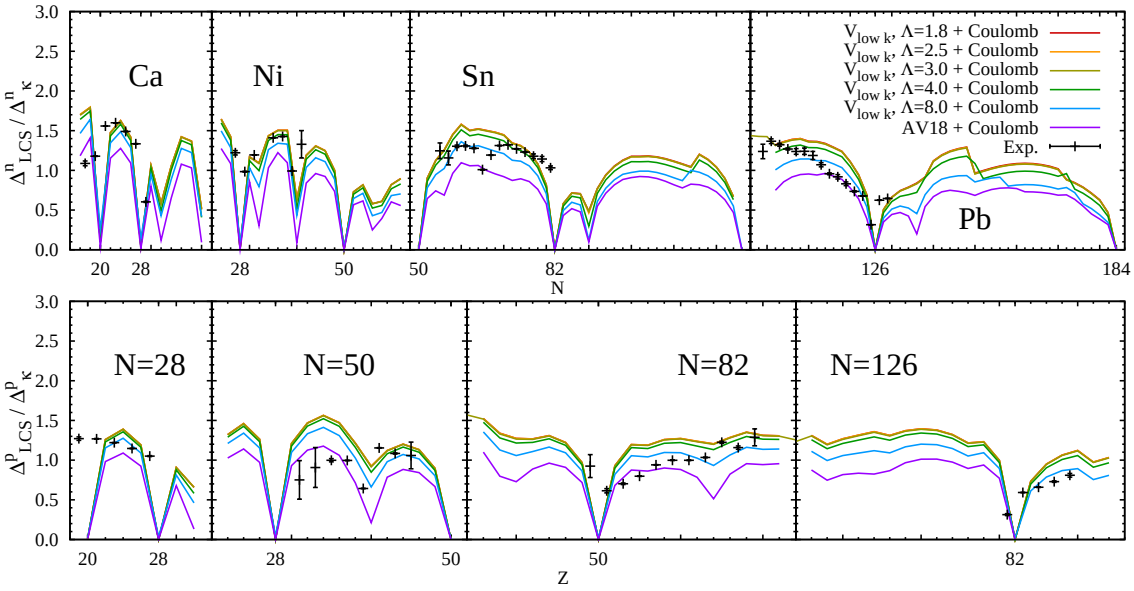

Figure 6.3: LCS gaps obtained with $V_{\text{low k}}$ interactions obtained from the CD-Bonn potential at various RG scales Λ and our separable representation of the Argonne v_{18} potential.

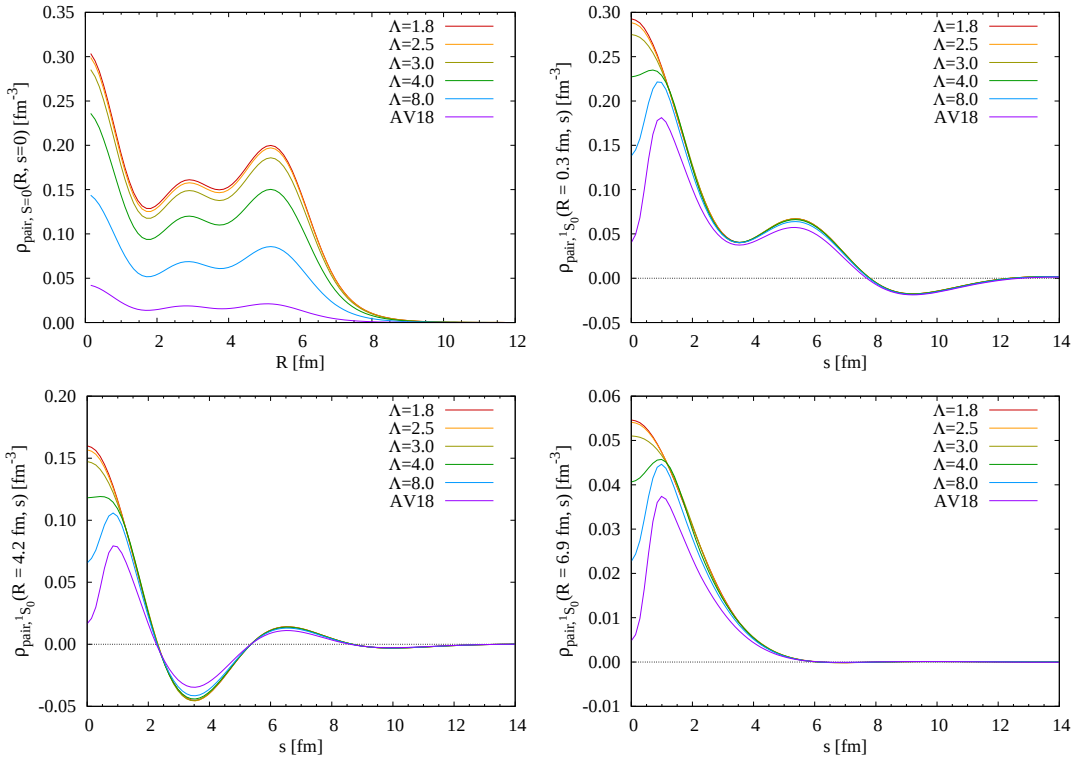

Figure 6.4: Pair density in ^{120}Sn. Top-left panel: local part. Other panels: non-local, $^1S_0$ part $\tilde{\rho}^{^1S_0}(R,s)$ with R fixed at 0.3, 4.2 and 6.9 fm.

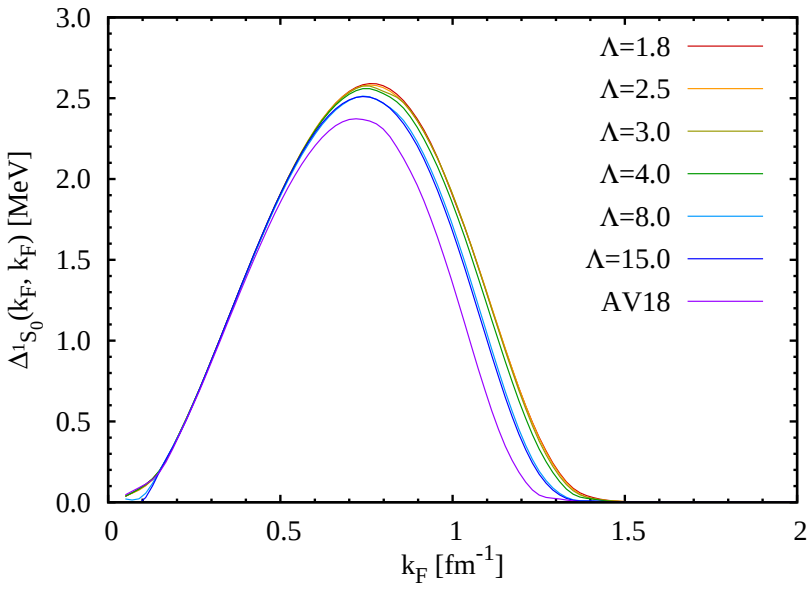

Figure 6.5: Neutron-neutron pairing gaps obtained at the Fermi level with the separable $V_{\text{low }k}$ /CD-Bonn interactions at indicated RG cutoffs, as well as the Argonne V18 potential, and a s.p. spectrum produced by the SLy4 Skyrme EDF in SNM.

no surprise that a hard-core interaction suppresses this amplitude.

The structure of the non-local part obtained with the various $V_{\text{low }k}$ interactions used differs mostly in the short-range region ($s < 1$ fm), where the gradual increase of Λ results in a depletion of $\tilde{\rho}(\mathbf{R}, \mathbf{s})$, including in the $\Lambda < 3$ fm^{-1} domain where gaps are Λ-independent. The long-range part is essentially unaffected for $\Lambda < 4$ fm^{-1} , whereas in the case of the hardest potentials, there also appears a reduction of $\tilde{\rho}(\mathbf{R}, \mathbf{s})$ in this region. Recalling the similar behavior of pairing gaps, one can conclude that their evolution with the "hardness" of the pairing interaction is correlated to the effect seen on the *long-range part* of the *non-local* pair density. It appears that at a certain point in the RG evolution, short-range physics integrated out by the RG equations interferes with long-range, low-energy physics, to which the observables we are interested in belong.

Given that the RG equations conserve two-body observables, this effect must be specific to the calculation we carried out and the underlying assumptions. We have seen that at the BCS level, no significant Λ-dependence occurred when using a free-particle spectrum. However, the case is different when self-energy effects are taken into account. Results displayed on Fig. 6.5 were obtained by performing a BCS calculation with the pairing interactions used on this section and a single-particle spectrum obtained from the SLy4 EDF in symmetric nuclear matter. We recall that this spectrum is determined by a constant effective mass given by

$$\frac{m^*}{m} = \left[1 + \frac{2m}{\hbar^2}\, C_0^\tau\, \rho_0\right]^{-1}, \qquad \rho_0 = \frac{2k_F^3}{3\pi^2}, \tag{6.1}$$

and independent from the particle's momentum. Thus, m^*/m decreases from 1 in the vacuum down to 0.7 at saturation density. With increasing k_F, values of $\Delta(k_F, k_F)$ are lowered more and more, for the $\Lambda = 8.0$ fm^{-1} $V_{\text{low }k}$ and Argonne v_{18},

when compared to low-Λ $V_{\mathrm{low}\,k}$ potentials. The amplitude of this reduction, taken at $k_F \sim 1.1$ fm^{-1} i.e. slightly below saturation density, corresponds for each of these interactions to the amplitude observed in nuclei. The CD-Bonn interaction evolved to $\Lambda = 15$ fm^{-1} yields results very similar to the one with $\Lambda = 8$ fm^{-1} , confirming that (reverse) RG evolution saturates at these cutoffs, which indicates that these interactions can be expected to yield results comparable to the bare CD-Bonn.

The only parameter which changes between Fig. 5.3 and Fig. 6.5 is the effective mass driving the s.p. spectrum. The observed reduction of pairing gaps must thus originate from the combination of this modification and the RG evolution of the potential eliminating high-momentum components. Indeed, whereas the RG evolution produces interactions yielding the same low-momentum gaps as a solution of the BCS gap equation solved with a kinetic spectrum, it is not the case with a low effective mass which reduces the density of states in the high-momentum sector of the s.p. spectrum, thus reducing their contribution to the pair density. Stated another way, the quasiparticle energy E_k entering the Δ_k/E_k factor increases, reducing the contribution of each state to the gap-equation integrand. With such a spectrum, the repulsive matrix elements coupling low- and high-momentum states, which are multiplied by negative gaps in the BCS gap equation, and thus give a positive contribution to the Fermi-level gap, see their contribution reduced.

Effective masses extracted from self-energies calculated at the (Dirac-)Brueckner-Hartree-Fock level with hard-core interactions such as CD-Bonn or Argonne v_{18} depend on the particle momentum. As seen, for example, from Fig. 3 in Ref. [Dal05b], they are actually larger at high k than at the Fermi level. It is thus possible that the pairing gaps calculated with hard-core interactions and SLy4 in nuclei underestimate values stemming from a more microscopic calculation (yet to be performed as of today) due to the trivial effective mass characterizing the Skyrme EDF. These results, as well as those of the Milan group concerning pairing gaps calculated with the bare Argonne v_{14}, should thus be taken with caution if one expects consistency with ab-initio theory.

It is not sure, yet, to what extent the low-Λ potentials are devoid of spurious effects from the neglected momentum and energy-dependence of self-energies, however they are potentially less affected by the effective-mass approximation due to working in a smaller model space where the spectrum density is reasonably under control. As stated at the beginning of this chapter, the quasi-local Skyrme functional allows to describe low-energy degrees of freedom and should not be expected to be predictive outside of this domain. We thus have more confidence in the results obtained with the $V_{\mathrm{low}\,k}$ potentials, where a certain consistency between resolution scales of the p-h and p-p functionals can be expected, than those stemming from hard-core ones. Beyond this qualitative argument, and short of a complete ab-initio calculation of self-energies in the finite nuclear medium, a thorough investigation would involve quantitatively validating in infinite matter the string of approximations leading to our calculation. This procedure is currently underway [Heb08], but beyond the present work.

6.4 Summary and outlook

The fact that the bare NN interaction, used in the pairing channel of a SR-EDF calculation, yields pairing gaps so close to values extracted from experimental masses

comes as a surprise, since it was expected from earlier works that effects beyond this first-order approximation to the pairing interaction kernel would yield significant contributions. At the present point it can not be completely excluded that this results from a cancellation of neglected effects, whose individual magnitude is hard to assess. Nevertheless, already at first order, a firm result that we have obtained is the significance of the reduction of proton gaps due to the Coulomb interaction, which is overall consistent with previous works [Ang01a].

Beyond that, several ingredients, in principle, are missing in this calculation.

First, our calculations are based on quasiparticle and effective-mass approximations. The implied re-summation of self-energy effects in the non-locality of the functional is not quantitatively under control. As already mentioned, this will be checked in detail.

Second, collective vibrations, in finite nuclei, are expected to enter as an attractive induced-interaction contribution due to the presence of surface modes [Gio02], which is the opposite of their effect in infinite matter where spin fluctuations dominate and bring a repulsive contribution [Gor05a]. To provide a clear picture of effects beyond the first order, a calculation should be made involving the description of collective modes using the same interaction as the one included at first order. Indeed, just as in the first-order case, a dependence on the renormalization scale may be encountered in this case. Such a calculation would be much more involved than the ones presented here, or even those of Refs. [Bar04, Pas08a] which employ quite a schematic model for the description of phonons.

Also, the three-nucleon force yields repulsive pairing matrix elements when included in the gap equation in nuclear matter. Its effect becomes sizeable principally for proton pairing in highly isospin-asymmetric matter [Bal07c], which may translate into a correction to proton gaps in nuclei near the neutron drip-line. Including it in our scheme is potentially achievable, by devising a separable representation of an in-medium vertex. The latter should sum a two-body interaction and a three-body one averaged over the third particle, calculated in infinite matter. The density-dependent separable representation would then be used with a local density approximation for the effective three-body part.

Finally, we have only considered the $^1S_0$ channel of the interaction. While this relative-motion state is clearly the main component of the Cooper pair wave function, the decoupling between partial waves which occurs in infinite matter may not be as complete in finite systems, resulting in the admixture of higher partial-wave components to the pair density. Such components, through the corresponding matrix elements of the interaction, which have been neglected here, will yield a contribution to the pairing energy and gaps. Including these components in our framework is part of our plans for the future.

As already stated, systematic calculations are desirable in studies of pairing due to the sensitivity of the latter to non-controlled details of single-particle spectra. The present work has been limited, due to technical constraints linked with the use of a non-local interaction, to spherical nuclei. However, it would be interesting to investigate the interplay between pairing and deformation in such a microscopic scheme and across the nuclear chart, in order to see, for example, if the distribution of gaps mentioned in section 5.1.2 can be reproduced. This would require a model of the NN interaction tractable in deformed calculations, either as a local pairing functional or the parametrization of a Brink-Boeker-type potential which could be

used as an input to a Gogny-HFB code. Work along the lines of the latter case is in progress, the main difficulty being the non-locality of the interaction [Rot08b].

Whereas we have focused on pairing gaps in this study, being mainly concerned by the origin of nuclear pairing and by providing a benchmark for the construction of future pairing functionals, other observables of interest will be studied in the near future, starting with a comparison of binding energies obtained with various pairing schemes. Quasiparticle spectra will be checked for state-dependent effects linked with the range of the interaction, among others.

Above all, we intend to undertake a systematic comparison of local and quasi-local pairing functionals. The range in mass and isospin of the nuclei for which we were able to perform ab-initio calculations and produce theoretical pseudo-data will be a key asset in devising a non-empirical, but local pairing functionals. The fact that our results are compatible with experiment allows to expect direct fits of such functionals, or a derivation through density-matrix expansion, to yield pairing models with more sound predictive power than current empirical ones. Again, this does not prevent us from checking the exact origin of this agreement by more sophisticated calculations.

Chapter 7

Conclusion

Nuclear energy density functional models based on Skyrme effective interactions and quasi-local functionals are undergoing a deep revision. We have participated in this process, aiming at a better connection with current knowledge of experimental data, microscopic interactions and ab-initio calculations. Our envisioned long-term goal is an improvement of the predictive power of this model and the construction of a functional accurately describing all known and relevant nuclear observables while having a solid formal, experimental and theoretical motivation, making it reliable in extrapolations to exotic nuclear systems. In this work we have studied several paths to an improved predictive power and given some new (or revised) constraints to be used in the construction of future density-functional parametrizations.

Although particular attention has been paid in the last decade to the properties of nuclear energy density functional models with respect to isospin, the spin-isospin structure of local nuclear functionals is not yet fully under control when deriving the latter from a Skyrme effective interaction. We have shown, moreover, that various aspects of this problem, namely the spin-isospin content of the nuclear matter equation of state and the behavior of nucleon effective masses with isospin, could not be put in agreement with predictions of ab-initio many-body theory at the same time. This points to deficiencies of a fifty-year-old model which, despite having known considerable success in several aspects of nuclear structure, remains rather schematic. We also have pointed out the necessity to fully understand and control the stability of the functional, i.e. its very ability to yield predictions at all ! We take this as an example of the amount of attention which must be paid to details of effective models. However, we also showed the potential of using methods generally employed *a posteriori*, with the intent to obtain physical predictions, in the construction and analysis of a functional. Such is the case of RPA response functions, which give an efficient, if not straightforward way, to ensure the consistency of ground states and excitation spectra of nuclei.

The inaccuracies observed in the individual and collective spectroscopy predicted by SR- or MR-EDF calculations using Skyrme functionals have been largely attributed to the lack of a tensor interaction in the underlying interaction, or equivalently to the lack of attention paid to the quadratic spin-current couplings of the functional. By performing a systematic exploration of the corresponding parameter space, including a systematic refit of the functional to basic physical constraints, we have emphasized the role of the "tensor terms" and devised constraints for them. We found again that the Skyrme energy functional was limited in terms of the con-

trol it allowed on the observables under consideration, such as spin-orbit splittings and binding energies of magic calcium and nickel isotopes, or single-particle spectra and their evolution along isotopic chains. It was found that the various constraints on Skyrme EDF parametrizations could not be simultaneously satisfied with the available parameters.

Therefore, our approach consisted in disentangling as much as possible the effect of the tensor terms from other parameters and finding the most model-independent possible constraint. Admittedly, the result was non-optimal with respect to even simple criteria. We concluded that new terms and parameters had to be found to control the position of spin-orbit doublet centroids, the state- and isospin-dependence of spin-orbit splittings, to name a few.

The fact that the Skyrme functional has to be extended and generalized to become really predictive starts to be routinely mentioned in research papers. The question then becomes, what term to add ? In an scheme based on an effective interaction, adding density-dependence to non-local terms, including the term proportional to t_2 acting in the P-wave, would allow to decouple spin-isospin properties from the equation of state and effective mass parameters, while conserving antisymmetry of the nuclear part of the functional. An extended spin-orbit part of the functional also seems necessary to gain control over spin-orbit splittings.

It is likely, however, that systematic investigations will develop. Investigating the relevance of the parameters of an extended functional with respect to the reproduction of available data, aided by rigorous analysis techniques such as singular value decomposition [Kor08] seems promising. So does density matrix expansion applied to an effective vertex deduced from low-momentum interactions [Neg72, Bog08c].

The pairing part added to quasi-local particle-hole nuclear functionals has been largely phenomenological until now. We showed that low-momentum nucleon-nucleon interactions, as well as any force amenable to a separable approximation, could be used in an efficient way in the pairing channel of Skyrme-EDF calculations. We thus performed, for the first time, systematic calculations of pairing gaps using the bare nucleon-nucleon force as a pairing interaction, also exhibiting the importance of the Coulomb interaction. The results came surprisingly close to experiment for a first step. A more thorough study of self-energy effects, partial waves different from $^1S_0$ and the three-body force will either show that these contributions cancel out or demonstrate that yet another ingredient is missing. One will then have to include many-body effects in the pairing interaction itself, in a scheme to be defined.

There remains to study other observables, such as masses and density distributions, and to use the large amount of theoretical data generated to build a microscopic local or quasi-local pairing functional. The latter shall be essential for reliably calculating properties of deformed and odd nuclei far from the valley of stability. Note however that as long as one keeps spherical symmetry, our method is about as efficient as a local pairing functional, which might allow to envision MR-EDF calculations for the study of pair vibrations or pair transfer reactions.

Looking back at this manuscript, the work presented therein may seem unfinished. Indeed, we have started exploring different directions leading to an increased predictive power for nuclear energy density functionals. We have utilized phenomenology, and systematic comparison with data, but also microscopic inputs. These aspects are both essential. A predictive functional first has to reproduce known observables before allowing for extrapolation into uncharted territory. On

the other hand, reliable extrapolations can hardly be achieved without a firm connection of the model with underlying physics. Only by combining these aspects can we expect to build a truly universal nuclear energy density functional.

Appendix

Appendix A

Coupling constants of the Skyrme energy functional

The coupling constants of the central Skyrme energy density functional in terms of the parameters of the central Skyrme force are given by

$$\begin{aligned}
A_0^\rho &= \tfrac{3}{8}t_0 + \tfrac{3}{48}t_3\,\rho_0^\gamma(\mathbf{r}) + \tfrac{3}{48}t_6\,\rho_0^{\gamma'}(\mathbf{r}) \\
A_1^\rho &= -\tfrac{1}{4}t_0\big(\tfrac{1}{2}+x_0\big) - \tfrac{1}{24}t_3\big(\tfrac{1}{2}+x_3\big)\,\rho_0^\gamma(\mathbf{r}) - \tfrac{1}{24}t_6\big(\tfrac{1}{2}+x_6\big)\,\rho_0^{\gamma'}(\mathbf{r}) \\
A_0^s &= -\tfrac{1}{4}t_0\big(\tfrac{1}{2}-x_0\big) - \tfrac{1}{24}t_3\big(\tfrac{1}{2}-x_3\big)\,\rho_0^\gamma(\mathbf{r}) - \tfrac{1}{24}t_6\big(\tfrac{1}{2}-x_6\big)\,\rho_0^{\gamma'}(\mathbf{r}) \\
A_1^s &= -\tfrac{1}{8}t_0 - \tfrac{1}{48}t_3\,\rho_0^\gamma(\mathbf{r}) - \tfrac{1}{48}t_6\,\rho_0^{\gamma'}(\mathbf{r}) \\
A_0^\tau &= \tfrac{3}{16}\,t_1 + \tfrac{1}{4}t_2\,\big(\tfrac{5}{4}+x_2\big) \\
A_1^\tau &= -\tfrac{1}{8}t_1\big(\tfrac{1}{2}+x_1\big) + \tfrac{1}{8}t_2\big(\tfrac{1}{2}+x_2\big) \\
A_0^T &= -\tfrac{1}{8}t_1\big(\tfrac{1}{2}-x_1\big) + \tfrac{1}{8}t_2\big(\tfrac{1}{2}+x_2\big) \\
A_1^T &= -\tfrac{1}{16}t_1 + \tfrac{1}{16}t_2 \\
A_0^{\Delta\rho} &= -\tfrac{9}{64}t_1 + \tfrac{1}{16}t_2\big(\tfrac{5}{4}+x_2\big) \\
A_1^{\Delta\rho} &= \tfrac{3}{32}t_1\big(\tfrac{1}{2}+x_1\big) + \tfrac{1}{32}t_2\big(\tfrac{1}{2}+x_2\big) \\
A_0^{\Delta s} &= \tfrac{3}{32}t_1\big(\tfrac{1}{2}-x_1\big) + \tfrac{1}{32}t_2\big(\tfrac{1}{2}+x_2\big) \\
A_1^{\Delta s} &= \tfrac{3}{64}t_1 + \tfrac{1}{64}t_2\,.
\end{aligned} \tag{A.1}$$

The coupling constants of the spin-orbit energy density functional in terms of the parameters of the spin-orbit force are given by

$$A_0^{\nabla J} = -\tfrac{3}{4}W_0\,, \qquad A_1^{\nabla J} = -\tfrac{1}{4}W_0\,. \tag{A.2}$$

The coupling constants of the tensor energy density functional in terms of the parameters of Skyrme's tensor force are given by (Table I in [Per04])

$$B_0^T = -\tfrac{1}{8}(t_e+3t_o) \qquad B_1^T = \tfrac{1}{8}(t_e-t_o) \tag{A.3}$$

$$B_0^F = \tfrac{3}{8}(t_e+3t_o) \qquad B_1^F = -\tfrac{3}{8}(t_e-t_o) \tag{A.4}$$

$$B_0^{\Delta s} = \tfrac{3}{32}(t_e-t_o) \qquad B_1^{\Delta s} = -\tfrac{1}{32}(3t_e+t_o) \tag{A.5}$$

$$B_0^{\nabla s} = \tfrac{9}{32}(t_e-t_o) \qquad B_1^{\nabla s} = -\tfrac{3}{32}(3t_e+t_o)\,. \tag{A.6}$$

Skyrme interaction parameters used in Chapters 3 and 4 are given in Table A.1. Tensor-interaction parameters are given in terms of U and V parameters. For use in the above formulae, we recall that $T = 3t_e$ and $U = 3t_o$.

Table A.1: Values of the Skyrme-interaction parameters for fits performed and used in this manuscript. Omitted values are zero.

Name	t_0	t_1	t_2	t_3	t_6
	x_0	x_1	x_2	x_3	x_6
	W_0	T	U	γ	γ'
f$_-$	-1847.562	477.387	-495.987	14003.89	-4302.16
	0.821426	-0.393945	-0.971838	1.792787	2.622989
	133.187			1/3	2/3
f$_0$	-1849.082	477.277	-412.825	14035.19	-4331.24
	0.824349	-0.137469	-0.915580	1.780474	3.295755
	129.190			1/3	2/3
f$_+$	-1849.486	478.078	-324.437	14050.84	-4351.54
	0.826648	0.085961	-0.821841	1.770010	3.932000
	127.855			1/3	2/3
T11	-2484.690	480.674	-522.233	13785.81	
	0.734532	-0.357956	-0.981127	1.195657	
	103.738	86.322	-114.259	1/6	
T12	-2482.571	480.605	-523.692	13762.34	
	0.741577	-0.357895	-0.984520	1.208913	
	112.506	38.788	-66.072	1/6	
T13	-2481.315	480.343	-531.133	13749.16	
	0.741208	-0.346965	-0.989822	1.209875	
	120.411	-6.946	-17.241	1/6	
T14	-2479.458	479.870	-530.397	13732.47	
	0.744308	-0.348138	-0.990900	1.215762	
	128.506	-55.122	30.824	1/6	
T15	-2482.479	478.923	-317.302	13764.91	
	0.733926	-0.677015	-0.813783	1.196671	
	136.554	-166.980	57.775	1/6	
T16	-2485.640	481.672	-316.779	13791.07	
	0.736004	-0.680207	-0.805749	1.198185	
	144.925	-215.394	104.916	1/6	
T21	-2486.267	484.633	-445.880	13807.35	
	0.721464	-0.480492	-0.924422	1.173067	
	115.277	158.983	-123.119	1/6	
T22	-2484.397	484.495	-471.454	13786.97	
	0.730120	-0.442635	-0.944655	1.188194	
	123.225	118.685	-72.504	1/6	
T23	-2483.501	484.291	-440.089	13776.29	
	0.732464	-0.492071	-0.924856	1.193100	
	131.435	61.309	-27.567	1/6	
T24	-2482.931	484.346	-433.185	13768.56	
	0.729639	-0.503889	-0.921044	1.190192	
	139.272	11.246	19.739	1/6	

Table A.1: Skyrme interaction parameters (continued).

Name	t_0	t_1	t_2	t_3	t_6
	x_0	x_1	x_2	x_3	x_6
	W_0	T	U	γ	γ'
T25	-2480.434	485.519	-478.822	13735.27	
	0.754456	-0.439566	-0.956135	1.231884	
	147.887	-23.126	72.006	1/6	
T26	-2476.673	484.490	-482.591	13699.04	
	0.767612	-0.434554	-0.962725	1.254753	
	156.146	-69.885	120.698	1/6	
T31	-2486.963	490.158	-418.307	13808.78	
	0.724547	-0.532406	-0.894940	1.178613	
	126.989	246.186	-127.507	1/6	
T32	-2486.155	489.073	-438.565	13804.97	
	0.712439	-0.499144	-0.912063	1.160360	
	133.590	204.352	-77.176	1/6	
T33	-2486.688	489.683	-405.609	13804.20	
	0.728149	-0.551901	-0.885872	1.184753	
	142.019	146.435	-32.623	1/6	
T34	-2485.496	488.412	-351.129	13799.05	
	0.716858	-0.632712	-0.829737	1.167295	
	149.734	82.186	10.278	1/6	
T35	-2483.136	490.586	-377.114	13762.06	
	0.740390	-0.601400	-0.863924	1.208476	
	158.994	41.846	60.306	1/6	
T36	-2478.946	488.365	-427.188	13729.53	
	0.752195	-0.522097	-0.912891	1.227180	
	166.212	9.055	113.945	1/6	
T41	-2492.261	494.721	-262.766	13874.45	
	0.689383	-0.767147	-0.653878	1.117874	
	138.146	294.978	-144.519	1/6	
T42	-2492.153	494.635	-251.272	13869.06	
	0.690625	-0.785802	-0.630399	1.121129	
	145.089	243.562	-97.619	1/6	
T42	-2492.150	494.635	-251.272	13869.06	
	0.690625	-0.785802	-0.630399	1.121129	
	145.089	243.562	-97.619	1/6	
T42	-2492.150	494.635	-251.272	13869.06	
	0.690625	-0.785802	-0.630399	1.121129	
	145.089	243.562	-97.619	1/6	
T43	-2490.275	494.608	-255.534	13847.12	
	0.698702	-0.781655	-0.646302	1.135795	
	153.103	196.868	-49.160	1/6	
T44	-2485.670	494.477	-337.961	13794.75	
	0.721557	-0.661848	-0.803184	1.175908	
	161.367	173.661	7.174	1/6	

Table A.1: Skyrme interaction parameters (continued).

Name	t_0	t_1	t_2	t_3	t_6
	x_0	x_1	x_2	x_3	x_6
	W_0	T	U	γ	γ'
T45	-2485.014	492.671	-304.046	13793.28	
	0.727016	-0.710368	-0.755428	1.182969	
	168.213	115.642	52.299	1/6	
T46	-2484.405	495.225	-356.435	13769.07	
	0.735176	-0.639443	-0.833399	1.201318	
	176.279	83.204	104.873	1/6	
T51	-2492.672	500.414	-272.332	13871.38	
	0.691985	-0.760015	-0.663662	1.123486	
	148.934	393.316	-145.233	1/6	
T52	-2494.783	499.204	-141.125	13886.86	
	0.692186	-0.955937	-0.126512	1.123414	
	155.371	306.098	-109.968	1/6	
T53	-2486.978	499.333	-363.964	13807.83	
	0.719761	-0.627515	-0.823595	1.171935	
	163.931	324.972	-39.688	1/6	
T54	-2489.087	497.774	-248.404	13829.43	
	0.710724	-0.797929	-0.625993	1.156397	
	170.383	242.449	-2.787	1/6	
T55	-2487.084	497.823	-227.658	13815.23	
	0.711011	-0.829103	-0.567634	1.157022	
	179.006	188.196	43.100	1/6	
T56	-2484.179	497.603	-258.182	13775.24	
	0.725926	-0.788228	-0.661928	1.185298	
	185.960	149.446	94.289	1/6	
T61	-2494.625	501.033	-125.512	13895.88	
	0.683145	-0.977518	0.040183	1.107100	
	156.389	445.173	-160.136	1/6	
T62	-2495.048	499.981	-197.374	13901.24	
	0.690739	-0.868510	-0.431559	1.117413	
	162.688	418.830	-104.641	1/6	
T63	-2492.495	500.627	-121.265	13875.17	
	0.680914	-0.985108	0.076440	1.105776	
	171.897	347.945	-64.433	1/6	
T64	-2487.323	501.096	-284.539	13818.03	
	0.705320	-0.746420	-0.694782	1.148322	
	180.135	348.930	-0.197	1/6	
T65	-2489.413	497.528	-194.992	13841.04	
	0.699857	-0.875605	-0.446926	1.137559	
	183.698	274.403	39.899	1/6	
T66	-2485.363	500.799	-228.479	13794.56	
	0.715164	-0.832653	-0.566420	1.165944	
	195.349	236.170	90.314	1/6	

Appendix B

Separation of the energy into spin-isospin channels

When the EDF is defined as the expectation value of an effective Hamiltonian, separating it into spin-isospin channels is straightforward, as in Eq. (3.11). However, one can extend this definition to the case of any Hartree-like functional: let us start by recalling that in the case of the Skyrme force, the direct and exchange terms have the same analytical structure; one thus usually uses the expressions

$$\mathcal{E}_{\rm pot} = \frac{1}{2}\sum_{kl}\left\langle kl\left|\hat{V}_{\rm Skyrme}\right|\overline{kl}\right\rangle \rho_{kk}\ \rho_{ll}, \tag{B.1}$$

$$\left|\overline{kl}\right\rangle = |kl\rangle - |lk\rangle = (1-\hat{P}_r\hat{P}_\sigma\hat{P}_\tau)\,|kl\rangle\,, \tag{B.2}$$

where the last expression uses the position, spin and isospin exchange operators to define an antisymmetrized and non-normalized two-body state. One then writes down the antisymmetrized form of the Skyrme interaction and the EDF by using the definition of densities entering Eqs. (C.29)-(C.32).

Leaving the antisymmetrized Hamiltonian framework, it is always possible to define the potential part of the functional as the *direct term* of the expectation value of a certain operator, as in

$$\mathcal{E}_{\rm pot} = \sum_{kl}\left\langle kl\left|\hat{V}_{\rm EDF}\right|kl\right\rangle \rho_{kk}\ \rho_{ll}, \tag{B.3}$$

recalling that $\hat{V}_{\rm EDF} = \hat{V}_{\rm Skyrme}(1-\hat{P}_r\hat{P}_\sigma\hat{P}_\tau)$ in the Hamiltonian case. One then defines the energy per channel as

$$\mathcal{E}^{ST}_{\rm EDF} = \sum_{kl}\left\langle kl\left|V_{\rm EDF}\ \hat{P}_S\hat{P}_T\right|kl\right\rangle \rho_{kk}\ \rho_{ll}, \tag{B.4}$$

which, with the definitions (C.29)-(C.32) for coupling constants, yields (retaining

only terms acting in infinite matter)

$$
\begin{aligned}
\mathcal{E}^{ST}_{\rm pot} &= \int \mathrm{d}^3\mathbf{r}\ \mathcal{H}^{ST}(\mathbf{r}),\\
\mathcal{H}^{ST} &= \left[C_0^\rho + (4S-3)C_0^s + (4T-3)C_1^\rho + (4S-3)(4T-3)C_1^s\right]\\
&\quad \times \frac{1}{16}\left[(2S+1)(2T+1)\rho_0^2 + (2S-1)(2T+1)\mathbf{s}_0^2\right.\\
&\quad \left. + (2S+1)(2T-1){\rho_1}^2 + (2S-1)(2T-1){\mathbf{s}_1}^2\right]\\
&\quad + \left[C_0^\tau + (4S-3)C_0^{sT} + (4T-3)C_1^\tau + (4S-3)(4T-3)C_1^{sT}\right]\\
&\quad \times \frac{1}{16}\big[(2S+1)(2T+1)\rho_0\tau_0 + (2S-1)(2T+1)\mathbf{s}_0\cdot\mathbf{T}_0\\
&\quad + (2S+1)(2T-1)\rho_1\tau_1 + (2S-1)(2T-1)\mathbf{s}_1\cdot\mathbf{T}_1\big].
\end{aligned}
\tag{B.5}
$$

Appendix C

Particle-Hole Potentials and Residual Interaction from a Quasi-Local Functional

In this appendix we derive the expression of the particle-hole effective potential and residual interaction arising from a quasi-local energy density functional. We present the results in a way which allows them to be directly put to use in the formula for the response function of Ref. [GR92].

C.1 Principle

Our starting point is a functional of the normal density matrix. Anomalous terms giving a pairing field and particle-particle residual interaction will not be considered here. This functional reads

$$\mathcal{E}[\rho] \;=\; \mathcal{F}\left[Q[\hat{\rho}]\right], \quad Q(x) \;=\; \mathrm{Tr}\left(\hat{Q}(x)\hat{\rho}\right) \;=\; \sum_{ij} q(x)_{ij}\rho_{ji}, \tag{C.1}$$

where $Q(x)$ plays the role of one or several "densities" as they are usually called in the Skyrme EDF, x representing the set of coordinates and discrete indices necessary to fully define each density operator/value. The ρ_{ji} then are matrix elements of the density matrix expressed in any complete representation including space, spin and isospin degrees of freedom, while $\hat{Q}(x)$ is a family of local one-body operators defining the densities, themselves independent from $\hat{\rho}$, and $q(x)_{ij}$ their matrix elements. For example, a functional of the local density can be recovered by making the substitutions (omitting spin and isospin for simplicity)

$$x \;\rightarrow\; \mathbf{r} \tag{C.2}$$

$$\rho_{ij} \;\rightarrow\; \rho(\mathbf{x},\mathbf{x}') \tag{C.3}$$

$$q(x)_{ij} \;\rightarrow\; \delta(\mathbf{r}-\mathbf{x})\;\delta(\mathbf{r}-\mathbf{x}') \tag{C.4}$$

$$Q(x) \;\rightarrow\; \rho(\mathbf{r}) \tag{C.5}$$

The effective potential entering the HF/Kohn-Sham equations can be derived as

$$h_{ij} \;=\; \frac{\delta\mathcal{F}}{\delta\rho_{ji}} \;=\; \sum\!\!\!\!\!\!\int_x \frac{\partial\mathcal{F}}{\partial Q(x)}\,\frac{\delta Q(x)}{\delta\rho_{ji}} \;=\; \sum\!\!\!\!\!\!\int_x \frac{\partial\mathcal{F}}{\partial Q(x)}\,q(x)_{ij} \tag{C.6}$$

$$\hat{h} \;=\; \sum\!\!\!\!\!\!\int_x \frac{\partial\mathcal{F}}{\partial Q(x)}\,\hat{Q}(x), \tag{C.7}$$

while the particle-hole residual interaction is given by the second functional derivative. Similarly, we can write

$$\begin{aligned} V^{\rm ph}_{ijkl} &= \frac{\delta^2\mathcal{F}}{\delta\rho_{ki}\,\delta\rho_{lj}} = \sum\!\!\!\!\!\!\int_{xy} \frac{\partial^2\mathcal{F}}{\partial Q(x)\,\partial Q(y)}\, q(x)_{ik}\, q(y)_{jl} \\ \hat{V}^{\rm ph} &= \sum\!\!\!\!\!\!\int_{xy} \frac{\partial^2\mathcal{F}}{\partial Q(x)\,\partial Q(y)}\, \hat{Q}(x)^{(1)}\, \hat{Q}(y)^{(2)}, \end{aligned} \tag{C.8}$$

where we use the notation $\hat{Q}^{(1)}$ or $\hat{Q}^{(2)}$ to indicate that the one-body operator acts on the first or the second interacting particle, respectively.

C.2 Definitions

In order to derive the effective potentials and residual interaction from a Skyrme-like EDF, it is useful to rewrite the densities according to Eq. (C.1), working in coordinate space. We thus recall the expression of the non-local density matrix

$$\hat{\rho}(\mathbf{x}\sigma q, \mathbf{x}'\sigma' q') = \sum_k \varphi^*_k(\mathbf{x}'\sigma' q')\varphi_k(\mathbf{x}\sigma q) v^2_k, \tag{C.9}$$

where φ_k is a canonical wave function and v^2_k its occupation probability. Although the redefinition of densities below may look cumbersome, it allows for a systematic and straightforward derivation of the fields and residual interaction corresponding to any quasi-local functional.

We use in the following the operators $\boldsymbol{\nabla}$ and $\boldsymbol{\nabla}'$ (derivation with respect to, respectively, $\mathbf{x}$ and $\mathbf{x}'$), $\boldsymbol{\sigma}_{\sigma'\sigma}$ and $\tau_{q'q}$ (Pauli matrices acting in spin and isospin space).

Let us start by defining the time-even and isoscalar densities,

$$\rho_0(\mathbf{r}) = \int \mathrm{d}^3\mathbf{x}\mathrm{d}^3\mathbf{x}' \sum_{\sigma\sigma' qq'} \delta(\mathbf{r}-\mathbf{x})\,\delta(\mathbf{x}'-\mathbf{x})\;\delta_{q'q}\,\delta_{\sigma'\sigma}\;\hat{\rho}(\mathbf{x}\sigma q, \mathbf{x}'\sigma' q'), \tag{C.10}$$

$$\tau_0(\mathbf{r}) = \int \mathrm{d}^3\mathbf{x}\mathrm{d}^3\mathbf{x}' \sum_{\sigma\sigma' qq'} \delta(\mathbf{r}-\mathbf{x})\,\delta(\mathbf{x}'-\mathbf{x})\;\delta_{q'q}\,\delta_{\sigma'\sigma}\;\boldsymbol{\nabla}'\cdot\boldsymbol{\nabla}\hat{\rho}(\mathbf{x}\sigma q, \mathbf{x}'\sigma' q'), \tag{C.11}$$

$$\mathbb{J}_0(\mathbf{r}) = \int \mathrm{d}^3\mathbf{x}\mathrm{d}^3\mathbf{x}' \sum_{\sigma\sigma' qq'} \delta(\mathbf{r}-\mathbf{x})\,\delta(\mathbf{x}'-\mathbf{x})\;\delta_{q'q}\;\frac{1}{2i}(\boldsymbol{\nabla}'-\boldsymbol{\nabla})\otimes\boldsymbol{\sigma}_{\sigma'\sigma}\,\hat{\rho}(\mathbf{x}\sigma q, \mathbf{x}'\sigma' q'), \tag{C.12}$$

$$\mathbf{J}_0(\mathbf{r}) = \int \mathrm{d}^3\mathbf{x}\mathrm{d}^3\mathbf{x}' \sum_{\sigma\sigma' qq'} \delta(\mathbf{r}-\mathbf{x})\,\delta(\mathbf{x}'-\mathbf{x})\;\delta_{q'q}\;(-i\boldsymbol{\nabla})\times\boldsymbol{\sigma}_{\sigma'\sigma}\,\hat{\rho}(\mathbf{x}\sigma q, \mathbf{x}'\sigma' q'), \tag{C.13}$$

$\mathbf{J}$ being the rank-one part of the tensor $\mathbb{J}$.

Time-even isovector densities, similarly, read

$$\rho_1(\mathbf{r}) = \int \mathrm{d}^3\mathbf{x}\mathrm{d}^3\mathbf{x}' \sum_{\sigma\sigma' qq'} \delta(\mathbf{r}-\mathbf{x})\ \delta(\mathbf{x}'-\mathbf{x})\ \ \tau_{q'q}\ \delta_{\sigma'\sigma}\ \ \hat{\rho}(\mathbf{x}\sigma q, \mathbf{x}'\sigma' q'), \tag{C.14}$$

$$\tau_1(\mathbf{r}) = \int \mathrm{d}^3\mathbf{x}\mathrm{d}^3\mathbf{x}' \sum_{\sigma\sigma' qq'} \delta(\mathbf{r}-\mathbf{x})\ \delta(\mathbf{x}'-\mathbf{x})\ \ \tau_{q'q}\ \delta_{\sigma'\sigma}\ \ \boldsymbol{\nabla}'\cdot\boldsymbol{\nabla}\hat{\rho}(\mathbf{x}\sigma q, \mathbf{x}'\sigma' q'), \tag{C.15}$$

$$\mathbb{J}_1(\mathbf{r}) = \int \mathrm{d}^3\mathbf{x}\mathrm{d}^3\mathbf{x}' \sum_{\sigma\sigma' qq'} \delta(\mathbf{r}-\mathbf{x})\ \delta(\mathbf{x}'-\mathbf{x})\ \ \tau_{q'q}\ \ \frac{1}{2i}(\boldsymbol{\nabla}'-\boldsymbol{\nabla})\otimes\boldsymbol{\sigma}_{\sigma'\sigma}\ \hat{\rho}(\mathbf{x}\sigma q, \mathbf{x}'\sigma' q'), \tag{C.16}$$

$$\mathbf{J}_1(\mathbf{r}) = \int \mathrm{d}^3\mathbf{x}\mathrm{d}^3\mathbf{x}' \sum_{\sigma\sigma' qq'} \delta(\mathbf{r}-\mathbf{x})\ \delta(\mathbf{x}'-\mathbf{x})\ \ \tau_{q'q}\ \ (-i\boldsymbol{\nabla})\times\boldsymbol{\sigma}_{\sigma'\sigma}\ \hat{\rho}(\mathbf{x}\sigma q, \mathbf{x}'\sigma' q'), \tag{C.17}$$

while time-odd isoscalar,

$$\mathbf{s}_0(\mathbf{r}) = \int \mathrm{d}^3\mathbf{x}\mathrm{d}^3\mathbf{x}' \sum_{\sigma\sigma' qq'} \delta(\mathbf{r}-\mathbf{x})\ \delta(\mathbf{x}'-\mathbf{x})\ \ \delta_{q'q}\ \boldsymbol{\sigma}_{\sigma'\sigma}\ \ \hat{\rho}(\mathbf{x}\sigma q, \mathbf{x}'\sigma' q'), \tag{C.18}$$

$$\mathbf{T}_0(\mathbf{r}) = \int \mathrm{d}^3\mathbf{x}\mathrm{d}^3\mathbf{x}' \sum_{\sigma\sigma' qq'} \delta(\mathbf{r}-\mathbf{x})\ \delta(\mathbf{x}'-\mathbf{x})\ \ \delta_{q'q}\ \boldsymbol{\sigma}_{\sigma'\sigma}\ \ \boldsymbol{\nabla}'\cdot\boldsymbol{\nabla}\hat{\rho}(\mathbf{x}\sigma q, \mathbf{x}'\sigma' q'), \tag{C.19}$$

$$\mathbf{j}_0(\mathbf{r}) = \int \mathrm{d}^3\mathbf{x}\mathrm{d}^3\mathbf{x}' \sum_{\sigma\sigma' qq'} \delta(\mathbf{r}-\mathbf{x})\ \delta(\mathbf{x}'-\mathbf{x})\ \ \delta_{q'q}\ \delta_{\sigma'\sigma}\ \ \frac{1}{2i}(\boldsymbol{\nabla}'-\boldsymbol{\nabla})\hat{\rho}(\mathbf{x}\sigma q, \mathbf{x}'\sigma' q'), \tag{C.20}$$

and time-odd isovector densities,

$$\mathbf{s}_1(\mathbf{r}) = \int \mathrm{d}^3\mathbf{x}\mathrm{d}^3\mathbf{x}' \sum_{\sigma\sigma' qq'} \delta(\mathbf{r}-\mathbf{x})\ \delta(\mathbf{x}'-\mathbf{x})\ \ \tau_{q'q}\ \boldsymbol{\sigma}_{\sigma'\sigma}\ \ \hat{\rho}(\mathbf{x}\sigma q, \mathbf{x}'\sigma' q'), \tag{C.21}$$

$$\mathbf{T}_1(\mathbf{r}) = \int \mathrm{d}^3\mathbf{x}\mathrm{d}^3\mathbf{x}' \sum_{\sigma\sigma' qq'} \delta(\mathbf{r}-\mathbf{x})\ \delta(\mathbf{x}'-\mathbf{x})\ \ \tau_{q'q}\ \boldsymbol{\sigma}_{\sigma'\sigma}\ \ \boldsymbol{\nabla}'\cdot\boldsymbol{\nabla}\hat{\rho}(\mathbf{x}\sigma q, \mathbf{x}'\sigma' q'), \tag{C.22}$$

$$\mathbf{j}_1(\mathbf{r}) = \int \mathrm{d}^3\mathbf{x}\mathrm{d}^3\mathbf{x}' \sum_{\sigma\sigma' qq'} \delta(\mathbf{r}-\mathbf{x})\ \delta(\mathbf{x}'-\mathbf{x})\ \ \tau_{q'q}\ \delta_{\sigma'\sigma}\ \ \frac{1}{2i}(\boldsymbol{\nabla}'-\boldsymbol{\nabla})\hat{\rho}(\mathbf{x}\sigma q, \mathbf{x}'\sigma' q'), \tag{C.23}$$

can be subject to the same treatment.

It is equally useful to reexpress the following derivatives of densities

$$\begin{aligned}
\Delta\rho_0(\mathbf{r}) &= \int \mathrm{d}^3\mathbf{x}\mathrm{d}^3\mathbf{x}' \sum_{\sigma\sigma' qq'} \delta(\mathbf{r}-\mathbf{x})\ \delta(\mathbf{x}'-\mathbf{x})\ \ \delta_{q'q}\ \delta_{\sigma'\sigma} \\
&\quad (\boldsymbol{\nabla}'^2 + 2\boldsymbol{\nabla}'\cdot\boldsymbol{\nabla} + \boldsymbol{\nabla}^2)\hat{\rho}(\mathbf{x}\sigma q, \mathbf{x}'\sigma' q'), \qquad \text{(C.24)} \\
\boldsymbol{\nabla}\cdot\mathbf{J}_0(\mathbf{r}) &= \int \mathrm{d}^3\mathbf{x}\mathrm{d}^3\mathbf{x}' \sum_{\sigma\sigma' qq'} \delta(\mathbf{r}-\mathbf{x})\ \delta(\mathbf{x}'-\mathbf{x})\ \ \delta_{q'q}\ \delta_{\sigma'\sigma} \\
&\quad \boldsymbol{\nabla}'\cdot(-i\boldsymbol{\nabla}\times\boldsymbol{\sigma}_{\sigma'\sigma}\ )\hat{\rho}(\mathbf{x}\sigma q, \mathbf{x}'\sigma' q'), \qquad \text{(C.25)} \\
\boldsymbol{\nabla}\cdot\mathbf{s}_0(\mathbf{r}) &= \int \mathrm{d}^3\mathbf{x}\mathrm{d}^3\mathbf{x}' \sum_{\sigma\sigma' qq'} \delta(\mathbf{r}-\mathbf{x})\ \delta(\mathbf{x}'-\mathbf{x})\ \ \delta_{q'q}\ (\boldsymbol{\nabla}'+\boldsymbol{\nabla})\cdot\boldsymbol{\sigma}_{\sigma'\sigma}\ \hat{\rho}(\mathbf{x}\sigma q, \mathbf{x}'\sigma' q') \\
\boldsymbol{\nabla}\times\mathbf{j}_0(\mathbf{r}) &= \int \mathrm{d}^3\mathbf{x}\mathrm{d}^3\mathbf{x}' \sum_{\sigma\sigma' qq'} \delta(\mathbf{r}-\mathbf{x})\ \delta(\mathbf{x}'-\mathbf{x})\ \ \delta_{q'q}\ \delta_{\sigma'\sigma}\ \ (-i)\boldsymbol{\nabla}'\times\boldsymbol{\nabla}\hat{\rho}(\mathbf{x}\sigma q, \mathbf{x}'\sigma' q'). \qquad \text{(C.26)}
\end{aligned}$$

The corresponding expressions for $\Delta\rho_1$, $\Delta\mathbf{s}_0$, $\Delta\mathbf{s}_1$, $\boldsymbol{\nabla}\cdot\mathbf{J}_1$, $\boldsymbol{\nabla}\cdot\mathbf{s}_1$ and $\boldsymbol{\nabla}\times\mathbf{j}_1$ can be deduced from the above immediately, by a simple replacement of spin and isospin operators.

Let us recall the general form of the energy density (omitting Coulomb and tensor terms)

$$\begin{aligned}
\mathcal{E} &= \int d^3\mathbf{r}\left(\frac{\hbar^2}{2m}\tau_0 + \mathcal{H}_{\mathrm{Skyrme}}\right), \qquad \text{(C.27)} \\
\mathcal{H}_{\mathrm{Skyrme}} &= \mathcal{H}_0^{\mathrm{even}} + \mathcal{H}_1^{\mathrm{even}} + \mathcal{H}_0^{\mathrm{odd}} + \mathcal{H}_1^{\mathrm{odd}}, \qquad \text{(C.28)}
\end{aligned}$$

with

$$\begin{aligned}
\mathcal{H}_0^{\mathrm{even}} &= C_0^\rho\rho_0^2 + C_0^{\Delta\rho}\rho_0\Delta\rho_0 + C_0^\tau\rho_0\tau_0 + C_0^J\mathbb{J}_0^2 + C_0^{\nabla J}\rho_0\boldsymbol{\nabla}\cdot\mathbf{J}_0, \qquad \text{(C.29)} \\
\mathcal{H}_1^{\mathrm{even}} &= C_1^\rho\rho_1^2 + C_1^{\Delta\rho}\rho_1\circ\Delta\rho_1 + C_1^\tau\rho_1\circ\tau_1 + C_1^J\mathbb{J}_1^2 + C_1^{\nabla J}\rho_1\circ\boldsymbol{\nabla}\cdot\mathbf{J}_1, \qquad \text{(C.30)} \\
\mathcal{H}_0^{\mathrm{odd}} &= C_0^s\mathbf{s}_0^2 + C_0^{\Delta s}\mathbf{s}_0\cdot\Delta\mathbf{s}_0 + C_0^{sT}\mathbf{s}_0\cdot\mathbf{T}_0 + C_0^{\nabla s}(\boldsymbol{\nabla}\cdot\mathbf{s}_0)^2 + C_0^j\mathbf{j}_0^2 + C_0^{\nabla j}\mathbf{s}_0\cdot(\boldsymbol{\nabla}\times\mathbf{j}_0), \qquad \text{(C.31)} \\
\mathcal{H}_1^{\mathrm{odd}} &= C_1^s\mathbf{s}_1^2 + C_1^{\Delta s}\mathbf{s}_1\cdot\circ\Delta\mathbf{s}_1 + C_1^{sT}\mathbf{s}_1\cdot\circ\mathbf{T}_1 + C_1^{\nabla s}(\boldsymbol{\nabla}\cdot\mathbf{s}_1)^2 + C_1^j\mathbf{j}_1^2 + C_1^{\nabla j}\mathbf{s}_1\cdot\circ(\boldsymbol{\nabla}\times\mathbf{j}_1). \qquad \text{(C.32)}
\end{aligned}$$

Let us also recall the constraints imposed between coupling constants due to time-reversal invariance

$$C_T^j = -C_T^\tau, \quad C_T^J = -C_T^{sT}, \quad C_T^{\nabla j} = C_T^{\nabla J}. \qquad \text{(C.33)}$$

We shall hereafter restrict density-depence to strictly local terms. A single density-dependent term will be considered, the generalization to two such terms being straightforward.

$$C_T^\rho = C_T^{\rho,0} + C_T^{\rho,\gamma}\rho_0^\gamma, \quad C_T^s = C_T^{s,0} + C_T^{s,\gamma}\rho_0^\gamma \qquad \text{(C.34)}$$

C.3 Potential and Residual Interaction

The coordinate-spin-isospin-space matrix element of the particle-hole residual interaction is defined by:

$$\langle\mathbf{x}'_a q'_a\sigma'_a\mathbf{x}'_b q'_b\sigma'_b|\hat{V}^{\mathrm{ph}}|\mathbf{x}_a q_a\sigma_a\mathbf{x}_b q_b\sigma_b\rangle = \frac{\delta^2\mathcal{E}}{\delta\rho(\mathbf{x}_b\sigma_b q_b, \mathbf{x}'_b\sigma'_b q'_b)\delta\rho(\mathbf{x}_a\sigma_a q_a, \mathbf{x}'_a\sigma'_a q'_a)}. \qquad \text{(C.35)}$$

In the following formulae for the effective potential terms, an identity operator $\delta(\mathbf{x}'-\mathbf{x})\ \delta_{q'q}\,\delta_{\sigma'\sigma}$ is implied, except when spin and/or isospin operators are present, in which case they should replace the one in the latter expression. If gradient operators are present, $\delta(\mathbf{x}'-\mathbf{x})$ should be placed left of $\boldsymbol{\nabla}$ (which acts on the right) and right of $\boldsymbol{\nabla}'$ (which acts on the left).

In the corresponding expressions for the residual interaction, we use the subscripts a and b to denote operators acting in the space of the first and second interacting particle, respectively. This convention has been chosen so as not to be confused with subscripts corresponding to spatial or isospin-space components. Similarly, an operator $\delta(\mathbf{x}'_a-\mathbf{x}_a)\delta(\mathbf{x}'_b-\mathbf{x}_b)\delta(\mathbf{x}_a-\mathbf{x}_b)\ \delta_{q'_aq_a}\delta_{q'_bq_b}\delta_{\sigma'_a\sigma_a}\delta_{\sigma'_b\sigma_b}$ is implied in each term of the residual interaction, with spin and isospin parts being replaced by those present in the specific expressions, and the δ-functions being inserted so gradient operators act to the left ($\boldsymbol{\nabla}'_{a,b}$) or right ($\boldsymbol{\nabla}_{a,b}$) before them.

Due to the length of the expressions involved, the effective potentials and residual interaction shall be broken down into terms denoted according to the terms of the functional they stem from. In any case, the complete expressions for $\hat{h}$ and $\hat{V}^{\mathrm{ph}}$ can be recovered by adding all the h- and V-terms, respectively, written down below.

C.3.1 Local, density-dependent terms

$$\begin{aligned}\hat{h}_0^{\rho} &= C_0^{\rho,0}2\rho_0 + C_0^{\rho,\gamma}\,(\gamma+2)\,\rho_0^{\gamma+1} \\ \hat{V}_0^{\rho}|_{ab} &= 2C_0^{\rho,0} + C_0^{\rho,\gamma}\,(\gamma+2)\,(\gamma+1)\,\rho_0^{\gamma}\end{aligned} \tag{C.36}$$

$$\begin{aligned}\hat{h}_1^{\rho} &= (C_1^{\rho,0}+C_1^{\rho,\gamma}\rho_0^{\gamma})2\rho_1\circ\hat{\tau} + C_1^{\rho,\gamma}\gamma\rho_0^{\gamma-1}\rho_1^2 \\ \hat{V}_1^{\rho}|_{ab} &= (C_1^{\rho,0}+C_1^{\rho,\gamma}\rho_0^{\gamma})2\hat{\tau}_a\circ\hat{\tau}_b + C_1^{\rho,\gamma}\left(2\gamma\rho_0^{\gamma-1}\rho_1\circ(\hat{\tau}_a+\hat{\tau}_b) + \gamma\,(\gamma-1)\,\rho_0^{\gamma-2}\rho_1^2\right)\end{aligned} \tag{C.37}$$

$$\begin{aligned}\hat{h}_0^{s} &= (C_0^{s,0}+C_0^{s,\gamma}\rho_0^{\gamma})2\mathbf{s}_0\cdot\hat{\boldsymbol{\sigma}} + C_0^{s,\gamma}\gamma\rho_0^{\gamma-1}\mathbf{s}_0^2 \\ \hat{V}_0^{s}|_{ab} &= (C_0^{s,0}+C_0^{s,\gamma}\rho_0^{\gamma})2\hat{\boldsymbol{\sigma}}_a\cdot\hat{\boldsymbol{\sigma}}_b + C_0^{s,\gamma}\left(2\gamma\rho_0^{\gamma-1}\mathbf{s}_0\cdot(\hat{\boldsymbol{\sigma}}_a+\hat{\boldsymbol{\sigma}}_b) + \gamma\,(\gamma-1)\,\rho_0^{\gamma-2}\mathbf{s}_0^2\right)\end{aligned} \tag{C.38}$$

$$\begin{aligned}\hat{h}_1^{s} &= (C_1^{s,0}+C_1^{s,\gamma}\rho_0^{\gamma})2\mathbf{s}_1\cdot\hat{\boldsymbol{\sigma}}\circ\hat{\tau} + C_1^{s,\gamma}\gamma\rho_0^{\gamma-1}\mathbf{s}_1^2 \\ \hat{V}_1^{s}|_{ab} &= (C_1^{s,0}+C_1^{s,\gamma}\rho_0^{\gamma})2\hat{\boldsymbol{\sigma}}_a\cdot\hat{\boldsymbol{\sigma}}_b\hat{\tau}_a\circ\hat{\tau}_b \\ &\quad + C_1^{s,\gamma}\left(2\gamma\rho_0^{\gamma-1}\mathbf{s}_1\cdot\circ(\hat{\boldsymbol{\sigma}}_a\hat{\tau}_a+\hat{\boldsymbol{\sigma}}_b\hat{\tau}_b) + \gamma\,(\gamma-1)\,\rho_0^{\gamma-2}\mathbf{s}_1^2\right)\end{aligned} \tag{C.39}$$

C.3.2 Non-local (effective-mass and current) terms

Terms of the form $C_T^{\tau}(\rho_T\tau_T-\mathbf{j}_T^2)$, $C_T^{sT}(\mathbf{s}_T\cdot\mathbf{T}_T-\mathbb{J}_T^2)$

$$\begin{aligned}\hat{h}_0^{\rho\tau-j^2} &= C_0^{\tau}\left(\rho_0\boldsymbol{\nabla}'\cdot\boldsymbol{\nabla}+\tau_0-\mathbf{j}_0\cdot\frac{1}{i}(\boldsymbol{\nabla}'-\boldsymbol{\nabla})\right) \\ \hat{V}_0^{\rho\tau-j^2}|_{ab} &= C_0^{\tau}\left(\boldsymbol{\nabla}'_a\cdot\boldsymbol{\nabla}_a+\boldsymbol{\nabla}'_b\cdot\boldsymbol{\nabla}_b+\frac{1}{2}(\boldsymbol{\nabla}'_a-\boldsymbol{\nabla}_a)\cdot(\boldsymbol{\nabla}'_b-\boldsymbol{\nabla}_b)\right)\end{aligned} \tag{C.40}$$

$$\begin{aligned}\hat{h}_1^{\rho\tau-j^2} &= C_1^\tau \left(\rho_1 \boldsymbol{\nabla}'\cdot\boldsymbol{\nabla}\hat{\tau} + \tau_1 \circ \hat{\tau} - \mathbf{j}_1 \cdot \frac{1}{i}(\boldsymbol{\nabla}' - \boldsymbol{\nabla})\hat{\tau}\right) \qquad \text{(C.41)}\\ \hat{V}_1^{\rho\tau-j^2}|_{ab} &= C_1^\tau \ \hat{\tau}_a \circ \hat{\tau}_b \ \left(\boldsymbol{\nabla}'_a\cdot\boldsymbol{\nabla}_a + \boldsymbol{\nabla}'_b\cdot\boldsymbol{\nabla}_b + \frac{1}{2}(\boldsymbol{\nabla}'_a - \boldsymbol{\nabla}_a)\cdot(\boldsymbol{\nabla}'_b - \boldsymbol{\nabla}_b)\right)\end{aligned}$$

$$\begin{aligned}\hat{h}_0^{sT-J^2} &= C_0^{sT} \left(\boldsymbol{\nabla}'\cdot\boldsymbol{\nabla}\mathbf{s}_0\cdot\hat{\boldsymbol{\sigma}} + \mathbf{T}_0\cdot\hat{\boldsymbol{\sigma}} - \frac{1}{i}(\boldsymbol{\nabla}' - \boldsymbol{\nabla})\cdot\mathbb{J}_0\cdot\hat{\boldsymbol{\sigma}}\right) \qquad \text{(C.42)}\\ \hat{V}_0^{sT-J^2}|_{ab} &= C_0^{sT} \ \hat{\boldsymbol{\sigma}}_a\cdot\hat{\boldsymbol{\sigma}}_b \ \left(\boldsymbol{\nabla}'_a\cdot\boldsymbol{\nabla}_a + \boldsymbol{\nabla}'_b\cdot\boldsymbol{\nabla}_b + \frac{1}{2}(\boldsymbol{\nabla}'_a - \boldsymbol{\nabla}_a)\cdot(\boldsymbol{\nabla}'_b - \boldsymbol{\nabla}_b)\right)\end{aligned}$$

$$\begin{aligned}\hat{h}_1^{sT-J^2} &= C_1^{sT} \left(\boldsymbol{\nabla}'\cdot\boldsymbol{\nabla}\mathbf{s}_1\cdot\hat{\boldsymbol{\sigma}}\circ\hat{\tau} + \mathbf{T}_1\cdot\hat{\boldsymbol{\sigma}}\circ\hat{\tau} - \frac{1}{i}(\boldsymbol{\nabla}' - \boldsymbol{\nabla})\cdot\mathbb{J}_1\cdot\hat{\boldsymbol{\sigma}}\circ\hat{\tau}\right) \qquad \text{(C.43)}\\ \hat{V}_1^{sT-J^2}|_{ab} &= C_1^{sT} \ \hat{\boldsymbol{\sigma}}_a\cdot\hat{\boldsymbol{\sigma}}_b \ \hat{\tau}_a\circ\hat{\tau}_b \ \left(\boldsymbol{\nabla}'_a\cdot\boldsymbol{\nabla}_a + \boldsymbol{\nabla}'_b\cdot\boldsymbol{\nabla}_b + \frac{1}{2}(\boldsymbol{\nabla}'_a - \boldsymbol{\nabla}_a)\cdot(\boldsymbol{\nabla}'_b - \boldsymbol{\nabla}_b)\right)\end{aligned}$$

Terms of the form $C_T^{\Delta\rho}\rho_T\Delta\rho_T$

$$\begin{aligned}\hat{h}_0^{\Delta\rho} &= C_0^{\Delta\rho}\left(\Delta\rho_0 + \rho_0(\boldsymbol{\nabla}'^2 + 2\boldsymbol{\nabla}'\cdot\boldsymbol{\nabla} + \boldsymbol{\nabla}^2)\right) \qquad \text{(C.44)}\\ \hat{V}_0^{\Delta\rho}|_{ab} &= C_0^{\Delta\rho}\left((\boldsymbol{\nabla}'^2_a + 2\boldsymbol{\nabla}'_a\cdot\boldsymbol{\nabla}_a + \boldsymbol{\nabla}^2_a) + (\boldsymbol{\nabla}'^2_b + 2\boldsymbol{\nabla}'_b\cdot\boldsymbol{\nabla}_b + \boldsymbol{\nabla}^2_b)\right)\end{aligned}$$

$$\begin{aligned}\hat{h}_1^{\Delta\rho} &= C_1^{\Delta\rho}\left(\Delta\rho_1\circ\hat{\tau} + \hat{\tau}\circ\rho_1(\boldsymbol{\nabla}'^2 + 2\boldsymbol{\nabla}'\cdot\boldsymbol{\nabla} + \boldsymbol{\nabla}^2)\right) \qquad \text{(C.45)}\\ \hat{V}_1^{\Delta\rho}|_{ab} &= C_1^{\Delta\rho}\ \hat{\tau}_a\circ\hat{\tau}_b\left((\boldsymbol{\nabla}'^2_a + 2\boldsymbol{\nabla}'_a\cdot\boldsymbol{\nabla}_a + \boldsymbol{\nabla}^2_a) + (\boldsymbol{\nabla}'^2_b + 2\boldsymbol{\nabla}'_b\cdot\boldsymbol{\nabla}_b + \boldsymbol{\nabla}^2_b)\right)\end{aligned}$$

$$\begin{aligned}\hat{h}_0^{\Delta\mathbf{s}} &= C_0^{\Delta s}\left(\Delta\mathbf{s}_0\cdot\hat{\boldsymbol{\sigma}} + \hat{\boldsymbol{\sigma}}\cdot\mathbf{s}_0(\boldsymbol{\nabla}'^2 + 2\boldsymbol{\nabla}'\cdot\boldsymbol{\nabla} + \boldsymbol{\nabla}^2)\right) \qquad \text{(C.46)}\\ \hat{V}_0^{\Delta\mathbf{s}}|_{ab} &= C_0^{\Delta s}\ \hat{\boldsymbol{\sigma}}_a\cdot\hat{\boldsymbol{\sigma}}_b\left((\boldsymbol{\nabla}'^2_a + 2\boldsymbol{\nabla}'_a\cdot\boldsymbol{\nabla}_a + \boldsymbol{\nabla}^2_a) + (\boldsymbol{\nabla}'^2_b + 2\boldsymbol{\nabla}'_b\cdot\boldsymbol{\nabla}_b + \boldsymbol{\nabla}^2_b)\right)\end{aligned}$$

$$\begin{aligned}\hat{h}_1^{\Delta\mathbf{s}} &= C_1^{\Delta s}\left(\Delta\mathbf{s}_1\cdot\hat{\boldsymbol{\sigma}}\circ\hat{\tau} + \hat{\boldsymbol{\sigma}}\cdot\hat{\tau}\circ\mathbf{s}_1(\boldsymbol{\nabla}'^2 + 2\boldsymbol{\nabla}'\cdot\boldsymbol{\nabla} + \boldsymbol{\nabla}^2)\right) \qquad \text{(C.47)}\\ \hat{V}_1^{\Delta\mathbf{s}}|_{ab} &= C_0^{\Delta s}\ \hat{\boldsymbol{\sigma}}_a\cdot\hat{\boldsymbol{\sigma}}_b\ \hat{\tau}_a\circ\hat{\tau}_b\left((\boldsymbol{\nabla}'^2_a + 2\boldsymbol{\nabla}'_a\cdot\boldsymbol{\nabla}_a + \boldsymbol{\nabla}^2_a) + (\boldsymbol{\nabla}'^2_b + 2\boldsymbol{\nabla}'_b\cdot\boldsymbol{\nabla}_b + \boldsymbol{\nabla}^2_b)\right)\end{aligned}$$

C.4 Infinite matter

C.4.1 Parameterization of the residual interaction

In a translation-invariant system, one can replace gradient operators by the momenta of s.p. states

$$\mathbf{p}_a = -i\boldsymbol{\nabla}_a, \quad \mathbf{p}'_a = i\boldsymbol{\nabla}'_a, \qquad \text{(C.48)}$$

and introduce relative momenta of the interacting particles, in the incoming (right) and outgoing (left) states,

$$\mathbf{k} = \frac{1}{2}(\mathbf{p}_a - \mathbf{p}_b), \qquad \mathbf{k}' = \frac{1}{2}(\mathbf{p}'_a - \mathbf{p}'_b), \tag{C.49}$$

while the incoming and outgoing total momenta, in turn, read

$$\mathbf{K} = \mathbf{p}_a + \mathbf{p}_b, \qquad \mathbf{K}' = \mathbf{p}'_a + \mathbf{p}'_b. \tag{C.50}$$

One can also define the direct and exchange transferred momenta

$$\mathbf{q} = \mathbf{k}' - \mathbf{k}, \qquad \mathbf{q}' = \mathbf{k}' + \mathbf{k}. \tag{C.51}$$

In an infinite, translation-invariant system, the residual interaction conserves total momentum. In the case of our functional it is also independent from it (i.e. there is no non-locality with respect to the center-of-mass coordinate). It is thus enough to use three quantities to express the momentum-dependence of the interaction. One can use the notation

$$\mathbf{p}'_a = \mathbf{q}_1 + \mathbf{q}, \qquad \mathbf{p}'_b = \mathbf{q}_2, \tag{C.52}$$

$$\mathbf{p}_a = \mathbf{q}_1, \qquad \mathbf{p}_b = \mathbf{q}_2 + \mathbf{q}, \tag{C.53}$$

where the exchange transferred momentum is $\mathbf{q}' = \mathbf{q}_1 - \mathbf{q}_2$.

The various terms of the interaction can be regrouped according to their spatial part on the one hand, and their spin-isospin structure on the other hand. One can then define four channels corresponding to the operators

$$\hat{\mathcal{O}}^{\rm ss}_{ab} = 1, \quad \hat{\mathcal{O}}^{\rm sv}_{ab} = \hat{\tau}_a \circ \hat{\tau}_b, \quad \hat{\mathcal{O}}^{\rm vs}_{ab} = \hat{\boldsymbol{\sigma}}_a \cdot \hat{\boldsymbol{\sigma}}_b, \quad \hat{\mathcal{O}}^{\rm vv}_{ab} = \hat{\boldsymbol{\sigma}}_a \cdot \hat{\boldsymbol{\sigma}}_b \; \hat{\tau}_a \circ \hat{\tau}_b. \tag{C.54}$$

For the spatial part, we group the local, effective mass/current, and pseudo-finite-range terms

$$\hat{V}^{\rho} = \hat{V}^{\rho}_0 + \hat{V}^{\rho}_1 + \hat{V}^{s}_0 + \hat{V}^{s}_1, \tag{C.55}$$

$$\hat{V}^{\tau} = \hat{V}^{\rho\tau-j^2}_0 + \hat{V}^{\rho\tau-j^2}_1 + \hat{V}^{sT-J^2}_0 + \hat{V}^{sT-J^2}_1, \tag{C.56}$$

$$\hat{V}^{\Delta\rho} = \hat{V}^{\Delta\rho}_0 + \hat{V}^{\Delta\rho}_1 + \hat{V}^{\Delta\mathbf{s}}_0 + \hat{V}^{\Delta\mathbf{s}}_1. \tag{C.57}$$

Let us first re-label the coupling constants in order to use a compact and general notation:

$$\begin{array}{llll} C^{\rho,0}_{\rm ss} = C^{\rho,0}_0, & C^{\rho,0}_{\rm vs} = C^{s,0}_0, & C^{\rho,0}_{\rm sv} = C^{\rho,0}_1, & C^{\rho,0}_{\rm vv} = C^{s,0}_1, \\ C^{\rho,\gamma}_{\rm ss} = C^{\rho,\gamma}_0, & C^{\rho,\gamma}_{\rm vs} = C^{s,\gamma}_0, & C^{\rho,\gamma}_{\rm sv} = C^{\rho,\gamma}_1, & C^{\rho,\gamma}_{\rm vv} = C^{s,\gamma}_1, \\ C^{\tau}_{\rm ss} = C^{\tau}_0, & C^{\tau}_{\rm vs} = C^{sT}_0, & C^{\tau}_{\rm sv} = C^{\tau}_1, & C^{\tau}_{\rm vv} = C^{sT}_1, \\ C^{\Delta\rho}_{\rm ss} = C^{\Delta\rho}_0, & C^{\Delta\rho}_{\rm vs} = C^{\Delta s}_0, & C^{\Delta\rho}_{\rm sv} = C^{\Delta\rho}_1, & C^{\Delta\rho}_{\rm vv} = C^{\Delta s}_1. \end{array} \tag{C.58}$$

Each of the above contributions can be decomposed according to

$$\hat{V}^{\rho} = 2C^{\rho,0}_{\rm ss} + C^{\rho,\gamma}_{\rm ss}\,(\gamma+2)\,(\gamma+1)\,\rho_0^{\gamma} + \sum_{(\alpha)\neq{\rm ss}} 2\hat{\mathcal{O}}^{(\alpha)}_{ab}(C^{\rho,0}_{(\alpha)} + C^{\rho,\gamma}_{(\alpha)}\rho_0^{\gamma}) \tag{C.59}$$

for the central part and rearrangement terms,

$$\begin{aligned} \hat{V}^{\tau} &= \sum_{(\alpha)} C^{\tau}_{(\alpha)}\hat{\mathcal{O}}^{(\alpha)}_{ab}\left[\mathbf{p}'_a\cdot\mathbf{p}_a + \mathbf{p}'_b\cdot\mathbf{p}_b - \frac{1}{2}(\mathbf{p}'_a+\mathbf{p}_a)\cdot(\mathbf{p}'_b+\mathbf{p}_b)\right] \\ &= \sum_{(\alpha)} C^{\tau}_{(\alpha)}\hat{\mathcal{O}}^{(\alpha)}_{ab}\left[(\mathbf{q}_1+\mathbf{q})\cdot\mathbf{q}_1 + \mathbf{q}_2\cdot(\mathbf{q}_2+\mathbf{q}) - \frac{1}{2}(2\mathbf{q}_1+\mathbf{q})\cdot(2\mathbf{q}_2+\mathbf{q})\right] \\ &= \sum_{(\alpha)} C^{\tau}_{(\alpha)}\hat{\mathcal{O}}^{(\alpha)}_{ab}\left[(\mathbf{q}_1-\mathbf{q}_2)^2 - \frac{1}{2}\mathbf{q}^2\right] \end{aligned} \tag{C.60}$$

for the non-local part, where the dependence on the exchange transferred momentum $\mathbf{q}' = \mathbf{q}_1 - \mathbf{q}_2$ arising from the differential non-locality of the functional is pointed out, with an additional contribution to the $\mathbf{q}$-dependence, and

$$\begin{aligned}
\hat{V}^{\Delta\rho} &= \sum_{(\alpha)} C^{\Delta\rho}_{(\alpha)} \hat{\mathcal{O}}^{(\alpha)}_{ab} \left((\boldsymbol{\nabla}'^2_a + 2\boldsymbol{\nabla}'_a \cdot \boldsymbol{\nabla}_a + \boldsymbol{\nabla}^2_a) + (\boldsymbol{\nabla}'^2_b + 2\boldsymbol{\nabla}'_b \cdot \boldsymbol{\nabla}_b + \boldsymbol{\nabla}^2_b) \right), \\
&= \sum_{(\alpha)} C^{\Delta\rho}_{(\alpha)} \hat{\mathcal{O}}^{(\alpha)}_{ab} \left((-\mathbf{p}'^2_a + 2\mathbf{p}'_a \cdot \mathbf{p}_a - \mathbf{p}^2_a) + (-\mathbf{p}'^2_b + 2\mathbf{p}'_b \cdot \mathbf{p}_b - \mathbf{p}^2_b) \right), \\
&= \sum_{(\alpha)} C^{\Delta\rho}_{(\alpha)} \hat{\mathcal{O}}^{(\alpha)}_{ab} \big(-(\mathbf{q}_1 + \mathbf{q})^2 + 2(\mathbf{q}_1 + \mathbf{q}) \cdot \mathbf{q}_1 - \mathbf{q}_1^2 \\
&\qquad - \mathbf{q}_2^2 + 2\mathbf{q}_2 \cdot (\mathbf{q}_2 + \mathbf{q}) - (\mathbf{q}_2 + \mathbf{q})^2 \big), \\
&= \sum_{(\alpha)} -2C^{\Delta\rho}_{(\alpha)} \hat{\mathcal{O}}^{(\alpha)}_{ab} \mathbf{q}^2, \qquad \text{(C.61)}
\end{aligned}$$

for the pseudo-finite-range part, where the $\mathbf{q}$-dependence, i.e. the range of $\hat{V}^{\rm ph}$ is linked to the gradient terms.

We finally write $\hat{V}^{\rm ph}$ following Ref. [GR92]

$$\hat{V}^{\rm ph} = \sum_{(\alpha)} \frac{1}{4} \hat{\mathcal{O}}^{(\alpha)}_{ab} \left(W^{(\alpha)}_1(q) + W^{(\alpha)}_2(q) (\mathbf{q}_1 - \mathbf{q}_2)^2 \right), \qquad \text{(C.62)}$$

with the W functions defined as

$$\frac{W^{\rm ss}_1(q)}{4} = 2C^{\rho,0}_{\rm ss} + C^{\rho,\gamma}_{\rm ss} (\gamma + 2)(\gamma + 1) \rho^\gamma_0 - \left[2C^{\Delta\rho}_{\rm ss} + \frac{1}{2} C^{\tau}_{\rm ss} \right] q^2, \qquad \text{(C.63)}$$

$$\frac{W^{(\alpha)\neq{\rm ss}}_1(q)}{4} = 2C^{\rho,0}_{(\alpha)} + 2C^{\rho,\gamma}_{(\alpha)} \rho^\gamma_0 - \left[2C^{\Delta\rho}_{(\alpha)} + \frac{1}{2} C^{\tau}_{(\alpha)} \right] q^2, \qquad \text{(C.64)}$$

$$\frac{W^{(\alpha)}_2(q)}{4} = C^{\tau}_{(\alpha)}, \qquad \text{(C.65)}$$

which generalizes the expression for the residual interaction obtained in Ref. [GR92]. The same expressions are found when replacing the coupling constants by the corresponding combinations of parameters of the Skyrme interaction.

Appendix D

Formal aspects of separable interactions

D.1 Potentials

Let us consider an arbitrary nucleon-nucleon potential expressed through a set of coordinate-/momentum-space operators V_{ST}. The exact expression of the whole potential involves projectors on spin and isospin space. For example, in each isospin channel V_T, we can write

$$\hat{V}_T \;=\; \hat{P}_{S=0}\hat{V}_{0TT_3} + \hat{P}_{S=1}\hat{V}_{1TT_3} \tag{D.1}$$

where $\hat{P}_{S=0} = \frac{1}{4}(1 - \hat{\boldsymbol{\sigma}}_1 \cdot \hat{\boldsymbol{\sigma}}_2)$, $\hat{P}_{S=1} = \frac{1}{4}(3 + \hat{\boldsymbol{\sigma}}_1 \cdot \hat{\boldsymbol{\sigma}}_2)$ are the usual spin projectors, while the index T refers to the total isospin and T_3 the third isospin component of the pair ($T_3 = -1, 0, +1$ resp. for pp, np, nn). For potentials breaking charge invariance and charge symmetry, one then has to consider the nn, pp and np isospin channels separately.

In the following we use the usual convention for unnormalized plane waves which are subject to the following continuum orthonormality relations:

$$\int d^3\mathbf{r}\; e^{i\mathbf{k}\cdot\mathbf{r}}\;\; e^{-i\mathbf{k}'\cdot\mathbf{r}} \;=\; (2\pi)^3\;\delta^3(\mathbf{k}-\mathbf{k}'), \tag{D.2}$$

$$\int \frac{d^3\mathbf{k}}{(2\pi)^3}\; e^{i\mathbf{k}\cdot\mathbf{r}}\;\; e^{-i\mathbf{k}\cdot\mathbf{r}'} \;=\; \delta^3(\mathbf{r}-\mathbf{r}'). \tag{D.3}$$

In such a momentum representation, it is useful to extract the center-of-mass motion from the matrix elements such that

$$\langle \mathbf{k}_1\mathbf{k}_2|\hat{V}_{ST}|\mathbf{k}'_1\mathbf{k}'_2\rangle \;\equiv\; \langle \mathbf{k}|\hat{V}_{ST}|\mathbf{k}'\rangle (2\pi)^3\;\delta^3(\mathbf{K}-\mathbf{K}') \tag{D.4}$$

where $\mathbf{k} = \frac{1}{2}(\mathbf{k}_1 - \mathbf{k}_2)$ is the relative momentum of outgoing particles and $\mathbf{K} = \mathbf{k}_1 + \mathbf{k}_2$ is the center-of-mass momentum of the outgoing pair, with similar expressions for the incoming momenta $\mathbf{k}'$ and $\mathbf{K}'$.

D.1.1 Partial-wave expansion

One can perform a partial-wave expansion of the matrix elements by first expanding the plane waves,

$$e^{i\mathbf{k}\cdot\mathbf{r}} = 4\pi \sum_{\ell m} i^\ell \, Y_m^{\ell *}(\hat{k}) \, Y_m^\ell(\hat{r}) \, j_\ell(kr), \tag{D.5}$$

$$|\mathbf{k}\rangle = 4\pi \sum_{\ell m} i^\ell \, Y_m^{\ell *}(\hat{k}) \, |k\ell m\rangle, \tag{D.6}$$

where k the norm and $\hat{k}$ the unit vector (which we use to refer to the angular coordinates) of $\mathbf{k}$, and $|k\ell m\rangle$ is a spherical wave,

$$\langle \mathbf{r}|k\ell m\rangle = j_\ell(kr) \, Y_m^\ell(\hat{r}), \tag{D.7}$$

which is in turn unnormalized so that

$$\langle k\ell m|k'\ell' m'\rangle = \int d^3\mathbf{r} \, Y_m^{\ell *}(\hat{r}) \, j_\ell(kr) Y_{m'}^{\ell'}(\hat{r}) \, j_{\ell'}(k'r), \tag{D.8}$$

$$= \delta_{\ell\ell'}\delta_{mm'} \int r^2 dr \, j_\ell(kr) j_\ell(kr) = \delta_{\ell\ell'}\delta_{mm'} \, \frac{\pi}{2kk'} \delta(k-k'). \tag{D.9}$$

The general expansion of the relative-momentum matrix element thus reads:

$$\langle \mathbf{k}|\hat{V}_{ST}|\mathbf{k}'\rangle = (4\pi)^2 \sum_{\ell\ell' mm'} i^{\ell'-\ell} Y_m^\ell(\hat{k}) Y_{m'}^{\ell' *}(\hat{k}') \langle k\ell m|\hat{V}_{ST}|k'\ell' m'\rangle. \tag{D.10}$$

In the absence of a tensor force (or simply if $S = 0$), V_{ST} does not couple partial waves with $\ell \neq \ell'$, and is independent from the projection of angular momentum, i.e.

$$\langle k\ell m|\hat{V}_{ST}|k'\ell' m'\rangle = \langle k\ell|\hat{V}_{ST}|k'\ell\rangle \, \delta_{\ell'\ell} \, \delta_{m'm} \tag{D.11}$$

thus

$$\langle \mathbf{k}|\hat{V}_{ST}|\mathbf{k}'\rangle = (4\pi)^2 \sum_{\ell m} Y_m^\ell(\hat{k}) Y_m^{\ell *}(\hat{k}') \langle k\ell|\hat{V}_{ST}|k'\ell\rangle \tag{D.12}$$

$$= 4\pi \sum_\ell (2\ell+1) P_\ell(\cos\theta) \langle k\ell|\hat{V}_{ST}|k'\ell\rangle \tag{D.13}$$

where θ is the angle between $\hat{k}$ and $\hat{k}'$.

For solving the two-body problem explicitly in momentum space, e.g. computing the deuteron bound state, one should work with normalized spherical waves, i.e. $|k\ell m\rangle_N \equiv \sqrt{2/\pi}|k\ell m\rangle$. One then has

$${}_N\langle k\ell|\hat{V}_{ST}|k'\ell\rangle_N = \frac{2}{\pi}\langle k\ell|\hat{V}_{ST}|k'\ell\rangle \tag{D.14}$$

The way we will write our separable interaction for subsequent use in HFB codes implies dropping all prefactors in Eq. (D.13), obtaining an expression for the potential matrix elements directly related to functions $V_{\ell ST}(k,k')$:

$$\langle \mathbf{k}|\hat{V}_{ST}|\mathbf{k}'\rangle \equiv \sum_\ell V_{\ell ST}(k,k') P_\ell(\cos\theta) \tag{D.15}$$

One thus has:

$$V_{\ell ST}(k,k') = 4\pi(2\ell+1) \, \langle k\ell|\hat{V}_{ST}|k'\ell\rangle \tag{D.16}$$

$$= 2\pi^2(2\ell+1) \, {}_N\langle k\ell|\hat{V}_{ST}|k'\ell\rangle_N \tag{D.17}$$

D.1.2 Two-particle scattering and the Lippmann-Schwinger equation

In discussing the scattering of a pair of particles, it is customary (since useful) to rephrase the Schrödinger equation in terms of an integral equation for an amplitude matrix in momentum space which then holds all information about observables such as cross-sections. We have, in operator form,

$$\hat{T} = \hat{V} + \hat{V}\hat{G}_0\hat{T}, \tag{D.18}$$

$\hat{G}_0$ being the free particle pair propagator expressed, in terms of the free Hamiltonian $\hat{H}_0 = \frac{\hbar^2 k^2}{m}$, as $\hat{G}_0 = (E - \hat{H}_0)^{-1}$ (One uses the reduced mass μ of the NN pair, $2\mu = m$). Plugging closure relations in, one gets

$$\langle \mathbf{k}|\hat{T}_{ST}(E)|\mathbf{k}'\rangle = \frac{m}{\hbar^2}\langle \mathbf{k}|\hat{V}_{ST}|\mathbf{k}'\rangle + \mathcal{P}\int \frac{d^3\mathbf{k}''}{(2\pi)^3}\frac{\langle \mathbf{k}|\hat{V}_{ST}|\mathbf{k}''\rangle\ \langle \mathbf{k}''|\hat{T}_{ST}(E)|\mathbf{k}'\rangle}{E - E(k'')}, \tag{D.19}$$

where $E(k'') = \hbar^2 k''^2/m$ is the energy associated with the intermediate state with momentum k'' and $\mathcal{P}$ indicates a principal value integral. Plugging the expansion of Eq. (D.10) (assuming no coupling between partial waves) into the above expression yields a set of uncoupled equations for each value of ℓ,

$$\begin{aligned}\langle k\ell|\hat{T}_{ST}(E)|k'\ell\rangle &= \frac{m}{\hbar^2}\langle k\ell|\hat{V}_{ST}|k'\ell\rangle \\ &\quad + \frac{2}{\pi}\mathcal{P}\int k''^2 dk'' \frac{\langle k\ell|\hat{V}_{ST}|k''\ell\rangle\ \langle k''\ell|\hat{T}_{ST}(E)|k'\ell\rangle}{E - E_{k''}}.\end{aligned} \tag{D.20}$$

The scattering phase shift in each partial wave is given by

$$\langle k\ell|\hat{T}_{ST}(E_k)|k\ell\rangle = -\tan(\delta_{\ell ST})/k \tag{D.21}$$

which implies that T should be expressed in fm, and justifies the $\hbar^2/m$ factor in Eqs. (D.19-D.20) since V is in MeV fm^3. If V is expressed in fm, the factor before the Born term should be dropped and E and $E_{k''}$ replaced by just k_0^2 and k''^2.

Assuming that the NN interaction can be expressed as a sum of uncoupled terms acting each in one partial wave, as in

$$\langle \mathbf{k}|\hat{V}_{ST}|\mathbf{k}'\rangle \equiv \sum_\ell V_{\ell ST}(k,k')P_\ell(\cos(\mathbf{k},\mathbf{k}')) \tag{D.22}$$

we would like as a first step to represent $V_0(k,k')$ as a sum of separable terms:

$$V_{\ell ST}(k,k') = \sum_{\alpha\beta} g_\alpha(k)\ \lambda_{\alpha\beta}\ g_\beta(k') \tag{D.23}$$

where the $g(k)$'s are form factors. In the following sections $\ell ST \equiv 001$ as we focus on the $T = 1$, $^1S_0$ channel.

D.2 Phase shifts

Plugging the separable form of our potential in the LS equation yields

$$\begin{aligned}\langle k\ell|\hat{T}_{ST}(E)|k'\ell\rangle &= \frac{m}{4\pi\hbar^2}\sum_{\alpha\beta} g_\alpha(k)\lambda_{\alpha\beta}g_\beta(k') \\ &\quad + \frac{1}{2\pi^2}\mathcal{P}\int k''^2 dk''\ \frac{g_\alpha(k)\lambda_{\alpha\beta}g_\beta(k')\ \langle k''\ell|\hat{T}_{ST}(E)|k'\ell\rangle}{E - E(k'')}.\end{aligned} \tag{D.24}$$

It is quite easy to see that the solution has the form

$$\langle k\ell|\hat{T}_{ST}(E)|k'\ell\rangle \equiv \sum_{\alpha\beta} g_\alpha(k)\tau_{\alpha\beta}(E)g_\beta(k'). \tag{D.25}$$

We thus have

$$\sum_{\alpha\beta} g_\alpha(k)\tau_{\alpha\beta}(E)g_\beta(k') = \frac{m}{4\pi\hbar^2}\sum_{\alpha\beta} g_\alpha(k)\lambda_{\alpha\beta}g_\beta(k') + \frac{1}{2\pi^2}\sum_{\alpha\beta\gamma\delta}\mathcal{P}\int k''^2dk'' \times \frac{g_\alpha(k)\lambda_{\alpha\gamma}g_\gamma(k'')\ g_\delta(k'')\tau_{\delta\beta}(E)g_\beta(k')}{E-E(k'')}, \tag{D.26}$$

which, assuming the linear independence of our form factors, leads to an equation for the couplings between form factors in the T-matrix,

$$\tau_{\alpha\beta}(E) = \frac{m}{4\pi\hbar^2}\ \lambda_{\alpha\beta} + \frac{1}{2\pi^2}\sum_{\gamma\delta}\ \lambda_{\alpha\gamma}\mathcal{P}\int k''^2dk''\ \frac{g_\gamma(k'')\ g_\delta(k'')}{E-E(k'')}\ \tau_{\delta\beta}(E), \tag{D.27}$$

$$\tau(E) = \frac{m}{4\pi\hbar^2}\ [1-\lambda\mathcal{G}(E)]^{-1}\ \lambda, \tag{D.28}$$

where the matrix $\mathcal{G}(E)$ corresponds to

$$\mathcal{G}_{\alpha\beta}(E) \equiv \frac{1}{2\pi^2}\mathcal{P}\int k^2dk\ \frac{g_\alpha(k)\ g_\beta(k)}{E-E(k)}. \tag{D.29}$$

The LS equation is thus reduced to some integrals and a (small) matrix inversion. The phase shifts can then be computed the usual way from the fully-on-shell T-matrix.

D.3 Gap equation in infinite matter

The pairing problem treated at the BCS appoximation, i.e. including the bare potential in the particle-particle channel, and using a kinetic single-particle spectrum, is characterized by the standard gap equation

$$\Delta(\mathbf{k}) = -\int\frac{d^3\mathbf{k}'}{(2\pi)^3}\ \langle\mathbf{k}|\hat{V}|\mathbf{k}'\rangle\frac{\Delta(\mathbf{k}')}{2E_{\mathbf{k}'}}, \tag{D.30}$$

where $E_{\mathbf{k}} = \sqrt{(\varepsilon_k-\lambda)^2+\Delta_{\mathbf{k}}^2}$, ε_k being the single-particle energy and λ the chemical potential. We'll take $\lambda = \varepsilon_{k_\mathrm{F}}$, which modifies the dependence between k_F and the density, albeit too little to be relevant for our qualitative use of the gap equation. Again, we plug our separable potential in, which selects the ${}^1S_0$ partial wave and makes all quantities independent from angular coordinates,

$$\Delta(k) = -\frac{1}{2\pi^2}\int k'^2dk'\ V_{001}(k,k')\frac{\Delta(k')}{2E_{k'}} \tag{D.31}$$

$$= -\sum_{\alpha\beta}\ g_\alpha(k)\lambda_{\alpha\beta}\frac{1}{2\pi^2}\int k'^2dk'\ g_\beta(k')\frac{\Delta(k')}{2E_{k'}}, \tag{D.32}$$

which shows, examining the k-dependence of the gap, that it can be written as

$$\Delta(k) \equiv \sum_\alpha \Delta_\alpha^0\ g_\alpha(k), \tag{D.33}$$

where the Δ^0's become the new unknowns of the problem. They obey a rewritten gap equation which involves the pair densities $\breve{\chi}_\alpha$,

$$\Delta^0_\alpha = -\frac{1}{2}\sum_\beta \lambda_{\alpha\beta}\ \breve{\chi}_\beta \tag{D.34}$$

$$\breve{\chi}_\beta = \frac{1}{2\pi^2}\int k'^2 dk'\ g_\beta(k')\frac{\Delta(k')}{E_{k'}}, \tag{D.35}$$

which correspond to the same quantities written in coordinate space for the spherical HFB case. The solution of the BCS gap equation can then be found by starting from some initial values of the Δ^0's, then iterating Eqs. (D.35), (D.33) and (D.34) until convergence is reached. Note that as is, this procedure will diverge for non-perturbative interactions [Ram07]. The latter reference thus uses an elaborate procedure to solve the gap equation, which amounts to separating the potential matrix elements into a separable term and a residual one which vanishes at the Fermi level. The resulting equations can be solved directly. However, we found that a simple damping factor modifying the self-consistent equations was enough to obtain convergence.

Appendix E

Parameters of separable interactions

The parameters of the separable interactions used in chapter 5 are given below, in Table E.1. For each interaction, a header specifies the starting (hard) interaction, isospin channel, cutoff function (see Eq. (5.37)), cutoff value (in fm^{-1}), rank M of the separable representation and number of terms m in each form factor. See Eqs. (5.44) and (5.57) and accompanying discussion for the meaning of the parameters and fit procedure. The actual separable parameterizations use diagonal couplings, i.e. $\lambda_{\alpha\beta} = \lambda_\alpha \delta_{\alpha\beta}$.

Table E.1: Parameters defining the separable operator representations of the hadronic parts of $V_{\mathrm{low}\,k}$ and Argonne v_{18} nucleon-nucleon interactions used in this work.

α	a_α [fm]	λ_α [MeV fm^3]	n_0	n_1 (n_5) $x_{\alpha 1}$ ($x_{\alpha 5}$)	n_2 $x_{\alpha 2}$	n_3 $x_{\alpha 3}$	n_4 $x_{\alpha 4}$
Argonne v_{18}, nn, exponential ($n = 6$), $\Lambda = 2.5$, $M = 3$, $m = 5$							
1	1.7400	-983.79	0	1 0.41483	2 0.23365	4 0.0077974	9 $-3.6629\,10^{-6}$
				10 $2.8335\,10^{-7}$			
2	1.6631	0.15436	0	6 -0.71971	7 0.37599	8 -0.083656	9 0.0074367
				10 $-2.2078\,10^{-4}$			
3	1.8234	-354.78	1	0 -0.033729	3 0.17602	8 $6.7379\,10^{-6}$	9 $-7.1010\,10^{-6}$
				10 $3.7713\,10^{-7}$			

Table E.1: Parameters defining the separable operator representations of interactions (continued).

Argonne v_{18}, pp, exponential ($n = 6$), $\Lambda = 2.5$, $M = 3$, $m = 5$							
1	1.7415	-978.26	0	1 0.41681	2 0.23341	4 0.0075925	9 $-3.7560\,10^{-6}$
				10 $2.9035\,10^{-7}$			
2	1.6680	0.15743	0	6 -0.73884	7 0.38570	8 -0.085207	9 0.0075197
				10 $-2.2182\,10^{-4}$			
3	1.8264	-347.42	1	0 -0.042636	3 0.17591	8 $4.9746\,10^{-6}$	9 $-6.8307\,10^{-6}$
				10 $3.6046\,10^{-7}$			
CD-Bonn, nn, Fermi-Dirac ($\epsilon = 0.5$), $\Lambda = 1.8$, $M = 2$, $m = 5$							
1	2.1847	-799.96	0	1 0.91829	3 0.47722	4 -0.19001	5 0.049102
				6 -0.0033185			
2	2.5000	-177.29	0	1 -0.21869	3 0.21610	4 -0.19555	5 0.035250
				6 -0.0024611			
CD-Bonn, nn, exponential ($n = 6$), $\Lambda = 2.5$, $M = 3$, $m = 4$							
1	1.7214	-930.12	0	1 0.25068	2 0.22550	5 .0022877	7 $-5.7267\,10^{-5}$
2	1.7881	32.091	1	0 0.0071364	4 0.13522	9 $5.4076\,10^{-5}$	10 $-4.0494\,10^{-6}$
3	1.7278	-580.64	1	0 0.26980	3 0.13974	9 $-2.8858\,10^{-6}$	10 $2.3252\,10^{-7}$
CD-Bonn, nn, exponential ($n = 6$), $\Lambda = 3.0$, $M = 4$, $m = 4$							
1	1.0908	-431.50	0	1 0.35315	2 0.59492	3 -0.37945	4 0.027775
2	1.1184	3235.3	3	1 17.596	2 -1.9937	0 0.28038	4 -8.4643
3	1.2473	-1371.1	1	0 -0.52693	2 -0.66651	3 0.22395	4 -0.010229
4	1.3007	-1948.6	2	1 -1.7907	0 -0.45939	3 -0.16783	4 -0.086305

Table E.1: Parameters defining the separable operator representations of interactions (continued).

CD-Bonn, nn, exponential ($n = 6$), $\Lambda = 4.0$, $M = 4$, $m = 4$							
1	0.78980	698.80	0	1	2	3	4
				-0.96576	0.87481	-1.9379	0.19910
2	0.83339	2885.2	1	0	2	3	4
				-0.030759	-1.9616	2.6650	-0.16114
3	1.7570	-91.515	1	0	2	3	4
				-1.4831	0.068112	0.067679	-0.0093729
4	0.89377	-5792.0	2	1	0	3	4
				-0.57060	-0.086000	-1.0777	-0.079829
CD-Bonn, nn, exponential ($n = 6$), $\Lambda = 8.0$, $M = 6$, $m = 4$							
1	0.63814	619.02	1	0	3	7	9
				0.51263	0.36902	$4.6330\,10^{-4}$	$-4.5753\,10^{-6}$
2	0.68468	-823.15	0	1	2	3	7
				-0.65990	0.062127	-0.054548	$-3.3780\,10^{-6}$
3	0.58589	0.43824	2	3	8	9	10
				-1.7986	-0.011990	0.0021446	$-9.3238\,10^{-5}$
4	0.60762	-0.026378	6	7	8	9	10
				-0.95561	0.25908	-0.027532	$9.3569\,10^{-4}$
5	0.94121	-1059.3	1	0	2	3	4
				-0.32739	-0.41297	0.14277	-0.032034
6	1.58513	-401.24	1	0	2	9	10
				-0.43268	-0.31717	$-5.6151\,10^{-6}$	$7.6408\,10^{-7}$
Argonne v_{18}, nn, $M = 9$, $m = 3$							
1	0.61544	-503.86	0	1	4	10	
				-1.9502	-0.052278	$1.5580\,10^{-8}$	
2	0.62603	169.58	0	1	3	7	
				2.8735	0.90026	$7.5516\,10^{-4}$	
3	0.28021	63.333	2	1	0	6	
				1.9134	0.90423	-0.0010905	
4	0.20451	6.0742	3	2	1	8	
				2.1766	1.9611	$4.8087\,10^{-5}$	
5	0.94442	-1131.1	1	0	2	10	
				-0.29080	-0.30625	$8.5078\,10^{-8}$	
6	0.32235	2.3871	3	2	1	10	
				-1.0497	0.0083717	$-4.2195\,10^{-6}$	
7	1.5158	-451.08	1	0	2	10	
				-0.41003	-0.37097	$1.2622\,10^{-7}$	
8	0.20000	33.447	2	4	6	10	
				-0.037752	-0.0044057	$-5.5173\,10^{-7}$	
9	0.75360	-0.99053	2	3	4	10	
				0.27823	2.6542	$1.7662\,10^{-5}$	

Appendix F

Separable Force in Spherical Symmetry

In this Appendix, we give the expressions actually used in the numerical implementation of the Hartree-Fock-Bogolyubov equations in spherical symmetry.

F.1 General expression of interaction matrix elements

Let us start from a general interaction acting in the ${}^1S_0$ channel :

$$\hat{V}^{^1S_0} = \hat{V}^S \hat{P}_{S=0}, \tag{F.1}$$

where $\hat{V}^S$ is the spatial part acting in the $L = 0$ state of relative motion and $\hat{P}_{S=0}$ is the spin singlet projector stemming from the definition

$$\hat{P}_S = \frac{1 + (-1)^S \hat{P}_\sigma}{2}, \tag{F.2}$$

$$\tag{F.3}$$

$\hat{P}_\sigma$ being the spin-exchange operator. First, we express the non-antisymmetrized matrix elements in coordinate space.

$$v_{ijkl}^{^1S_0} = \langle ij|\hat{V}^{^1S_0}|kl\rangle \tag{F.4}$$

$$= \langle ij|\hat{P}^\dagger_{S=0}\hat{V}^S\hat{P}_{S=0}|kl\rangle \tag{F.5}$$

$$= \int d^3\mathbf{r}_{1,2,3,4}\ \langle ij|\hat{P}^\dagger_{S=0}|\mathbf{r}_1\mathbf{r}_2\rangle\langle\mathbf{r}_1\mathbf{r}_2|\hat{V}^S|\mathbf{r}_3\mathbf{r}_4\rangle\langle\mathbf{r}_3\mathbf{r}_4|\hat{P}_{S=0}|kl\rangle, \tag{F.6}$$

where $|ij\rangle$, $|\mathbf{r}_1\mathbf{r}_2\rangle$, etc. are two-particle direct product states, non-antisymmetrized and normalized. $|i\rangle$ is a state from the single-particle basis we will be working with, to be defined later. The index i includes all space, spin and isospin coordinates. Basis functions are notably considered the same for neutrons and protons, which shall eventually be treated separately.

The spin-singlet part of the two-body wave function can be expressed as :

$$\hat{P}_{S=0}|ij\rangle = \sum_{\sigma_1\sigma_2}\sum_{q_1q_2}\int d^3\mathbf{r}_1 d^3\mathbf{r}_2 \times \varphi_i(\mathbf{r}_1\sigma_1q_1)\ \varphi_j(\mathbf{r}_2\sigma_2q_2)\ |\mathbf{r}_1\mathbf{r}_2\rangle\ |q_1q_2\rangle\hat{P}_{S=0}|\sigma_1\sigma_2\rangle, \tag{F.7}$$

with the spin part reduced through

$$\begin{aligned}
&\sum_{\sigma_1\sigma_2} \ \varphi_i(\mathbf{r}_1\sigma_1 q_1)\ \varphi_j(\mathbf{r}_2\sigma_2 q_2)\ \hat{P}_{S=0}|\sigma_1\sigma_2\rangle \\
&= \sum_{\sigma_1\sigma_2} \varphi_i(\mathbf{r}_1\sigma_1 q_1)\ \varphi_j(\mathbf{r}_2\sigma_2 q_2)\ \frac{1}{2}\left(|\sigma_1\sigma_2\rangle - |\sigma_2\sigma_1\rangle\right), && \text{(F.8)}\\
&= \sum_{\sigma} \varphi_i(\mathbf{r}_1\sigma q_1)\ \varphi_j(\mathbf{r}_2\overline{\sigma} q_2)\ \frac{1}{2}\left(|\sigma\overline{\sigma}\rangle - |\overline{\sigma}\sigma\rangle\right), && \text{(F.9)}\\
&= \sum_{\sigma} \varphi_i(\mathbf{r}_1\sigma q_1)\ \varphi_j(\mathbf{r}_2\overline{\sigma} q_2)\ \frac{1}{2}(-)^{s-\sigma}\left(|\uparrow\downarrow\rangle - |\downarrow\uparrow\rangle\right), && \text{(F.10)}\\
&= \sum_{\sigma} (-)^{s-\sigma}\ \varphi_i(\mathbf{r}_1\sigma q_1)\ \varphi_j(\mathbf{r}_2\overline{\sigma} q_2)\ \frac{1}{\sqrt{2}}|00\rangle. && \text{(F.11)}
\end{aligned}$$

We get the expression for the matrix element of Eq. (F.4) :

$$\begin{aligned}
\langle ij|\hat{V}^{^1S_0}|kl\rangle \ = \ & \int d^3\mathbf{r}_{1,2,3,4} \ \sum_{q_1q_2}\sum_{\sigma_1}(-)^{s-\sigma_1}\ \varphi_i^*(\mathbf{r}_1\sigma_1 q_1)\ \varphi_j^*(\mathbf{r}_2\overline{\sigma}_1 q_2) \\
& \times \ \sum_{q_3q_4}\sum_{\sigma_3}(-)^{s-\sigma_3}\ \varphi_k(\mathbf{r}_3\sigma_3 q_3)\ \varphi_l(\mathbf{r}_4\overline{\sigma}_3 q_4) \\
& \times \ \frac{1}{2}\langle \mathbf{r}_1\mathbf{r}_2|\hat{V}^S|\mathbf{r}_3\mathbf{r}_4\rangle\ \langle q_1q_2|q_3q_4\rangle, && \text{(F.12)}
\end{aligned}$$

The antisymmetrized matrix element (containing both direct and exchange terms), which shall be written

$$\begin{aligned}
\overline{v}^{^1S_0}_{ijkl} \ = \ v^{^1S_0}_{ij\overline{kl}} \ &= \ \langle ij|\hat{\overline{V}}^{^1S_0}|kl\rangle, && \text{(F.13)}\\
&= \ \langle ij|\hat{V}^{^1S_0}(1 - P_r\hat{P}_\sigma\hat{P}_\tau)kl\rangle, && \text{(F.14)}\\
&= \ v^{^1S_0}_{ijkl} - v^{^1S_0}_{ijlk} \ = \ v^{^1S_0}_{ijkl} - v^{^1S_0}_{jikl}, && \text{(F.15)}
\end{aligned}$$

(the last equality holds for a Hermitian interaction) reads

$$\begin{aligned}
\overline{v}^{^1S_0}_{ijkl} \ &= \ \langle ij|\hat{V}^{^1S_0}(1 + \hat{P}_\sigma)|kl\rangle, && \text{(F.16)}\\
&= \ \int d^3\mathbf{r}_{1,2,3,4} \ \sum_{q_1q_2}\sum_{\sigma_1}(-)^{s-\sigma_1}\ \varphi_i^*(\mathbf{r}_1\sigma_1 q_1)\ \varphi_j^*(\mathbf{r}_2\overline{\sigma}_1 q_2) \\
&\qquad \times \ \sum_{q_3q_4}\sum_{\sigma_3}(-)^{s-\sigma_3}\ \varphi_k(\mathbf{r}_3\sigma_3 q_3)\ \varphi_l(\mathbf{r}_4\overline{\sigma}_3 q_4) \\
&\qquad \times \ \frac{1}{2}\langle \mathbf{r}_1\mathbf{r}_2|\hat{V}^S|\mathbf{r}_3\mathbf{r}_4\rangle\ \langle q_1q_2|1 + \hat{P}_\tau|q_3q_4\rangle. && \text{(F.17)}
\end{aligned}$$

In the case of isospin-pure states, we can omit isospin indices where they are contained in the single-particle states i, j, k, l. We obtain :

$$\begin{aligned}
\overline{v}^{^1S_0}_{ijkl} \ &= \ \langle ij|\hat{V}^{^1S_0}(1 + \hat{P}_\sigma)|kl\rangle, && \text{(F.18)}\\
&= \ \int d^3\mathbf{r}_{1,2,3,4}\ \Psi^*_{ij}(\mathbf{r}_1, \mathbf{r}_2)\ \frac{1}{2}\langle \mathbf{r}_1\mathbf{r}_2|\hat{V}^S|\mathbf{r}_3\mathbf{r}_4\rangle\ \Psi_{kl}(\mathbf{r}_3, \mathbf{r}_4) \\
&\qquad \times (\delta_{q_iq_k}\delta_{q_jq_l} + \delta_{q_iq_l}\delta_{q_jq_k}), && \text{(F.19)}
\end{aligned}$$

where we introduce the spin-singlet part of the two-body wavefunction (non-normalized) :

$$\Psi_{ij}(\mathbf{r}_1,\mathbf{r}_2) \;=\; \sum_{\sigma}(-)^{s-\sigma}\;\varphi_i(\mathbf{r}_1\sigma)\;\varphi_j(\mathbf{r}_2\overline{\sigma}). \tag{F.20}$$

The latter guarantees the antisymmetry of the matrix element in Eq. (F.18): if we exchange the spin variables,

$$\Psi_{ji}(\mathbf{r}_1,\mathbf{r}_2) \;=\; \sum_{\sigma}(-)^{s-\sigma}\;\varphi_j(\mathbf{r}_1\sigma)\;\varphi_i(\mathbf{r}_2\overline{\sigma}), \tag{F.21}$$

$$\;=\; -\sum_{\sigma}(-)^{s-\sigma}\;\varphi_i(\mathbf{r}_2\sigma)\;\varphi_j(\mathbf{r}_1\overline{\sigma}), \tag{F.22}$$

we get the opposite of the original wavefunction where the coordinates have been exchanged. If the spatial part of the interaction is symmetric w.r.t. this exchange (it then selects even-parity states of relative motion), the matrix element is indeed antisymmetric.

In the case of identical-particle pairing, $q_1 = q_2 = q_3 = q_4$ and the isospin part of the antisymmetrized matrix element reduces to a factor 2. We then have :

$$\overset{\hat{}}{\overline{V}}{}^{^1S_0}_{ijkl} \;=\; \int d^3\mathbf{r}_{1,2,3,4}\;\Psi^*_{ij}(\mathbf{r}_1,\mathbf{r}_2)\;\langle\mathbf{r}_1\mathbf{r}_2|\hat{V}^S|\mathbf{r}_3\mathbf{r}_4\rangle\;\Psi_{kl}(\mathbf{r}_3,\mathbf{r}_4), \tag{F.23}$$

where the spin-singlet two-body wave functions take care of the spin part and exchange term.

F.2 Computation of the pairing field

F.2.1 General technical aspects

In spherical symmetry, single-particle basis functions are labelled by quantum numbers n, ℓ, j, m:

$$\varphi_{n\ell jm}(\mathbf{r},\sigma) = \frac{u_{n\ell j}(r)}{r}\langle\ell m_\ell s\sigma|jm\rangle Y^\ell_{m_\ell}(\hat{r}) \tag{F.24}$$

The effective potentials are rotationally invariant: $\breve{\Delta}$ (see Eq. (5.56)) only depends on the radial coordinate in use. This isotropy stems from that of the density matrix: states labelled with the same value of quantum numbers n, ℓ, j (and different values of the projection m) are degenerate, have identical occupancies and have the same radial dependance. It is thus possible to perform analytical presummations over m whenever applicable, especially in the calculation of $\breve{\chi}$.

F.2.2 Center-of-mass/relative coordinate separation

The calculation of pairing matrix elements with a non-local separable vertex requires to perform the transformation of the two-body product wave function from the set of coordinates $(\mathbf{r}_1, \mathbf{r}2)$ corresponding to the interacting particles to the set $(\mathbf{R}, \mathbf{s})$, where $\mathbf{R} = \frac{1}{2}(\mathbf{r}_1 + \mathbf{r}_2)$ is the center-of-mass (COM) coordinate and $\mathbf{s} = \mathbf{r}_1 - \mathbf{r}_2$ is the separation vector. Whereas this is immediate in Cartesian coordinates, in a spherical coordinate system or basis, some algebra is involved to obtain useful expressions. There are standard techniques to achieve this in a harmonic oscillator

basis, most based on Brody-Moshinsky coefficients [Mos59]. However, since one of the purposes of this work is to provide a description of pairing up to the drip-lines, we used a basis more suited to the treatment of continuum effects. Thus, we used the coordinate separation method of Sawaguri and Tobocman [Saw67]:

$$\phi_{\ell m}(\alpha\mathbf{r}_a+\beta\mathbf{r}_b) = \sum_{l'\lambda'} A_l^{l'\lambda'}(r_a,r_b)\sum_{m'\mu'}\frac{1}{\sqrt{4\pi}}C^{lm}_{l'\overline{m}'\lambda'\overline{\mu}'}Y^{l'}_{m'}(\hat{r}_a)Y^{\lambda'}_{\mu'}(\hat{r}_b) \quad \text{(F.25)}$$

$$A_l^{l'\lambda'}(r_a,r_b) = 8\,i^{l'-\lambda'-\ell}\int k^2dk\; j_{l'}(\alpha kr_a)j_{\lambda'}(\beta kr_b)\int r^2dr\; j_\ell(kr)\phi_\ell(r) \quad \text{(F.26)}$$

(this expression is readily obtained by rewriting the wave function $\phi(\mathbf{r})$ as the direct-then-reverse Fourier transform (FT) of itself, replacing $\mathbf{r}=\alpha\mathbf{r}_a+\beta\mathbf{r}_b$ in the reverse FT part, then replacing the three exponentials by their spherical expansion and integrating over angular coordinates). Using this expression, we find

$$\begin{aligned}\Psi_{n_1\ell jm,n_2\ell j\overline{m}}(\mathbf{R},\mathbf{s}) &= \sum_{m_\ell\sigma}(-)^{s-\sigma}\langle\ell m_\ell s\sigma|jm\rangle\langle\ell\overline{m}_\ell s\overline{\sigma}|j\overline{m}\rangle\\ &\times\sum_{l'_1l'_2\lambda'_1\lambda'_2}A^{l'_1\lambda'_1}_{n_1\ell j}(R,s)A^{l'_2\lambda'_2}_{n_2\ell j}(R,s)\\ &\times\frac{1}{4\pi}\sum_{m'_1m'_2\mu'_1\mu'_2}C^{\ell m_\ell}_{l'_1\overline{m}'_1\lambda'_1\overline{\mu}'_1}C^{\ell\overline{m}_\ell}_{l'_2m'_2\lambda'_2\mu'_2}\\ &\times Y^{l'_1}_{m'_1}(\hat{R})Y^{l'_2}_{\overline{m}'_2}(\hat{R})Y^{\lambda'_1}_{\mu'_1}(\hat{s})Y^{\lambda'_2}_{\overline{\mu}'_2}(-\hat{s}),\end{aligned} \quad \text{(F.27)}$$

with

$$A^{l'\lambda'}_{nlj}(R,s) = 8\,i^{l'-\lambda'-l}\int kdk\; j_{l'}(kR)j_{\lambda'}\left(\frac{ks}{2}\right)\breve{u}_{nlj}(k) \quad \text{(F.28)}$$

$$\breve{u}_{nlj}(k) = k\int rdr\; j_\ell(kr)u_{n\ell j}(r) \quad \text{(F.29)}$$

Multiplying by the separable-interaction form factor $G_\alpha(s)$ and integrating over $\mathbf{s}$ yields

$$\begin{aligned}\breve{\Psi}^\alpha_{n_1\ell jm,n_2\ell j\overline{m}}(\mathbf{R}) &= \sum_{m_\ell\sigma}(-)^{s-\sigma}\langle\ell m_\ell s\sigma|jm\rangle\langle\ell\overline{m}_\ell s\overline{\sigma}|j\overline{m}\rangle\\ &\times\sum_{l'_1l'_2\lambda'}\int s^2ds\; G_\alpha(s)\,A^{l'_1\lambda'}_{n_1\ell j}(R,s)A^{l'_2\lambda'}_{n_2\ell j}(R,s)\\ &\times\frac{1}{4\pi}\sum_{m'\mu'}C^{\ell m_\ell}_{l'_1\overline{m}'\lambda'\overline{\mu}'}C^{\ell\overline{m}_\ell}_{l'_2m'\lambda'\mu'}(-)^{\lambda'+\mu'}\\ &\times Y^{l'_1}_{m'}(\hat{R})Y^{l'_2}_{\overline{m}'}(\hat{R}),\end{aligned} \quad \text{(F.30)}$$

where the integration with respect to the angular coordinates yields the spherical harmonic coupling coefficients.

F.2.3 Pair densities

Pair densities $\breve{\chi}_\alpha$ can be expressed as (Eq. (5.52))

$$\breve{\chi}_\alpha(\mathbf{R}) = \sum_{n_{1,2}\ell_{1,2}j_{1,2}m_{1,2}}\breve{\Psi}^\alpha_{n_1\ell_1j_1m_1,n_2\ell_1j_1\overline{m}_2}(\mathbf{R})\;\kappa_{n_1\ell_1j_1m_1,n_2\ell_1j_1\overline{m}_2}. \quad \text{(F.31)}$$

In spherical systems, the pair tensor κ takes the simplified form

$$\kappa_{n_1\ell_1 j_1 m_1, n_2\ell_1 j_1 \overline{m}_2} = \kappa_{n_1,n_2;\ell_1 j_1}\ (-)^{\ell-j-m}\ \delta_{\ell_1\ell_2}\ \delta_{j_1 j_2}\ \delta_{m_1 m_2}, \tag{F.32}$$

where $(-)^{\ell-j-m}$ is the phase $\eta_{\ell jm}$ acquired by state $|n\ell jm\rangle$ under a time-reversal transformation, which determines the splitting in two parts of the single-particle basis, such that

$$\breve{\chi}_\alpha(\mathbf{R}) = \sum_{\ell j}\sum_{n_1 n_2} \kappa_{n_1,n_2;\ell j} \sum_m (-)^{\ell-j-m} \breve{\Psi}^\alpha_{n_1\ell jm, n_2\ell j\overline{m}}(\mathbf{R}) \tag{F.33}$$

Due to the spherical degeneracy of single-particle states and the specific structure of κ, the summation with respect to m can be separated and performed analytically. It is thus beneficial to define the function

$$\overline{\breve{\Psi}}^\alpha_{n_1\ell j, n_2\ell j}(\mathbf{R}) \ = \ \sum_m (-)^{\ell-j-m} \breve{\Psi}^\alpha_{n_1\ell jm, n_2\ell j\overline{m}}(\mathbf{R}). \tag{F.34}$$

In order to express this function, let us first give the result of the reduction of its algebraic factor:

$$\begin{aligned}
&\sum_{mm_\ell\sigma m'\mu'} (-)^{\ell-j-m+s-\sigma} \langle \ell m_\ell s\sigma | jm\rangle \langle \ell\overline{m}_\ell s\overline{\sigma}|j\overline{m}\rangle \\
&\quad \times C^{\ell m_\ell}_{l'_1\overline{m}'\lambda'\overline{\mu}'} C^{\ell\overline{m}_\ell}_{l'_2 m'\lambda'\mu'} (-)^{\lambda'+\mu'}\ Y^{l'_1}_{m'}(\hat{R})\ Y^{l'_2}_{\overline{m}'}(\hat{R}) \\
&\quad = \ -\frac{2j+1}{4\pi}\frac{(2l'_1+1)(2\lambda'+1)}{2\ell+1}\langle l'_1 0\lambda' 0|\ell 0\rangle^2 \delta_{l'_1 l'_2}(-)^{\lambda'},
\end{aligned} \tag{F.35}$$

which yields

$$\begin{aligned}
\overline{\breve{\Psi}}^\alpha_{n_1\ell j, n_2\ell j}(\mathbf{R}) \ &= \ -\frac{2j+1}{(4\pi)^2} \\
&\quad \times \sum_{l'\lambda'} \int s^2 ds\ G_\alpha(s) A^{l'\lambda'}_{n_1\ell j}(R,s) A^{l'\lambda'}_{n_2\ell j}(R,s) \\
&\quad \times (-)^{\lambda'} \frac{(2l'+1)(2\lambda'+1)}{2\ell+1}\langle l'0\lambda'0|\ell 0\rangle^2
\end{aligned} \tag{F.36}$$

once this reduction has been made, it is possible to rewrite the radial integral with respect to s:

$$(-1)^{l'-\lambda'-\ell}\frac{1}{4\pi}\int s^2 e^{-\frac{s^2}{4\alpha^2}} A^{l'\lambda'}_{n_1\ell j}(R,s) A^{l'\lambda'}_{n_2\ell j}(R,s) \tag{F.37}$$

$$\begin{aligned}
&= \ \frac{16}{\pi}\int k_1 dk_1\ j_{l'}(k_1 R)\ \breve{u}_{n_1\ell j}(k_1) \int k_2 dk_2\ j_{l'}(k_2 R)\ \breve{u}_{n_1\ell j}(k_2) \\
&\quad \times \int s^2\ G_\alpha(s)\ j_{\lambda'}\left(\frac{k_1 s}{2}\right)\ j_{\lambda'}\left(\frac{k_2 s}{2}\right)
\end{aligned} \tag{F.38}$$

$$= \ \int k_1 dk_1\ \breve{u}_{n_1\ell j}(k_1) \int k_2 dk_2\ \breve{u}_{n_2\ell j}(k_2)\ \breve{\psi}^{\alpha,l'\lambda'}(k_1,k_2;R), \tag{F.39}$$

where we introduce the representation-independent functions (mind the small ψ)

$$\begin{aligned}
\check{\psi}^{\alpha,l'\lambda'}(k_1,k_2;R) &= \frac{16}{\pi}\, j_{l'}(k_1R)\, j_{l'}(k_2R) \\
&\quad \times \int s^2\, G_\alpha(s)\, j_{\lambda'}\left(\frac{k_1 s}{2}\right)\, j_{\lambda'}\left(\frac{k_2 s}{2}\right), \qquad \text{(F.40)} \\
\overline{\check{\psi}}^{\alpha}_{\ell}(k_1,k_2;R) &= \sum_{l'\lambda'} \check{\psi}^{\alpha,l'\lambda'}(k_1,k_2;R) \\
&\quad \times (-)^{\ell-l'}\frac{(2l'+1)(2\lambda'+1)}{2\ell+1}\langle l'0\lambda'0|\ell 0\rangle^2. \qquad \text{(F.41)}
\end{aligned}$$

Using the latter function one can finally write

$$\overline{\breve{\Psi}}^{\alpha}_{n_1\ell j,n_2\ell j}(\mathbf{R}) = -\frac{2j+1}{4\pi}\int k_1dk_1\; k_2dk_2\; \overline{\check{\psi}}^{\alpha}_{\ell}(k_1,k_2;R)\; \breve{u}_{n_1\ell j}(k_1)\; \breve{u}_{n_1\ell j}(k_2). \qquad \text{(F.42)}$$

F.2.4 Pairing fields

Matrix elements of the pairing fields are obtained through (Eq. (5.55))

$$\begin{aligned}
\Delta_{n_1\ell jm,n_2\ell j\overline{m}} &= \sum_\alpha \int d^3\mathbf{R}\; \breve{\Psi}^{\alpha}_{n_1\ell jm,n_2\ell j\overline{m}}(\mathbf{R})\; \breve{\Delta}_\alpha(\mathbf{R}) \qquad \text{(F.43)} \\
&= \sum_\alpha \int R^2dR\; d\hat{R}\; \breve{\Psi}^{\alpha}_{n_1\ell jm,n_2\ell j\overline{m}}(\mathbf{R})\; \breve{\Delta}_\alpha(R), \qquad \text{(F.44)}
\end{aligned}$$

an expression where the angular integral with respect to the direction $\hat{R}$ allows one to reduce the sums involving projection indices, viz.

$$\begin{aligned}
&\sum_{m_\ell\sigma m'\mu'} (-)^{s-\sigma}\langle \ell m_\ell s\sigma|jm\rangle\langle \ell\overline{m}_\ell s\overline{\sigma}|j\overline{m}\rangle \\
&\quad\times C^{\ell m_\ell}_{l'_1\overline{m}'\lambda'\overline{\mu}'} C^{\ell\overline{m}_\ell}_{l'_2 m'\lambda'\mu'}(-)^{\lambda'+\mu'}\int d\hat{R}\; Y^{l'_1}_{m'}(\hat{R})\; Y^{l'_2}_{\overline{m}'}(\hat{R}) \\
&\quad= -(-)^{\ell-j-m}\frac{(2l'_1+1)(2\lambda'+1)}{2\ell+1}\langle l'0\lambda'0|\ell 0\rangle^2\delta_{l'_1l'_2}(-)^{\lambda'}. \qquad \text{(F.45)}
\end{aligned}$$

Given this expression, one obtains

$$\begin{aligned}
\Delta_{n_1\ell jm,n_2\ell j\overline{m}} &= -(-)^{\ell-j-m}\,\frac{1}{4\pi}\sum_\alpha \\
&\quad\times\sum_{l'\lambda'}\int R^2dR\int s^2ds\; G_\alpha(s)A^{l'\lambda'}_{n_1\ell j}(R,s)A^{l'\lambda'}_{n_2\ell j}(R,s)\breve{\Delta}_\alpha(R) \\
&\quad\times(-)^{\lambda'}\frac{(2l'+1)(2\lambda'+1)}{2\ell+1}\langle l'0\lambda'0|l0\rangle^2. \qquad \text{(F.46)}
\end{aligned}$$

It is then useful to use the representation-independent functions (F.39), yielding

$$\begin{aligned}
\Delta_{n_1\ell jm,n_2\ell j\overline{m}} &= -(-)^{\ell-j-m}\int R^2dR\; \breve{\Delta}_\alpha(R) \qquad \text{(F.47)} \\
&\quad\times\int k_1dk_1\; k_2dk_2\; \overline{\breve{\psi}}_{\alpha,\ell}(k_1,k_2;R)\; \breve{u}_{n_1\ell j}(k_1)\; \breve{u}_{n_2\ell j}(k_2),
\end{aligned}$$

Eq. (F.42) allows one to work with any basis for which one can compute $\check{u}(k)$ functions. A particularly simple and efficient choice is to use a basis of spherical Bessel functions, in this case we have $\check{u}_{n_i\ell j}(k) \propto \delta(k - k_i)$ and the double integral becomes trivial. See appendix G.

F.3 Evaluation of Bessel-form factor integrals

The formulae given above for $\overline{\check{\psi}}$ and $\overline{\check{\Psi}}$ functions involve an integral of the product of two Bessel functions, an interaction form factor and a s^2 weight.

$$\mathcal{I}^{\alpha}_{\lambda'_1\lambda'_2}(k_1,k_2) \equiv \int s^2\, G_\alpha(s)\, j_{\lambda'_1}\left(\frac{k_1 s}{2}\right) j_{\lambda'_2}\left(\frac{k_2 s}{2}\right). \tag{F.48}$$

This section deals with the evaluation of this integral for a number of given form factors $g(k)$ and their inverse Fourier transforms $G(s)$ (see Eq. (5.46)).

F.3.1 Simple Gaussian form factor

For $g(k) = e^{-a^2k^2}$, the inverse Fourier transform yields

$$G(s) = \tfrac{1}{(4\pi a^2)^{3/2}}\, e^{-\frac{s^2}{4a^2}} \tag{F.49}$$

In the case where $\lambda'_1 = \lambda'_2 \equiv \lambda'$, the integral (F.48) can be evaluated using an analytical expression (F.70), yielding :

$$\mathcal{I}^{\alpha}_{\lambda'\lambda'}(k_1,k_2) = \frac{1}{4\pi}\, \exp\left(-\frac{a^2(k_1^2+k_2^2)}{4}\right)\, b_{\lambda'}\left(-\frac{a^2 k_1 k_2)}{2}\right), \tag{F.50}$$

where $b_{\lambda'}$ is a modified spherical Bessel function of the first kind, Eq. (F.71). If $\lambda_1 \neq \lambda_2$, one should use the more general method described below.

F.3.2 Gaussian $\times$ polynomial form factor

In fits of an operator representation of the $V_{\text{low } k}$ interaction, we found the following form of form factors to be the most useful one:

$$g_\alpha(k) = \left[\sum_n x_{\alpha n}\left(\frac{a_\alpha^2 k^2}{2}\right)^n\right] \exp\left(-\frac{a_\alpha^2 k^2}{2}\right). \tag{F.51}$$

where a_α is a range parameter, while the $x_{\alpha n}$'s control the way the shape of the Gaussian function is modulated by powers of k^2. The inverse Fourier transform reads

$$G_\alpha(s) = \frac{1}{(2\pi)^{3/2}a^3}\left[\sum_n x_{\alpha n}\left(-\tfrac{1}{2}\right)^n \left(\frac{a}{s}\right) \mathrm{He}_{2n+1}\left(\frac{s}{a}\right)\right]\, \exp\left(-\frac{s^2}{2a_\alpha^2}\right), \tag{F.52}$$

where He_{2n+1} is a "probabilist's" Hermite polynomial [Abr64]. The integral in Eq. (F.48) can be evaluated by Gauss-Hermite integration [Pre92], which is based on the formula

$$\int_{-\infty}^{\infty} f(x) e^{-x^2} = \sum_{i=1}^{N} w_i\, f(x_i) \tag{F.53}$$

where the x_i are the roots of $H_N(x)$, the (more common) "physicist's" Hermite polynomial[1]. To apply the formula above, one needs to perform the change of variable $x = \frac{s}{a_\alpha\sqrt{2}}$, which depends on the range a_α. For the sake of performance, one should use a single variable for all form factors, as the Bessel functions have to be evaluated for each integration point : different sets of s_i stemming from each set of x_i would multiply an important contribution to the CPU time by the number of form factors. It is advisable to simply re-express $G_\alpha(s)$ as

$$\begin{aligned} G_\alpha(s) &= \frac{1}{(2\pi)^{3/2}a^3}\left[\sum_n x_{\alpha n}\left(-\tfrac{1}{2}\right)^n\left(\frac{a_\alpha}{s}\right)\mathrm{He}_{2n+1}\left(\frac{s}{a_\alpha}\right)\right] \\ &\quad\times\ \exp\left[-\left(\frac{1}{2a_\alpha^2}-\frac{1}{2a_{\max}^2}\right)s^2\right]\ \exp\left(-\frac{s^2}{2a_{\max}^2}\right), \end{aligned} \tag{F.54}$$

where $a_{\max} = \max_\alpha(a_\alpha)$, and use the variable $x = \frac{s}{a_{\max}\sqrt{2}}$. The sign of the argment of the first exponential guarantees that it is a well-behaved function which poses no problem with the quadrature scheme.

F.3.3 Coulomb expansion form factor

The separable representation for a truncated Coulomb potential involves the form factor $g_\alpha(k) = \sqrt{2\pi}\, j_\alpha^2(\frac{ak}{2})$. The inverse Fourier transform yields

$$G_\alpha(s) = \frac{1}{\sqrt{2\pi}a^2}\begin{cases} \frac{1}{s}P_\alpha\left(1-2(\frac{s}{a})^2\right) & \text{for} \quad s \le a \\ 0 & \text{for} \quad s > a \end{cases}, \tag{F.55}$$

where P_α is the Legendre polynomial of order α. The integral to be calculated is thus :

$$\mathcal{I}^\alpha_{\lambda'_1\lambda'_2}(k_1,k_2) = \frac{1}{\sqrt{2\pi}a^2}\int_0^a s\ P_\alpha\left(1-2(\tfrac{s}{a})^2\right)\ j_{\lambda'_1}\left(\frac{k_1 s}{2}\right)\ j_{\lambda'_2}\left(\frac{k_2 s}{2}\right). \tag{F.56}$$

There is no useful analytical expression for this integral, but it can be evaluated efficiently by using a Gauss-Legendre integration scheme [Pre92].

F.4 Some useful expressions

Spherical harmonics

We define spherical-harmonic coupling coefficients

$$C^{LM}_{l_1m_1l_2m_2} = \sqrt{\frac{(2l_1+1)(2l_2+1)}{(2L+1)}}\langle l_1 0 l_2 0|L0\rangle\langle l_1 m_1 l_2 m_2|LM\rangle, \tag{F.57}$$

which thus follow :

$$C^{LM}_{l_1m_1l_2m_2} = (-)^{m_2}C^{l_1m_1}_{LMl_2\overline{m}_2}, \tag{F.58}$$

$$= (-)^{m_1}C^{l_2m_2}_{l_1\overline{m}_1LM}, \tag{F.59}$$

$$= (-)^{l_1+l_2-L}C^{L\overline{M}}_{l_1\overline{m}_1l_2\overline{m}_2}, \tag{F.60}$$

[1] We shall use only the points $x_i > 0$ to calculate the integral from 0 to ∞. One can show that this remains a valid Gauss quadrature scheme, which is equivalent to the Gauss-Laguerre one with a change of variable $u = x^2$.

and

$$\sum_{m_1 m_2} C^{LM}_{l_1 m_1 l_2 m_2} C^{L'M'}_{l_1 m_1 l_2 m_2} = \frac{(2l_1+1)(2l_2+1)}{(2L+1)} \langle l_1 0 l_2 0 | L0 \rangle^2 \delta_{LL'} \delta_{MM'}. \tag{F.61}$$

the later expression involves the coefficient $\langle l_1 0 l_2 0 | L0 \rangle$, which is non-vanishing only in the case of even $l_1 + l_2 + L$.

The following expressions hold:

$$\int d\hat{r}\ Y^{l_1}_{m_1}(\hat{r}) Y^{l_2}_{m_2}(\hat{r}) Y^{L*}_{M}(\hat{r}) = \frac{1}{\sqrt{4\pi}} C^{LM}_{l_1 m_1 l_2 m_2} \tag{F.62}$$

$$Y^{l*}_{m}(\hat{r}) = (-)^m\ Y^{l}_{\overline{m}}(\hat{r}) \tag{F.63}$$

$$Y^{l}_{m}(-\hat{r}) = (-)^l\ Y^{l}_{m}(\hat{r}) \tag{F.64}$$

$$\int d\hat{r}\ Y^{l}_{m}(\hat{r}) Y^{l'*}_{m'}(\hat{r}) = \delta_{ll'} \delta_{mm'} \tag{F.65}$$

$$\sum_{m} Y^{l}_{m}(\hat{r}) Y^{l*}_{m}(\hat{r}') = \frac{2l+1}{4\pi} P_l(\cos\theta) \tag{F.66}$$

$$\sum_{lm} Y^{l}_{m}(\hat{r}) Y^{l*}_{m}(\hat{r}') = \delta(\hat{r} - \hat{r}') \tag{F.67}$$

where P_l is the l^{th}-order Legendre polynomial, θ the angle between $\hat{r}$ and $\hat{r}'$; for $\hat{r} = \hat{r}'$, $P_l(cos\theta) = P_l(1) = 1$.

Spherical Bessel functions

The normalization condition for spherical Bessels over a finite interval reads

$$\int_0^1 t^2 dt\ j_l(a_i t) j_l(a_j t) = \delta_{ij} \frac{1}{2} [j'_l(a_i)]^2, \tag{F.68}$$

where a_i is the i^{th} zero of j_l. Additionally, the following integral relations are useful:

$$\int_0^\infty r^2 dr\ j_l(kr) j_l(k'r) = \frac{\pi}{2kk'} \delta(k - k') \tag{F.69}$$

$$\int_0^\infty x^2 dx\ e^{-c^2 x^2} j_l(ax) j_l(bx) = \frac{\sqrt{\pi}}{4c^3} e^{-\frac{a^2+b^2}{4c^2}} b_l\left(\frac{ab}{2c^2}\right) \tag{F.70}$$

where

$$b_l(x) = i^{-l} j_l(ix) = \sqrt{\frac{\pi}{2x}}\, I_{l+\frac{1}{2}}(x) \tag{F.71}$$

is the modified spherical Bessel function of the first kind.

Appendix G

Spherical Bessel Function Basis

In the spherical calculations performed in this work, we use a basis of single-particle states relying on spherical Bessel functions, which correspond to the radial part of free spherical waves. Labelled $j_\ell(kr)$, these functions are the solutions (non-divergent at $r = 0$) of

$$\left[\frac{1}{r^2}\frac{d}{dr}\left(r^2\frac{d}{dr}\right) + \left(k^2 - \frac{\ell(\ell+1)}{r^2}\right)\right] j_\ell(kr) = 0. \tag{G.1}$$

Considering an infinite spherically-symmetric square well (a "box") of radius $R_{\rm box}$, one can build the sequence of its eigenstates. They are given by Eq. (G.1) with the boundary condition $j_\ell(kR_{\rm box}) = 0$, which produces a discrete spectrum for each value of ℓ. Let us call $k_{i,\ell}, i = 1 \ldots N_\ell$ the solutions of the above in the interval $[0, k_{\rm cut}]$. In the case $\ell = 0$, $j_0(kr) = sin(kr)/kr$ and $k_{i,0} = i(\pi/R_{\rm box})$.

Actual basis functions are defined in the direct product of three-dimensional coordinate space and spin space, and should be normalized. First in a spin-independent case, one can check that such a basis can be taken as

$$\phi_{i,\ell m_\ell}(\mathbf{r}) = \sqrt{\frac{2}{R_{\rm box}^3}}\frac{1}{|j'_\ell(k_{i,\ell}R_{\rm box})|}\; j_\ell(k_{i,\ell}r)Y^\ell_{m_\ell}(\hat{r}), \tag{G.2}$$

where j'_ℓ is the derivative of j_ℓ with respect to its argument. Next we apply spin-orbit coupling to the latter, yielding

$$\begin{aligned}
\varphi_{i,\ell jm}(\mathbf{r},\sigma) &= \langle \ell m_\ell s\sigma | jm\rangle\; \phi_{i,\ell m_\ell}(\mathbf{r}), & \text{(G.3)}\\
&= \langle \ell m_\ell s\sigma | jm\rangle\; \frac{u_{i,\ell}(r)}{r}Y^\ell_{m_\ell}(\hat{r}), & \text{(G.4)}\\
u_{i,\ell}(r) &= \begin{cases} \sqrt{\frac{2}{R_{\rm box}^3}}\frac{r}{|j'_\ell(k_{i,\ell}R_{\rm box})|}\; j_\ell(k_{i,\ell}r) & \text{for} \quad r < R_{\rm box} \\ 0 & \text{for} \quad r \geq R_{\rm box} \end{cases} & \text{(G.5)}
\end{aligned}$$

Spherical Bessel functions occur naturally in the coordinate separation method summarized by Eq. (F.42), which can be simplified when using the basis above. Let us consider the definition of $\check{u}$ functions (Eq. (F.29), with adapted notation)

$$\check{u}_{i,\ell}(k) = k\int_0^\infty rdr\; j_\ell(kr)\; u_{i,\ell}(r), \tag{G.6}$$

Replacing $u_{i,\ell}(r)$ with Eq. (G.5) yields

$$\check{u}_{i,\ell}(k) = \sqrt{\frac{2}{R_{\rm box}^3}}\frac{1}{|j'_\ell(k_{i,\ell}R_{\rm box})|}k\int_0^{R_{\rm box}} r^2dr\; j_\ell(kr)\; j_\ell(k_{i,\ell}r), \tag{G.7}$$

which can be evaluated, albeit into a non-trivial function. However, it is possible to achieve considerable simplification by performing the above integral with an infinite upper bound. This amounts to continuing the wave function $u(r)$ beyond the limits of the box. The spherical expansion for the two-body wave function will thus contain components corresponding to particles outside of the box. Nevertheless, since we work with finite-range interactions, we are only interested in components with an interparticle separation less than this range. Consequently, spurious components can only be expected to have an effect near the box boundary. The pair tensor, in turn, can be expected to have non-vanishing components only in regions of significant density in the nucleus, which means the effective pairing fields themselves vanish outside of the nucleus. This approximation thus seems reasonable, only having to be confirmed by checking the independence of results with respect to the box radius, as should always be checked anyway.

Using the normalization condition in the continuum, Eq. (F.69), to evaluate Eq. (G.7), yields

$$\check{u}_{i,\ell}(k) = \frac{\pi}{\sqrt{2R_{\text{box}}^3}} \frac{1}{k_{i,\ell}|j'_\ell(k_{i,\ell}R_{\text{box}})|} \delta(k - k_{i,\ell}). \tag{G.8}$$

Reduced two-body basis functions then read

$$\overline{\check{\Psi}}_{i_1\ell j,i_2\ell j}(\mathbf{R}) = -\frac{(2j+1)}{4\pi}\frac{\pi^2}{2R_{\text{box}}^3} \frac{1}{|j'_\ell(k_{i_1,\ell}R_{\text{box}})\ j'_\ell(k_{i_2,\ell}R_{\text{box}})|} \overline{\check{\psi}}^{\alpha}_{\ell}(k_{i_1,\ell}, k_{i_2,\ell}; R), \tag{G.9}$$

recalling the expression for $\overline{\check{\psi}}^{\alpha}_{\ell}$ (F.41)

$$\begin{aligned}\overline{\check{\psi}}^{\alpha}_{\ell}(k_1, k_2; R) &= \frac{16}{\pi} \sum_{\ell'\lambda'} (-)^{\ell-\ell'} \frac{(2\ell'+1)(2\lambda'+1)}{2\ell+1} \langle \ell' 0 \lambda' 0 | \ell 0 \rangle^2\ j_{\ell'}(k_1 R)\ j_{\ell'}(k_2 R) \\ &\quad \times \int s^2\ G_\alpha(s)\ j_{\lambda'}\left(\frac{k_1 s}{2}\right) j_{\lambda'}\left(\frac{k_2 s}{2}\right)\end{aligned} \tag{G.10}$$

The function $\overline{\check{\Psi}}$ can thus be expressed as

$$\begin{aligned}\overline{\check{\Psi}}_{i_1\ell j,i_2\ell j}(\mathbf{R}) &= -\frac{(2j+1)}{4\pi}\ \frac{8\pi}{R_{\text{box}}^3} \frac{1}{|j'_\ell(k_{i_1,\ell}R_{\text{box}})\ j'_\ell(k_{i_2,\ell}R_{\text{box}})|} \\ &\quad \times \sum_{l'\lambda'} (-)^{\ell-\ell'} \frac{(2\ell'+1)(2\lambda'+1)}{2\ell+1} \langle \ell' 0 \lambda' 0 | \ell 0 \rangle^2\ j_{\ell'}(k_{i_1,\ell}R)\ j_{\ell'}(k_{i_2,\ell}R) \\ &\quad \times \int s^2\ G_\alpha(s)\ j_{\lambda'}\left(\frac{k_{i_1,\ell} s}{2}\right) j_{\lambda'}\left(\frac{k_{i_2,\ell} s}{2}\right).\end{aligned} \tag{G.11}$$

The integral can be evaluated with the methods exposed in appendix F.3, which completes the set of equations we need to work with a separable, finite-ranged and non-local force in the particle-particle channel of HFB equations.

Bibliography

[Abr63] A. A. Abrikosov, L. P. Gorkov, I. E. Dzyaloshinski, *Methods of Quantum Field Theory in Statistical Physics*, Prentice-Hall (1963)

[Abr64] M. Abramowitz, I. A. Stegun, editors, *Handbook of Mathematical Functions* (1964)

[Akm98] A. Akmal, V. R. Pandharipande, D. G. Ravenhall, *Equation of state of nucleon matter and neutron star structure*, Phys. Rev. C 58 (1998) 1804–1828

[Ald56] K. Alder, A. Bohr, T. Huus, B. Mottelson, A. Winther, *Study of Nuclear Structure by Electromagnetic Excitation with Accelerated Ions*, Rev. Mod. Phys. 28 (1956) 432

[Alm96] T. Alm, G. Röpke, A. Schnell, N. H. Kwong, H. S. Köhler, *Nucleon spectral function at finite temperature and the onset of superfluidity in nuclear matter*, Phys. Rev. C 53 (1996) 2181–2193

[Amu85] L. Amundsen, E. Østgaard, *Superfluidity of neutron matter : (II). Triplet pairing*, Nucl. Phys. A 442 (1985) 163–188

[And59] P. W. Anderson, *Theory of dirty superconductors*, Jour. Phys. Chem. Sol. 11 (1959) 26–30

[And84] P. W. Anderson, *Structure of "triplet" superconducting energy gaps*, Phys. Rev. B 30 (1984) 4000

[Ang01a] M. Anguiano, J. L. Egido, L. M. Robledo, *Coulomb exchange and pairing contributions in nuclear Hartree-Fock-Bogoliubov calculations with the Gogny force*, Nucl. Phys. A 683 (2001) 227–254

[Ang01b] M. Anguiano, J. L. Egido, L. M. Robledo, *Particle number projection with effective forces*, Nucl. Phys. A 696 (2001) 467–493

[Ang04] I. Angeli, Atom. Data Nucl. Data Tables 87 (2004) 185

[Aud03] G. Audi, A. H. Wapstra, C. Thibault, *The 2003 atomic mass evaluation: (II). Tables, graphs and references*, Nucl. Phys. A 729 (2003) 337 – 676

[Avo07] P. Avogadro, F. Barranco, R. A. Broglia, E. Vigezzi, *Quantum calculation of vortices in the inner crust of neutron stars*, Phys. Rev. C 75 (2007) 012805–5

[Bal86] M. Baldo, L. S. Ferreira, L. Streit, T. Vertse, *Gamow separable approximations for realistic N-N interactions: Single channel case*, Phys. Rev. C 33 (1986) 1587

[Bal87] M. Baldo, L. S. Ferreira, L. Streit, *Eigenvalue problem for Gamow vectors and a separable approximation for the N-N interaction*, Phys. Rev. C 36 (1987) 1743

[Bal90] M. Baldo, J. Cugnon, A. Lejeune, U. Lombardo, *Superfluidity in neutron matter and nuclear matter with realistic interactions*, Nucl. Phys. A 515 (1990) 409–432

[Bal98] M. Baldo, O. Elgarøy, L. Engvik, M. Hjorth-Jensen, H.-J. Schulze, $^3P_2 - ^3F_2$ *pairing in neutron matter with modern nucleon-nucleon potentials*, Phys. Rev. C 58 (1998) 1921–1928

[Bal99] M. Baldo, *Nuclear methods and the nuclear equation of state*, Int. Rev. Nucl. Phys., Vol 9, World Scientific, Singapore (1999)

[Bal00a] M. Baldo, A. Grasso, *Dispersive effects in neutron matter superfluidity*, Phys. Lett. B 485 (2000) 115–120

[Bal00b] M. Baldo, U. Lombardo, E. Saperstein, M. Zverev, *A simple model for the microscopic effective pairing interaction*, Phys. Lett. B 477 (2000) 410–415

[Bal01] M. Baldo, A. Grasso, *Microscopic theory of strong superfluidity*, Phys. At. Nucl. 64 (2001) 611–618

[Bal02] M. Baldo, U. Lombardo, H. J. Schulze, Z. Wei, *Self-energy effects on isospin singlet pairing in nuclear matter*, Phys. Rev. C 66 (2002) 054304

[Bal03] M. Baldo, M. Farine, U. Lombardo, E. Saperstein, P. Schuck, M. Zverev, *Surface behaviour of the pairing gap in a slab of nuclear matter*, Eur. Phys. Jour. A 18 (2003) 17–23

[Bal06] M. Baldo (2006). Private communication

[Bal07a] M. . Baldo, C. Maieron, *Equation of state of nuclear matter at high baryon density*, Jour. Phys. G 34 (2007) R243–R283

[Bal07b] M. Baldo, P. Schuck, X. V. nas, *Khon-Sham Density Functional Inspired Approach to Nuclear Binding* ArXiv:0706.0658

[Bal07c] M. Baldo, H. J. Schulze, *Proton pairing in neutron stars*, Phys. Rev. C 75 (2007) 025802–6

[Bar57a] J. Bardeen, L. N. Cooper, J. R. Schrieffer, *Microscopic Theory of Superconductivity*, Phys. Rev. 106 (1957) 162

[Bar57b] J. Bardeen, L. N. Cooper, J. R. Schrieffer, *Theory of Superconductivity*, Phys. Rev. 108 (1957) 1175

[Bar82a] J. Bartel, P. Quentin, M. Brack, C. Guet, H. B. Hakansson, *Towards a better parametrisation of Skyrme-like effective forces: A critical study of the SkM force*, Nucl. Phys. A 386 (1982) 79–100

[Bar82b] J. Bartel, P. Quentin, M. Brack, C. Guet, H. B. Håkansson, *Towards a better parametrisation of Skyrme-like effective forces: A critical study of the SkM force*, Nucl. Phys. A 386 (1982) 79 – 100

[Bar99] F. Barranco, R. A. Broglia, G. Gori, E. Vigezzi, P. F. Bortignon, J. Terasaki, *Surface Vibrations and the Pairing Interaction in Nuclei*, Phys. Rev. Lett. 83 (1999) 2147

[Bar04] F. Barranco, R. A. Broglia, G. Coló, G. Gori, E. Vigezzi, P. F. Bortignon, *Many-body effects in nuclear structure*, Eur. Phys. Jour. A 21 (2004) 57–60

[Bar05] F. Barranco, P. F. Bortignon, R. A. Broglia, G. Coló, P. Schuck, E. Vigezzi, X. Viñas, *Pairing matrix elements and pairing gaps with bare, effective, and induced interactions*, Phys. Rev. C 72 (2005) 054314–11

[Bec68] R. L. Becker, A. D. MacKellar, B. M. Morris, *Brueckner Theory in an Oscillator Basis. I. The Method of Reference Bethe-Goldstone Equations and Comparison of the Yale, Reid (Hard-Core), and Hamada-Johnston Interactions*, Phys. Rev. 174 (1968) 1264–1290

[Bec74] R. L. Becker, K. T. R. Davies, M. R. Patterson, *Renormalized Brueckner-Hartree-Fock calculations of ^{4}He and ^{16}O with center-of-mass corrections*, Phys. Rev. C 9 (1974) 1221–1242

[Bei75a] M. Beiner, H. Flocard, N. V. Giai, P. Quentin, *Nuclear ground-state properties and self-consistent calculations with the skyrme interaction: (I). Spherical description*, Nucl. Phys. A 238 (1975) 29 – 69

[Bei75b] M. Beiner, H. Flocard, Nguyen Van Giai, P. Quentin, *Nuclear ground-state properties and self-consistent calculations with the skyrme interaction: (I). Spherical description*, Nucl. Phys. A238 (1975) 29–69

[Bel56] J. S. Bell, T. H. R. Skyrme, *The nuclear spin-orbit coupling*, Phil. Mag. 1 (1956) 1055–1068

[Ben99a] M. Bender, K. Rutz, P.-G. Reinhard, J. A. Maruhn, W. Greiner, *Shell structure of superheavy nuclei in self-consistent mean-field models*, Phys. Rev. C 60 (1999) 034304

[Ben99b] M. Bender, K. Rutz, P.-G. Reinhard, J. A. Maruhn, W. Greiner, *Shell structure of superheavy nuclei in self-consistent mean-field models*, Phys. Rev. C 60 (1999) 034304

[Ben99c] K. Bennaceur, J. Dobaczewski, M. Płoszajczak, *Continuum effects for the mean-field and pairing properties of weakly bound nuclei*, Phys. Rev. C 60 (1999) 034308

[Ben00] K. Bennaceur, J. Dobaczewski, M. Ploszajczak, *Pairing anti-halo effect*, Phys. Lett. B 496 (2000) 154–160

[Ben01] M. Bender, W. Nazarewicz, P. G. Reinhard, *Shell stabilization of super- and hyperheavy nuclei without magic gaps*, Phys. Lett. B 515 (2001) 42 – 48

[Ben02] M. Bender, J. Dobaczewski, J. Engel, W. Nazarewicz, *Gamow-Teller strength and the spin-isospin coupling constants of the Skyrme energy functional*, Phys. Rev. C 65 (2002) 054322

[Ben03a] M. Bender, P. Bonche, T. Duguet, P. H. Heenen, *Skyrme mean-field study of rotational bands in transfermium isotopes*, Nucl. Phys. A723 (2003) 354–364

[Ben03b] M. Bender, P.-H. Heenen, P.-G. Reinhard, *Self-consistent mean-field models for nuclear structure*, Rev. Mod. Phys. 75 (2003) 121–180

[Ben04] M. Bender, P. Bonche, T. Duguet, P.-H. Heenen, *Configuration mixing of angular momentum projected self-consistent mean-field states for neutron-deficient Pb isotopes*, Phys. Rev. C 69 (2004) 064303

[Ben05] K. Bennaceur, J. Dobaczewski, *Coordinate-space solution of the Skyrme-Hartree-Fock- Bogolyubov equations within spherical symmetry. The program HFBRAD (v1.00)*, Comp. Phys. Comm. 168 (2005) 96–122

[Ben06a] M. Bender, G. F. Bertsch, P.-H. Heenen, *Global study of quadrupole correlation effects*, Phys. Rev. C 73 (2006) 034322

[Ben06b] M. Bender, P. Bonche, P. H. Heenen, *Shape coexistence in neutron-deficient Kr isotopes: Constraints on the single-particle spectrum of self-consistent mean-field models from collective excitations*, Phys. Rev. C 74 (2006) 024312–12

[Ben08] M. Bender, P.-H. Heenen, *Configuration mixing of angular-momentum and particle-number projected triaxial HFB states using the Skyrme energy density functional* (2008). ArXiv:0805.4383

[Ben09] M. Bender, K. Bennaceur, T. Duguet, P.-H. Heenen, T. Lesinski, J. Meyer (2009). In preparation

[Ber72] W. Bertozzi, J. Friar, J. Heisenberg, J. W. Negele, *Contributions of neutrons to elastic electron scattering from nuclei*, Phys. Lett. B41 (1972) 408–414

[Ber80] V. Bernard, Nguyen Van Giai, *Effects of collective modes on the single-particle states and the effective mass in* ^{208}Pb, Nucl. Phys. A348 (1980) 75–92

[Ber91] J. F. Berger, M. Girod, D. Gogny, *Time-dependent quantum collective dynamics applied to nuclear fission*, Comp. Phys. Comm. 63 (1991) 365–374

[Ber01] J. F. Berger, L. Bitaud, J. Dechargé, M. Girod, K. Dietrich, *Superheavy, hyperheavy and bubble nuclei*, Nucl. Phys. A 685 (2001) 1 – 16

[Ber05] G. F. Bertsch, B. Sabbey, M. Uusnäkki, *Fitting theories of nuclear binding energies*, Phys. Rev. C 71 (2005) 054311

[Ber07] G. F. Bertsch, M. Girod, S. Hilaire, J.-P. Delaroche, H. Goutte, S. Péru, *Systematics of the First 2^+ Excitation with the Gogny Interaction*, Phys. Rev. Lett. 99 (2008) 032502

[Bet56] H. A. Bethe, *Nuclear Many-Body Problem*, Phys. Rev. 103 (1956) 1353–1390

[Bet57] H. A. Bethe, J. Goldstone, *Effect of a Repulsive Core in the Theory of Complex Nuclei*, Proc. Roy. Soc. London A 238 (1957) 551–567

[Bet68] H. A. Bethe, *Thomas-Fermi Theory of Nuclei*, Phys. Rev. 167 (1968) 879

[Bet90] H. A. Bethe, *Supernova mechanisms*, Rev. Mod. Phys. 62 (1990) 801–866

[Bha05] A. Bhattacharyya, R. J. Furnstahl, *Single-particle properties from Kohn-Sham Green's functions*, Phys. Lett. B 607 (2005) 259–266

[Bla77] J. Blaizot, D. Gogny, *Theory of elementary excitations in closed shell nuclei*, Nucl. Phys. A 284 (1977) 429 – 460

[Blo62] C. Bloch, A. Messiah, *The canonical form of an antisymmetric tensor and its application to the theory of superconductivity*, Nucl. Phys. 39 (1962) 95 – 106

[Bog58] N. Bogolyubov, *On a new method in the theory of superconductivity*, Il Nuovo Cimento 7 (1958) 794–805

[Bog01] S. K. Bogner, A. Schwenk, T. T. S. Kuo, G. E. Brown, *Renormalization Group Equation for Low Momentum Effective Nuclear Interactions* (2001). ArXiv:nucl-th/0111042

[Bog02] S. Bogner, T. T. S. Kuo, L. Coraggio, A. Covello, N. Itaco, *Low momentum nucleon-nucleon potential and shell model effective interactions*, Phys. Rev. C 65 (2002) 051301–5

[Bog03a] S. K. Bogner, T. T. S. Kuo, A. Schwenk, *Model-independent low momentum nucleon interaction from phase shift equivalence*, Phys. Rep. 386 (2003) 1–27

[Bog03b] S. K. Bogner, T. T. S. Kuo, A. Schwenk, D. R. Entem, R. Machleidt, *Towards a model-independent low momentum nucleon-nucleon interaction*, Phys. Lett. B 576 (2003) 265–272

[Bog05] S. K. Bogner, A. Schwenk, R. J. Furnstahl, A. Nogga, *Is nuclear matter perturbative with low-momentum interactions?*, Nucl. Phys. A 763 (2005) 59–79

[Bog06a] S. K. Bogner, R. J. Furnstahl, *Variational calculations using low-momentum potentials with smooth cutoffs*, Phys. Lett. B 639 (2006) 237–241

[Bog06b] S. K. Bogner, R. J. Furnstahl, S. Ramanan, A. Schwenk, *Convergence of the Born series with low-momentum interactions*, Nucl. Phys. A 773 (2006) 203–220

[Bog07a] S. K. Bogner, R. J. Furnstahl, R. J. Perry, *Similarity renormalization group for nucleon-nucleon interactions*, Phys. Rev. C 75 (2007) 061001–5

[Bog07b] S. K. Bogner, R. J. Furnstahl, R. J. Perry, A. Schwenk, *Are low-energy nuclear observables sensitive to high-energy phase shifts?*, Phys. Lett. B 649 (2007) 488–493

[Bog07c] S. K. Bogner, R. J. Furnstahl, S. Ramanan, A. Schwenk, *Low-momentum interactions with smooth cutoffs*, Nucl. Phys. A 784 (2007) 79–103

[Bog08a] S. K. Bogner, R. J. Furnstahl, P. Maris, R. J. Perry, A. Schwenk, J. P. Vary, *Convergence in the no-core shell model with low-momentum two-nucleon interactions*, Nucl. Phys. A 801 (2008) 21–42

[Bog08b] S. K. Bogner, R. J. Furnstahl, R. J. Perry, *Three-body forces produced by a similarity renormalization group transformation in a simple model*, Ann. Phys. 323 (2008) 1478–1501

[Bog08c] S. K. Bogner, R. J. Furnstahl, L. Platter, *Density Matrix Expansion for Low-Momentum Interactions* To be published

[Boh39] N. Bohr, J. A. Wheeler, *The Mechanism of Nuclear Fission*, Phys. Rev. 56 (1939) 426–450

[Boh55] A. Bohr, B. R. Mottelson, Kgl. Danske Videnskab. Selskab, Mat-fys. Medd. 30 (1955) 1

[Boh58] A. Bohr, B. R. Mottelson, D. Pines, *Possible Analogy between the Excitation Spectra of Nuclei and Those of the Superconducting Metallic State*, Phys. Rev. 110 (1958) 936

[Boh79] O. Bohigas, A. M. Lane, J. Martorell, *Sum rules for nuclear collective excitations*, Phys. Rep. 51 (1979) 267 – 316

[Boh98] A. Bohr, B. R. Mottelson, *Nuclear Structure*, World Scientific, Singapore (1998)

[Bom91] I. Bombaci, U. Lombardo, *Asymmetric nuclear matter equation of state*, Phys. Rev. C 44 (1991) 1892–1900

[Bon87] P. Bonche, H. Flocard, P. H. Heenen, Nucl. Phys. A467 (1987) 115

[Bon90] P. Bonche, J. Dobaczewski, H. Flocard, P. H. Heenen, S. J. Krieger, J. Meyer, M. S. Weiss, *Quadrupole collective correlations and the depopulation of the superdeformed bands in mercury*, Nucl. Phys. A 519 (1990) 509–520

[Bon91] P. Bonche, J. Dobaczewski, H. Flocard, P. H. Heenen, *Generator coordinate method for triaxial quadrupole collective dynamics in strontium isotopes*, Nucl. Phys. A530 (1991) 149–170

[Boz99] P. Bożek, *Superfluid nuclear matter calculations*, Nucl. Phys. A 657 (1999) 187–215

[Boz03] P. Bożek, *Superfluidity with dressed nucleons*, Phys. Lett. B 551 (2003) 93–97

[Bra67] B. H. Brandow, *Linked-Cluster Expansions for the Nuclear Many-Body Problem*, Rev. Mod. Phys. 39 (1967) 771–828

[Bri67] D. M. Brink, E. Boeker, *Effective interactions for Hartree-Fock calculations*, Nucl. Phys. A 91 (1967) 1–26

[Bri07] D. M. Brink, F. Stancu, *Evolution of nuclear shells with the Skyrme density dependent interaction*, Phys. Rev. C 75 (2007) 064311

[Bro76] G. E. Brown, A. D. Jackson, *The Nucleon-Nucleon Interaction*, North-Holland (1976)

[Bro98] B. A. Brown, *New Skyrme interaction for normal and exotic nuclei*, Phys. Rev. C 58 (1998) 220–231

[Bro06a] B. A. Brown, T. Duguet, T. Otsuka, D. Abe, T. Suzuki, *Tensor interaction contributions to single-particle energies*, Phys. Rev. C 74 (2006) 061303

[Bro06b] B. A. Brown, W. A. Richter, *New "USD" Hamiltonians for the sd shell*, Phys. Rev. C 74 (2006) 034315

[Bro07] B. A. Brown (2007). Private communication

[Bru54a] K. A. Brueckner, *Nuclear Saturation and Two-Body Forces. II. Tensor Forces*, Phys. Rev. 96 (1954) 508

[Bru54b] K. A. Brueckner, C. A. Levinson, H. M. Mahmoud, *Two-Body Forces and Nuclear Saturation. I. Central Forces*, Phys. Rev. 95 (1954) 217

[Bru55a] K. A. Brueckner, *Many-Body Problem for Strongly Interacting Particles. II. Linked Cluster Expansion*, Phys. Rev. 100 (1955) 36

[Bru55b] K. A. Brueckner, *Two-Body Forces and Nuclear Saturation. III. Details of the Structure of the Nucleus*, Phys. Rev. 97 (1955) 1353

[Bru55c] K. A. Brueckner, C. A. Levinson, *Approximate Reduction of the Many-Body Problem for Strongly Interacting Particles to a Problem of Self-Consistent Fields*, Phys. Rev. 97 (1955) 1344

[Bru99] G. Bruun, Y. Castin, R. Dum, K. Burnett, *BCS theory for trapped ultracold fermions*, Eur. Phys. Jour. D 7 (1999) 433–439

[Bul02a] A. Bulgac, *Local density approximation for systems with pairing correlations*, Phys. Rev. C 65 (2002) 051305

[Bul02b] A. Bulgac, Y. Yu, *Renormalization of the Hartree-Fock-Bogoliubov equations in the case of a zero range pairing interaction*, Phys. Rev. Lett. 88 (2002) 042504

[Cam78] X. Campi, A. Bouyssy, Phys. Lett. 73B (1978) 263

[Cao06] L. G. Cao, U. Lombardo, C. W. Shen, N. V. Giai, *From Brueckner approach to Skyrme-type energy density functional*, Phys. Rev. C 73 (2006) 014313

[Cau01] E. Caurier, K. Langanke, G. Martinez-Pinedo, F. Nowacki, P. Vogel, *Shell model description of isotope shifts in calcium*, Phys. Lett. B522 (2001) 240–244

[Cau05] E. Caurier, G. Martínez-Pinedo, F. Nowacki, A. Poves, A. P. Zuker, *The shell model as a unified view of nuclear structure*, Rev. Mod. Phys. 77 427

[Cha32] J. Chadwick, *Possible Existence of a Neutron*, Nature 129 (1932) 312–312

[Cha97] E. Chabanat, P. Bonche, P. Haensel, J. Meyer, R. Schaeffer, *A Skyrme parametrization from subnuclear to neutron star densities*, Nucl. Phys. A627 (1997) 710–746

[Cha98] E. Chabanat, P. Bonche, P. Haensel, J. Meyer, R. Schaeffer, *A Skyrme parametrization from subnuclear to neutron star densities Part II. Nuclei far from stabilities*, Nucl. Phys. A635 (1998) 231–256. Erratum Nucl. Phys. A643, (1998) 441

[Cha04] S. Y. Chang, J. J. Morales, V. R. Pandharipande, D. G. Ravenhall, J. Carlson, S. C. Pieper, R. B. Wiringa, K. E. Schmidt, *Neutron matter: a superfluid gas*, Nucl. Phys. A 746 (2004) 215–221

[Cha06a] F. Chappert, M. Girod, J.-F. Berger (2006). Private communication

[Cha06b] R. J. Charity, L. G. Sobotka, W. H. Dickhoff, *Asymmetry Dependence of Proton Correlations*, Phys. Rev. Lett. 97 (2006) 162503

[Cha06c] A. Chatillon, C. Theisen, P. T. Greenlees, G. Auger, J. E. Bastin, E. Bouchez, B. Bouriquet, J. M. Casandjian, R. Cee, E. Clément, et al., *Spectroscopy and single-particle structure of the odd- Z heavy elements* ^{255}Lr, ^{251}Md *and* ^{247}Es, Eur. Phys. J. A30 (2006) 397–411

[Che95] B. Chen, J. Dobaczewski, K. L. Kratz, K. Langanke, B. Pfeiffer, F.-K. Thielemann, P. Vogel, *Influence of shell-quenching far from stability on the astrophysical r-process*, Phys. Lett. B355 (1995) 37–44

[Che05] L.-W. Chen, C. M. Ko, B.-A. Li, *Determination of the Stiffness of the Nuclear Symmetry Energy from Isospin Diffusion*, Phys. Rev. Lett. 94 (2005) 032701

[Coc04] B. Cochet, K. Bennaceur, P. Bonche, T. Duguet, J. Meyer, *Compressibility, effective mass and density dependence in skyrme forces*, Nucl. Phys. A 731 (2004) 34 – 40

[Coe70] F. Coester, S. Cohen, B. Day, C. M. Vincent, *Variation in Nuclear-Matter Binding Energies with Phase-Shift-Equivalent Two-Body Potentials*, Phys. Rev. C 1 (1970) 769

[Col95] G. Colò, N. V. Giai, H. Sagawa, *Isovector properties of Skyrme-type effective interactions*, Phys. Lett. B 363 (1995) 5 – 11

[Col07] G. Colò, H. Sagawa, S. Fracasso, P. F. Bortignon, *Spin-orbit splitting and the tensor component of the Skyrme interaction*, Phys. Lett. B646 (2007) 227–231

[Coo56] L. N. Cooper, *Bound Electron Pairs in a Degenerate Fermi Gas*, Phys. Rev. 104 (1956) 1189

[Cor02] L. Coraggio, A. Covello, A. Gargano, N. Itaco, *Structure of Sn isotopes beyond $N = 82$*, Phys. Rev. C 65 (2002) 051306

[Dal05a] E. N. E. van Dalen, C. Fuchs, A. Faessler, *Effective Nucleon Masses in Symmetric and Asymmetric Nuclear Matter*, Phys. Rev. Lett. 95 (2005) 022302

[Dal05b] E. N. E. van Dalen, C. Fuchs, A. Faessler, *Momentum, density, and isospin dependence of symmetric and asymmetric nuclear matter properties*, Phys. Rev. C 72 (2005) 065803–9

[Day78] B. D. Day, *Current state of nuclear matter calculations*, Rev. Mod. Phys. 50 (1978) 495–521

[Dea03] D. J. Dean, M. Hjorth-Jensen, *Pairing in nuclear systems: from neutron stars to finite nuclei*, Rev. Mod. Phys. 75 (2003) 607

[Dec80] J. Dechargé, D. Gogny, *Hartree-Fock-Bogolyubov calculations with the $D1$ effective interaction on spherical nuclei*, Phys. Rev. C 21 (1980) 1568–1593

[Dec99] J. Dechargé, J. F. Berger, K. Dietrich, M. S. Weiss, *Superheavy and hyperheavy nuclei in the form of bubbles or semi-bubbles*, Phys. Lett. B451 (1999) 275–282

[Dob84] J. Dobaczewski, H. Flocard, J. Treiner, *Hartree-Fock-Bogolyubov description of nuclei near the neutron-drip line*, Nucl. Phys. A422 (1984) 103–139

[Dob94] J. Dobaczewski, I. Hamamoto, W. Nazarewicz, J. A. Sheikh, *Nuclear shell structure at particle drip lines*, Phys. Rev. Lett. 72 (1994) 981–984

[Dob95a] J. Dobaczewski, J. Dudek, *Time-odd components in the mean field of rotating superdeformed nuclei*, Phys. Rev. C 52 (1995) 1827–1839. Erratum Phys. Rev. C **55**, 3177 (1997)

[Dob95b] J. Dobaczewski, A. Nazarewicz, T. R. Werner, *Closed shells at drip-line nuclei*, Phys. Scr. T56 (1995) 15

[Dob96a] J. Dobaczewski, J. Dudek, *Time-odd components in the rotating mean field and identical bands*, Acta Phys. Pol. B27 (1996) 45

[Dob96b] J. Dobaczewski, W. Nazarewicz, T. R. Werner, J. F. Berger, C. R. Chinn, J. Dechargé, *Mean-field description of ground-state properties of drip-line nuclei: Pairing and continuum effects*, Phys. Rev. C 53 (1996) 2809–2840

[Dob00] J. Dobaczewski, J. Dudek, S. G. Rohoziński, T. R. Werner, *Point symmetries in the Hartree-Fock approach. I. Densities, shapes, and currents*, Phys. Rev. C 62 (2000) 014310

[Dob01] J. Dobaczewski, P. Magierski, W. Nazarewicz, W. Satuła, Z. Szymański, *Odd-even staggering of binding energies as a consequence of pairing and mean-field effects*, Phys. Rev. C 63 (2001) 024308

[Dob04] J. Dobaczewski, M. V. Stoitsov, W. Nazarewicz, *Skyrme-HFB deformed nuclear mass table*, in *Proc. Int. Conf. on Nuclear Physics, Large and Small, Cocoyoc, Mexico, April 19-22, 2004*, R. Bijker, R. F. Casten, A. Frank, editors (2004) pages 51–56. Nucl-th/0404077

[Dob06] J. Dobaczewski, in *Proceedings of the Third ANL/MSU/JINA/INT RIA Workshop*, volume 15 of *Proceedings from the Institute for Nuclear Theory*, T. Duguet, H. Esbensen, K. M. Nollett, C. D. Roberts, editors, World Scientific (2006) Preprint nucl-th/0604043

[Dob07] J. Dobaczewski, M. V. Stoitsov, W. Nazarewicz, P.-G. Reinhard, *Particle-number projection and the density functional theory*, Phys. Rev. C 76 (2007) 054315

[Dug01a] T. Duguet, P. Bonche, P. H. Heenen, J. Meyer, *Pairing correlations. I. Description of odd nuclei in mean-field theories*, Phys. Rev. C 65 (2001) 014310

[Dug01b] T. Duguet, P. Bonche, P. H. Heenen, J. Meyer, *Pairing correlations. II. Microscopic analysis of odd-even mass staggering in nuclei*, Phys. Rev. C 65 (2001) 014311

[Dug03] T. Duguet, M. Bender, P. Bonche, P. H. Heenen, *Shape coexistence in ^{186}Pb: beyond-mean-field description by configuration mixing of symmetry restored wave functions*, Phys. Lett. B 559 (2003) 201–206

[Dug04] T. Duguet, *Bare vs effective pairing forces: A microscopic finite-range interaction for Hartree-Fock-Bogolyubov calculations in coordinate space*, Phys. Rev. C 69 (2004) 054317–18

[Dug05] T. Duguet, K. Bennaceur, P. Bonche, *Pairing schemes for HFB calculations of nuclei*, in *New developments in Nuclear Self-Consistent Mean-Field Theories*, Yukawa Institute for Theoretical Physics Report, Yukawa Institute for Theoretical Physics (2005) ArXiv:nucl-th/0508054v1

[Eis72] J. M. Eisenberg, W. Greiner, *Nuclear Theory. III. Microscopic theory of the nucleus*, North Holland, Amsterdam, London (1972)

[Elg96] Ø. Elgarøy, L. Engvik, M. Hjorth-Jensen, E. Osnes, *Model-space approach to $^1S_0$ neutron and proton pairing in neutron star matter with the Bonn meson-exchange potentials*, Nucl. Phys. A 604 (1996) 466–490

[Eme59] V. J. Emery, *On the existence of solutions of the Brueckner equations for a many-fermion system*, Nucl. Phys. 12 (1959) 69–83

[Eme60] V. J. Emery, *Reaction matrix singularities and the energy gap in an infinite system of Fermions*, Nucl. Phys. 19 (1960) 154–163

[Eng75] Y. M. Engel, D. M. Brink, K. Goeke, S. J. Krieger, D. Vautherin, *Time-dependent hartree-fock theory with Skyrme's interaction*, Nucl. Phys. A249 (1975) 215–238

[Eng99] J. Engel, M. Bender, J. Dobaczewski, W. Nazarewicz, R. Surman, *β decay of r–process waiting–point nuclei in a self-consistent approach*, Phys. Rev. C 60 (1999) 014302

[Eng07] J. Engel, *Intrinsic-density functionals*, Phys. Rev. C 75 (2007) 014306

[Ent03] D. R. Entem, R. Machleidt, *Accurate charge-dependent nucleon-nucleon potential at fourth order of chiral perturbation theory*, Phys. Rev. C 68 (2003) 041001

[Epe05] E. Epelbaum, W. Glöckle, U.-G. Meißner, *The two-nucleon system at next-to-next-to-next-to-leading order*, Nucl. Phys. A 747 (2005) 362–424

[Epe07] E. Epelbaum, H. Krebs, U.-G. Meißner, *Delta-excitations and the three-nucleon force* Preprint arXiv:0712.1969

[Ere86] A. Erell, J. Alster, J. Lichtenstadt, M. A. Moinester, J. D. Bowman, M. D. Cooper, F. Irom, H. S. Matis, E. Piasetzky, U. Sennhauser, *Measurements on isovector giant resonances in pion charge exchange*, Phys. Rev. C 34 (1986) 1822–1844

[Ern73] D. J. Ernst, C. M. Shakin, R. M. Thaler, D. L. Weiss, *Numerical Study of a Separable Approximation to a Local Potential*, Phys. Rev. C 8 (1973) 2056

[Fab05] A. Fabrocini, S. Fantoni, A. Y. Illarionov, K. E. Schmidt, *$^1S_0$ Superfluid Phase Transition in Neutron Matter with Realistic Nuclear Potentials and Modern Many-Body Theories*, Phys. Rev. Lett. 95 (2005) 192501–4

[Far97] M. Farine, J. M. Pearson, F. Tondeur, *Nuclear-matter incompressibility from fits of generalized Skyrme force to breathing-mode energies*, Nucl. Phys. A 615 (1997) 135 – 161

[Far01] M. Farine, J. M. Pearson, F. Tondeur, *Skyrme force with surface-peaked effective mass*, Nucl. Phys. A 696 (2001) 396 – 412

[Fay97] M. S. Fayache, L. Zamick, B. Castel, *The nuclear tensor interaction*, Phys. Rep. 290 (1997) 201–282

[Fay98] S. Fayans, *Towards a universal nuclear density functional*, JETP Letters 68 (1998) 169–174

[Fay00] S. A. Fayans, S. V. Tolokonnikov, E. L. Trykov, D. Zawischa, *Nuclear isotope shifts within the local energy–density functional approach*, Nucl. Phys. A676 (2000) 49–119

[Fee49] E. Feenberg, K. C. Hammack, *Nuclear Shell Structure*, Phys. Rev. 75 (1949) 1877–1893

[Fet71] A. L. Fetter, J. D. Walecka, *Quantum Theory of Many-Particle Systems*, McGraw-Hill, New-York (1971)

[Flo75] H. Flocard, Ph.D. thesis, Orsay, Série A, No. 1543, Université Paris Sud (1975)

[Foc30] V. Fock, *NÄherungsmethode zur Lösung des quantenmechanischen Mehrkörperproblems*, Z. Phys. 61 (1930) 126–148

[Fri81] B. Friedman, V. R. Pandharipande, *Hot and cold, nuclear and neutron matter*, Nucl. Phys. A 361 (1981) 502–520

[Fri86] J. Friedrich, P. G. Reinhard, *Skyrme-force parametrization: Least-squares fit to nuclear ground-state properties*, Phys. Rev. C 33 (1986) 335

[Gan08] S. Gandolfi, A. Y. Illarionov, S. Fantoni, F. Pederiva, K. E. Schmidt, *Equation of State of Superfluid Neutron Matter and the Calculation of the $^1S_0$ Pairing Gap*, Phys. Rev. Lett. 101 (2008) 132501

[Gei09] H. Geiger, E. Marsden, *On a Diffuse Reflection of the α-Particles*, Proc. Roy. Soc. London 82 (1909) 495–500

[Gil75] T. L. Gilbert, *Hohenberg-Kohn theorem for nonlocal external potentials*, Phys. Rev. B 12 (1975) 2111–2120

[Gio02] N. Giovanardi, F. Barranco, R. A. Broglia, E. Vigezzi, *Surface effects in nuclear Cooper pair formation*, Phys. Rev. C 65 (2002) 041304

[Gir82] M. Girod, P.-G. Reinhard, *A Microscopic Calculation of the Collective Ground–State Correlations in the Fe–Ni–Zn Isotopes*, Nucl. Phys. A384 (1982) 179–189

[Gir07] B. Giraud, B. K. Jennings, B. Barrett, *Existence of a Density Functional for an Intrinsic State* ArXiv:0707.3099

[Gir08a] B. G. Giraud, *Density functionals in the laboratory frame*, Phys. Rev. C 77 (2008) 014311

[Gir08b] B. G. Giraud, *Scalar nature of the nuclear density functional*, Phys. Rev. C 78 014307

[GM48] M. Goeppert Mayer, *On Closed Shells in Nuclei*, Phys. Rev. 74 (1948) 235–239

[GM49] M. Goeppert Mayer, *On Closed Shells in Nuclei. II*, Phys. Rev. 75 (1949) 1969–1970

[GM50a] M. Goeppert Mayer, *Nuclear Configurations in the Spin-Orbit Coupling Model. I. Empirical Evidence*, Phys. Rev. 78 (1950) 16–21

[GM50b] M. Goeppert Mayer, *Nuclear Configurations in the Spin-Orbit Coupling Model. II. Theoretical Considerations*, Phys. Rev. 78 (1950) 22–23

[GM51] M. Gell-Mann, F. Low, *Bound States in Quantum Field Theory*, Phys. Rev. 84 (1951) 350–354

[Gog70] D. Gogny, P. Pires, R. De Tourreil, *A smooth realistic local nucleon-nucleon force suitable for nuclear Hartree-Fock calculations*, Phys. Lett. B 32 (1970) 591–595

[Gog75a] D. Gogny, *Simple separable expansions for calculating matrix elements of two-body local interactions with harmonic oscillator functions*, Nucl. Phys. A 237 (1975) 399–418

[Gog75b] D. Gogny, *Simple separable expansions for calculating matrix elements of two-body local interactions with harmonic oscillator functions*, Nucl. Phys. A237 (1975) 399–418

[Gol57] J. Goldstone, *Derivation of the Brueckner Many-Body Theory*, Proc. Roy. Soc. London A 239 (1957) 267–279

[Goo78] A. L. Goodman, J. Borysowicz, *The mass dependence of the spin-orbit splitting in the A = 176-208 mass region*, Nucl. Phys. A295 (1978) 333–344

[Gor58] L. P. Gorkov, Sov. Phys. JETP 7 (1958) 505

[Gor85] L. P. Gor'kov, *Exotic Superconductors*, Phys. Scr. 32 (1985) 6–10

[Gor96] A. Görling, *Density-functional theory for excited states*, Phys. Rev. A 54 (1996) 3912–3915

[Gor03] S. Goriely, M. Samyn, M. Bender, J. M. Pearson, *Further explorations of Skyrme-Hartree-Fock-Bogoliubov mass formulas. II. Role of the effective mass*, Phys. Rev. C 68 (2003) 054325

[Gor05a] G. Gori, F. Ramponi, F. Barranco, P. F. Bortignon, R. A. Broglia, G. Coló, E. Vigezzi, *Attractive and repulsive contributions of medium fluctuations to nuclear superfluidity*, Phys. Rev. C 72 (2005) 011302–5

[Gor05b] S. Goriely, M. Samyn, J. M. Pearson, M. Onsi, *Further explorations of Skyrme-Hartree-Fock-Bogoliubov mass formulas. IV: Neutron-matter constraint*, Nucl. Phys. A750 (2005) 425–443

[Gor06] S. Goriely, M. Samyn, J. M. Pearson, *Further explorations of Skyrme-Hartree-Fock-Bogoliubov mass formulas; VI: Weakened pairing*, Nucl. Phys. A 773 (2006) 279–299

[GR92] C. García-Recio, J. Navarro, V. G. Nguyen, L. Salcedo, *Response functions for infinite fermion systems with velocity dependent interactions*, Ann. Phys. (NY) 214 (1992) 293 – 340

[Gra89] P. Grangé, A. Lejeune, M. Martzolff, J.-F. Mathiot, *Consistent three-nucleon forces in the nuclear many-body problem*, Phys. Rev. C 40 (1989) 1040–1060

[Gre01] V. Greco, M. Colonna, M. Di Toro, G. Fabbri, F. Matera, *Asymmetric nuclear matter in a Hartree-Fock approach to nonlinear quantum hadrodynamics*, Phys. Rev. C 64 (2001) 045203

[Hae82] P. Haensel, A. J. Jerzak, *Tensor forces and spin susceptibility of a Fermi liquid*, Phys. Lett. B112 (1982) 285

[Hag07] G. Hagen, D. J. Dean, M. Hjorth-Jensen, T. Papenbrock, A. Schwenk, *Benchmark calculations for ^3H, ^4He, ^{16}O, and ^{40}Ca with ab initio coupled-cluster theory*, Phys. Rev. C 76 (2007) 044305–8

[Hag08] G. Hagen, T. Papenbrock, D. J. Dean, M. Hjorth-Jensen, *Medium-Mass Nuclei from Chiral Nucleon-Nucleon Interactions*, Phys. Rev. Lett. 101 (2008) 092502

[Hai84] J. Haidenbauer, W. Plessas, *Separable representation of the Paris nucleon-nucleon potential*, Phys. Rev. C 30 (1984) 1822

[Ham62] T. Hamada, I. D. Johnston, *A potential model representation of two-nucleon data below 315 MeV*, Nucl. Phys. 34 (1962) 382–403

[Hau01] K. Hauschild, M. Rejmund, H. Grawe, E. Caurier, F. Nowacki, F. Becker, Y. Le Coz, W. Korten, J. Döring, M. Górska, et al., *Isomer Spectroscopy in $^{216}_{90}Th_{126}$ and the Magicity of $^{218}_{92}U_{126}$*, Phys. Rev. Lett. 87 (2001) 072501

[Hax49] O. Haxel, J. H. D. Jensen, H. E. Suess, *On the "Magic Numbers" in Nuclear Structure*, Phys. Rev. 75 (1949) 1766

[Heb08] K. Hebeler, T. Duguet, A. Schwenk (2008). Private communication

[Hee93] P. H. Heenen, P. Bonche, J. Dobaczewski, H. Flocard, *Generator-coordinate method for triaxial quadrupole dynamics in Sr isotopes. (II). Results for particle-number-projected states*, Nucl. Phys. A561 (1993) 367–386

[Hei32] W. Heisenberg, *Über den Bau der Atomkerne. II*, Z. Phys. 78 (1932) 156–164

[Hei00] H. Heiselberg, C. J. Pethick, H. Smith, L. Viverit, *Influence of Induced Interactions on the Superfluid Transition in Dilute Fermi Gases*, Phys. Rev. Lett. 85 (2000) 2418–2421

[Hen64] E. M. Henley, L. Wilets, *Energy Gap in Nuclear Matter. I. Extended Theory*, Phys. Rev. 133 (1964) B1118

[Hil53] D. L. Hill, J. A. Wheeler, *Nuclear Constitution and the Interpretation of Fission Phenomena*, Phys. Rev. 89 (1953) 1102–1145

[Hil06] S. Hilaire, M. Girod, *Hartree-Fock-Bogoliubov results based on the Gogny force* (2006). Url: www-phynu.cea.fr

[Hil07] S. Hilaire, M. Girod, *Large-scale mean-field calculations from proton to neutron drip lines usi ng the D1S Gogny force*, Eur. Phys. Jour. A 33 (2007) 237–241

[Hof01] F. Hofmann, C. M. Keil, H. Lenske, *Density dependent hadron field theory for asymmetric nuclear matter and exotic nuclei*, Phys. Rev. C 64 (2001) 034314

[Hoh64] P. Hohenberg, W. Kohn, *Inhomogeneous Electron Gas*, Phys. Rev. 136 (1964) B864–B871

[Hon02] M. Honma, T. Otsuka, B. A. Brown, T. Mizusaki, *Effective interaction for pf-shell nuclei*, Phys. Rev. C 65 (2002) 061301

[Hos05] P. T. Hosmer, H. Schatz, A. Aprahamian, O. Arndt, R. R. C. Clement, A. Estrade, K.-L. Kratz, S. N. Liddick, P. F. Mantica, W. F. Mueller, et al., *Half-Life of the Doubly Magic r-Process Nucleus ^{78}Ni*, Phys. Rev. Lett. 94 (2005) 112501

[Hug57] N. M. Hugenholtz, *Perturbation theory of large quantum systems*, Physica 23 (1957) 481–532

[Jah37] H. A. Jahn, E. Teller, Proc. Roy. Soc. London 161 (1937) 220

[Jam89] M. Jaminon, C. Mahaux, *Effective masses in relativistic approaches to the nucleon-nucleus mean field*, Phys. Rev. C 40 (1989) 354–367

[Jan64] B. Jancovici, D. H. Schiff, *The collective vibrations of a many-fermion system*, Nucl. Phys. 58 (1964) 678–686.

[JD01] M. S. J. Dobaczewski, W. Nazarewicz, *Contact pairing interaction for the Hartree-Fock-Bogoliubov calculations* NATO Advanced Research Workshop: The Nuclear Many-Body Problem 2001, Brijuni National Park, Pula, Croatia, June 2-5, 2001. Preprint arXiv:nucl-th/0109073

[Jen86] A. S. Jensen, A. Miranda, *The skyrme-plus-pairing effective interaction and the global neutron-excess dependence of the pairing gap*, Nucl. Phys. A 449 (1986) 331–353

[Jeu76] J. P. Jeukenne, A. Lejeune, C. Mahaux, *Many-body theory of nuclear matter*, Phys. Rep. 25 (1976) 83 – 174

[Joh71] A. Johnson, H. Ryde, J. Sztarkier, *Evidence for a "singularity" in the nuclear rotational band structure*, Phys. Lett. B 34 (1971) 605–608

[KH51] O. Kofoed-Hansen, K. O. Nielsen, *Short-Lived Krypton Isotopes and Their Daughter Substances*, Phys. Rev. 82 (1951) 96–97

[Kim97] K.-H. Kim, T. Otsuka, P. Bonche, *Three-dimensional TDHF calculations for reactions of unstable nuclei*, Jour. Phys. G 23 (1997) 1267–1273

[Koh65] W. Kohn, L. J. Sham, *Self-Consistent Equations Including Exchange and Correlation Effects*, Phys. Rev. 140 (1965) A1133–A1138

[Koo34] T. Koopmans, *Über die Zuordnung von Wellenfunktionen und Eigenwerten zu den Einzelnen Elektronen Eines Atoms*, Physica 1 (1934) 104 – 113

[Kor04] W. Korten, E. Bouchez, E. Clément, A. Chatillon, A. Görgen, Y. Le Coz, C. Theisen, J. Wilson, J. M. Casandjian, G. de France, et al., *Shape coexistence in Krypton isotopes studied through Coulomb excitation of radioactive Krypton ion beams*, Nucl. Phys. A 746 (2004) 90–95

[Kor08] M. Kortelainen, J. Dobaczewski, K. Mizuyama, J. Toivanen, *Dependence of single-particle energies on coupling constants of the nuclear energy density functional*, Phys. Rev. C 77 (2008) 064307

[Kre01] T. Kreibich, E. K. U. Gross, *Multicomponent Density-Functional Theory for Electrons and Nuclei*, Phys. Rev. Lett. 86 (2001) 2984–2987

[Kri80] H. Krivine, J. Treiner, O. Bohigas, *Derivation of a fluid-dynamical lagrangian and electric giant resonances*, Nucl. Phys. A 336 (1980) 155–184

[Kru00] A. T. Kruppa, M. Bender, W. Nazarewicz, P.-G. Reinhard, T. Vertse, S. Ćwiok, *Shell corrections of superheavy nuclei in self-consistent calculations*, Phys. Rev. C 61 (2000) 034313

[Kub97] S. Kubis, M. Kutschera, *Nuclear matter in relativistic mean field theory with isovector scalar meson*, Phys. Lett. B 399 (1997) 191 – 195

[Kur99] S. Kurth, M. Marques, M. Lüders, E. K. U. Gross, *Local Density Approximation for Superconductors*, Phys. Rev. Lett. 83 (1999) 2628–2631

[Lac80] M. Lacombe, B. Loiseau, J. M. Richard, R. V. Mau, J. Côté, P. Pirès, R. de Tourreil, *Parametrization of the Paris N-N potential*, Phys. Rev. C 21 (1980) 861

[Lac08] D. Lacroix, T. Duguet, M. Bender (2008). To be published

[Lag81] I. E. Lagaris, V. R. Pandharipande, *Variational calculations of realistic models of nuclear matter*, Nucl. Phys. A 359 (1981) 349–364

[Lal98a] G. A. Lalazissis, D. Vretenar, W. Pöschl, P. Ring, *Reduction of the spin-orbit potential in light drip-line nuclei*, Phys. Lett. B418 (1998) 7–12

[Lal98b] G. A. Lalazissis, D. Vretenar, W. Pöschl, P. Ring, *Relativistic Hartree-Bogoliubov description of the neutron drip-line in light nuclei*, Nucl. Phys. A632 (1998) 363–382

[Lan62] A. Lane, *Isobaric spin dependence of the optical potential and quasi-elastic (p, n) reactions*, Nucl. Phys. 35 (1962) 676 – 685

[Lan03] K. Langanke, J. Terasaki, F. Nowacki, D. J. Dean, W. Nazarewicz, *How magic is the magic ^{68}Ni nucleus?*, Phys. Rev. C 67 (2003) 044314

[Lat04] J. M. Lattimer, M. Prakash, *The Physics of Neutron Stars*, Science 304 (2004) 536

[Lej00] A. Lejeune, U. Lombardo, W. Zuo, *Nuclear matter EOS with a three-body force*, Phys. Lett. B 477 (2000) 45 – 50

[Les06] T. Lesinski, K. Bennaceur, T. Duguet, J. Meyer, *Isovector splitting of nucleon effective masses, ab initio benchmarks and extended stability criteria for Skyrme energy functionals*, Phys. Rev. C 74 (2006) 044315

[Les07] T. Lesinski, M. Bender, K. Bennaceur, T. Duguet, J. Meyer, *Tensor part of the Skyrme energy density functional: Spherical nuclei*, Phys. Rev. C 76 (2007) 014312

[Li04a] B.-A. Li, *Constraining the neutron-proton effective mass splitting in neutron-rich matter*, Phys. Rev. C 69 (2004) 064602

[Li04b] B.-A. Li, C. B. Das, S. Das Gupta, C. Gale, *Momentum dependence of the symmetry potential and nuclear reactions induced by neutron-rich nuclei at RIA*, Phys. Rev. C 69 (2004) 011603

[Li08] Z. H. Li, U. Lombardo, H. J. Schulze, W. Zuo, *Consistent nucleon-nucleon potentials and three-body forces*, Phys. Rev. C 77 (2008) 034316–10

[Lit05] Y. A. Litvinov, T. J. Burvenich, H. Geissel, Y. N. Novikov, Z. Patyk, C. Scheidenberger, F. Attallah, G. Audi, K. Beckert, F. Bosch, et al., *Isospin Dependence in the Odd-Even Staggering of Nuclear Binding Energies*, Phys. Rev. Lett. 95 (2005) 042501–4

[Lit06] E. Litvinova, P. Ring, *Covariant theory of particle-vibrational coupling and its effect on the single-particle spectrum*, Phys. Rev. C 73 044328

[Liu76] K. F. Liu, N. V. Giai, *A self-consistent microscopic description of the giant resonances including the particle continuum*, Phys. Lett. B 65 (1976) 23 – 26

[Liu91] K.-F. Liu, H. Luo, Z. Ma, Q. Shen, S. A. Moszkowski, *Skyrme-Landau parameterization of effective interactions (I). Hartree-Fock ground states*, Nucl. Phys. A534 (1991) 1–24

[Liu02] B. Liu, V. Greco, V. Baran, M. Colonna, M. Di Toro, *Asymmetric nuclear matter: The role of the isovector scalar channel*, Phys. Rev. C 65 (2002) 045201

[Loi67] B. A. Loiseau, Y. Nogami, *Three-nucleon force*, Nucl. Phys. B 2 (1967) 470–478

[Lom01] U. Lombardo, P. Schuck, W. Zuo, *Self-energy effects in the superfluidity of neutron matter*, Phys. Rev. C 64 (2001) 021301

[Lon06] W.-H. Long, Nguyen Van Giai, J. Meng, *Density-dependent relativistic Hartree-Fock approach*, Phys. Lett. B640 (2006) 150–154

[Lon08] W. H. Long, H. Sagawa, J. Meng, N. V. Giai, *Evolution of nuclear shell structure due to the pion exchange potential*, Europhys. Lett. 82 (2008) 12001

[LQ00] M. López-Quelle, Nguyen Van Giai, S. Marcos, L. N. Savushkin, *Spin-orbit splitting in nonrelativistic and relativistic self-consistent models*, Phys. Rev. C 61 (2000) 064321

[Lun03] D. Lunney, J. M. Pearson, C. Thibault, *Recent trends in the determination of nuclear masses*, Rev. Mod. Phys. 75 (2003) 1021

[Ma04] Z.-Y. Ma, J. Rong, B.-Q. Chen, Z.-Y. Zhu, H.-Q. Song, *Isospin dependence of nucleon effective mass in Dirac Brueckner-Hartree-Fock approach*, Phys. Lett. B 604 (2004) 170 – 174

[Mac87] R. Machleidt, K. Holinde, C. Elster, *The bonn meson-exchange model for the nucleon–nucleon interaction*, Phys. Rep. 149 (1987) 1–89

[Mac89a] H. Mach, M. Moszynski, R. L. Gill, F. K. Wohn, J. A. Winger, J. C. Hill, G. Molnár, K. Sistemich, *Deformation and shape coexistence of 0^+ states in 98Sr and 100Zr*, Phys. Lett. B 230 (1989) 21–26

[Mac89b] R. Machleidt, *The Meson Theory of Nuclear Forces and Nuclear Structure*, pages 189–380, Plenum, New York (1989)

[Mac01] R. Machleidt, *High-precision, charge-dependent Bonn nucleon-nucleon potential*, Phys. Rev. C 63 (2001) 024001

[Mad88] D. G. Madland, J. R. Nix, *New model of the average neutron and proton pairing gaps*, Nucl. Phys. A 476 (1988) 1–38

[Mar06] J. Margueron, N. V. Giai, J. Navarro, *Effects of spin-orbit interaction on nuclear response and neutrino mean free path*, Phys. Rev. C 74 (2006) 015805

[Mar07] J. Margueron, H. Sagawa, K. Hagino, *BCS-BEC crossover of neutron pairs in symmetric and asymmetric nuclear matter*, Phys. Rev. C 76 (2007) 064316–11

[Mar08] J. Margueron, H. Sagawa, K. Hagino, *Effective pairing interactions with isospin density dependence*, Phys. Rev. C 77 (2008) 054309–10

[Mat06] M. Matsuo, *Spatial structure of neutron Cooper pair in low density uniform matter*, Phys. Rev. C 73 (2006) 044309

[Mei39] L. Meitner, O. R. Frisch, *Disintegration of Uranium by Neutrons: a New Type of Nuclear Reaction*, Nature 143 (1939) 239–240

[Mes58] A. Messiah, *Quantum Mechanics*, Wiley (1958)

[Mey95] J. Meyer, P. Bonche, M. S. Weiss, J. Dobaczewski, H. Flocard, P. H. Heenen, *Quadrupole and octupole correlations in normal, superdeformed and hyperdeformed states of 194Pb*, Nucl. Phys. A 588 (1995) 597 – 622

[Mig60] A. B. Migdal, Sov. Phys. JETP 10 (1960) 176

[Mig67] A. B. Migdal, *Theory of Finite Fermi Systems and Applications to Atomic Nuclei*, Interscience, London (1967)

[Möl92] P. Möller, J. R. Nix, *Nuclear pairing models*, Nucl. Phys. A 536 (1992) 20–60

[Mon07] C. Monrozeau, J. Margueron, N. Sandulescu, *Nuclear superfluidity and cooling time of neutron star crusts*, Phys. Rev. C 75 065807

[Mos59] M. Moshinsky, *Transformation brackets for harmonic oscillator functions*, Nucl. Phys. 13 (1959) 104 – 116

[Mos96] S. A. Moszkowski, *Maria Goeppert Mayer* (1996). Talk Presented at APS meeting, Indianapolis

[Mot60] B. R. Mottelson, J. G. Valatin, *Effect of Nuclear Rotation on the Pairing Correlation*, Phys. Rev. Lett. 5 (1960) 511

[Mut05] H. Muther, W. H. Dickhoff, *Pairing properties of nucleonic matter employing dressed nucleons*, Phys. Rev. C 72 (2005) 054313–11

[Nag04] H. Nagaoka, *Kinetics of a system of particles illustrating the line and the band spectrum and the phenomena of radioactivity*, Phil. Mag. 7 (1904) 445–455

[Nam60] Y. Nambu, *Quasi-Particles and Gauge Invariance in the Theory of Superconductivity*, Phys. Rev. 117 (1960) 648

[Nav03] P. Navrátil, W. E. Ormand, *Ab initio shell model with a genuine three-nucleon force for the p-shell nuclei*, Phys. Rev. C 68 (2003) 034305

[Nef03] T. Neff, H. Feldmeier, *Tensor correlations in the unitary correlation operator method*, Nucl. Phys. A713 (2003) 311–371

[Neg70] J. W. Negele, *Structure of Finite Nuclei in the Local-Density Approximation*, Phys. Rev. C 1 (1970) 1260

[Neg72] J. W. Negele, D. Vautherin, *Density-Matrix Expansion for an Effective Nuclear Hamiltonian*, Phys. Rev. C 5 (1972) 1472–1493

[Neg75] J. W. Negele, D. Vautherin, *Density-matrix expansion for an effective nuclear Hamiltonian. II*, Phys. Rev. C 11 (1975) 1031–1041

[Neg82] J. W. Negele, *The mean-field theory of nuclear structure and dynamics*, Rev. Mod. Phys. 54 (1982) 913

[Nem62] P. E. Nemirovsky, Y. V. Adamchuk, *Neutron and proton pair interaction energy*, Nucl. Phys. 39 (1962) 551–562

[Nij] *Nijmegen NN-OnLine database*. Url: nn-online.org

[Nil95] S. G. Nilsson, I. Ragnarsson, *Shapes and Shells in Nuclear Structure*, Cambridge University Press, Cambridge, England (1995)

[Nog04] A. Nogga, S. K. Bogner, A. Schwenk, *Low-momentum interaction in few-nucleon systems*, Phys. Rev. C 70 (2004) 061002

[Noz63] P. Nozières, *Le problème à N corps*, Dunod, Paris (1963)

[Oli88] L. N. Oliveira, E. K. U. Gross, W. Kohn, *Density-Functional Theory for Superconductors*, Phys. Rev. Lett. 60 (1988) 2430–2433

[Oni78] N. Onishi, J. W. Negele, *Two-body and three-body effective interactions in nuclei*, Nucl. Phys. A301 (1978) 336–348

[Ots05] T. Otsuka, T. Suzuki, R. Fujimoto, H. Grawe, Y. Akaishi, *Evolution of Nuclear Shells due to the Tensor Force*, Phys. Rev. Lett. 95 (2005) 232502–4

[Ots06] T. Otsuka, T. Matsuo, D. Abe, *Mean Field with Tensor Force and Shell Structure of Exotic Nuclei*, Phys. Rev. Lett. 97 (2006) 162501–4

[Ott89] E. W. Otten, *Nuclear Radii and Moments of unstable Isotopes*, in *Treatise on Heavy-Ion Science*, volume 8. Nuclei far from Stability, A. D. Bromley, editor, pages 517–638, Plenum, New York (1989)

[Paa05] N. Paar, T. Niksic, D. Vretenar, P. Ring, *Isotopic dependence of the pygmy dipole resonance*, Phys. Lett. B 606 (2005) 288 – 294

[Pan79] V. R. Pandharipande, R. B. Wiringa, *Variations on a theme of nuclear matter*, Rev. Mod. Phys. 51 (1979) 821–861

[Pan06] S. Pankratov, E. Saperstein, M. Zverev, *Chemical-potential dependence of the pairing gap in a nuclear-matter slab*, Phys. At. Nucl. 69 (2006) 2009–2019

[Pan07] S. Pankratov, M. Baldo, U. Lombardo, E. Saperstein, M. Zverev, *Effective pairing interaction for the Argonne nucleon-nucleon potential v18*, Phys. At. Nucl. 70 (2007) 658–668

[Pas08a] A. Pastore, F. Barranco, R. A. Broglia, E. Vigezzi, *Microscopic calculation and LDA of the spatial dependence of the pairing field with bare and induced interactions* (2008). ArXiv:0801.1385

[Pas08b] A. Pastore, E. Vigezzi (2008). Private communication

[Pat99] Z. Patyk, A. Baran, J. F. Berger, J. Dechargé, J. Dobaczewski, P. Ring, A. Sobiczewski, *Masses and radii of spherical nuclei calculated in various microscopic approaches*, Phys. Rev. C 59 (1999) 704–713

[Pea96] J. M. Pearson, R. C. Nayak, S. Goriely, *Nuclear mass formula with Bogolyubov-enhanced shell-quenching: application to r-process*, Phys. Lett. B387 (1996) 455–459

[Per81] J. P. Perdew, A. Zunger, *Self-interaction correction to density-functional approximations for many-electron systems*, Phys. Rev. B 23 (1981) 5048–5079

[Per04] E. Perlińska, S. G. Rohoziński, J. Dobaczewski, W. Nazarewicz, *Local density approximation for proton-neutron pairing correlations: Formalism*, Phys. Rev. C 69 (2004) 014316

[Pfe97] B. Pfeiffer, K.-L. Kratz, F.-K. Thielemann, *Analysis of the solar-system r-process abundance pattern with the new ETFSI-Q mass formula*, Z. Phys. A357 (1997) 235

[Pie01a] S. C. Pieper, V. R. Pandharipande, R. B. Wiringa, J. Carlson, *Realistic models of pion-exchange three-nucleon interactions*, Phys. Rev. C 64 (2001) 014001

[Pie01b] S. C. Pieper, R. B. Wiringa, *Quantum Monte-Carlo Calculations of Light Nuclei*, Ann. Rev. Nucl. Part. Sci. 51 (2001) 53–90

[Pil07] N. Pillet, N. Sandulescu, P. Schuck, *Generic strong coupling behavior of Cooper pairs on the surface of superfluid nuclei*, Phys. Rev. C 76 (2007) 024310

[Por05] M. G. Porquet, S. Péru, M. Girod, *Crossing of the $\pi d_{5/2}$ and $\pi g_{7/2}$ orbitals in the $_{51}Sb$ isotopes*, Eur. Phys. J. A25 (2005) 319–323

[Pre92] W. H. Press, S. A. Teukolsky, W. T. Vetterling, B. P. Flannery, *Numerical Recipes*, Cambridge, New York, second edition (1992)

[Pud95] B. S. Pudliner, V. R. Pandharipande, J. Carlson, R. B. Wiringa, *Quantum Monte Carlo Calculations of $A \leq 6$ Nuclei*, Phys. Rev. Lett. 74 (1995) 4396

[Ram07] S. Ramanan, S. K. Bogner, R. J. Furnstahl, *Weinberg eigenvalues and pairing with low-momentum potentials*, Nucl. Phys. A 797 (2007) 81–93

[Rei68] R. V. Reid, *Local phenomenological nucleon-nucleon potentials,*, Ann. Phys. (NY) 50 (1968) 411–448

[Rei79] P.-G. Reinhard, D. Drechsel, *Ground–State Correlations and the Nuclear Charge Distribution*, Z. Phys. A290 (1979) 85–91

[Rei95] P. G. Reinhard, H. Flocard, *Nuclear effective forces and isotope shifts*, Nucl. Phys. A 584 (1995) 467–488

[Rei99] P.-G. Reinhard, D. J. Dean, W. Nazarewicz, J. Dobaczewski, J. A. Maruhn, M. R. Strayer, *Shape coexistence and the effective nucleon-nucleon interaction*, Phys. Rev. C 60 (1999) 014316

[Rei06] P.-G. Reinhard, M. Bender, W. Nazarewicz, T. Vertse, *From finite nuclei to the nuclear liquid drop: Leptodermous expansion based on self-consistent mean-field theory*, Phys. Rev. C 73 (2006) 014309

[Rii94] K. Riisager, *Nuclear halo states*, Rev. Mod. Phys. 66 (1994) 1105–1116

[Rin00] P. Ring, P. Schuck, *The Nuclear Many-Body Problem*, Springer, Berlin, Heidelberg (2000)

[Rit93] J. Ritman, F.-D. Berg, W. Kühn, V. Metag, R. Novotny, M. Notheisen, P. Paul, M. Pfeiffer, O. Schwalb, H. Löhner, et al., *First observation of the Coulomb-excited double giant dipole resonance in ^{208}Pb via double-γ decay*, Phys. Rev. Lett. 70 (1993) 533–536

[Riz04] J. Rizzo, M. Colonna, M. D. Toro, V. Greco, *Transport properties of isospin effective mass splitting*, Nucl. Phys. A 732 (2004) 202 – 217

[Rot04] R. Roth, T. Neff, H. Hergert, H. Feldmeier, *Nuclear structure based on correlated realistic nucleon-nucleon potentials*, Nucl. Phys. A745 (2004) 3–33

[Rot07a] R. Roth, P. Navrátil, *Ab Initio Study of ^{40}Ca with an Importance-Truncated No-Core Shell Model*, Phys. Rev. Lett. 99 (2007) 092501

[Rot07b] V. Rotival, K. Bennaceur, T. Duguet, *Halo phenomenon in medium-mass nuclei. II. Impact of pairing correlations and large scale analysis* Preprint arXiv:0711.1275

[Rot07c] V. Rotival, T. Duguet, *Halo Phenomenon in Medium-Mass Nuclei. I. New Analysis Method and First Applications* ArXiv:nucl-th/0702050

[Rot08a] V. Rotival (2008). Private communication

[Rot08b] V. Rotival, *Fonctionnelles d'énergie non-empiriques pour la structure nucléaire*, Ph.D. thesis, Université Denis Diderot – Paris VII (2008)

[Rut11] E. Rutherford, *The Scattering of α and β Particles by Matter and the Structure of the Atom*, Phil. Mag. 21 (1911) 669–688

[Rut98] K. Rutz, M. Bender, P. G. Reinhard, J. A. Maruhn, W. Greiner, *Odd nuclei and single-particle spectra in the relativistic mean-field model*, Nucl. Phys. A634 (1998) 67–88

[Rut99] K. Rutz, M. Bender, P. G. Reinhard, J. A. Maruhn, *Pairing gap and polarisation effects*, Phys. Lett. B 468 (1999) 1–6

[SAI] *Scattering Analysis Interactive Dial-in*. Url: gwdac.phys.gwu.edu

[Sam02] M. Samyn, S. Goriely, P. H. Heenen, J. M. Pearson, F. Tondeur, *A Hartree-Fock-Bogoliubov mass formula*, Nucl. Phys. A700 (2002) 142–156

[Sam05] F. Sammarruca, W. Barredo, P. Krastev, *Predicting the single-proton and single-neutron potentials in asymmetric nuclear matter*, Phys. Rev. C 71 (2005) 064306

[Sat97] W. Satuła, D. J. Dean, J. Gary, S. Mizutori, W. Nazarewicz, *On the origin of the Wigner energy*, Phys. Lett. B407 (1997) 103–109

[Sat98] W. Satuła, J. Dobaczewski, W. Nazarewicz, *Odd-Even Staggering of Nuclear Masses: Pairing or Shape Effect?*, Phys. Rev. Lett. 81 (1998) 3599

[Sat06] W. Satuła, R. A. Wyss, M. Rafalski, *Global properties of the Skyrme-force-induced nuclear symmetry energy*, Phys. Rev. C 74 (2006) 011301

[Saw67] T. Sawaguri, W. Tobocman, *Finite-Range Effects in Distorted-Wave Born-Approximation Calculations of Nucleon Transfer Reactions*, Jour. Math. Phys. 8 (1967) 2223–2230

[Sch64] J. R. Schrieffer, *Theory of Superconductivity*, Benjamin, New York (1964)

[Sch76] R. R. Scheerbaum, *The role of spin-unsaturated closed shells in nuclear spin-orbit splitting*, Phys. Lett. B63 (1976) 381–384

[Sch04] J. P. Schiffer, S. J. Freeman, J. A. Caggiano, C. Deibel, A. Heinz, C.-L. Jiang, R. Lewis, A. Parikh, P. D. Parker, K. E. Rehm, et al., *Is the Nuclear Spin-Orbit Interaction Changing with Neutron Excess?*, Phys. Rev. Lett. 92 (2004) 162501

[Sch08] N. Schunck, J. L. Egido, *Nuclear Halos and Drip Lines in Symmetry-Conserving Continuum HFB Theory* Preprint arXiv:0809.4037

[Sev02] A. P. Severyukhin, C. Stoyanov, V. V. Voronov, N. Van Giai, *Quasiparticle random phase approximation with finite rank approximation for Skyrme interactions*, Phys. Rev. C 66 (2002) 034304

[Sev06] A. P. Severyukhin, M. Bender, P.-H. Heenen, *Beyond mean field study of excited states: Analysis within the Lipkin model*, Phys. Rev. C 74 (2006) 024311

[Sha85] L. J. Sham, M. Schlüter, *Density-functional theory of the band gap*, Phys. Rev. B 32 (1985) 3883–3889

[Sha95] M. M. Sharma, G. Lalazissis, J. König, P. Ring, *Isospin Dependence of the Spin-Orbit Force and Effective Nuclear Potentials*, Phys. Rev. Lett. 74 (1995) 3744–3747

[She00] J. A. Sheikh, P. Ring, *Symmetry-projected Hartree-Fock-Bogoliubov equations*, Nucl. Phys. A 665 (2000) 71–91

[She03] C. Shen, U. Lombardo, P. Schuck, W. Zuo, N. Sandulescu, *Screening effects on ^1S pairing in neutron matter*, Phys. Rev. C 67 (2003) 061302

[She05] J. Shergur, D. J. Dean, D. Seweryniak, W. B. Walters, A. Wohr, P. Boutachkov, C. N. Davids, I. Dillmann, A. Juodagalvis, G. Mukherjee, et al., *Identification of low-spin states in ^{111}Sb: Test of spin-orbit coupling in light nuclei*, Phys. Rev. C 71 (2005) 064323–8

[Ska93] J. Skalski, P. H. Heenen, P. Bonche, *Shape coexistence and low-lying collective states in $A \simeq 100$ Zr nuclei*, Nucl. Phys. A 559 (1993) 221–238

[Ska01] J. Skalski, *Self-consistent calculations of the exact Coulomb exchange effects in spherical nuclei*, Phys. Rev. C 63 (2001) 024312

[Sky56] T. H. R. Skyrme, *The nuclear surface*, Phil. Mag. 1 (1956) 1043–1054

[Sky58a] T. H. R. Skyrme, *The effective nuclear potential*, Nucl. Phys. 9 (1958) 615–634

[Sky58b] T. H. R. Skyrme, *The spin-orbit interaction in nuclei*, Nucl. Phys. 9 (1958) 635–640

[Sla51] J. C. Slater, *A Simplification of the Hartree-Fock Method*, Phys. Rev. 81 (1951) 385–390

[Son98] H. Q. Song, M. Baldo, G. Giansiracusa, U. Lombardo, *Bethe-Brueckner-Goldstone Expansion in Nuclear Matter*, Phys. Rev. Lett. 81 (1998) 1584–1587

[sp206] *Physics case of SPIRAL 2* (2006). `http://www.ganil.fr/`

[Sta77] F. Stancu, D. M. Brink, H. Flocard, *The tensor part of Skyrme's interaction*, Phys. Lett. B68 (1977) 108–112

[Ste72] F. S. Stephens, R. S. Simon, *Coriolis effects in the yrast states*, Nucl. Phys. A 183 (1972) 257–284

[Sto07] M. V. Stoitsov, J. Dobaczewski, R. Kirchner, W. Nazarewicz, J. Terasaki, *Variation after particle-number projection for the Hartree-Fock-Bogoliubov method with the Skyrme energy density functional*, Phys. Rev. C 76 (2007) 014308

[Tab64] F. Tabakin, *An effective interaction for nuclear hartree-fock calculations,*, Ann. Phys. (NY) 30 (1964) 51–94

[Taj93a] N. Tajima, P. Bonche, H. Flocard, P. H. Heenen, M. S. Weiss, *Self-consistent calculation of charge radii of Pb isotopes*, Nucl. Phys. A551 (1993) 434–450

[Taj93b] N. Tajima, H. Flocard, P. Bonche, J. Dobaczewski, P. H. Heenen, *Diabatic effects in 186Pb: A generator-coordinate analysis*, Nucl. Phys. A 551 (1993) 409–433

[Tan85a] I. Tanihata, H. Hamagaki, O. Hashimoto, S. Nagamiya, Y. Shida, N. Yoshikawa, O. Yamakawa, K. Sugimoto, T. Kobayashi, D. E. Greiner, et al., *Measurements of interaction cross sections and radii of He isotopes*, Phys. Lett. B 160 (1985) 380–384

[Tan85b] I. Tanihata, H. Hamagaki, O. Hashimoto, Y. Shida, N. Yoshikawa, K. Sugimoto, O. Yamakawa, T. Kobayashi, N. Takahashi, *Measurements of Interaction Cross Sections and Nuclear Radii in the Light p-Shell Region*, Phys. Rev. Lett. 55 (1985) 2676–2679

[Tan88] I. Tanihata, T. Kobayashi, O. Yamakawa, S. Shimoura, K. Ekuni, K. Sugimoto, N. Takahashi, T. Shimoda, H. Sato, *Measurement of interaction cross sections using isotope beams of Be and B and isospin dependence of the nuclear radii*, Phys. Lett. B 206 (1988) 592 – 596

[Ter02] J. Terasaki, F. Barranco, R. A. Broglia, E. Vigezzi, P. F. Bortignon, *Solution of the Dyson equation for nucleons in the superfluid phase*, Nucl. Phys. A 697 (2002) 127–140

[Ter05a] J. Terasaki, J. Engel, M. Bender, J. Dobaczewski, W. Nazarewicz, M. Stoitsov, *Self-consistent description of multipole strength in exotic nuclei: Method*, Phys. Rev. C 71 (2005) 034310

[Ter05b] J. Terasaki, J. Engel, M. Bender, J. Dobaczewski, W. Nazarewicz, M. V. Stoitsov, *Self-Consistent Description of Multipole Strength in Exotic Nuclei. The Method*, Phys. Rev. C 71 (2005) 034310

[Ter07] J. Terasaki, J. Engel, *Excited-state density distributions in neutron-rich nuclei*, Phys. Rev. C 76 (2007) 044320

[Ter08] J. Terasaki, J. Engel, *Systematics of the first 2^+ excitation in spherical nuclei with the Skryme-QRPA* ArXiv:0801.2346

[Ton83] F. Tondeur, *A Skyrme functional for Hartree-Fock calculations of nuclear masses and density distributions*, Phys. Lett. B 123 (1983) 139–142

[Ton84] F. Tondeur, M. Brack, M. Farine, J. M. Pearson, *Static nuclear properties and the parametrisation of Skyrme forces*, Nucl. Phys. A420 (1984) 297–319

[Ton00] F. Tondeur, S. Goriely, J. M. Pearson, M. Onsi, *Towards a Hartree-Fock mass formula*, Phys. Rev. C 62 (2000) 024308

[Typ01] S. Typel, B. A. Brown, *Neutron radii and the neutron equation of state in relativistic models*, Phys. Rev. C 64 (2001) 027302

[Val58] J. Valatin, *Comments on the theory of superconductivity*, Il Nuovo Cimento 7 (1958) 843–857

[Val97] M. Valiev, G. W. Fernando, *Generalized Kohn-Sham Density-Functional Theory via Effective Action Formalism* ArXiv:cond-mat/9702247

[Val00] A. Valor, P. H. Heenen, P. Bonche, *Configuration mixing of mean-field wave functions projected on angular momentum and particle number: Application to 24Mg*, Nucl. Phys. A 671 (2000) 145–164

[Vau72] D. Vautherin, D. M. Brink, *Hartree-Fock Calculations with Skyrme's Interaction. I. Spherical Nuclei*, Phys. Rev. C 5 (1972) 626–647

[VG81] N. Van Giai, H. Sagawa, *Spin-isospin and pairing properties of modified Skyrme interactions*, Phys. Lett. B 106 (1981) 379–382

[Vog84] P. Vogel, B. Jonson, P. G. Hansen, *Is there neutron-proton pairing in medium heavy nuclei?*, Phys. Lett. B 139 (1984) 227–230

[Wal74] J. D. Walecka, *A theory of highly condensed matter*, Ann. Phys. (NY) 83 (1974) 491–529

[Wam93] J. Wambach, T. L. Ainsworth, D. Pines, *Quasiparticle interactions in neutron matter for applications in neutron stars*, Nucl. Phys. A 555 (1993) 128–150

[Wei63] S. Weinberg, *Quasiparticles and the Born Series*, Phys. Rev. 131 (1963) 440

[Wir84] R. B. Wiringa, R. A. Smith, T. L. Ainsworth, *Nucleon-nucleon potentials with and without Delta (1232) degrees of freedom*, Phys. Rev. C 29 (1984) 1207

[Wir88] R. B. Wiringa, V. Fiks, A. Fabrocini, *Equation of state for dense nucleon matter*, Phys. Rev. C 38 (1988) 1010–1037

[Wir95] R. B. Wiringa, V. G. J. Stoks, R. Schiavilla, *Accurate nucleon-nucleon potential with charge-independence breaking*, Phys. Rev. C 51 (1995) 38

[Woh86] F. K. Wohn, J. C. Hill, C. B. Howard, K. Sistemich, R. F. Petry, R. L. Gill, H. Mach, A. Piotrowski, *Shape coexistence and level structure of* ^{100}Zr *from decay of the low-spin isomer of* ^{100}Y, Phys. Rev. C 33 (1986) 677–690

[Yuk35] H. Yukawa, *On the Interaction of Elementary Particles*, Proc. Phys. Math. Soc. Jap. 17 (1935) 48. Reprinted in: D. M. Brink, *Nuclear Forces*, Pergamon Press (1965) 214.

[Zal08] M. Zalewski, J. Dobaczewski, W. Satuła, T. R. Werner, *Spin-orbit and tensor mean-field effects on spin-orbit splitting including self-consistent core polarizations*, Phys. Rev. C 77 (2008) 024316

[Zdu05] H. Zduńczuk, W. Satuła, R. A. Wyss, *Probing the nuclear energy functional at band termination*, Phys. Rev. C 71 (2005) 024305

[Zhe91] D. C. Zheng, L. Zamick, *The effects of the spin-orbit and tensor interactions in nuclei*, Ann. Phys. (NY) 206 (1991) 106–121

[Zuo99] W. Zuo, I. Bombaci, U. Lombardo, *Asymmetric nuclear matter from an extended Brueckner-Hartree-Fock approach*, Phys. Rev. C 60 (1999) 024605

Contraintes microscopiques et au-delà du champ moyen pour une nouvelle génération de fonctionnelles de la densité nucléaires

La structure nucléaire connaît une véritable renaissance liée au développement des faisceaux d'ions radioactifs (tels les faisceaux SPIRAL 1 et 2 au GANIL). Les méthodes de champ moyen et/ou de fonctionnelle de la densité sont parmi les outils les plus généraux et les mieux adaptés pour étudier les noyaux qui sont produits auprès de tels instruments. Le but du travail présenté est de montrer comment les fonctionnelles existantes peuvent être améliorées afin d'avoir un meilleur pouvoir prédictif dans les régions encore peu explorées de la carte des noyaux. Il est en particulier proposé de mieux modéliser la dépendance en isospin de l'interaction effective, et l'intérêt d'y ajouter un couplage de type tensoriel est étudié. Nous mesurons également l'apport de calculs au-delà de l'approximation du champ moyen lors de la construction de la fonctionnelle. Finalement, nous tentons d'établir le lien avec l'interaction nue entre nucléons pour la description de l'appariement, participant ainsi au développement d'une fonctionnelle non-empirique.

Microscopic and Beyond-Mean-Field Constraints for a New Generation of Nuclear Energy Density Functionals

Nuclear structure is subject to a major renewal linked with the development of radioactive ion beams (such as the SPIRAL 1 and 2 beams at GANIL). Mean-field and density-functional methods are among the best suited for studying nuclei produced at such facilities. The present work aims at demonstrating how existing functionals can be improved so as to exhibit a better predictive power in little-explored regions of the nuclear chart. We propose a better description of the isospin-dependence of the effective interaction, and examine the relevance of adding a tensor coupling. We also show how a new generation of functionals can be better constrained by considering results obtained beyond the mean-field approximation. Finally, we attempt establishing a link with the bare nucleon-nucleon potential for the description of pairing, thus participating in the construction of a non-empirical functional.